



POLITECNICO DI MILANO

Facoltà di Ingegneria Edile - Architettura
Corso di laurea magistrale in Ingegneria dei Sistemi Edilizi

Analytical Modeling of the Cyclic Behaviour of a Replaceable Dissipater Device for Damage-Resisting Controlled Rocking System

Relatore: Prof. Paola RONCA
Correlatore: Prof. Alessandro PALERMO
Correlatore: Prof. Stefano PAMPANIN

Tesi di Laurea di:

Daniela BONARDI

Matr. 753175

Anno Accademico 2010 – 2011

INDEX OF CONTENTS

ABSTRACT.....	13
Prefazione.....	14
1. Introduction.....	15
1.1 Damping device systems.....	17
1.1.1 Base isolation devices.....	18
1.1 Dissipater devices.....	22
1.1.1 The hysteretic dampers.....	22
1.1.2 The Viscous and Viscoelastic Dampers.....	25
1.1.3 Tuned Mass Dampers.....	27
1.2 References.....	29
2. New Forms of Damage Resistant Structure.....	30
2.1 Controlled Rocking of Self Centering Systems.....	30
2.2 The Hybrid System: Concept, Mechanism and Design.....	33
2.3 Self Centering Resisting Systems.....	38
2.3.1 Self-Centering Systems for Concrete Structures.....	39
2.3.2 Self-Centering Systems For Steel Structures.....	40
2.3.3 Self-Centering Systems for Timber Structures.....	41
2.3.4 Self Centering Systems for Bridge Structures.....	42
2.4 Technological Solutions for Post Tensioned Walls.....	43
2.5 External “Plug And Play” Dissipators.....	49
2.5.1 Literature Review on External Dissipators.....	50
2.6 References.....	57
3. Plug and Play Experimental Program.....	59
3.1 Structural Instability.....	59
3.1.1 Steel Design.....	64
3.2 Design of the “PLUG and PLAY” Dissipators.....	65
3.3 Materials.....	70
3.3.1 Grade 300 Mild Steel.....	70
3.3.2 Epoxy.....	73
3.3.3 Grout.....	73
3.4 Fabrication of the Plug and Play Dissipators and Test Set Up.....	74
3.5 Displacement Time History.....	78

3.5.1	Test Schedules.....	89
3.6	Conclusions and Future Applications.....	91
3.7	References.....	92
4	Buckling Restrained Braces Behavior.....	94
4.1	Characteristics of Buckling Restrained Braces	94
4.2	Experimental Results on Buckling Restrained Braces	96
4.3	References.....	102
5	Plug and Play Hysteresis Loop.....	103
5.1	Physical Model of the Dissipator	103
5.2	Overall Buckling Criterion for Buckling Restrained Dissipators.....	104
5.3	The Effect of the Confinement.....	106
5.4	Buckling of a Bar on Elastic Supports	111
5.4.1	The Effect of the Tube	113
5.4.2	Critical Load of Bars on Elastic Supports	114
5.5	Finite Element Analysis	119
5.6	Parametric Analysis.....	125
5.7	Dissipator Hysteresis Loop Steps.....	130
5.8	Steel Dissipator Hysteresis Rule	153
5.1.1	Discussion	158
5.9	References.....	160
6	The effect of anchorage length of Fused Type Dissipation.....	162
6.1	Contribution of the Anchorage Length	162
6.2	The Effect of the Anchorage in the Elastic Range	167
6.2.1	Example of application of the k factor	169
6.3	The Effect of the Anchorage in the Plastic Range	171
6.1.1	Influence of the Anchorage after Yielding.....	173
6.4	Application of the Equivalent Length	174
6.1.2	<i>Determination of the Axial Stiffness of the Spring or Multi-Spring</i>	174
6.4.1	Evaluation of the Strain of the External Dissipator.....	176
6.5	Conclusions.....	177
6.6	References.....	178
7	Case Study – Carterton Events Center	179
7.1	Introduction to the Carterton Events Center.....	179
7.1.1	Material and Section Properties	180

7.2	Multi Spring Model.....	187
7.2.1	Quasi Static Analysis	189
	Push Over Analysis	190
	Capacity Spectrum Method.....	190
	Push Pull Analysis.....	194
	Truss to Wall Connection Analysis.....	196
7.2.2	Dynamic Time Hystory Analyses	202
7.3	Carterton Events Center – Parallel with “Plug And Play” Dissipator	204
7.3.1	Multi Spring Model.....	205
7.3.2	Quasi Static Analysis	207
	Push Over Analysis	208
	Push Pull Analysis.....	209
7.4	References	213
8	Conclusions	214
	Further Objective of the Research.....	216
APPENDIX A		217
	Introduction	217

INDEX OF FIGURES

Figure 1. Current performance Objective Matrix (Modified from[2]	15
Figure 2. Building resting directly on ground	18
Figure 3. Building on rollers without any friction.....	18
Figure 4. Building on Base Isolators (left); Details of the Base Isolator (right)	18
Figure 5. Schematic of Laminated Rubber Bearing and Example of Laminated Rubber Bearing [1].....	19
Figure 6. Schematic Design of the Base Isolator Device and Example of a Base Isolator Device [1].....	19
Figure 7. Te Papa Museum’s Base Isolator Devices.....	20
Figure 8. Schematic design of Spherical Sliding Isolation Bearing (left), Principle of Operation of the Friction Pendulum System [1](right)	20
Figure 9. Mississippi Rr. Bridge (left) and Spherical Sliding Isolation Bearing of Mississippi Rr. Bridge (right).....	20
Figure 10. Mechanism of Double Friction Pendulum System (Constantinou et al. 2004).....	21
Figure 11. Typical application of yielding dampers (left); Hysteresis Loop of Hysteretic Dampers (right)	22
Figure 12. Pin shaped damper (left); Crescent moon shaped damper; Butterfly shaped damper	23
Figure 13. Typical Application of Friction Dampers (left); possible arrangements of Steel Plates in Friction Dampers [3].....	23
Figure 14. Slotted Bolt Connection [4]	24
Figure 15. Components of BRB (left); Example of BRB of the Tzu-Chi Culture Building (Taipei, Taiwan).....	24
Figure 16. The World Trade Center, fitted with dampers (left); Placement (top right); Damper (bottom right) (http://accessscience.com/content/Smart-structures-and-materials/YB001370) .	25
Figure 17. Example of Application of a Fiscous Damping Device (left); Hysteresis Loop of a Viscous Damping Device (right) [3]	25
Figure 18. Viscous fluid device [1]	26
Figure 19. Viscous Damping Wall [6]	26
Figure 20. Main Structure and TMD [1]	27
Figure 21. The Taipei 101, Taiwan (left); the Tuned Mass Damper (right) (http://en.wikipedia.org/wiki/File:Taipei_101_Tuned_Mass_Damper_2010.jpg).....	27
Figure 22. Earlier implementation of a self-centering limited-damage rocking system, for earthquake loading (Dionysus temple in Athen [2])	31
Figure 23. Test Building - Level 1 floor plan [3].....	32
Figure 24. Test Building - Level 4 floor plan [3].....	32
Figure 25. Hybrid Post Tensioned Connection (top left); TCY Gap Connection (top right); Hybrid Post Tensioned Connection (bottom left); TCY Connection (bottom right) [3]	32
Figure 26. Elevation of jointed shear wall system	33
Figure 27. Idealized Flag Shape Hysteresis Loop (left) and ..(right)	34
Figure 28. Monolithic Beam Analogy [5].....	34
Figure 29. Extended Monolithic Beam Analogy [1]	35
Figure 30. Schematic flow chart of the moment-rotation procedure [5].....	37
Figure 31. Idealized Seismic Response of Yielding Structure [7]	38

Figure 32. Rangitikei Railway Bridge [7] [8]	38
Figure 33. Jointed precast hybrid frame and wall systems developed in the PRESSS-Program [2]	39
Figure 34. Comparison of monolithic wall and precast rocking wall [2].....	39
Figure 35. Hybrid Post Tensioned Connection for Steel Frames [10]	40
Figure 36. Steel Moment Resisting Connection [9]	40
Figure 37. Application of Hybrid Concept to LVL frame system [11].....	41
Figure 38. Examples of beam-column joint, wall to foundation joint and column to foundation joint [12].....	42
Figure 39. Controlled Rocking concept of bridge piers (Palermo, 2005)	42
Figure 40. (a) Post Tensioned Rocking Wall System, (b) Detail of U shaped dissipators [7] ...	43
Figure 41. Wall with Supplemental Viscous Damping [14]	43
Figure 42. (a) Hybrid Reinforced Concrete Cantilever Wall System, (b) Energy dissipator installed [16].....	44
Figure 43. Coupled wall system: a) multistorey wall, b) beam-wall connection [17]	45
Figure 44. Confined Masonry Rocking Walls: Front view (left) ; view of base of the wall (top right); geometry of hysteretic dissipation device (bottom right) [18]	45
Figure 45 . Internal versus External Replaceable Dissipaters at the base of the wall [2].....	46
Figure 46. (a) Hybrid Timber Wall with Internal Dissipaters, (b) Energy Dissipation Devices, (c) Wall base [1].....	46
Figure 47. Wall-foundation joint using external dissipators [21].....	46
Figure 48. Scheme of Coupled Wall System with UFP devices (left), Test set up of Coupled Wall System (center), Particular of UFP devices (right) [22]	47
Figure 49. Damper details, Mild Steel Damper (left), FIP Industriale Viscous Damper (right) [23]	47
Figure 50. Wall Test Set Up, Wall with external mild steel devices (left), Wall with external mild steel devices and viscous damper (right) [23].....	48
Figure 51. Example of Plug and Play dissipater: Schematic Design (top), Example of a Dissipator (bottom)	49
Figure 52. (a) Test Set Up, (b) Model of the Connection, (c) Detail of the Connection [25]	50
Figure 53. Force-Displacement Response of the Hybrid Solution under Uni Directional or Combined testing Regime [25]	50
Figure 54. Post Tensioned Precast Rocking Wall System with Externally Mounted Mild Steel Dissipators (left) and Controlled Rocking (right) [23].....	51
Figure 55. Detail of the Dissipator (top left), Experimental Response of the Dissipator (top right); As-Build Wall unit (Bottom Left); Experimental Response of the Wall (Bottom Right) [23]	51
Figure 56. Dissipator Connection Details ([26]	52
Figure 57. Dissipator Device Testing [26]	52
Figure 58. Cyclic Testing of Dampers. Test Specimens C1 & C2 Positive Displacements only, Test Specimens C3 & C4 Positive and Negative Displacements [26]	53
Figure 59. The Effect of the Epoxy, increasing the Axial Stiffness of the Damper in Compression [26]	53
Figure 60. Energy Dissipator Footing (left), Particular of Energy Dissipation Device (right) [27]	54

Figure 61. Hysteresis Response of the Hybrid Solution (Left) and Gap Opening at 3.5% of Drift (right) [27].....	54
Figure 62. Test Set Up of External Dissipator Elements and Detail of the Dissipator [27].....	54
Figure 63. Hysteresis Response with two Different Energy Dissipators [27].....	55
Figure 64. Stress Strain Force of External Dissipators [27].....	55
Figure 65. Connection Detail (left) and Dissipator Detail (right) [27].....	55
Figure 66. Components of Beam-Column Joint Assembly (left); Mild Steel Energy Dissipator [12].....	56
Figure 67. Load-Drift Plot of Hybrid Solution with External Dissipators [12].....	56
Figure 68. Buckling of a Column with Pin Connected Ends [1].....	60
Figure 69. Example of a Buckled Column [1].....	60
Figure 70. Euler's Curve [1].....	61
Figure 71. Effective Length of Column for Various End Conditions [1].....	61
Figure 72. Idealized and Empirical Relation of Critical Stress [1].....	62
Figure 73. Buckling of Column under Eccentric Load [1].....	63
Figure 74. Load per Unit Area causing Yield in Column [1].....	63
Figure 75. Variation of σ_{cr} with $L/1$ [1].....	64
Figure 76. External Dissipator Device.....	65
Figure 77. Effect of Buckling Restrain [3].....	65
Figure 78. Profile of the Screw Thread.....	67
Figure 79. Stress - Slenderness Relationship.....	68
Figure 80. Dissipators to be Tested at University of Canterbury.....	68
Figure 81. Simplified Scheme of Buckling.....	69
Figure 82. Typical Stress Strain Relationship for Steel Bars (left), Typical Stress Strain Relationship for Steel with repeated Loading of the Same Sign [5].....	70
Figure 83. Typical Stress Strain Relationship for Steel with Cyclic Loading [5].....	71
Figure 84. Histograms of Yield Strengths for Grade 275 Deformed Bars [5].....	71
Figure 85. Yield Strength Values of Various Deformed Bars Diameter of Grade 275 [5].....	72
Figure 86. Histogram of the Ultimate Strength of Grade 275 Deformed Bars [5].....	72
Figure 87. Possible Buckling Shapes [6].....	74
Figure 88. Example of the Dissipator.....	75
Figure 89. Strain Gauging of the Dissipator at the mid length (top), Detail of the Strain Gauging (bottom).....	75
Figure 90. Manufacturing of External “Plug and Play” Dissipators.....	76
Figure 91. Dissipators Test Set Up.....	77
Figure 92. Details of the Wall. Vertical Section of the Wall (left), Detail of the base of the Wall (top right), Horizontal Section of the Wall(bottom right).....	78
Figure 93. Post Tensioned Wall Sections with D24 External Mild Steel Dissipators.....	86
Figure 94. Post Tensioned Wall Section with $\phi 12$ External Mild Steel Dissipators.....	87
Figure 95. Post Tensioned Wall Section with $\phi 16$ External Mild Steel Dissipators.....	87
Figure 96. Post Tensioned Wall Section with $\phi 20$ External Mild Steel Dissipators.....	88
Figure 97. Post Tensioned Wall Section with $\phi 26$ External Mild Steel Dissipators.....	88
Figure 98. Test Schedule of $\phi 12$ External Mild Steel Dissipators.....	89
Figure 99. Test Schedule of $\phi 16$ External Mild Steel Dissipators.....	89
Figure 100. Test Schedule of $\phi 20$ External Mild Steel Dissipators.....	90

Figure 101. Test Schedule of $\phi 24$ External Mild Steel Dissipators	90
Figure 102. Test Schedule of $\phi 26$ External Mild Steel Dissipators	91
Figure 103. Component of BRB [1].....	95
Figure 104. Cross Sections of BRBs [2]	95
Figure 105. Behavior of Conventional Brace and BRB.....	96
Figure 106. Buckling - Restrained Brace Hysteresis [2].....	97
Figure 107. Frame test of X-Shape BRB [2].....	97
Figure 108. Brace Hysteretic Behavior : loading Protocol (top left), Test 1 (top right), Test 2 (bottom left), Test 3 (bottom right) [3]	98
Figure 109 Load Displacement Relation of Test Specimens: Test 1 (top left), Test 2 (top right), Test 3 (middle left), Test 4 (middle right), Test 5 (bottom left), Test 6 (bottom right).	99
Figure 110. Experimental and Analytical Cyclic Response: Test 1 (top left), Test 2(top right), Test 3 (bottom left), Test 4 (bottom right) [5].....	100
Figure 111. Steel Buckling Hysteresis Rule.....	101
Figure 112. Different Failure modes of the brace: Plastic buckling (top right), Fatigue Failure mode (bottom right).	101
Figure 113. Dissipator and model of the dissipator.....	103
Figure 114. Detail of the Plug and Play Dissipators	104
Figure 115. Analysis on a Dissipators, Force in the System.....	105
Figure 116. Dissipator and model of the dissipator.....	106
Figure 117. Dissipator and Model of the Dissipator for $P < P_{cr}$	107
Figure 118. Dissipator and Model of the Dissipator for $P \approx P_{cr}$	108
Figure 119. Dissipator and Model of the Dissipator for $P \approx P_c$	108
Figure 120. Dissipator and Model of the Dissipator for $P > P_{cr}$ (left), Detail of the Mid Length of the Dissipator (top right), Force – Displacement of the filler material	109
Figure 121. Dissipator and Detail of the Dissipator for $P > P_{cr}$	110
Figure 122. Dissipator and Detail of the Dissipator for $P > P_{cr}$	110
Figure 123. Deformation of a Column with Increasing Load [5].....	112
Figure 124. Two Springs in series modeling the grout/epoxy and the steel tube.....	113
Figure 125. Sap Model of the Confinement subjected to a force in the Y axis.....	113
Figure 126. “Slice” of the Confinement subjected to a force F.....	114
Figure 127. Critical Load and Effective Length Factor versus Thickness of the Confinement	115
Figure 128. Critical Load and Effective Length Factor versus Thickness of the Confinement	116
Figure 129. Critical Load and Effective Length Factor versus Thickness of the Confinement	116
Figure 130. Critical Load and Effective Length Factor versus Thickness of the Confinement	117
Figure 131. Critical Load and Effective Length Factor versus Thickness of the Confinement	117
Figure 132. Critical Load and Effective Length Factor versus Thickness of the Confinement	118
Figure 133. Graph of Effective Length Factor versus Thickness of the Epoxy	118
Figure 134. Graph of Critical Load versus Thickness of the Epoxy	119
Figure 135. Fully Fixed Column Supporting a Load P	120
Figure 136. SAP 2000 Model (left) and Section of the model (right).....	120
Figure 137. Fully Fixed Column Supporting a load P	121
Figure 138. Fully Fixed Restrained Column Supporting a Load P	123
Figure 139. Fully Fixed Column Supporting a Load P	123
Figure 140. Graph of Stiffness versus Outer Diameter of the Tube.....	127
Figure 141 . Stiffness versus Thickness of the Confinement	127

Figure 142. Graph of Stiffness versus Outer Diameter of the Tube.....	128
Figure 143. Stiffness versus Thickness of the Confinement	128
Figure 144. Displacement Time History, Compression - Tension.....	130
Figure 145 "Step by Step" Analysis of the Dissipator	131
Figure 146. Stress Strain Relationship.....	132
Figure 147. "Step by Step" Analysis of the Dissipator	136
Figure 148. Force-Displacement Relationship of Dissipator	137
Figure 149. Displacement Time History, Compression - Tension.....	137
Figure 150. "Step by Step" Analysis of the Dissipator	144
Figure 151. Force-Displacement Relationship of Dissipator	145
Figure 152. Stiffness versus Outer Diameter of the tube with an Epoxy Confinement	145
Figure 153. Fitting of Results.....	146
Figure 154. Fitting of Results obtained with the Equation and Sap 2000.....	147
Figure 155. Stiffness versus Thickness of the Confinement	147
Figure 156. Stiffness versus Outer Diameter with a Grout Confinement	148
Figure 157. Fitting of the Results.....	149
Figure 158. Fitting of the Results obtained with the Equation and Sap 2000	150
Figure 159. Stiffness versus Thickness of the Confinement	150
Figure 160. Stiffness versus Outer Diameter of the Tube.....	151
Figure 161. Fitting of Results obtained with the Equation and Sap 2000.....	152
Figure 162. Steel Buckling Hysteresis Loop.....	153
Figure 163. Different Failure modes of the Dissipator: Plastic buckling (top right), Fatigue Failure mode (bottom right).	153
Figure 164. Hysteretic Loop.....	154
Figure 165. Required Datas of the Hysteresis Loop (top) and P- δ Curve, P- ϕ Curve, P – M Curve (bottom).....	156
Figure 166. Deformation of the Dissipator when subjected to Compression-Tension Cycles..	157
Figure 167. Example of Dissipator Device	158
Figure 168. Test Schedule.....	158
Figure 169. Specimen type - dissipator device.....	163
Figure 170. Displacement of the fuse, displacement of the external part and total displacement of specimen 1	165
Figure 171. Displacement of the fuse, displacement of the external part and total displacement of specimen 2	165
Figure 172. Displacement of the fuse, displacement of the external part and total displacement of specimen 3	166
Figure 173. Displacement of the fuse, displacement of the external part and total displacement of specimen 4	166
Figure 174. Displacement of the fuse, displacement of the external part and total displacement of specimen 5	167
Figure 175. Values of k with relation to ϕ_f/ϕ_e and L_f/L_{tot}	169
Figure 176. Specimen of upcoming UoC testing	169
Figure 177. Comparison between the values of strain	173
Figure 178. Alternative Solution using the Equivalent Length.....	176
Figure 179. Plan of the Carterton Events Centre (left); Auditorium Plan showing walls locations (right) [1]	179

Figure 180. Photos taken during construction and installation of LVL post-tensioned and coupled shear panels, NMIT Arts & Media Building	180
Figure 181. Manufacturing Process of LVL	181
Figure 182. Schematic View of LVL Manufacturing Process	182
Figure 183. Walls - Truss System	183
Figure 184. Wall Panel Erection	184
Figure 185. Macalloy Bar Connection (left); Construction Progress (right).....	184
Figure 186. Pres-Lam Wall General Arrangement (left); comparative response of a monolithic system and a dissipative rocking post-tensioned solution (right) [3]	185
Figure 187 Post Tensioned Wall and Lumped Plasticity Model.....	185
Figure 188 . (a) Side view of truss-wall system; (b) Transverse wall connection during construction; (c) Sketch and (d) Model of the truss-to-wall connection	186
Figure 189. Ruaumoko Model of the Walls-Truss System	187
Figure 190. Push Over Capacity of the Walls. Capacity of Wall 1 (top left), Capacity of Wall 2 (top right), Capacity of wall 3 (bottom left	190
Figure 191. Capacity Spectrum Method. Development of Push Over Curve (top left), Conversion of Push Over Curve to Capacity Diagram (top right), Conversion from Acceleration Spectrum to Displacement Spectrum (bottom right) [7]	191
Figure 192. ULS Response Spectrum and ULS Displacement Spectrum.....	192
Figure 193. Seismic Performance Assessment.....	193
Figure 194. Quasi Static Analysis. Lateral Force and Tendons Force Wall 1 (top left and right), Lateral Force and Tendons Force Wall 2 (center left and right), Lateral Force and Tendon Force Wall 3 (bottom left and right)	194
Figure 195. Quasi Static Analysis Total Shear Force – Drift.....	195
Figure 196. Quasi Static Analysis: Viscous Damping (left) and neutral axis vs. Drift (right)	195
Figure 197. Vertical Displacement of the Walls	196
Figure 198. Beam sign convention.....	197
Figure 200. Bending Moment, drift 1% (left), Drift 1.5% (right).....	197
Figure 199. Wall 1 - Truss connection.....	197
Figure 201. Axial Forces, Drift 1% (left), Drift 1.5% (right).....	198
Figure 202. Shear Forces, Drift 1% (left), Drift 1.5% (right)	198
Figure 204. Bending Moment, drift 1% (left), Drift 1.5% (right)	199
Figure 205, Axial Forces, Drift 1% (left), Drift 1.5% (right).....	199
Figure 203. Wall 2 - Truss connection	199
Figure 206. Shear Forces, Drift 1% (left), Drift 1.5% (right)	200
Figure 207. Wall 3- truss connection	200
Figure 208. Bending Moment, drift 1% (left), Drift 1.5% (right)	200
Figure 209. Axial Forces, Drift 1% (left), Drift 1.5% (right).....	201
Figure 210. Shear Forces, Drift 1% (left), Drift 1.5% (right)	201
Figure 211. Multi Spring Model Results.....	203
Figure 212. Flag Shape Hysteresis, Push Pull Analysis and Ground Motion Analysis (EQ2) .	203
Figure 213. Case Study with External Dissipator Devices; Sections of the Wall (top and center), Detail of the Dissipator (bottom)	204
Figure 214. Lumped Plasticity Model of the Wall with External Dissipators	205

Figure 215. Push Over Capacity of the Wall; Capacity of Wall 1 (top left), Capacity of Wall 2 (top right), Capacity of Wall 3 (bottom left)	208
Figure 216. Push Over Analysis up to Failure Point (left), Hysteresis of External Dissipator (right).....	209
Figure 217 . Quasi Static Analysis. Lateral Force and Tendons Force Wall 1 (top left and right), Lateral Force and Tendons Force Wall 2 (center left and right), Lateral Force and Tendon Force Wall 3 (bottom left and right)	210
Figure 218. Quasi Static Analysis Total Shear Force - Drift	210
Figure 219. Hysteresis Loop of External Dissipator Devices	211
Figure 220. Push Pull Analysis up to Failure Point	211
Figure 221. Flag Shape Hysteresis, Push Pull Analysis and Ground Motion Analysis	212

INDEX OF TABLES

Table 1. Damping Device Systems	17
Table 2. Fuse Diameters of Dissipators used in the Past Research	66
Table 3. Size of External and Internal Diameters of the Dissipators	66
Table 4. Threaded Diameters of the Dissipator Devices	67
Table 5. Diameters and Lengths of the Dissipators.....	69
Table 6. Determination of the Thickness of the Tube	70
Table 7. Properties of Grade 275 Steel.....	73
Table 8. Properties of Epoxy Resin.....	73
Table 9. Diameters and Lengths of the Dissipators.....	74
Table 10. Restrain Tubes Details	76
Table 11. Mild Steel Steel Properties	79
Table 12. Post Tensioned Steel Properties	79
Table 13. Number of Dissipators Required.....	81
Table 14. Unitary Values of Stiffness of a “Slice” of Dissipator	114
Table 15. Critical Value of a L = 300 mm Dissipator	115
Table 16. Critical Value of a L = 400 mm Dissipator	115
Table 17. Critical Value of a L = 500 mm Dissipator	116
Table 18. Critical Value of a L = 600 mm Dissipator	117
Table 19. Critical Value of a L = 600 mm Dissipator	117
Table 20. Critical Value of a L = 600 mm Dissipator	118
Table 21. Dimensions of the External Tube e Thicknesses of the Confinement	125
Table 22. Unitary Stiffness of the Dissipator Device for Different Values of Outer Diameter and Thickness of the Epoxy	126
Table 23. Unitary Stiffness of the Dissipator Device for Different Values of Outer Diameter and Thickness of the Epoxy	127
Table 24. Unitary Stiffness of the Dissipator Device for Different Values of Outer Diameter and Thickness of the Grout	128
Table 25. Data of Hysteresis Loop.....	156
Table 26. Diameters and Lengths of Dissipator Devices	164
Table 27. Displacements of a 12 mm and 16 mm Diameter Bars	164
Table 28. Equivalent Lengths for the Different Dissipators	168
Table 29. Values of k_1 and equivalent lengths for $\varepsilon = 0.01$	172
Table 30. Values of k_1 and equivalent lengths for $\varepsilon = 0.01$	172
Table 31. Comparison between the values of strain.....	173
Table 32. Values of equivalent length obtained with different displacements.....	174
Table 33. Structural Properties of LVL Wall	182
Table 34. Dimensions of LVL Wall and LVL Truss	182
Table 35. Materials Properties	183
Table 36. Design values of the Wall	186
Table 37. Multi Spring Model Members.....	189
Table 38. Spectrum Values	192
Table 39. Multi Spring Model Members.....	207

ABSTRACT

The present document has the purpose to investigate the key aspects of the design and modeling of external mild steel dissipators.

The first part of the thesis is focused on the design of dissipators and provides the information needed to carry out the forthcoming experimental tests. The development of a guide line for the design of dissipators is one of the objectives of the work. If not properly designed the devices can be subjected to instability; the dissipators are not able anymore to dissipate the same amount of energy as in compression as in tension.

Considering the dissipation device is important to know the exact value of the onset of dissipation and so the value of displacement needed to reach the yielding load. The definition of an equivalent length that keeps into account the effect of the anchorage on the global response is introduced. The aim is to supply a value of length that have to be used for the determination of the strain in order to define the exact value of the beginning of dissipation.

The modeling of the dissipators is carried out defining a new hysteresis loop (modified of Remennikov Hysteresis Loop) specific for Plug and Play dissipators. The behavior of the device depends on the global response of a bar restrained by a steel tube filled with grout or epoxy. The effect of the confinement provides an increasing of the critical load (or a decreasing of the effective length of the bar). Different ways to define the value of stiffness of the restrain have been carried out; as a result a general solution for the determination of the stiffness depending on the outer diameter of the tube and on the thickness of the filler material is determined.

The final part of the work presents the results of a finite element analysis on a truss-walls system. The walls are realized using the Press Lam System with internal dissipators. The advantages of the use of the external dissipators are highlighted by the results of a parallel analysis with external dissipators in place of the internal ones that show no stiffness degradation. The crisis of the wall is due to the rupture, and not buckling, of the dissipator.

Prefazione

L'elaborato di tesi ha lo scopo di investigare gli aspetti fondamentali della progettazione e modellazione dei dissipatori esterni "Plug and Play", sviluppati e testati all'"University of Canterbury" (New Zealand).

La prima parte della tesi tratta il progetto dei dissipatori e fornisce le informazioni necessarie per l'esecuzione di prove sperimentali finalizzate a caratterizzarne il comportamento. Particolare attenzione richiede il design dei dissipatori poiché, se non correttamente pensato, può comportare l'instabilità dell'elemento. Se soggetti a instabilità i dissipatori non sono in grado di dissipare a compressione la stessa quantità di energia dissipata in trazione poiché il valore di snervamento non è raggiunto.

La dissipazione isteretica può avere luogo solo con lo snervamento del metallo. E' dunque rilevante conoscere l'effettivo spostamento che l'elemento dovrà raggiungere prima di potersi attivare. In via approssimativa la soglia di attivazione può essere calcolata considerando che la deformazione avviene solo nel fuso ma in questo modo l'effetto delle parti terminali più rigide è trascurato. Una lunghezza equivalente è introdotta nel calcolo ed è ponderata per tenere in conto l'aumento di rigidità fornito dalle due estremità di diametro maggiore; considerando la deformazione in funzione di questa lunghezza si ottiene l'effettivo valore di spostamento necessario al dissipatore per iniziare a dissipare.

La modellazione dei dissipatori esterni è effettuata introducendo una nuova curva isteretica specifica per i "Plug and Play". Il comportamento del dissipatore dipende dalla risposta globale del sistema di barra di acciaio vincolata lateralmente per mezzo di un tubo di acciaio e colmando lo spazio tra barra e tubo con del materiale riempitivo. L'effetto del confinamento comporta un aumento del carico critico (o una diminuzione della lunghezza effettiva).

La parte conclusiva del lavoro mostra i risultati di un'analisi eseguita con Ruaumoko 2D su un sistema di muri in legno che sostengono una trave reticolare anch'essa in legno. I muri sono realizzati secondo la tecnica del Press Lam; la dissipazione avviene con dissipatori interni. Un'analisi parallela con dissipatori esterni a sostituzione di quelli interni mostra che la crisi del muro avviene per rottura, non quindi instabilità, del dissipatore.

1. Introduction

The main principle of earthquake resistant design is to ensure an acceptable safety level avoiding catastrophic failures and loss of life. There are then important buildings such as hospitals, police stations, communication centers,.. that need to be designed for higher performance level because must remain functional after an earthquake event. Indeed the basic performance objective of conventional seismic design is the life safety but this objective is not sufficient for important structures. In the last 30 years important improvement in innovative earthquake system have been carried out in order to raise the performance level of structures but always trying to keep the costs at a reasonable level.

The current philosophy for seismic engineering is the Performance Based Design that was first formulated in the Vision 2000 document [2]. In the document has been given a definition of the Performance Based Earthquake Engineering consisting of:

“a set of engineering procedures for design and construction of structures to achieve predictable levels of performance in response to specified levels of earthquake, within definable levels of reliability”.

Performance levels correspond to the maximum acceptable extent of damage under a given level of seismic ground motion.

The performance based design framework modified from SEAOC is shown below with the distinction of the buildings depending on their importance for the general public.

		Earthquake performance level			
		<i>Fully operational</i>	<i>Operational</i>	<i>Life safe</i>	<i>Near collapse</i>
		REPAIRABLE		NON REPAIRABLE	
Earthquake design level	Frequent (40 years)		Unacceptable	Unacceptable	Unacceptable
	Occasional (100 years)			Unacceptable	Unacceptable
	Rare (550 years)				Unacceptable
	Very rare (2500 years)				

Figure 1. Current performance Objective Matrix (Modified from[2])

Buildings respond to an earthquake shaking in different ways. If a building is designed to respond elastically it may fail when it is subjected to a force that is higher than the building strength. On the other hand when a building is designed to respond with ductility it will be damaged but it is able to resist without an unexpected failure.

Therefore there are different ways and so different design possibilities to resist to the same earthquake [3]

- to provide the building with high strength so that it will respond elastically
- to design the building to have normal strength following some design guidelines
- to modify the building characteristics with the use of damping devices.

Considering the first option the structure will have no damage but this approach is not completely safe because the maximum level of ground shaking is never known for certain. Another limit of this kind of design is that the construction cost will be too high.

On the other hand considering an elasto-plastic response, ductility is developed and the structure can reach the collapse for an exceptional earthquake.

The other possibility is to modify externally the building to reduce the demand or the response. There are two different alternatives: isolate the building from the ground shaking or dissipate the incoming energy.

These two options are described in the next paragraphs.

1.1 Damping device systems

There are two different ways to modify the answer of the building :

- to reduce the demand: damper devices
- to reduce the response: isolators

The dampers can be passive or semi active/active and the kind of dissipators within the two groups are listed below.

<i>Passive Dampers</i>	<i>Semi Active/ Active Dampers</i>
Metallic	Braces
Friction	Tuned Mass
Viscoelastic	Variable Stiffness
Viscous	Variable Damping
Self - Centering	Piezoelectric

In the group of the isolation system there are:

<i>Isolation system</i>
Elastomeric
Lead rubber
High damping rubber
Metallic
Lead extrusion
Friction Pendulum

Table 1. Damping Device Systems

The dampers can dissipate in different ways; there are then the displacement activated dampers (metallic dampers, friction dampers, self centering dampers), the velocity activated dampers (viscous dampers) and the motion activated dampers (tuned mass dampers).

Most of the damping systems are design to dissipate the seismic energy introduced into a structure and they work as supplemental damping mechanism designed to limit the transmission of seismic energy to the primary system of isolation.

The different kinds of primary isolation system and of the supplemental ones are explained in the following paragraphs.

1.1.1 Base isolation devices

The system of base isolation that has been adopted most widely in recent years is typified by the use of elastomeric bearings, the elastomer made of either natural rubber or neoprene. In this approach, the building or structure is decoupled from the horizontal components of the earthquake ground motion by interposing a layer with low horizontal stiffness between the structure and the foundation. The system decouples the building from its foundations resting on the shaking ground. Due to the presence of this layer the frequency of the building is much lower than the one that he should have if it is fixed on the ground.

The earthquake involves a deformation in the isolation system while the building moves rigidly.

The concept of base isolation is explained with some drawings below.

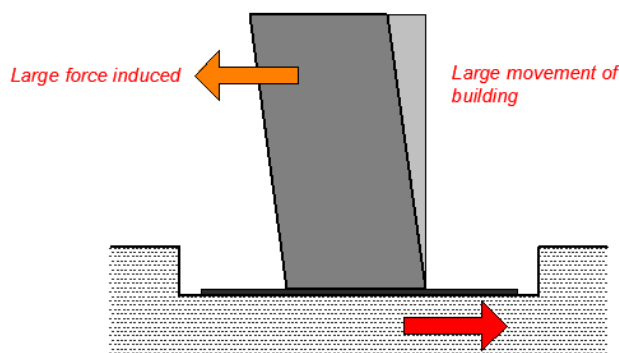


Figure 2. Building resting directly on ground

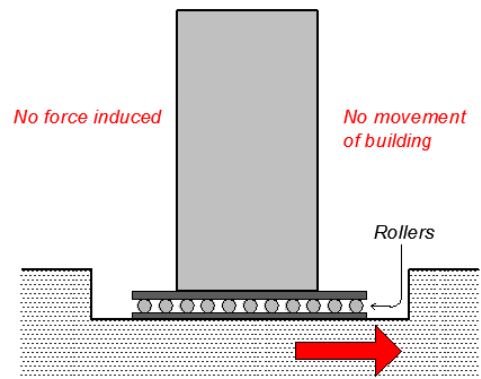


Figure 3. Building on rollers without any friction

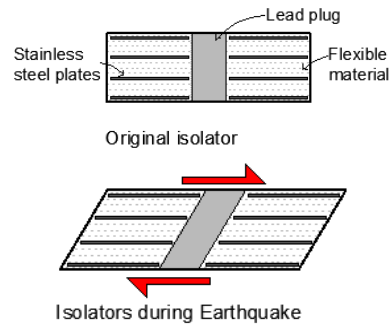
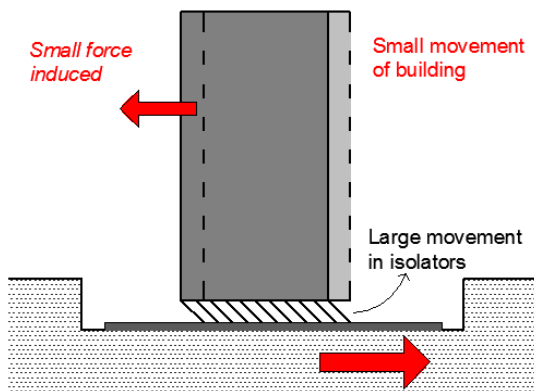


Figure 4. Building on Base Isolators (left); Details of the Base Isolator (right)

Figure 2 represents the case of the building fixed on the ground. The building is subjected to large movements and the large forces.

The concept of building isolated is explained in the Figure 4 where is shown a building resting on frictionless rollers. When there is an earthquake the rollers freely roll and the building above don't move. This is an ideal representation because if the building is located on the isolators it's subjected to a small movement and small forces are induced. Due to the resistance of the system to lateral displacements some effects are transferred to the building.

There are two basic kinds of isolation system: elastomeric bearings and sliding system. In the first case the building is decoupled from the ground with the interposition of a layer of rubber that is characterized by a low horizontal stiffness.

There are two main types of elastomeric bearings, the laminated rubber bearing and the lead rubber bearing.

The first one is composed of elastomeric rubber layers alternating with steel plates solidly jointed together under high pressure and temperature through a process called vulcanization.

A schematic drawing of the laminated rubber bearing and a picture are shown below.

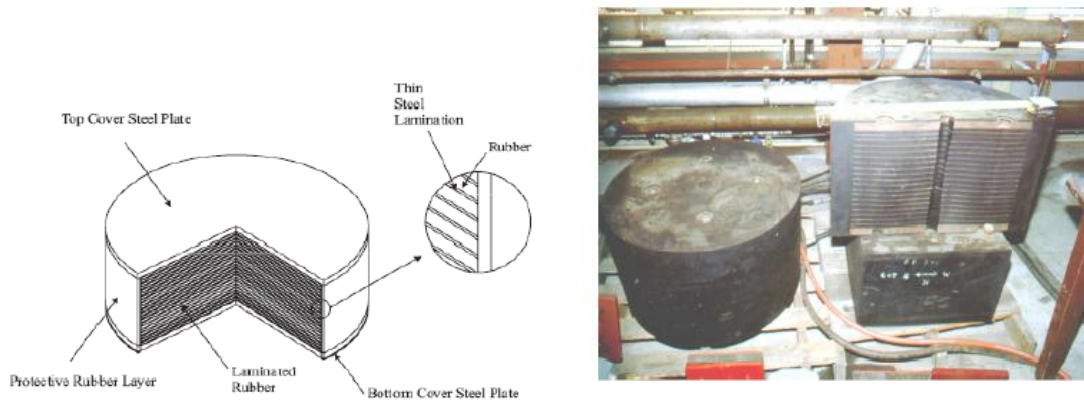


Figure 5. Schematic of Laminated Rubber Bearing and Example of Laminated Rubber Bearing [1]

The lead rubber bearing produced by Robinson Seismic typically consists of a rubber bearing with alternating laminations of thin rubber layers and steel plates with a cylindrical lead plug inserted in its center. In this way the isolator is very stiff in the vertical direction but flexible in the horizontal one and the damping by hysteretic shear deformation of the lead is increased. These characteristics of the base isolator elements are very important because it must be capable of undergoing to movement imposed by the ground shaking, while maintaining its ability to carry the gravity load.

A schematic design and a picture of the foundation of the Te Papa Museum in Wellington which uses this kind of dissipation devices are shown below.

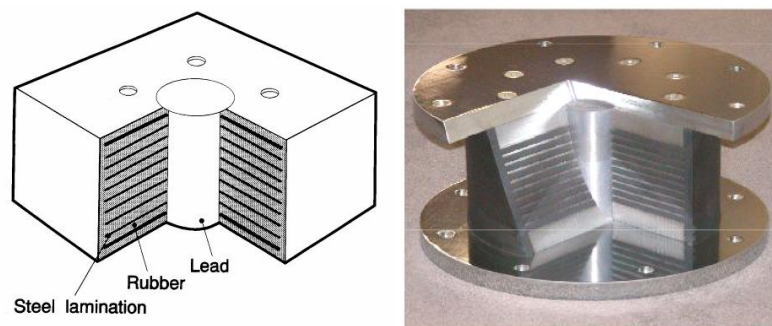


Figure 6. Schematic Design of the Base Isolator Device and Example of a Base Isolator Device [1]



Figure 7. Te Papa Museum's Base Isolator Devices

The sliding system works trying to limit the transfer of the shear across the isolation interface. The most common used is the spherical sliding bearing that is represented in the drawing below.

The friction pendulum system manufactured by Earthquake Protection System in Richmond California is a friction type sliding bearing that uses gravity as the restoring force. The system consists of a friction slider that travels on a large spherical concave sliding surface.

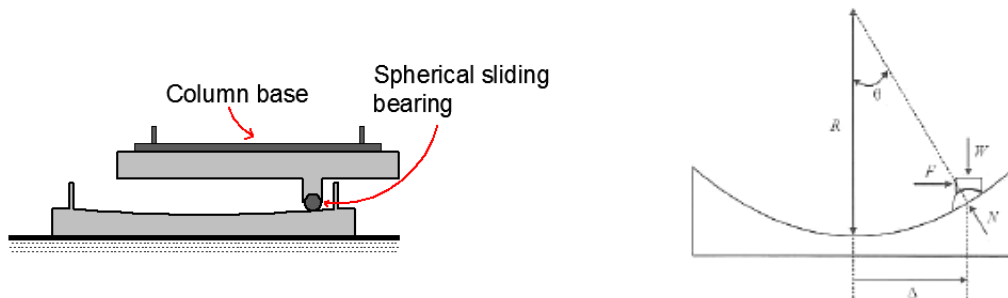


Figure 8. Schematic design of Spherical Sliding Isolation Bearing (left), Principle of Operation of the Friction Pendulum System [1](right)

An example of the use of the spherical sliding isolation bearing is the Mississippi Rr. Bridge, Memphis (Tennessee) as shown in Figure 9 (Figures from Earthquake Protection System Inc.).

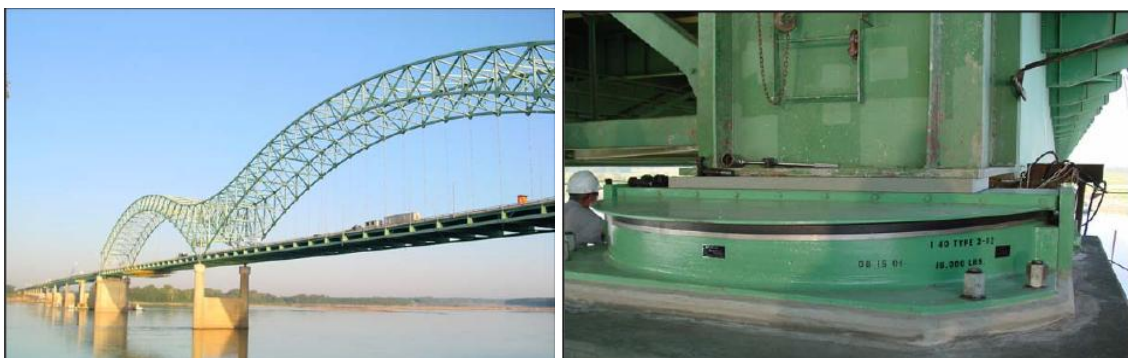


Figure 9. Mississippi Rr. Bridge (left) and Spherical Sliding Isolation Bearing of Mississippi Rr. Bridge (right)

In the last few years the double friction pendulum system has been proposed and validated (Constantinou, 2004). It is a combination of two friction pendulum systems and sliding is

possible on both the surface, the bottom first and then the top one. When the maximum displacement on the first plate has been reached the top surface starts sliding and as results the isolator can displace of a total distance of $2d$ (Christopoulos).

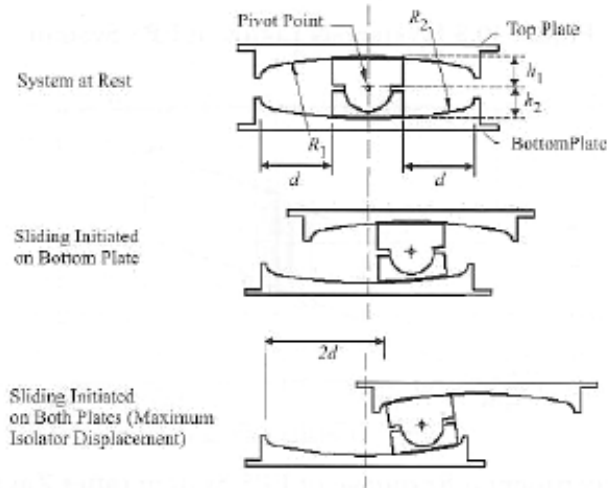


Figure 10. Mechanism of Double Friction Pendulum System (Constantinou et al. 2004)

In order to reduce the deformations of the isolators, supplemental damping systems can be provided. The system is so comprised of two main components:

- A kind of isolator like a base isolator device or a sliding spherical bearings installed between the foundation and the structure in the case of building and between the deck and the piers in the case of bridges
- A supplemental damping mechanism that dissipate the energy reducing the force transmitted to the isolators, and so their deformations, and to the structure.

The different possibility for dissipate energy are presented in the next paragraph.

1.1 Dissipater devices

The dissipater devices can absorb the energy due to an earthquake in order to reduce the energy that the building has to dissipate and limiting so the damages.

These devices can be combined with base isolation or placed elsewhere in the building. Retrofitting existing building is easier with dissipater devices instead of base isolators especially if the application is external.

There are different types of dampers used to mitigate the seismic effect like the hysteretic dissipation, the visco-elastic dissipation, the friction dissipation and the tuned mass dampers.

1.1.1 The hysteretic dampers

The *hysteretic dampers* are made of metal parts and the energy is absorbed by yielding deformation of critical metallic components. In this group there are the metallic dampers that take advantage of the hysteretic behavior of metal in the post elastic range to dissipate energy and the friction dampers that dissipate the energy by friction that develops at interface between two sliding solid bodies.

The metallic dampers are designed to yield in bending or in tension or compression. For this reason they are made of different shapes whose plasticization determines their mechanical characteristics.

A typical application of the yielding dampers and the hysteresis loop are shown below.

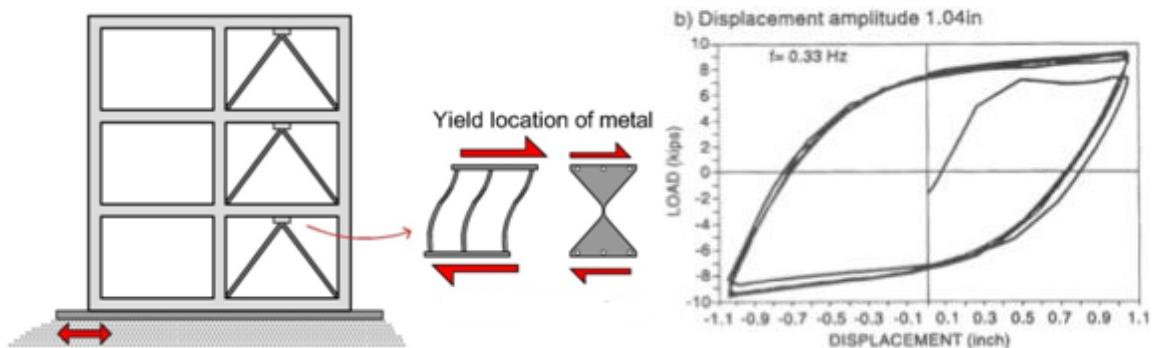


Figure 11. Typical application of yielding dampers (left); Hysteresis Loop of Hysteretic Dampers (right)

Some examples are shown in the pictures below (images from FIP Industriale SpA).



Figure 12. Pin shaped damper (left); Crescent moon shaped damper; Butterfly shaped damper

For dissipate this kind of dissipaters have to go over the activation mark so they start working only after that a certain displacement has been reached. For this reason they are called displacement activated dampers.

When the hysteretic dampers are used it's important to protect to the low cycle fatigue in order to prevent the crisis of the material after a low number of cycles. For this reason the mild steel is commonly used because of its property to resist to big deformations and also for its low price.

In the group of hysteretic dampers there are also the friction dampers that dissipate energy with the friction between two surfaces. The friction is due to unevenness of surfaces. During the sliding of the two close surfaces are subjected to elastic, elasto-plastic and visco-elastic deformation.

Usually the friction damper devices consist of several steel plates sliding against each other in opposite direction.

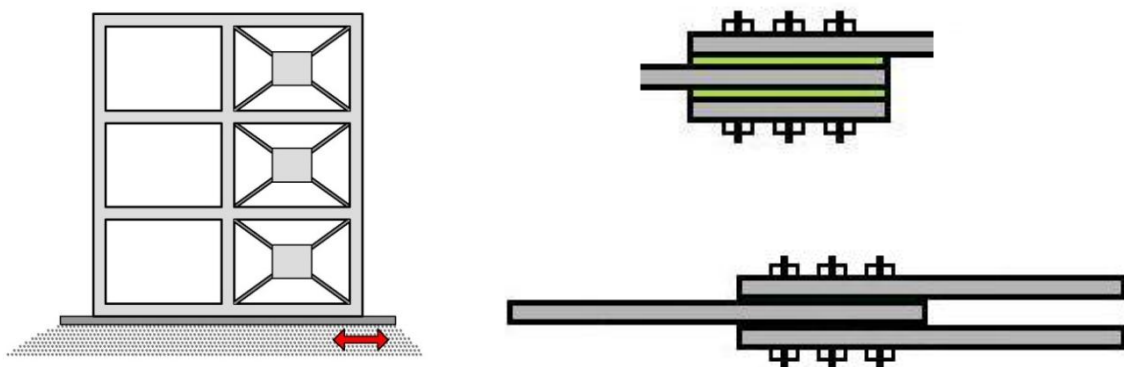


Figure 13. Typical Application of Friction Dampers (left); possible arrangements of Steel Plates in Friction Dampers [3]

The simplest form of friction dampers are the slotted bolt connection at the end of bracing members.

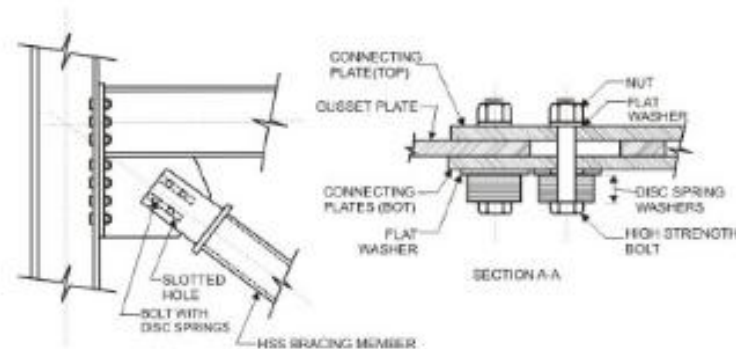


Figure 14. Slotted Bolt Connection [4]

The buckling restrained braces (BRB) are hysteretic dampers that dissipate energy when subjected to compression-tension cycles in such a way that the damper can yield in both axial tension and compression under reverse cyclic load. The BRB are formed of a steel core restrained by steel casing filled with mortar that prevent the buckling of the structure and then a steel casing.

The steel core carries the axial the axial load while the outer tube provides lateral support to the core and prevents global buckling.

Between the confining material and the tube there may be a separation material in order to avoid the transfer of tangential strains between the two materials. The components of the BRB are shown in the drawing below.

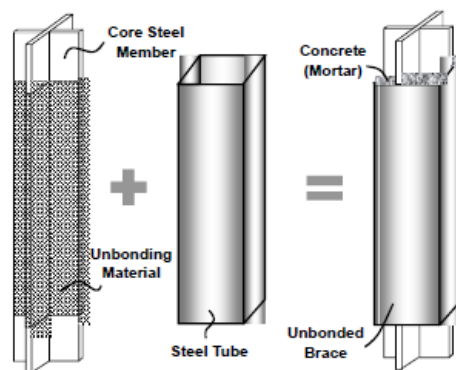


Figure 15. Components of BRB (left); Example of BRB of the Tzu-Chi Culture Building (Taipei, Taiwan) [5]

The advantage of the buckling restrained braces over the conventional brace is in their ability to carry load, yield and so dissipate energy in both tension and compression. In contrast, conventional brace dissipate when they reach the inelastic yielding in tension while they buckle without dissipating a substantial amount of energy in compression.

1.1.2 The Viscous and Viscoelastic Dampers

The viscous and viscoelastic material are used in Civil Engineering structures only since 1969 when over 10000 viscoelastic dampers were installed in each of the twin towers of the World trade center in New York. The purpose was to reduce the vibration caused by the wind.

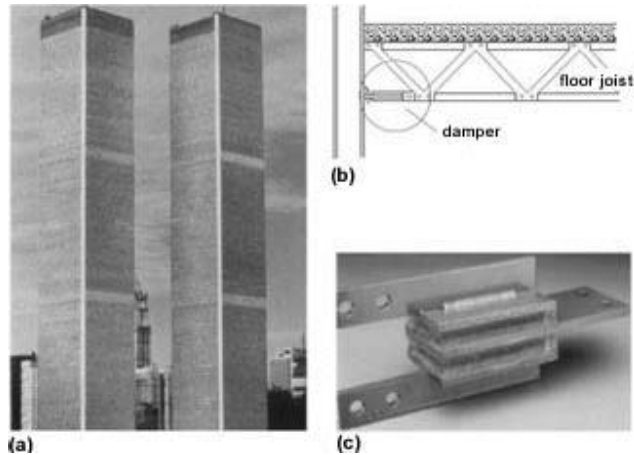


Figure 16. The World Trade Center, fitted with dampers (left); Placement (top right); Damper (bottom right) (<http://accessscience.com/content/Smart-structures-and-materials/YB001370>)

The *viscous dampers* provide only a velocity dependent force while *viscoelastic dampers* provide both a velocity dependant force and a displacement dependent restoring force. The typical hysteresis loops are shown in the graphs below.

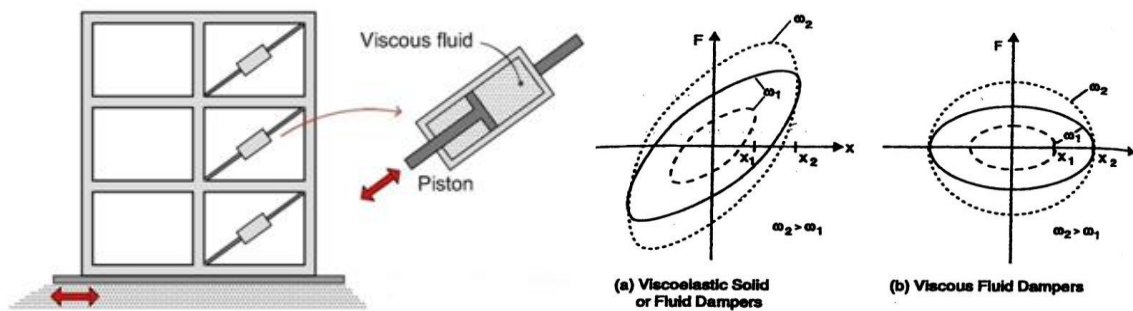


Figure 17. Example of Application of a Viscous Damping Device (left); Hysteresis Loop of a Viscous Damping Device (right) [3]

The viscoelastic dampers are often incorporated in bracing members and they dissipate through shear deformations.

In this category there are the solid viscous dampers, the fluid dampers or fluid viscous dampers if the liquid is viscous. The fluid viscous dampers consist of a stainless steel piston with bronze orifice head. The piston heads utilizes specially shaped passages which alter the flow of the damper fluid and thus alter the resistance characteristics of the damper.

The benefit of these kinds of dissipater devices is that they are always active so they don't need to go over an activation mark to work as the hysteretic dampers.

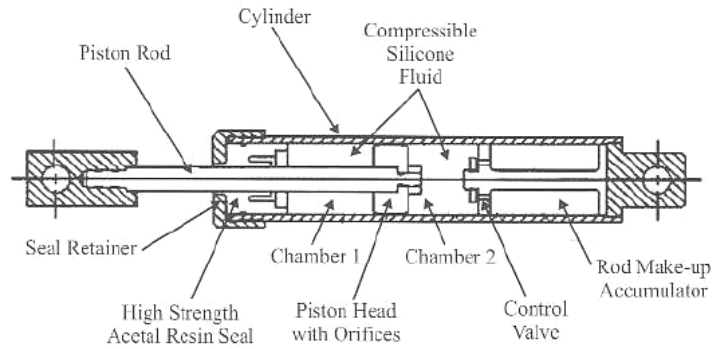


Figure 18. Viscous fluid device [1]

A structural implementation of this kind of dissipation device is the Viscous Wall Dampers that consist of an outer steel box filled with viscous fluid with an inner plate dipped in it. The inner plate is fixed to the upper floor while the outer plate is fixed to the lower floor. The relative displacements of the plates provide energy dissipation.

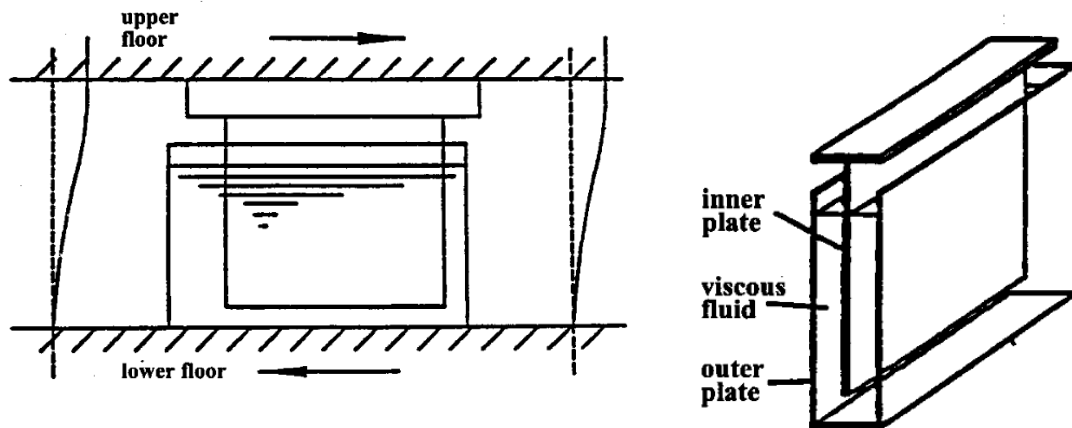


Figure 19. Viscous Damping Wall [6]

1.1.3 Tuned Mass Dampers

The tuned mass dampers (TMD) or vibration absorbers are mass spring systems that are calibrated to be in resonance with a particular mode of the structure on which they are installed. As the viscous dampers they have been used in order to reduce the wind vibrations and only recently for the seismic protection of buildings.

To the main structure that is characterized by its mass, damping and stiffness is coupled a secondary structure that is at the same time characterized by its mass, damping and stiffness.

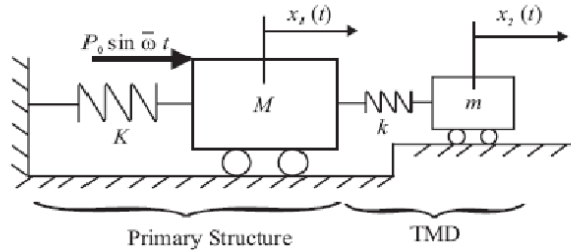


Figure 20. Main Structure and TMD [1]

The TMD has its own frequency and resonance and so it's possible to obtain not the attenuation of all the resonances of the structure but of only one. The TMD can be designed for whichever frequency and so can control whichever mode but usually it is designed to control the first mode that represent the weakest configuration.

The construction of a tuned mass damper is simple because only requires the assembly of a mass, a spring and a viscous damper at a given point of the structure but a relatively large mass is needed and consequently a large space of installation. The weight of this structure obviously will influence the design and has to be considered. Usually the mass undergo large relative displacements and requires large clearances. The mass is usually mad of lead, steel or concrete. Then the friction between TMD and the surface has to be minimized so that the system can work also for small accelerations.

Some of the highest building of the world used the Tuned Mass Dampers as dissipator devices like the Taipei 101 (Taipei, Taiwan) and the Shanghai World Financial Center (Shangai, China). The Taipei 101 has the biggest tuned mass damper and it's made of steel.



Figure 21. The Taipei 101, Taiwan (left); the Tuned Mass Damper (right)
http://en.wikipedia.org/wiki/File:Taipei_101_Tuned_Mass_Damper_2010.jpg

The mass is 660 ton of weight, it's located at 380 m height and it is hanged with long cables in order to realize a pendulum of five storeis high; 8 dissipator elements connect the mass to the structure below. It has been realized in loco because it was too heavy to be carried in the right position.

The dissipator elements can minimize the movements of the building up to the 40%.

Another example of building using the Tuned Mass Damper is the Canadian National Tower in Toronto, Canada (503 m). In this building the TMD have been used to control the second and fourth vibration modes; this means that the system can be used to control whichever mode as previously explained.

There are then several cases of TMD that have been realized without adding additional mass on the structure. Some structures like the Rokko-Island P&G Building (Kobe), Crystal Tower (Osaka), Sea Hawk Hotel & Resort (Fukuoka) use water or ice tanks.

1.2 References

1. Christopoulos, C.a.F., A., *Principle of Passive Supplemental Damping and Seismic Isolation*, ed. I. PRESS. 2006, Pavia.
2. SEAOC, *Vision 2000 Committee, Performance Based Seismic Engineering*. 1995
3. Buchanan, A., et al., *Base Isolation and Damage-Resistant Technologies for Improved Seismic Performance of Buildings 2011: Christchurch*.
4. Tremblay, R.S.S.F., *Energy dissipation through friction bolted connections in concentrically braced steel frames*, in *Seminar on Seismic Isolation, passive energy dissipation and active control*. 1993.
5. Lai, J.-W. and K.-C. Tsai, *Research and Application of Buckling Restrained Braces in Taiwan* 2004
6. Symans, M.D.C., M.C., *Passive fluid viscous damping systems for seismic energy dissipation*. *Journal of Earthquake Technology*, 1998
7. Dowrick, D.J., ed. *Earthquake Resistant Design*. ed. J.W. Sons. 1988: Chichester, UK.
8. Skinner, R.I., T.E. Kelly, and W.H. Robinson, eds. *Seismic Isolation for Designers and Structural Engineers*. ed. R.S.L.a.H.C. Group. 2000: Wellington.
9. Symans, M.D. and M.C. Constantinou, *Passive Fluid Viscous Damping Systems for Seismic Energy Dissipation*. *ISET Journal of Earthquake Technology*, 1995. 35: p. 22.

2. New Forms of Damage Resistant Structure

The increasing levels of expectations of buildings concerning their behavior during an earthquake have lead to a major effort toward the development of damage control design approaches and technologies. The current approach supposes that the structure remains elastic or develop a mechanism involving ductile inelastic deformations while maintaining a stable global response and avoiding loss of life.

The aims of the new target are to provide low cost, more affordable, high seismic performance structures capable to sustain a design level earthquake with limited or negligible damage. Generally the cost of repairing damages and considering also the cost of the loss of business operation during a moderately strong earthquake is comparable to the cost of the structure itself.

For this reason the last target of Earthquake Engineer is to expect building to survive to a moderately strong earthquake without no disturbance to business operation.

An overview of the recent developments of damage control self centering structure are presented in the following paragraphs.

2.1 Controlled Rocking of Self Centering Systems

An optimal earthquake resistant system should limit the transfer of seismic forces to the building and provide additional damping and in order to reduce the cost of repair of the building, to reduce or eliminate the residual deformation of the post-earthquake. Most of the structure designed according to the codes will sustain residual deformations that can result in partial or total loss of a building.

Allowing the movement of the structural elements, a self centering system provides an amount of energy dissipation with a controlled rocking. In the ancient Greek and Roman temples that

were constructed with blocks of stones, a rocking behavior was displayed. The structural elements resist to the lateral loads thanks to their own weight (they were approximately 0.6 to 1 m height) and to the friction between the elements themselves. The self weight of the columns provides the necessary amount of pre compression and so during an earthquake the elements separate at the junctions producing a rocking behavior.



Figure 22. Earlier implementation of a self-centering limited-damage rocking system, for earthquake loading (Dionysus temple in Athen [2])

A modern application of a self centering system will include the characteristics of yielding or hysteretically damping structures but also self centering properties that allow the system to come back to the original position after an earthquake limiting so the residual displacements.

The introduction of connection that re center using unbounded post tensioned cables combined with energy dissipation represents one of the last developments of controlled rocking.

This technology was developed in the 1990s from the PRESSS Program (PREcast Seismic Structural System) coordinated by the University of California, San Diego. The primary aim of the program was to develop innovative seismic resistant solutions for precast concrete building to replace the cast in situ concrete. The demand is achieved by the allowed movement of the structural elements through the opening and closing of an existing gap in order to obtain the rocking motion without the formation of a plastic hinge region [3].

The PRESSS Program has developed four main types of connection:

- The hybrid connection that utilize post tensioned cables in a central position and running in a duct that provide the re centering effects and mild steel dissipaters in correspondence of the bottom and the top of the beam grouted in the external parts.
- Pre tension frame connection where continuous partially bonded pretension beams are connected to the column and no additional mild steel reinforcement was provided across the beam column interface.
- TCY gap connection that is characterized by post tensioned cables in the center of the beam and mild steel dissipaters on the top and on the bottom and a gap between the beam and a column is left. The opening on the top and the closing of the bottom of the gap keep the frame of the same length even as the connection yield.
- TCY connection that uses mild steel reinforcing bars in grout ducts at the top and the bottom of the connection.

The PRESSS program is based on the design of two prototypes five storey precast buildings of 30 x 61.5 in plan and 3.81m heights. Both buildings use frames and shear walls to resist lateral load in the longitudinal and transversal direction respectively.

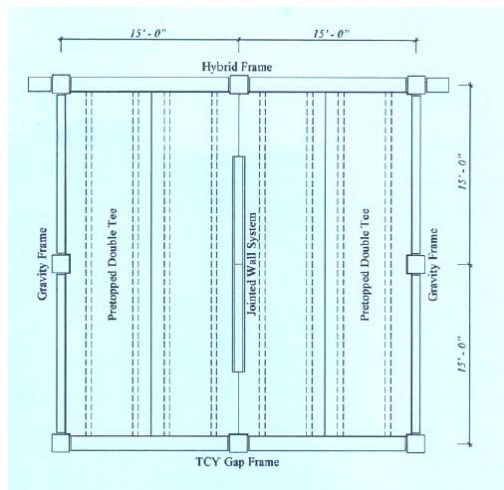


Figure 23. Test Building - Level 1 floor plan [3]

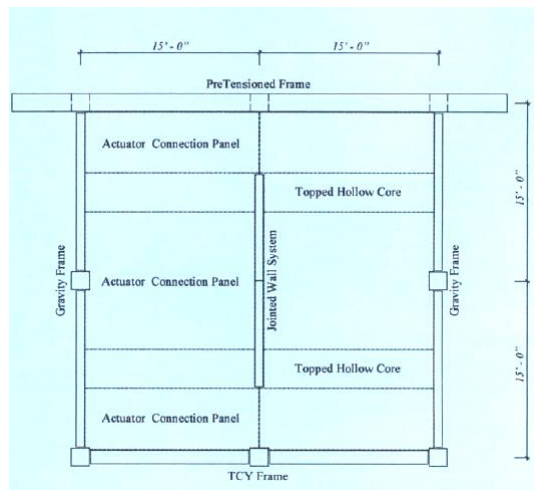


Figure 24. Test Building - Level 4 floor plan [3]

In the design of the test building there are so many combinations of systems included. The four different types of ductile connection systems used in the PRESSS building are shown in the pictures below.

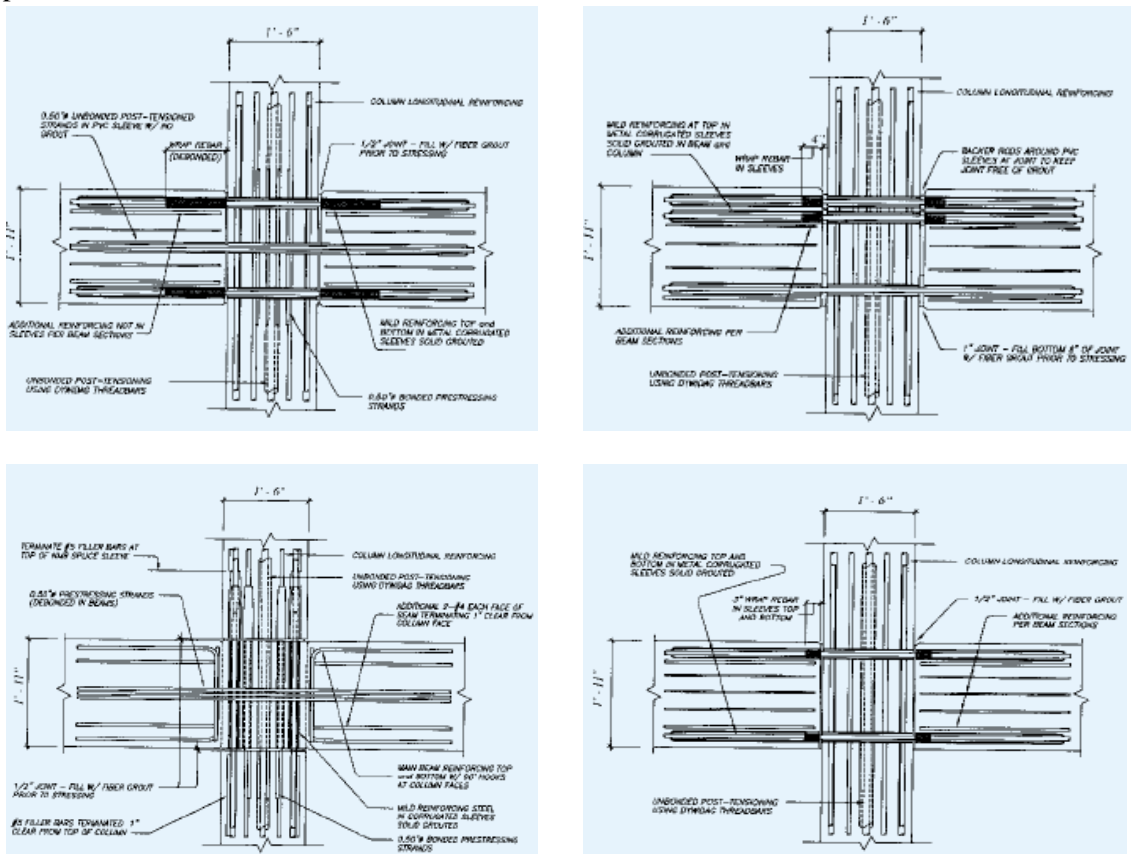


Figure 25. Hybrid Post Tensioned Connection (top left); TCV Gap Connection (top right); Hybrid Post Tensioned Connection (bottom left); TCV Connection (bottom right) [3]

Due to the limitations on the building size because of the dimensions of the laboratory, only one jointed wall system is incorporated in the test building. The walls are jointed with U-shaped flexural plates used as dissipator devices. Unbonded post tensioned cables are design to re-center the walls when the load is removed so that there is no residual displacement.

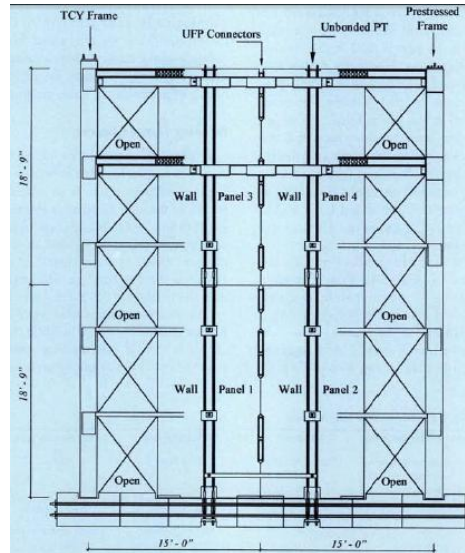


Figure 26. Elevation of jointed shear wall system

The building was tested with pseudo dynamic method under several different earthquakes ground motions. Under the largest motion the wall has reached a peak drift of 2.9%, yet returned to only 0.055% drift at the end of the motion. The structure would have been ready to the immediate occupancy after the earthquake.

An evolution of this system, “*the hybrid system*” [4], was then suggested and in this case the post tensioned cables were combined with energy dissipators designed to provide supplemental damping to the rocking system.

2.2 The Hybrid System: Concept, Mechanism and Design

The “*Hybrid system*” is a re centering solution that combines unbonded post tensioned cables to dissipater devices. The structure is so allowed to have relative displacements through a rocking motion. This solution can be achieved with different structural configurations like the beam column joint, the rock to foundation joint, segments of column rocking on each other,..

The hybrid system has been developed for concrete structures and then also timber and steel structures.

The post-tensioned cables work re-centering the structure while remaining elastic during the rocking movement and the mild steel bars act as energy dissipater and the peculiar dissipative-recentering hysteresis loop is shown in the drawing below. Depending on the moment

contribution ratio between self centering a wide range of hybrid solutions with different flag shapes can be obtained.

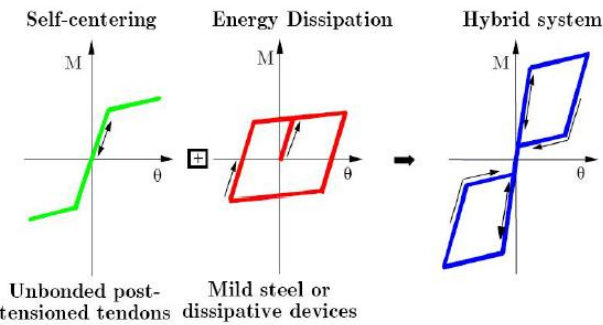


Figure 27. Idealized Flag Shape Hysteresis Loop (left) and ..(right)

The hybrid connection has the properties of both self centering and energy dissipation; by combining the moment contribution from the energy dissipators and the post tensioning, the hybrid flag shape is obtained.

The design parameter λ is the ratio between the moment contribution provided by the mild steel M_s and the total moment contribution M_t . For example a full recentering condition means that the cables are able to close the gap at each cycle. Usually a ratio of 40:60 for dissipation and recentering respectively is used.

For the analysis of the Hybrid Connection a member compatibility is applied, the Monolithic Beam Analogy [5]. The common presence of unbounded tendons violates the strain compatibility in the section and so a member compatibility condition is introduced. The relationship between the neutral axis position and the strain in the concrete is defined introducing an analogy between the precast connection and the monolithic one.

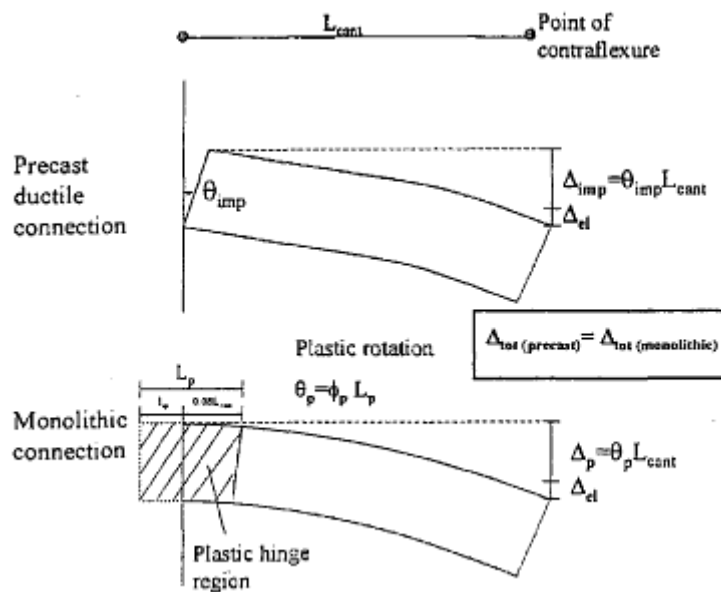


Figure 28. Monolithic Beam Analogy [5]

Assuming that the two beams are identically in terms of geometry, the elastic deformations would be the same and the plastic deformations can be equated.

$$\Delta_{tot,precast} = \Delta_{tot,monolithic} \quad (0.1)$$

$$\Delta_{imp} + \Delta_e = \Delta_p + \Delta_e \quad (0.2)$$

$$\Delta_{imp} = \Delta_e \quad (0.3)$$

Utilising the ultimate and yielding curvature and substituting in the equations, the value of strain is obtained as a function of the neutral axis position.

$$\varepsilon = f(c) \quad (0.4)$$

The procedure has been implemented by [6].

The initial analogy does not distinguish between the elastic and plastic phase of concrete. The extension of the analogy divides the member compatibility condition into three distinct ranges of the deflection: zero to decompression, decompression to yield, yield to ultimate.

In the case of LVL only the two first ranges are considered due to the linear stress strain-relationship.

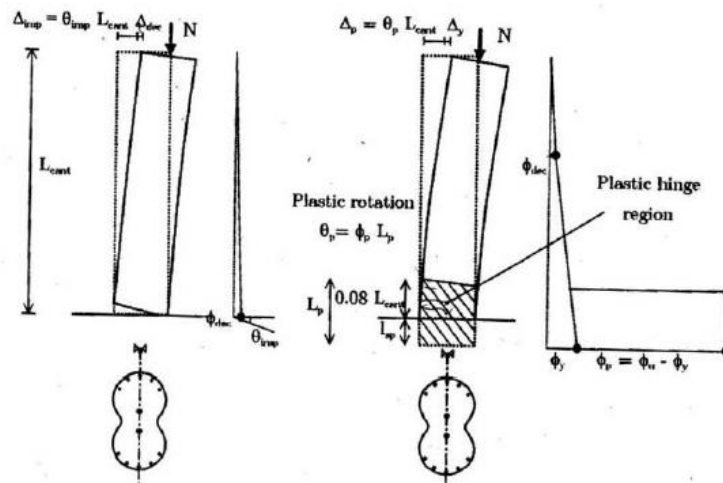


Figure 29. Extended Monolithic Beam Analogy [1]

The different steps of the procedure are summarized below.

The first step of the procedure is to fix beam end rotation.

Then as second step the depth of neutral axis has to be guessed so that it's possible to evaluate the strain in the unbounded post tensioned tendon and in the mild steel.

Post tensioning steel

$$\varepsilon_{pt} = \frac{n\Delta_{pt}}{L_{ub}} \quad (0.5)$$

Where:

n= number of total gap opening

Δ_{pt} is the elongation of the tendon

L_{ub} is the unbonded length.

$$\Delta_{pt} = \vartheta * \left(\frac{L}{2} - c \right) \quad (0.6)$$

Substituting the equation 2.2.6 in the equation 2.2.5:

$$\varepsilon_{pt} = \frac{n*\vartheta*(L/2-c)}{L_{ub}} \quad (0.7)$$

Mild steel

The displacement on the bar of mild steel due to the gap opening is:

$$\Delta_{si} = \vartheta * (d - c) \quad (0.8)$$

And the strain can be evaluated depending on the type of dissipater elements.

1) *Internal epoxied bars*

$$\varepsilon_{si} = \frac{\Delta_{si}}{2L_{si} + L_{ubi}} \quad (0.9)$$

Where:

L_{si} is the strain penetration length

L_{ubi} is the unbounded length of the bar.

2) *Fuse and bonded bars*

$$\left\{ \begin{array}{l} \varepsilon_{si} = \frac{\Delta_{si}}{\frac{A_{fuse}}{A_{bond}} * 2L_{si} + L_{ubi}} \quad \varepsilon_{si} < \varepsilon_y \\ \varepsilon_{si} = \frac{\Delta_{si} - \frac{A_{fuse}}{A_{bond}} * 2L_{si}}{L_{ubi}} \quad \varepsilon_{si} > \varepsilon_y \end{array} \right.$$

3) *External dissipator*

The strain of the external dissipator is calculated as:

$$\epsilon_{se} = \frac{\Delta_{sl}}{L_{ubi}} \quad (0.10)$$

Going on describing the procedure, the value of ϵ_t has to be defined. Two equations are required to solve the two unknown values (neutral axis depth and the strain in the timber). Section analysis and member compatibility conditions (the monolithic beam analogy), assuming so that a precast connection and a monolithic one are compatible, are used.

$$\epsilon_{t,max} = \left(\frac{3\theta_{imp}}{L_{cant}} + \phi_{dec} \right) * C \quad (0.11)$$

L_{cant} is the contraflexure length and ϕ_{dec} is the decompression curvature.

The next step is to evaluate the compressive force in the timber, the forces in the dissipater devices and the force in the tendon. After having verified the section equilibrium and the neutral axis position with an iterative method until convergence, the moment capacity can be obtained.

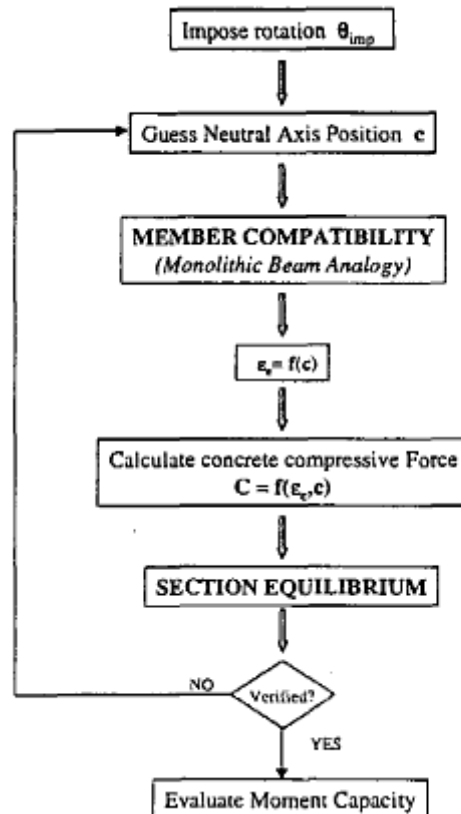


Figure 30. Schematic flow chart of the moment-rotation procedure [5]

2.3 Self Centering Resisting Systems

The self centering system is similar to the rocking concept combined with energy dissipation device.

Self centering system incorporates the non linear characteristics of yielding structures by using dissipater elements and has self centering properties allowing the structural system to return to its original position. The cumulative damage is so eliminated or at least reduced. Figure 31 illustrates the behavior of a self centering system.

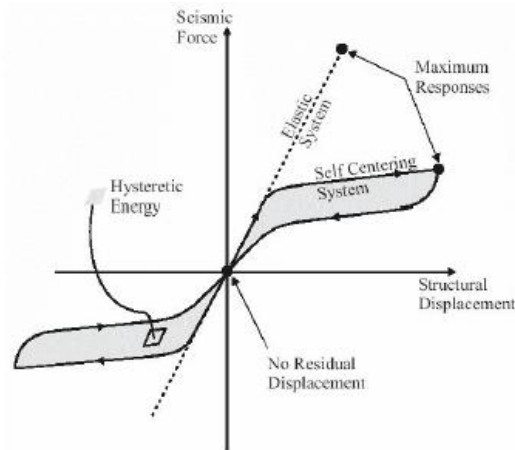


Figure 31. Idealized Seismic Response of Yielding Structure [7]

One of the first applications of the self centering system is the Rangitikei Railway Bridge in New Zealand that has been in operation since 1981. The bridge is 70 m tall and 315 m long. There are base isolation and torsional-beam dampers that limit the amount of rocking. Then the weight of the bridge allows the re-centering of the structure.

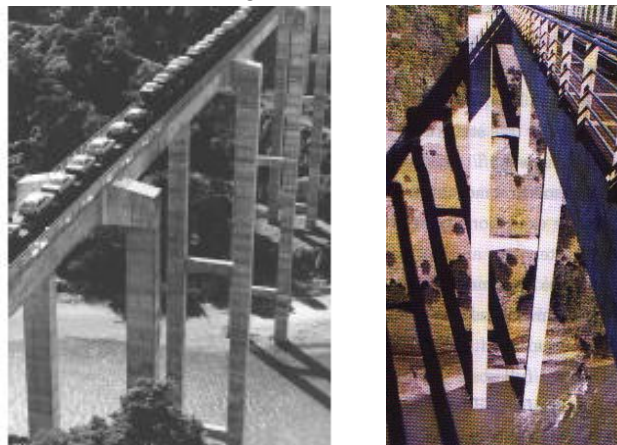


Figure 32. Rangitikei Railway Bridge [7] [8]

2.3.1 Self-Centering Systems for Concrete Structures

The hybrid system has firstly been developed on concrete on precast beam column subassembly where mild steel dissipators were coupled to post tensioned cables (Figure 33) [2]. The similar concept was used by Stanton and Nakaky in the development of post tensioned rocking wall system (Figure 33).

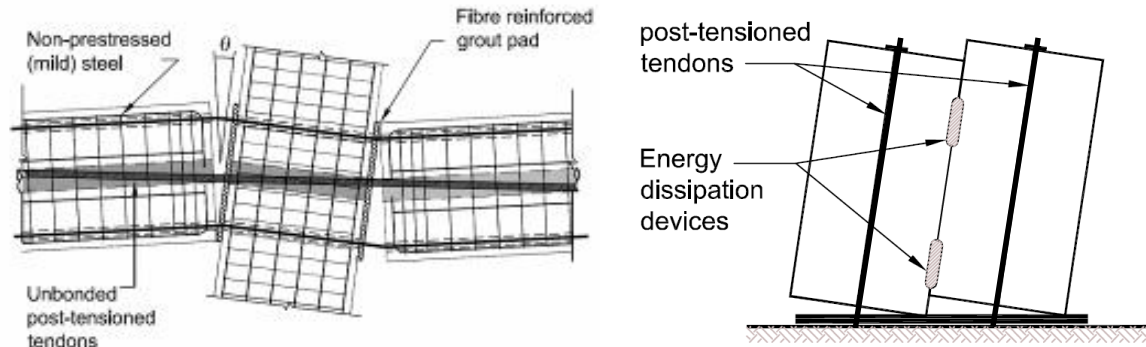


Figure 33. Jointed precast hybrid frame and wall systems developed in the PRESS-Program [2]

In a monolithic wall solution a plastic hinge region is formed at the base of the wall and the damage is concentrated there while in a precast rocking wall the only negligible deformations are achieved. The results from a non linear dynamic analysis show that the response of the precast hybrid wall is almost the same than the monolithic solution.

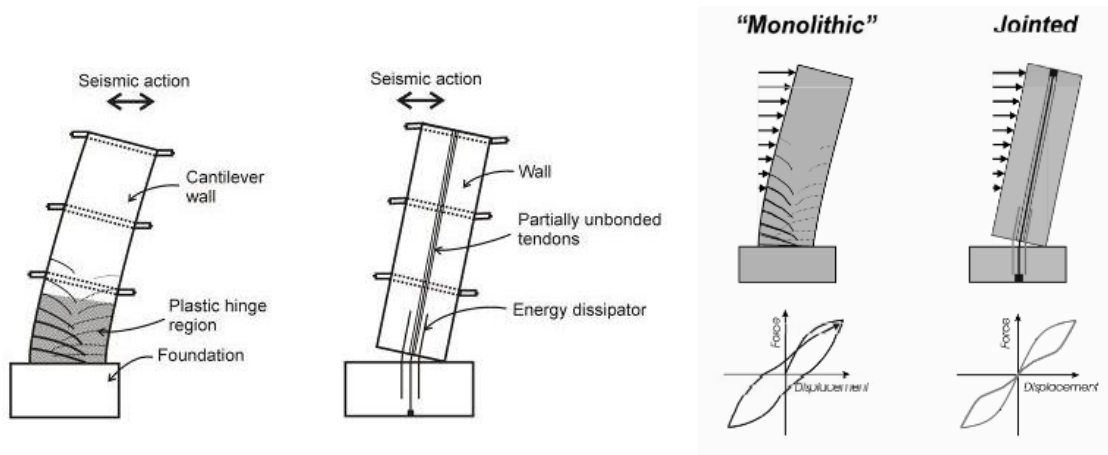


Figure 34. Comparison of monolithic wall and precast rocking wall [2]

2.3.2 Self-Centering Systems For Steel Structures

The PRESSS technology developed for concrete structures has also been extended to steel structures. The technology involves pre-stressing/post-tensioning prefabricated beams to the column face. During an earthquake the gap opens and the post tensioned tendons extends supplying additional force to close the gap. When the gap opens the beam rotate on the beam column contact point generating increase rotation. Different kinds of dissipaters have been used like the angles (Ricles et al.), high strength bars (Christopoulos), friction devices [9]. The connection proposed by Ricles consist of high strength steel cables that run all along the beam and are anchored outside the column frame.

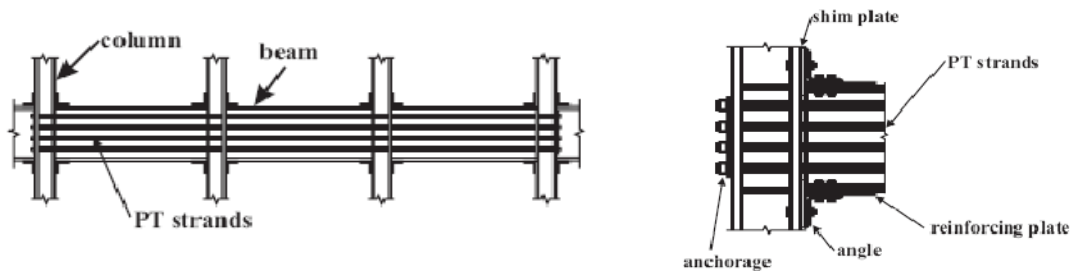


Figure 35. Hybrid Post Tensioned Connection for Steel Frames [10]

On the bottom and the top of the beam are bolted angles that dissipate the incoming energy yielding. The angles are outside and so after an earthquake it's easy to replace them that are the only sacrificial element.

The solution proposed later by Christopoulos consist of post tensioned tendons located at mid span and energy dissipation bars. In order to avoid the buckling the bars are inserted in steel sleeves that are welded to the beam flange for exterior connections and to the column plates for interior connections.

More recently Kim has suggested a post tensioned self centering friction damped steel moment resisting connections.

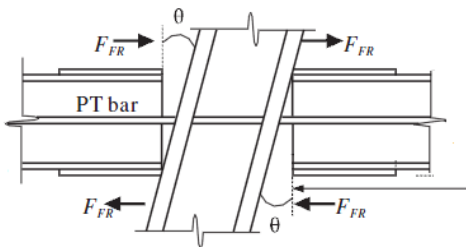


Figure 36. Steel Moment Resisting Connection [9]

The post tensioning bars are anchored outside the faces of the exterior columns and friction devices are used are dissipater elements on the top and bottom of the beam flanges.

2.3.3 Self-Centering Systems for Timber Structures

The self centering technology has also been extended to timber structures, both frame and wall systems, after the development of laminated veneer lumber (LVL) as an alternative to solid timber or glue laminated timber. The advantages using timber as the structural element is that it is lighter than steel and concrete and for this reason it's possible to design building for rapid construction and with more economic foundations. Consequently the operations of dismantling and re-assembly are easier compared to concrete and steel constructions. As a natural element timber has problem of durability in particular if exposed to humid conditions and the acoustic performance are not as good as concrete and this is why often a floor system using timber as a structural element and concrete topping is use (also to increase the thermal mass and provide a rigid diaphragm of lateral forces).

The use of post tension in timber has been developed at the University of Canterbury, Christchurch (New Zealand) following the example of the U.S. PRESSS coordinated by the University of California, San Diego which has proposed important post tension technology applied to the concrete.

The post tension in timber is conceptually identical to the post tension in concrete. The material used is the Laminated Veneer Lumber (LVL) which is obtained peeling logs into 3 mm veneers and gluing into billets of 1.2 m and thickness from 40 mm to 100 mm. The wood is usually stressed parallel to the grain and the pre-stressing loads are almost the same because the compressive strength of the LVL is similar to the concrete one (from 30 to 40 MPa).

The technology has been proposed by Palermo et al. (2005) and validated by experimental tests carried out at the University of Canterbury (Christchurch, NZ).

Laminated Veneer Lumber is safer than sawn timber or glulam because the thick veneers are selected and the defects are randomized to a point that the influence on the material properties can be assumed negligible. LVL members have high strength because of their higher homogeneity.

Unbonded post tension cables and dissipater elements provide to the structure the damping and self centering characteristics and so the system is subjected to a controlled rocking motion.

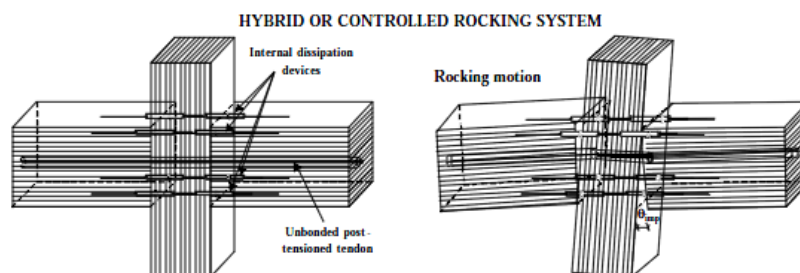


Figure 37. Application of Hybrid Concept to LVL frame system [11]

When has started, the research has investigated beam-column joint, wall to foundation joint and column to foundation joint considering different variable like considering only unbonded post tension cables only or coupling them with dissipator elements internal or external with different behavior.

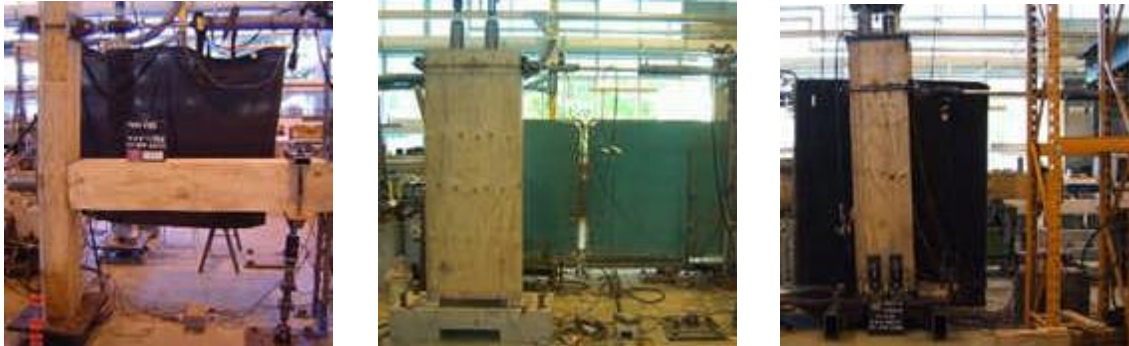


Figure 38. Examples of beam-column joint, wall to foundation joint and column to foundation joint [12]

2.3.4 Self Centering Systems for Bridge Structures

One of the first applications of the self centering concept concern bridges as already mentioned speaking about the Rangitikei River Bridge in New Zealand. The development of the hybrid systems in building is then extended also to bridges as an efficient solution for an improved seismic performance compared with the monolithic counterparts. The first example was proposed by Mander and Chen and post tensioned cable was combined with viscous dissipators. Then similarly to the solutions used for building mild steel dissipator elements have been used at the critical section of the piers as shown in the figure below where a comparison with the monolithic case is presented [13]

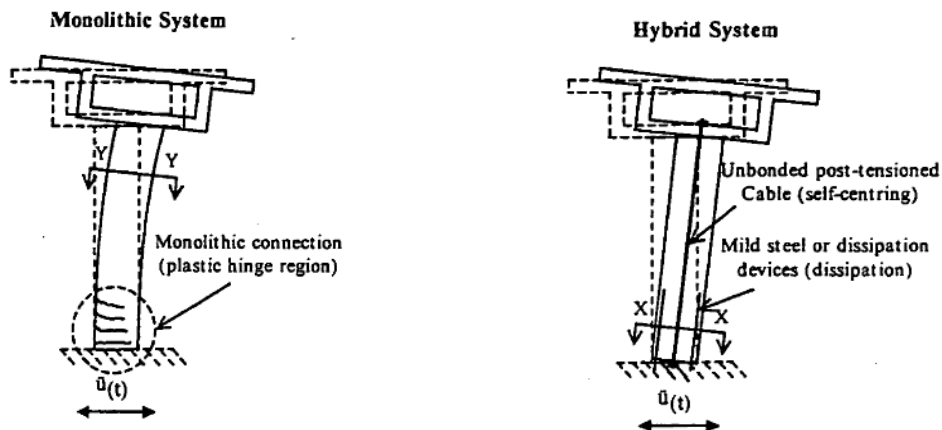


Figure 39. Controlled Rocking concept of bridge piers (Palermo, 2005)

2.4 Technological Solutions for Post Tensioned Walls

Rocking walls have many positive features from a seismic point of views; the most important is the capacity to sustain large lateral displacements without damage. The most negative feature, instead, is the low energy dissipation capacity.

The previous discussion has highlighted the possibility of the use of the hybrid system in the three main structural materials such as concrete, steel and timber. The following pages focus the attention to the technological solutions for post tensioned walls paying attention to all the dissipator systems that have been used.

The hybrid system has been proposed by [4] for a precast frame and then the same concept has been proposed by Stanton and Nakaki (2002) for a rocking wall system.

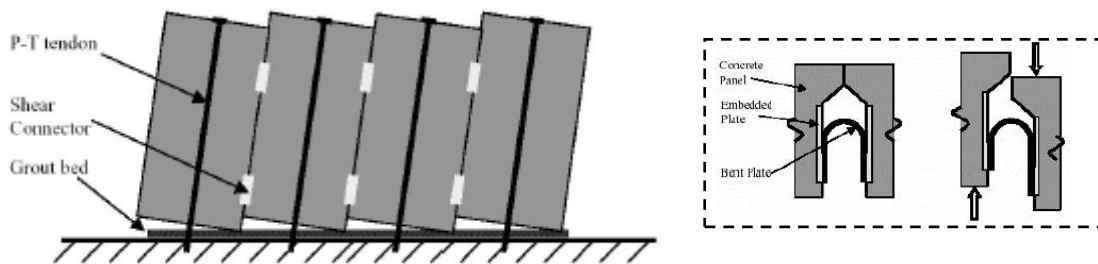


Figure 40. (a) Post Tensioned Rocking Wall System, (b) Detail of U shaped dissipators [7]

The panels are split to allow the rocking of the single walls about their base. The weight of the walls provide the re centering of the structure and, if necessary, post tensioned cables can be installed. In this system the dissipator devices are grouting reinforced bars inserted in vertical ducts at the edges of the wall and they are so able to dissipate in both compression and tension. An alternative to this system are ductile shear connections between the wall panels which deform cyclically in shear as the walls rock back and forth.

The U shaped rolling stainless steel plates have been studied and tested in PRESSS Phase II and then used for energy dissipation to couple the walls of the prototype buildings (Phase III).

A wall with supplemental passive energy dissipation system as then been proposed by [14]. Linear fluid dampers are used in brace elements and are located diagonally in plane with the wall.

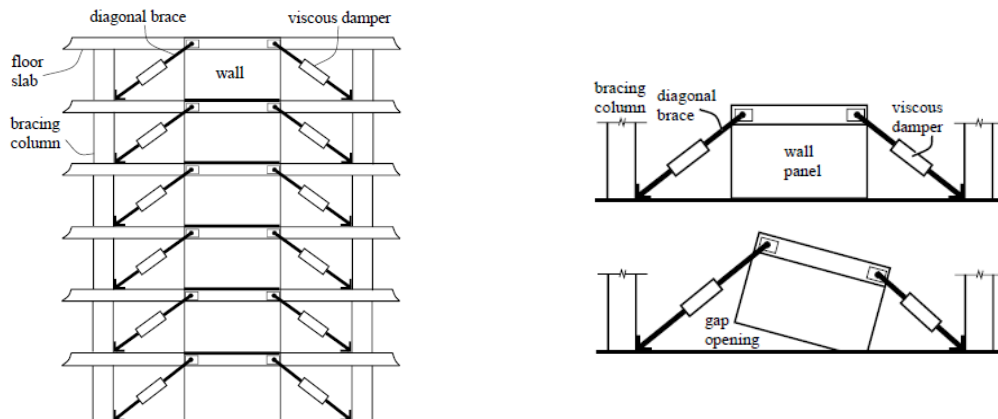


Figure 41. Wall with Supplemental Viscous Damping [14]

The brace is anchored to the wall at one end and to a column on the other end. The braces are designed to displace laterally when the gap opening occurs along the horizontal joints. The results have shown that a displacement of up to 4.6 cm can be achieved without significant damage to the wall.

Unbonded post tension precast concrete walls have also been connected with vertical joint [15] that consist of steel components that provide vertical shear force transfer between the wall panel and provide energy dissipation under seismic loading. These connectors dissipate by yielding in shear.

The self centering system has then been extended by [16] to reinforced cantilever walls using unbonded tendons and conventional reinforcement as energy dissipators. The unbonded length of the tendons is proportioned to ensure that the limit of proportionality is not reached as a result of the elongation due to the opening of the gap. The mild steel bars are cast in the foundation and then grouted into the wall. The energy dissipation takes place in tension and compression in the milled portion of the bar only. Buckling is avoid thank to the surrounded concrete. A scheme of the wall is shown in the picture below.

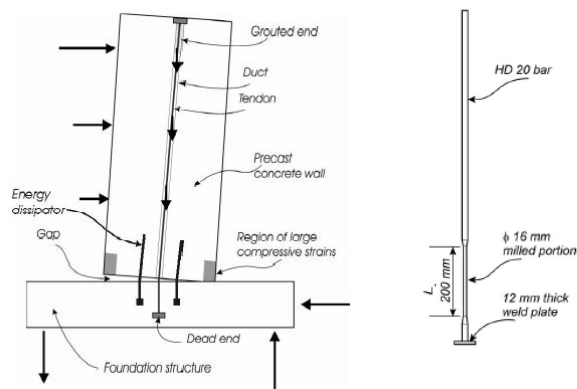


Figure 42. (a) Hybrid Reinforced Concrete Cantilever Wall System, (b) Energy dissipator installed [16]

The opening and closing of the gap implies the formation of a compressive region and this usually requires the use of confinement the enable the concrete to develop such strains without crashing.

This system has been tested at the University of Canterbury (Christchurch, New Zealand). A comparison between the monolithic solution and the hybrid one has highlighted the difference performances of the two walls. The monolithic wall presented residual cracks between 1 mm and 2.2 mm in width after unloading from a cycle to 1%. The buckling of the longitudinal bars has preceded a fracture at 2.5% drift. In the hybrid solution the gap always close when unloading and the structure has been cycled till 4% of drift without damage.

The self centering concept has been extended to other types of reinforced concrete structures with concrete coupled walls and cantilever walls with vertical joints. Kurama and Shen [17] proposed a new type of hybrid coupled wall system that use unbonded post tensioning to couple the walls without embedding the beams to the walls. Inside the walls the tendons are placed in ungrouted ducts. In this system it's shown that post tensioned steel beams can provide

significant levels of coupling over large cyclic lateral displacements. The beam-wall connection is realized with top and seat angles bolted to the flanges and a spiral or other reinforcement to confine the concrete. The purpose of the angles is to provide the energy dissipation by yielding.

The drawings of the multistory wall and the beam-wall connection are shown below.

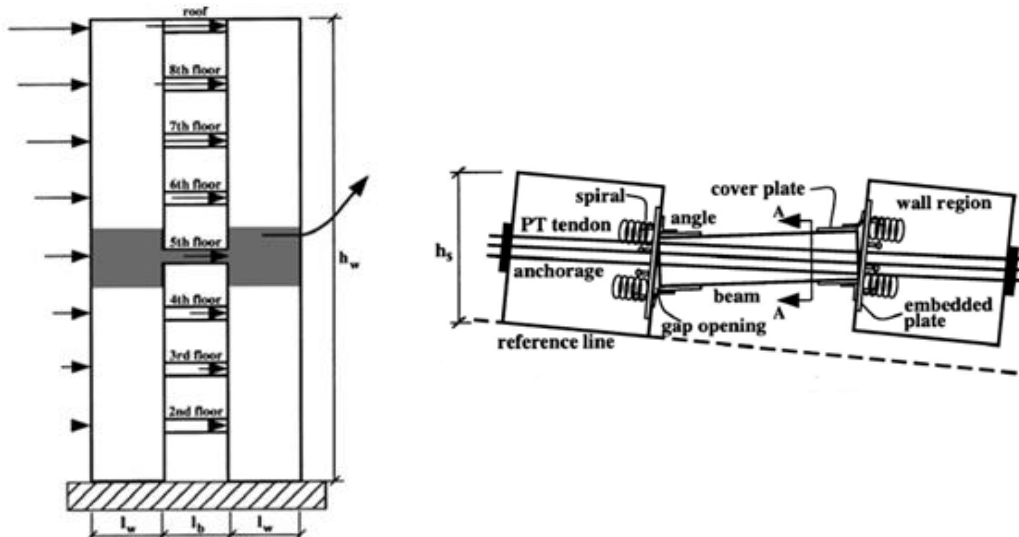


Figure 43. Coupled wall system: a) multistorey wall, b) beam-wall connection [17]

The self centering system has then been extended to confined masonry walls [18]. Confined masonry walls is a traditional method of construction that consist of un reinforced brick masonry panels surrounded by small reinforced concrete beams and columns. Energy dissipation devices are used at the wall's toes and they were designed to yield in bending. One end of the dissipator is fully fixed to the foundation and the other one is connected to the wall through a pin and this allow the device behave like a cantilever.

The shake table test has been carried out at the University of Canterbury and the system has been subjected to sixty dynamic tests. The seismic response was excellent, no cracking has occurred and the maximum residual drift of 0.13% was observed after an excursion of 1.8% drift.

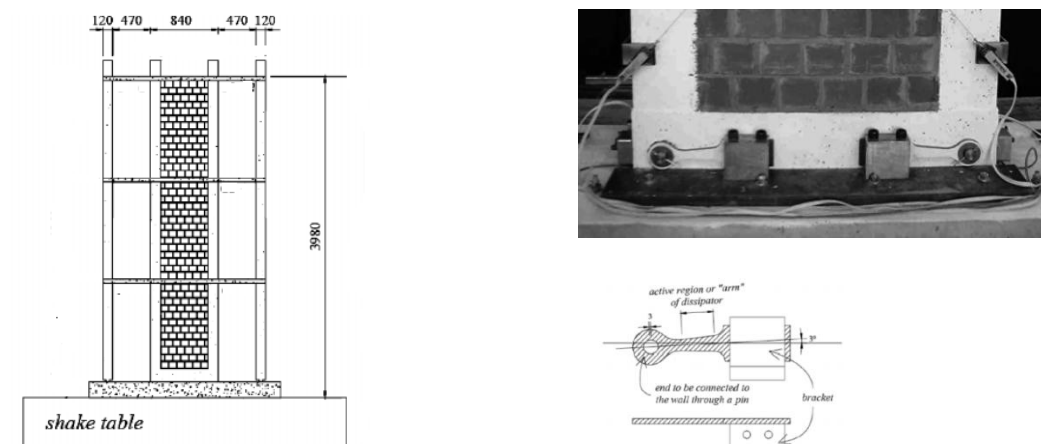


Figure 44. Confined Masonry Rocking Walls: Front view (left) ; view of base of the wall (top right); geometry of hysteretic dissipation device (bottom right) [18]

Following the declared target of no damage structural system and considering the cost associated to the damage of non structural components such as the sacrificial ones, the use of external dissipaters have been proposed [19]. The strong point of these devices called “*Plug and Play*” dissipaters is that they are easily replaceable after an earthquake if damaged.



Figure 45 . Internal versus External Replaceable Dissipaters at the base of the wall [2]

The same technology has been extended also to timber [11] and in particular to Laminated Veneer Lumber (LVL). LVL can be in fact considered as a superior alternative to sawn timber or glulam due to the higher homogeneity.

Laminated Veneer Lumber walls have been tested at the University of Canterbury using U shaped dissipaters, internal and external dissipaters [20]



Figure 46. (a) Hybrid Timber Wall with Internal Dissipaters, (b) Energy Dissipation Devices, (c) Wall base [1]

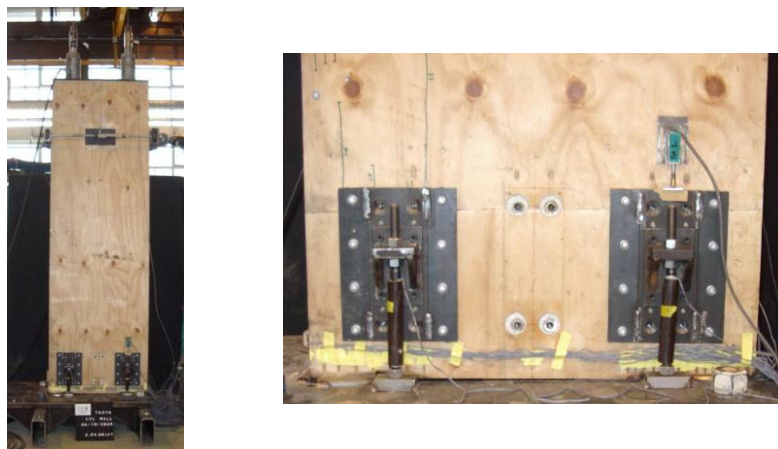


Figure 47. Wall-foundation joint using external dissipaters [21]

The U shaped have been used to couple post tensioned precast concrete walls to obtain a hybrid system where energy is dissipated through yielding of the mild steel U-shaped plates, while the post-tensioning in the walls provides the restoring force.

These solutions as already explained are independent of the mechanical properties of the adopted structural material and so the same principles have been applied to timber coupled walls [22]. The use of the U shaped dissipators allows following the target of easy replaceability and low cost. The UFP is welded to a plate in the terminal sides and then a semicircular strip is free to roll when the walls rock producing a relative displacement. Due to the relative displacement of the walls the elements yield.



Figure 48. Scheme of Coupled Wall System with UFP devices (left), Test set up of Coupled Wall System (center), Particular of UFP devices (right) [22]

The behavior of the U shaped walls is very stable and their configuration allows exploiting the rocking behavior of wall systems and translating it into energy dissipation. After an earthquake, if the U shaped connectors are damaged, the only repair cost consists of the replacement of these sacrificial elements.

Externally viscous dampers have been used as dissipator devices in the hybrid wall proposed by Kurama and then they have been used in combination with mild steel dampers [23]. Different tests on the walls have been carried out at the University of Canterbury comparing the walls without any kind of dissipation, with only external mild steel devices as dissipator device, with both mild steel and viscous dampers and with only viscous damper.

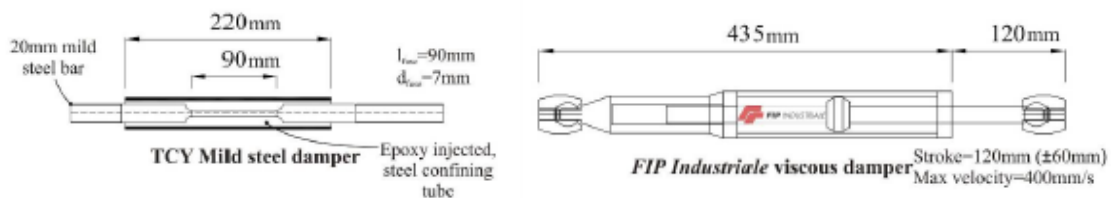


Figure 49. Damper details, Mild Steel Damper (left), FIP Industriale Viscous Damper (right) [23]

The two kind of devices provide a very stable dissipation; in particular the external mild steel dissipator provide very stable behavior when loaded in compression thanks to the filler material

and the confining tube that avoid the buckling of the specimen. The viscous damper used is highly non linear and so relatively small velocity dependant on the damper force.

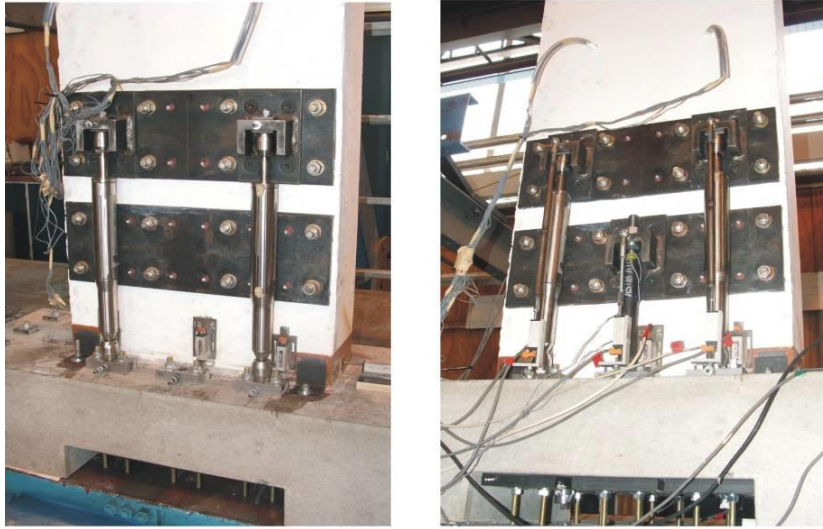


Figure 50. Wall Test Set Up, Wall with external mild steel devices (left), Wall with external mild steel devices and viscous damper (right) [23]

2.5 External “Plug And Play” Dissipators

An overview of different kind of dissipator devices has been done and the main properties of these elements have been explained; the study now is focused on external dissipator devices.

The “Plug and Play” dissipaters have been developed at the University of Canterbury and they have as further advantage the possibility to be potentially replaced after an earthquake event, if required. Considering that the energy dissipaters act as sacrificial fuses (“weakest link of the chain”) the possibility that they are damaged after an earthquake is quite high and so the replaceability is an important quality [24]

If the internal dissipaters are adopted some stiffness degradation has to be accepted due to the strain penetration while the external dissipaters guarantee a more stable hysteresis loop.

These dissipaters are realized with a mild steel bar surrounded by a confining material and encased in a steel tube. The manufacturing is quite easy and cost-effective according so with the declared target to achieve a low damage system.

The confining material avoids the buckling of the bar; if the buckling occurs in the dissipator a significant reduction in the strength of the system has to be expected. Avoiding the buckling the dissipater can yield in both axial tension and compression under reverse cyclic load and so often the crisis of the dissipater is due to the low cycle fatigue.

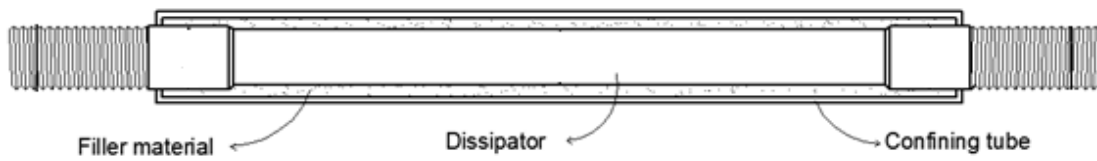


Figure 51. Example of Plug and Play dissipator: Schemratic Design (top), Example of a Dissipator (bottom)

2.5.1 Literature Review on External Dissipators

The external plug and play dissipators have been already tested in a beam-column or wall-foundation subassembly. A hybrid solution with external dissipators for a beam column joint has been tested by [25]. Four external dissipators consisting of 7 or 8 mm diameter of fuse and with 150 mm unbonded length have been installed in the X and Y directions and inserted in existing slots on both sides of the beam.

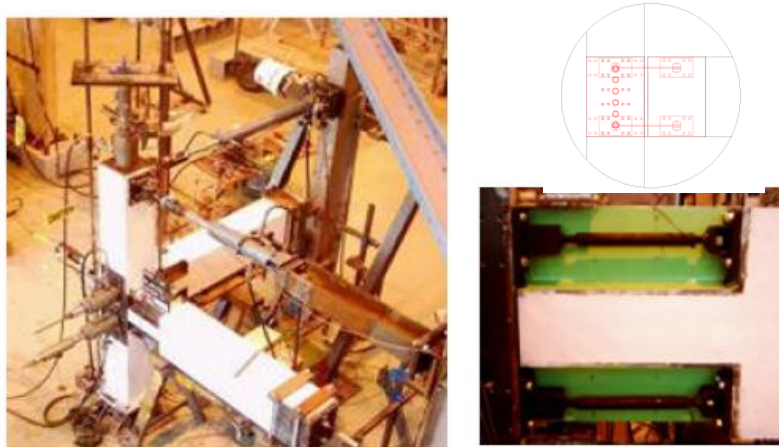


Figure 52. (a) Test Set Up, (b) Model of the Connection, (c) Detail of the Connection [25]

The results of the hybrid system under the bi directional testing regime were very stable.

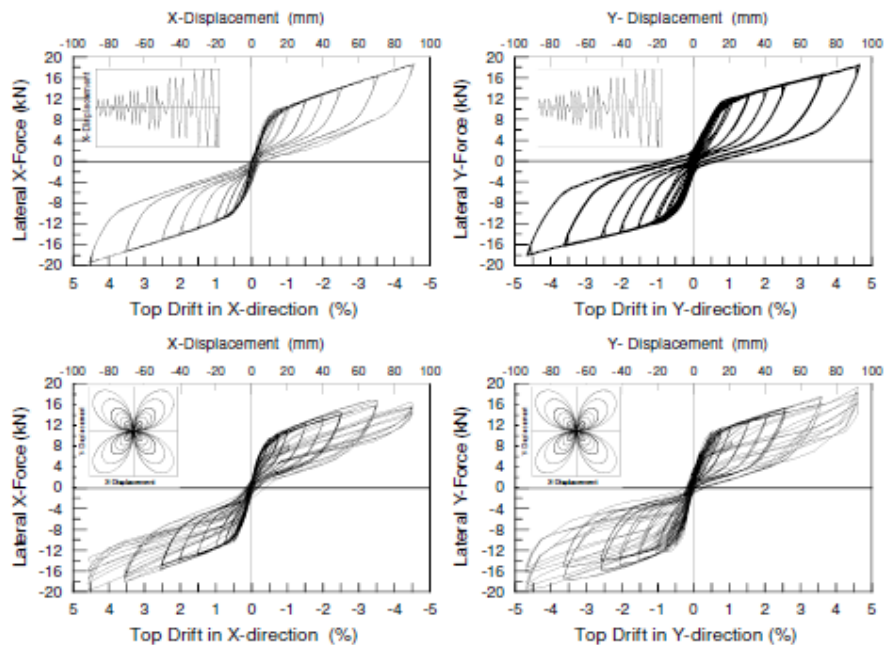


Figure 53. Force-Displacement Response of the Hybrid Solution under Uni Directional or Combined testing Regime [25]

The dynamic response of four post tensioned rocking walls with different dissipator devices have been tested by [23]. Each wall was installed with viscous fluid dampers, tension-compression yielding steel dampers, a combination of both and no device at all.

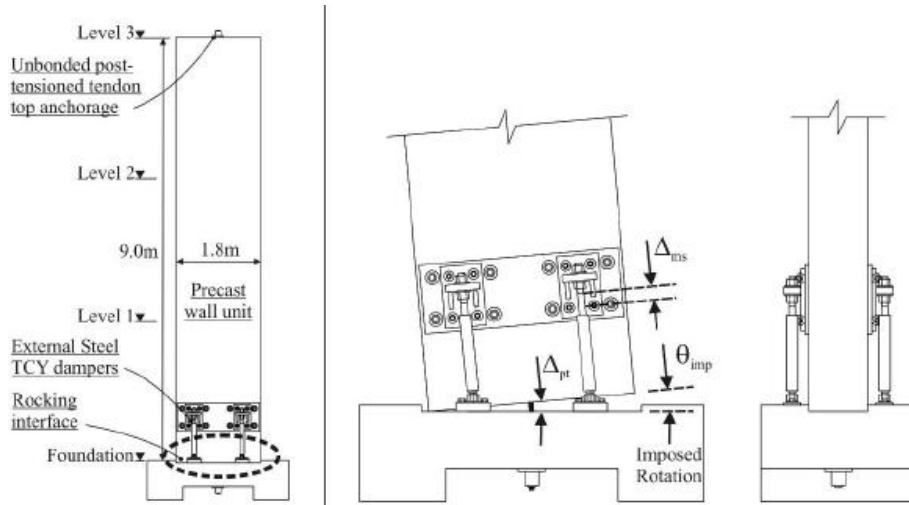


Figure 54. Post Tensioned Precast Rocking Wall System with Externally Mounted Mild Steel Dissipators (left) and Controlled Rocking (right) [23]

The detail of the “Plug and Play” and the experimental response of the dissipator are presented in Figure 55. The efficiency of the steel tube is confirmed by a very stable behavior when loaded in compression.

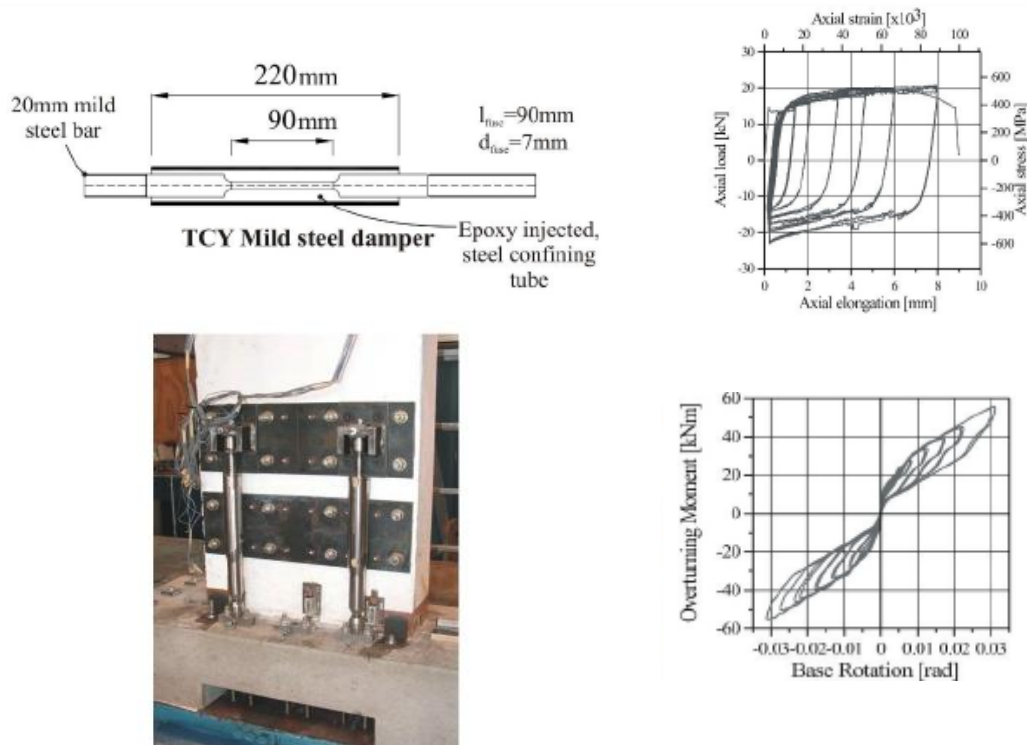


Figure 55. Detail of the Dissipator (top left), Experimental Response of the Dissipator (top right); As-Built Wall unit (Bottom Left); Experimental Response of the Wall (Bottom Right) [23]

Different tests on bridge piers with a monolithic solution, internal dissipators and external one have been carried out by [26].

The external dissipators were fabricated from 20 mm mild steel bar with different yielding regions. Some devices had a fused diameter of 10 mm over a length of 75 mm, some other had a fused diameter of 8 mm over a length of 115 mm.

The connection of the dampers to the structures is very similar to the one to the walls.

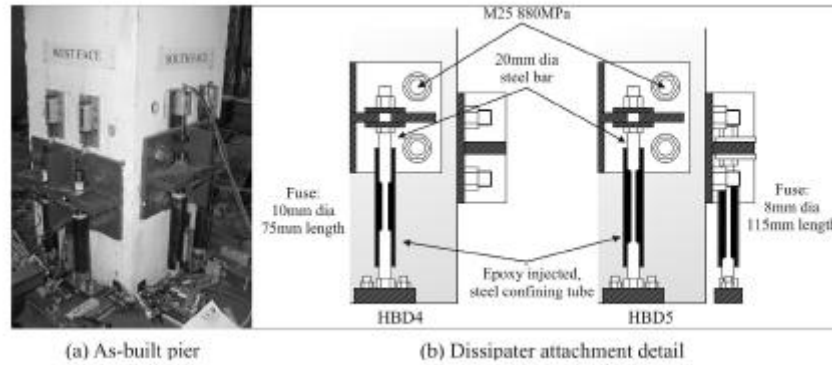


Figure 56. Dissipator Connection Details [26]

The dissipator devices have been tested before individually to characterize their stability under cyclic loading and energy dissipation capacity. The typical failure mechanism of the dissipator was the rupture of the mild steel due to low cycle fatigue.

The dissipator were subjected to the displacement time history shown in figure..

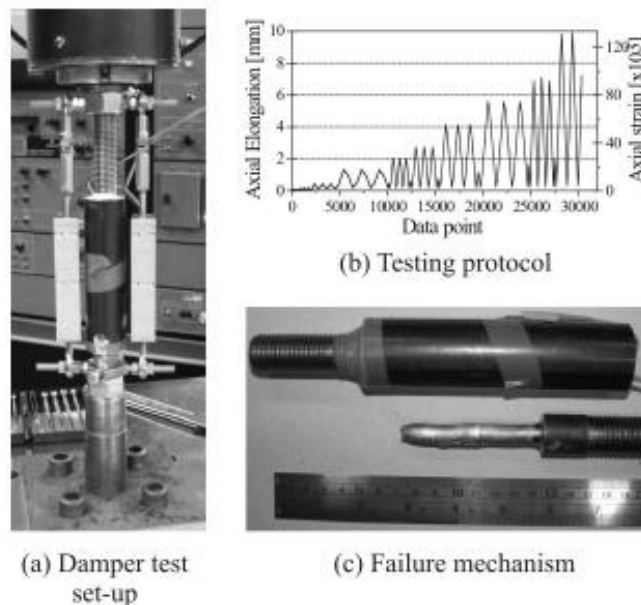


Figure 57. Dissipator Device Testing [26]

Some dissipators have also been subjected to negative displacements; the response of the devices is shown in Figure 58.

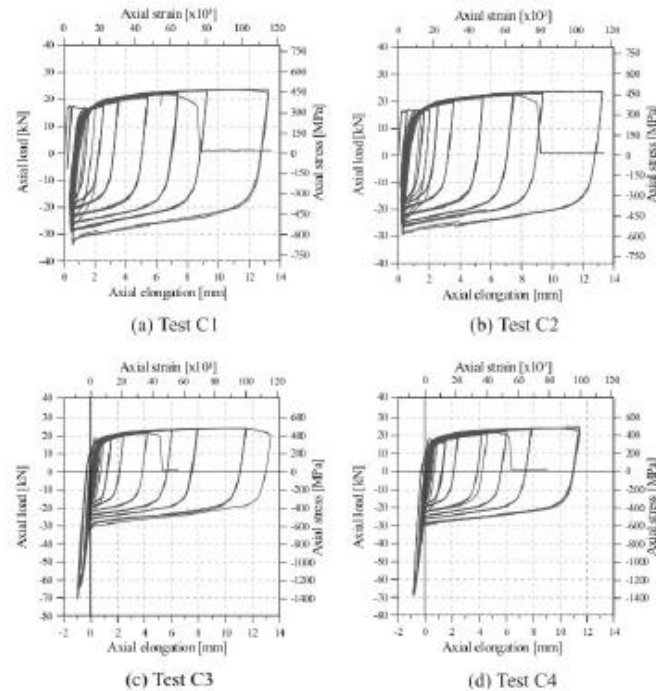


Figure 58. Cyclic Testing of Dampers. Test Specimens C1 & C2 Positive Displacements only, Test Specimens C3 & C4 Positive and Negative Displacements [26]

The increasing of stiffness when the damper is subjected to negative displacement has been explained by [26]. As the damper is compressed into the negative range the external part of the bar comes into contact with the surrounding epoxy, increasing the axial stiffness.

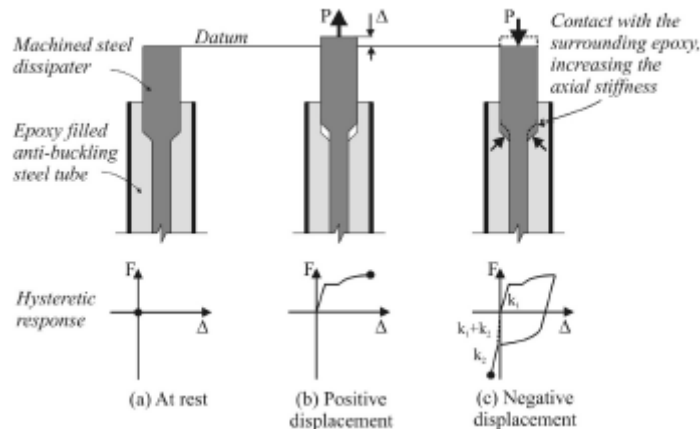


Figure 59. The Effect of the Epoxy, increasing the Axial Stiffness of the Damper in Compression [26]

Further studies have been carried out on beam column subassembly with external dissipators [27]. A five story monolithic reinforced concrete building has been used as prototype. Monolithic solutions of beam column joints have been compared with hybrid solutions as part of the experimental program. Three cases of hybrid solutions have been carried out: the first one with internal mild steel dissipator elements and the other ones with external replaceable mild steel dissipators.

One specimen is realized with external dissipator and a parabolic tendon profile while in the second specimen external devices are coupled with post tensioning profiles with several different arrangements. The external dissipator devices are in both cases realized with mild steel round bars of 12 mm diameter machined down at a 7 mm diameter with a 150 mm unbonded length. In the first solution the external part of the bar are threaded and the element goes through a flat bar and it's then fixed with a nut.

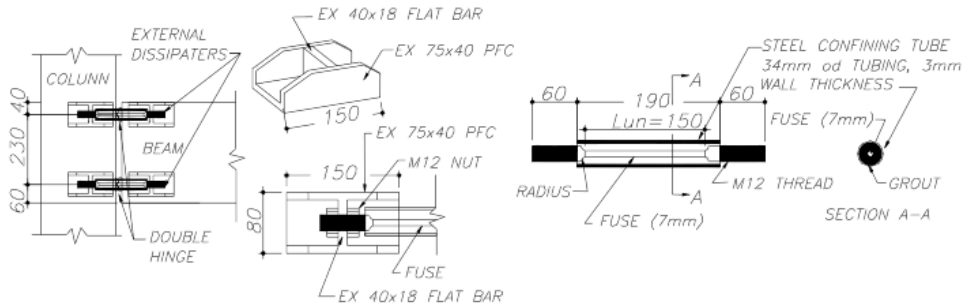


Figure 60. Energy Dissipator Footing (left), Particular of Energy Dissipation Device (right) [27]

A steel tube filled with epoxy is placed over the bar working as an anti buckling restraint. The total force displacement response and the gap opening at 3.5% of drift of the hybrid system are shown in Figure 61. The asymmetric behavior was due to the non central position of the cable within the section. The failure of the dissipator was observed at 6% of axial strain.

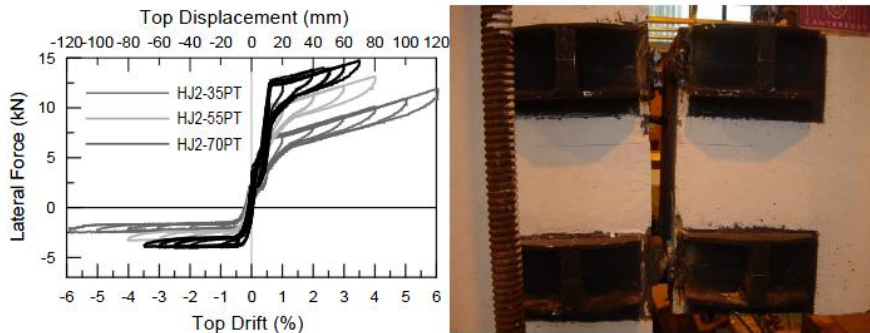


Figure 61. Hysteresis Response of the Hybrid Solution (Left) and Gap Opening at 3.5% of Drift (right) [27]

The second solution is realized likewise with external dissipators but they are located in a “pocket” hidden for architectural use. The devices are fabricated with two different diameters of the fuse, 7 mm and 8 mm respectively but with the same unbonded length.

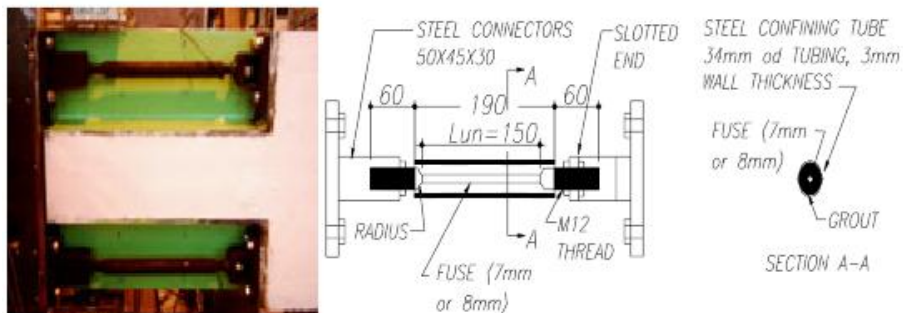


Figure 62. Test Set Up of External Dissipator Elements and Detail of the Dissipator [27]

The results of the hybrid system with the two different energy dissipaters are shown in figure .. Less energy dissipation is shown in the case of the 7 mm dissipator due to its smaller diameter.

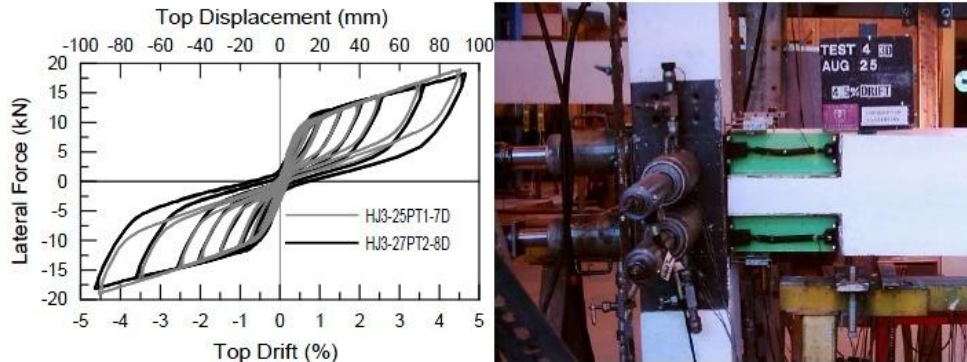


Figure 63. Hysteresis Response with two Different Energy Dissipators [27]

The stress strain relationships shows that the dissipator devices have failed at a level of elongation of 14 mm and 16 mm corresponding to a 9% and 11% of the axial strain for the 7 mm and 8 mm diameter of fuse respectively.

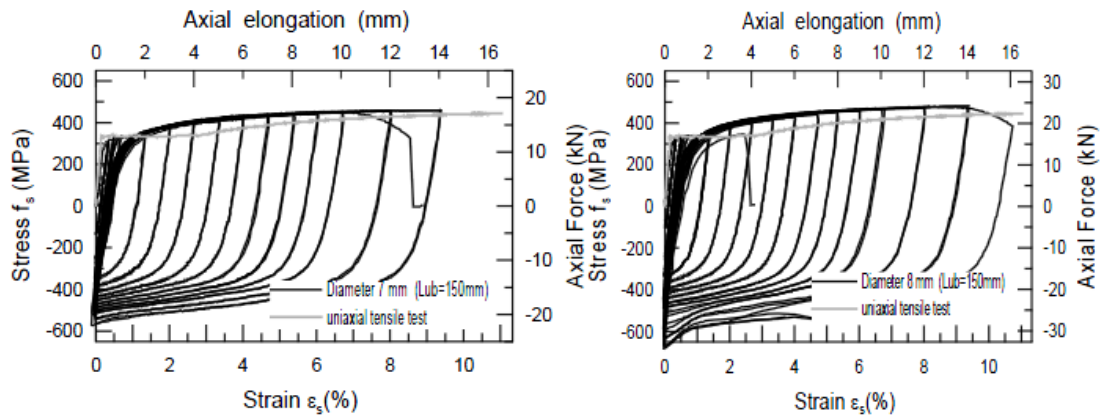


Figure 64. Stress Strain Force of External Dissipaters [27]

The loops show that the two dissipators fail at similar level of elongation and they reach in compression around the same value than in tension that means that they are stable also in compression due to the anti buckling restrain.

The study on hybrid connection has then been extended to non tearing floor connection using similarly mild steel dissipator devices to provide the required supplemental damping.

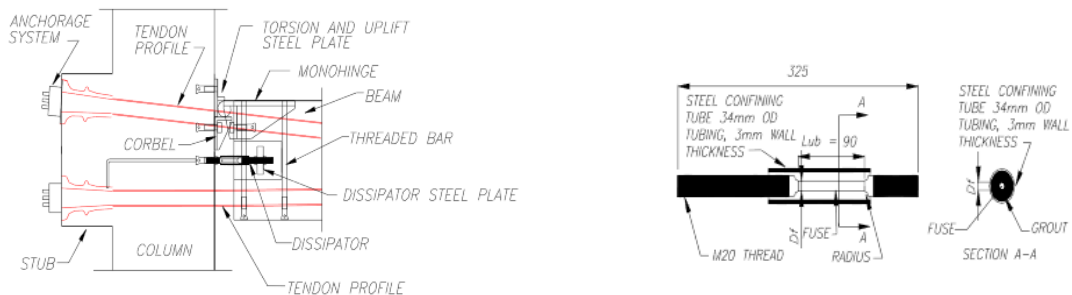


Figure 65. Connection Detail (left) and Dissipator Detail (right) [27]

Supplemental devices have been coupled with post tensioned tendons in timber systems made of laminated veneer lumber (LVL). Different tests of a full scale LVL beam column joint with internal and external dissipators have been carried out at the University of Canterbury [12]. Each joint interface was designed to have four mild steel dissipators, two each at top and bottom edge.



Figure 66. Components of Beam-Column Joint Assembly (left); Mild Steel Energy Dissipator [12]

The energy dissipator consists of steel rods designed to yield in both tension and compression, encased in steel tubes injected with epoxy to prevent the buckling in compression. Each dissipator is connected with one end to a steel bracket fixed to the beam and with the other end to a steel threaded bar inside the column through a metal coupler.

The results show that with energy dissipators only a small residual deformation due to the plastic deformation within the hybrid connection is present.

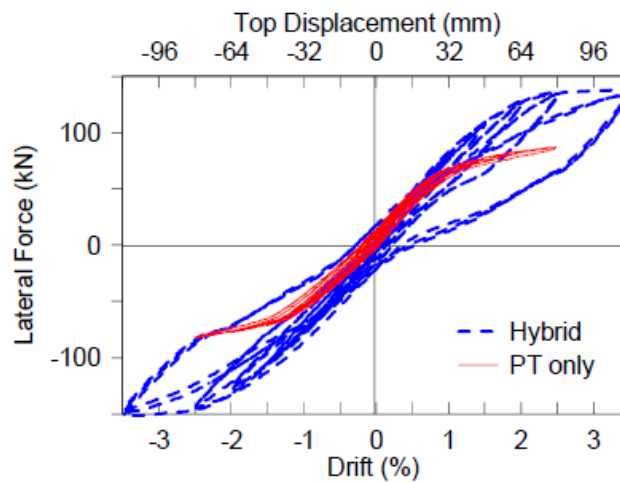


Figure 67. Load-Drift Plot of Hybrid Solution with External Dissipators [12]

2.6 References

1. Newcombe, M., *Beam to Column and Wall to Foundation Tests with Internal Dissipaters*. 2005.
2. Buchanan, A., et al., *Base Isolation and Damage-Resistant Technologies for Improved Seismic Performance of Buildings 2011*: Christchurch.
3. Nakaki, S.D., J.F. Stanton, and S. Sritharan, *An Overview of the PRESSS Five-Story Precast Test Building*. PCI Journal, 1999. **44**: p. 14.
4. Stanton, J.F., W.C. Stone, and G.S. Cheok, *A hybrid reinforced precast frame for seismic regions*. PCI Journal, 1997. **42**.
5. Pampanin, S., M.J.N. Priestley, and S. Sritharan, *Analytical Modelling of the Seismic Behaviour of Precast Concrete Frames Designed with Ductile Connections*. Journal of Earthquake Engineering, 2001. **Vol. 5**: p. 40.
6. Palermo, A., *The use of controlled rocking in the seismic design of bridges* 2004, Politecnico di Milano.
7. Filiatrault, A., J.I. Restrepo, and C. Christopoulos, *DEVELOPMENT OF SELF-CENTERING EARTHQUAKE RESISTING SYSTEMS*, in *13th World Conference on Earthquake Engineering*. 2004: Vancouver, Canada. p. 15.
8. Bruneau, M., et al., *Review of selected recent research on US seismic design and retrofit strategies for steel structures*. 2005.
9. Kim, H.-J. and C. Christopoulos, *Seismic design procedure and seismic response of post-tensioned self-centering steel frames*. Earthquake Engineering and Structural Dynamics, 2009. **38**(3): p. 355-376.
10. Christopoulos, C.a.F., A., *Principle of Passive Supplemental Damping and Seismic Isolation*, ed. I. PRESS. 2006, Pavia.
11. Palermo, A., et al., *Seismic Design of Multi-Storey Buildings using Laminated Veneer Lumber (LVL)*, in *NZSEE Conference*. 2005. p. 8.
12. Iqbal, A., S. Pampanin, and A. Buchanan, *Seismic Performance of Prestressed Timber Beam-Column Sub-Assemblies*, in *2010 NZSEE Conference*. 2010. p. 8.
13. Palermo, A., S. Pampanin, and G.M. Calvi, *Concept and Development of Hybrid Solutions for Seismic Resistant Bridge Systems*. Journal of Earthquake Engineering, 2005. **9**(6): p. 899-921.
14. Kurama, Y.C., *Unbonded Post-Tensioned Precast Concrete Walls With Supplemental Viscous Damping*. 2000. p. 8.
15. Perez, F.J., S. Pessiki, and R. Sause, *Seismic Design of Unbonded Post-Tensioned Precast Concrete Walls with Vertical Joint Connectors*. PCI Journal, 2004. **49**(1): p. 58-79.

16. Restrepo, J.I., J. Mander, and T.J. Holden, *New Generation of Structural Systems for Earthquake Resistance*, in *NZSEE Conference*. 2001. p. 9.
17. Kurama, Y.C. and Q. Shen, *Posttensioned hybrid coupled walls under lateral loads*. *Journal of Structural Engineering*, 2004. **130**(2): p. 297-309.
18. Toranzo, L.A., et al., *Shake-table tests of confined-masonry rocking walls with supplementary hysteretic damping*. *Journal of Earthquake Engineering*, 2009. **13**(6): p. 882-898.
19. Pampanin, S., *Emerging Solutions for High Seismic Performance of Precast - Prestressed Concrete Buildings*. *Journal of Advanced Concrete Technology (ACT)*, 2005. **3**: p. 202-222.
20. Palermo, A., S. Pampanin, and A. Buchanan, *EXPERIMENTAL INVESTIGATIONS ON LVL SEISMIC RESISTANT WALL AND FRAME SUBASSEMBLIES*, in *1st ECEES*. 2006: Geneva. p. 10.
21. Sarti, F., *Simplified design methods for post-tensioned timber buildings*. 2011, Politecnico of Milan.
22. Iqbal, A., S. Pampanin, and A. Buchanan, *Improved Seismic Performance of LVL Post-tensioned Walls Coupled with UFP devices*, in *8th Pacific Conference on Earthquake Engineering*. 2007: Singapore.
23. Marriott, D., et al., *Dynamic testing of precast, post-tensioned rocking wall systems with alternative dissipating solutions*. *Bulletin of the New Zealand Society for Earthquake Engineering*, 2008. **41**(2): p. 90-103.
24. NZCS, *Press Design Handbook*. 2010, Wellington, New Zealand.
25. Amaris, A., S. Pampanin, and A. Palermo, *Uni and Bidirectional Quasi Static Tests on Alternative Hybrid Precast Beam Column Joint Subassembly*, in *NZSEE Conference*. 2006. p. 8.
26. Marriott, D., *The Development of High-Performance Post-Tensioned Rocking Systems for the Seismic Design of Structures*, in *Civil Engineering*. 2009, University of Canterbury: Christchurch, New Zealand.
27. Amaris, A., *Advanced Seismic Performance of Jointed Ductile Precast Concrete Frame Systems*, in *Department of Civil Engineer*. 2010, University of Canterbury: Christchurch.

3. Plug and Play Experimental Program

The chapter investigates the key parameters regarding the design of the "Plug and Play" dissipators in order to facilitate the design and subsequently to allow the implementation to concrete, timber or steel structures.

An introduction on the buckling of structures follows; one of the crucial points of this kind of dissipators that work in both tension and compression in fact is the buckling in compression. If the buckling occurs, the devices are not able to dissipate the same amount of energy as in compression as in tension and they are no more stable.

The fabrication and the test set up of the dissipators are described and the analysis carried out in order to determine the test schedules for each kind of dissipator are presented.

All the information needed to carry out the forthcoming experimental tests on the devices are provided.

3.1 Structural Instability

Structures may fail in different ways depending of some factors like for example the type of structure, the condition of support, the kinds of load and the material used.

Failure is prevented by designing structures so that the maximum stresses and maximum displacement remains within tolerable limits. In the design of column the cross sectional area is selected such that:

$$\vartheta = \frac{P}{A} \leq \vartheta_{amm} \quad (0.1)$$

$$\delta = \frac{PL}{AE} \leq \delta_{spec} \quad (0.2)$$

After these verifications it may happen that the column is unstable under loading and that it suddenly becomes sharply curved or buckles. This kind of failure is the *buckling*.

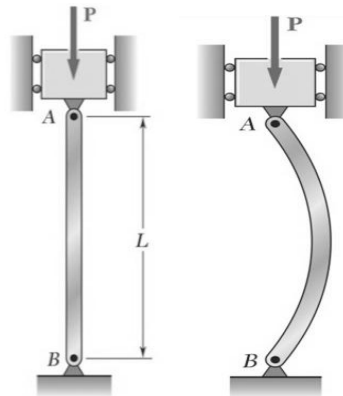


Figure 68. Buckling of a Column with Pin Connected Ends [1]

Buckling is a kind of instability that lead to a failure mode and theoretically is caused by a bifurcation in the solution to the equations of static equilibrium.

In an idealized situation buckling is the sudden onset of a very large displacement at the critical load of the structure with corresponding decrease in load carry capacity. Usually buckling occurs more gradually but as the load approaches the critical load, the displacement will increase rapidly.

Figure 1 shows an example of a column that has been loaded over the load it is design to support. The column instead of remaining straight it becomes sharply curved.



Figure 69. Example of a Buckled Column [1]

The most common problem involving buckling is the design of columns. The strength of a column and the manner in which it fails are greatly dependant on its effective length. A very short stocky column may be loaded until it reaches its yield point and maybe also the strain hardening range. It can support about the same load in compression than in tension. Increasing the effective length the buckling stress decreases. A long column may fail elastically if the buckling stress is less than the proportional limit of the material used.

In 18th century Euler has studied and solved the problem of buckling evaluating the critical value of a column depending on its stiffness and length. This classical approach is still valid for long slender pin ended columns.

$$P_{cr} = \frac{\pi^2 EI}{L^2} \quad (0.3)$$

Where:

- E is the elastic modulus
- I is the moment of inertia
- L is the length

of the element.

The most important parameter speaking about buckling is the slenderness of the column. Increasing the slenderness the critical value will decrease.

The critical stress can so be written as function of the slenderness ratio.

$$\sigma_{cr} = \frac{P_{cr}}{A} = \frac{\pi^2 E}{(L/r)^2} \quad (0.4)$$

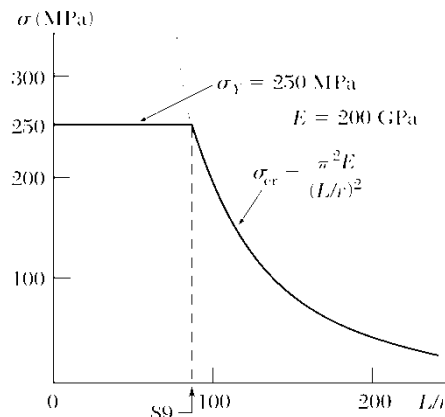


Figure 70. Euler's Curve [1]

The Euler's buckling formula was derived for a column with pivoted ends but the formula has also been extended to other end conditions.

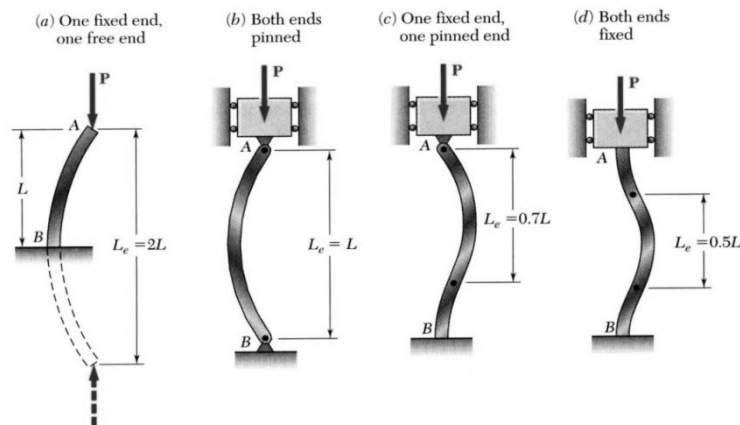


Figure 71. Effective Length of Column for Various End Conditions [1]

The critical load and critical stress are defined as:

$$P_{cr} = \frac{\pi^2 EI}{L_e^2} \quad (0.5)$$

$$\sigma_{cr} = \frac{P_{cr}}{A} = \frac{\pi^2 E}{(L_e/r)^2} \quad (0.6)$$

L_e in the equations is the effective length of the columns and it's the distance between successive points of zero bending.

$$L_E = kL$$

k is the effective length factor that depends to the end conditions as shown in Figure 71. The Euler's formula predicts very well the strength of long columns where the axial compressive stress remains below the proportional limit.

For intermediate columns some fibers will reach the yield stress and some other not; their failure will be dependent on both yielding strain and elastic modulus. The most of the columns fall into this range of the intermediate columns. Empirical formulas are used to approximate a value of the critical stress.

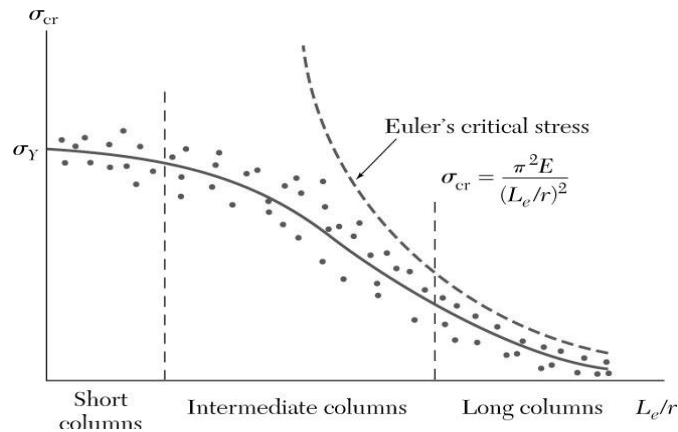


Figure 72. Idealized and Empirical Relation of Critical Stress [1]

Experimental data demonstrates that:

- for large L_e/r , σ_{cr} follows the Euler's formula and depends upon E but not σ_y .
- for small L_e/r , σ_{cr} is determined by the yield strength σ_y and not E
- for intermediate L_e/r , σ_{cr} depends on both σ_y and E .

The Euler buckling load does not take into account the initial eccentricity of the column and the eccentricity of the load.

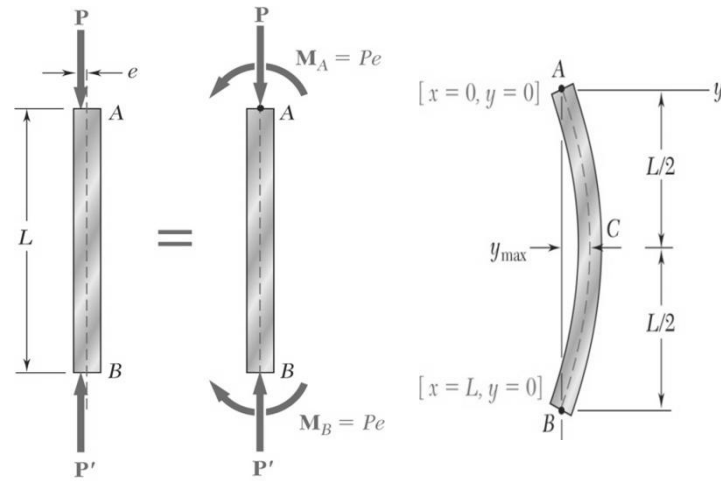


Figure 73. Buckling of Column under Eccentric Load [1]

An alternative formula known as the secant formula for the stress that considers the eccentricity of the load is presented below:

$$\frac{P}{A} = \frac{\sigma_{max}}{\left(1 + \frac{ec}{r^2} \sec\left(\frac{1}{2} \sqrt{\frac{PL_e}{EA}}\right)\right)} \quad (0.7)$$

Where:

σ_{max} is the maximum stress in a column of given effective slenderness ratio L_e/r
 e is the eccentricity of the applied load.

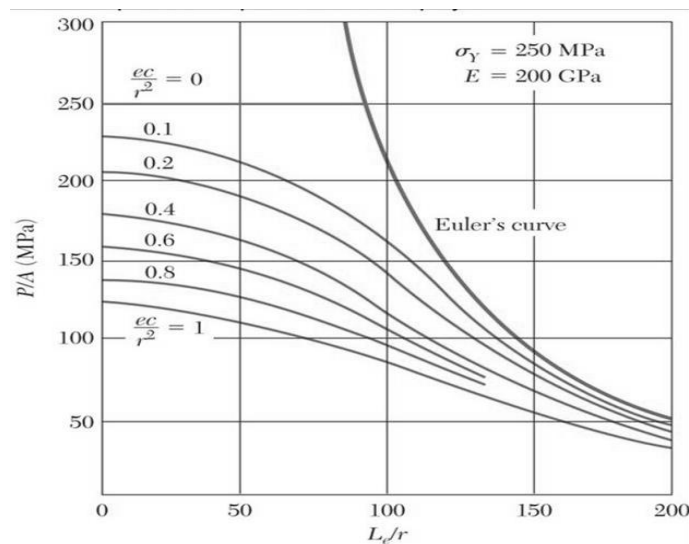


Figure 74. Load per Unit Area causing Yield in Column [1]

3.1.1 Steel Design

For the design of columns there are different formulas depending on the material used. The formulas most used for the allowable stress design of steel columns under a centric load are found in the Specification for Structural Steel Building of the American Institute of Steel Construction [2]. An exponential expression is used to predict the maximum stress for short and intermediate columns while the Euler's formula is used for long columns.

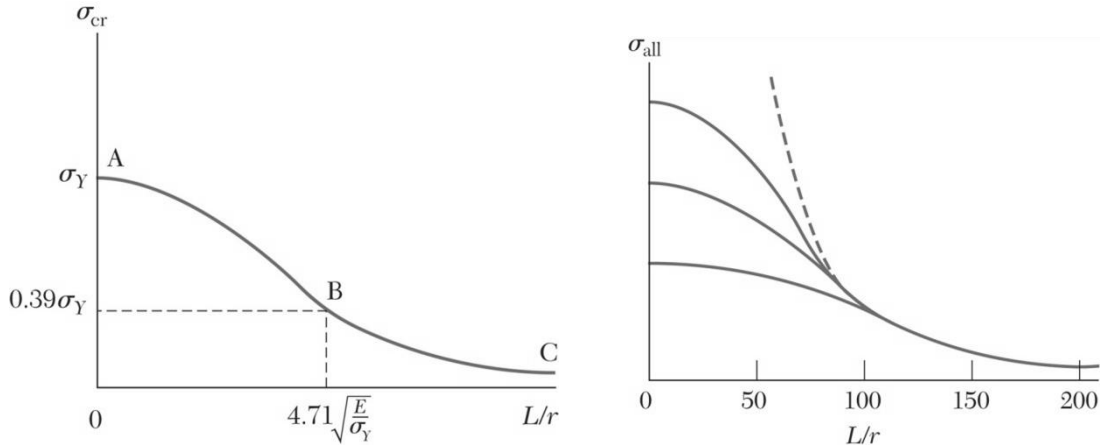


Figure 75. Variation of σ_{cr} with L/l [1]

The portion AB is defined by the equation:

$$\vartheta_{cr} = \left[0.658^{(\vartheta_y/\vartheta_e)} \right] \vartheta_y \quad (0.8)$$

Where σ_e is the Euler's critical stress:

$$\vartheta_{cr} = \frac{\pi^2 E}{(L_e/r)^2} \quad (0.9)$$

The portion BC is defined by the equation:

$$\vartheta_{cr} = 0.877 \vartheta_e \quad (0.10)$$

The value of slenderness at the junction of the two equations (point B)

is:

$$\frac{L}{r} = 4.71 \sqrt{\frac{E}{\vartheta_y}} \quad (0.11)$$

3.2 Design of the “PLUG and PLAY” Dissipators

The Plug and Play dissipators are realized with steel bars encased inside a steel tube and between them a filler material is injected. The steel bar has a fuse part with a diameter smaller than the one of the external part. Decreasing the stiffness the yielding will take place in the fused part of the bar.

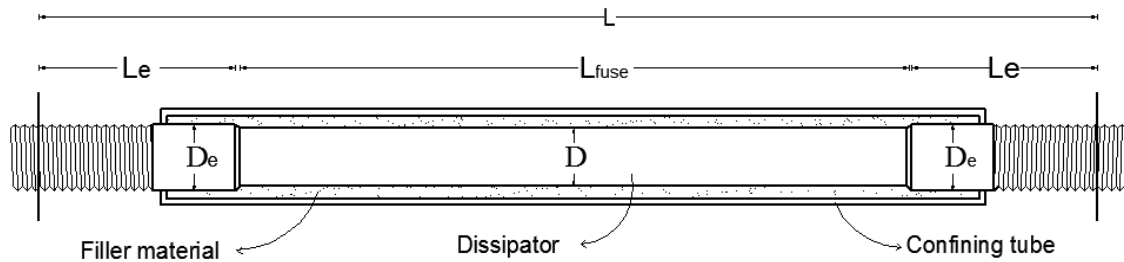


Figure 76. External Dissipator Device

The external parts of the dissipator are threaded in order to facilitate its attachment to the Uni Axial Machine.

A filler material confined by a steel casing is used in order to prevent the buckling. If the buckling occurs the element is not able to dissipate the same amount of energy as in compression as in tension. An external tube confines the material and provides additional stiffness to the system. With the confinement the element's length approaches to zero.

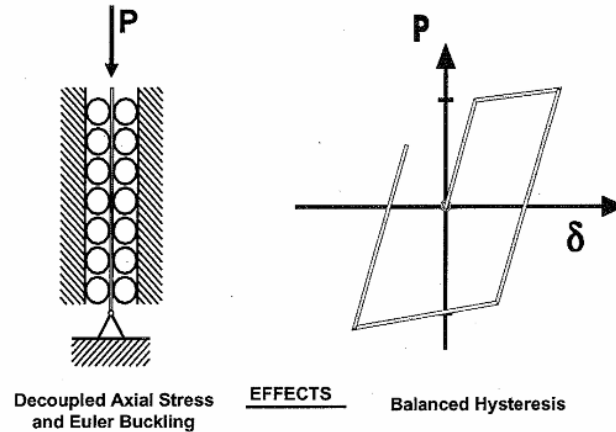


Figure 77. Effect of Buckling Restrain [3]

Different parameters, like the diameters of the bars, the slenderness of the devices, the confining material have been varied in order to have a complete idea of the behaviors of these kinds of dissipators.

Five different diameters have been chosen for the specimens that are surrounded by two different confining material, epoxy or grout; a benchmark test for every diameter will be realized without filler material, the bar will be only restrained by the steel tube.

The fuse diameter has been chosen according to the most used size of dissipators; table below shows the dissipators sizes used for experimental testing or as building's energy devices.

<i>TEST</i>	<i>STRUCTURE MATERIAL</i>	<i>FUSE DIAMETER (mm)</i>	<i>Internal/External Dissipator</i>
Restrepo 2001	Concrete	16	Internal
Amaris 2008	Concrete	7	External
Amaris 2008	Concrete	10	External
Amaris 2008	Concrete	13	External
Newcombe 2005	LVL	10	Internal
Pampanin 2006	Concrete	10	Internal
Pampanin 2006	Concrete	7	External
Smith 2007	LVL	8	Internal /External
Alan MacDiarmid Building 2009	Concrete	22	External
Marriott 2009	Concrete	7	Internal / External
Iqbal 2010	LVL	22	
Iqbal 2010	LVL	16	External
Carterton Events Center	LVL	32	Internal

Table 2. Fuse Diameters of Dissipators used in the Past Research

Considering the most used diameters and according to the standard sizes of bars, five different external and internal (fuse) diameters respectively are considered [4]:

External Diameters (mm)	Internal Diameters (mm)
16	12
20	16
24	20
32	24
32	26

Table 3. Size of External and Internal Diameters of the Dissipators

The external parts have to be enough stiffer to guarantee that the buckling, if happens, occurs in the fuse length. The internal thread diameter has to be bigger than the fuse diameter.

When threads are in the shear plane, the thread root area is approximately 70% to 75% of the gross (shank) area [2].

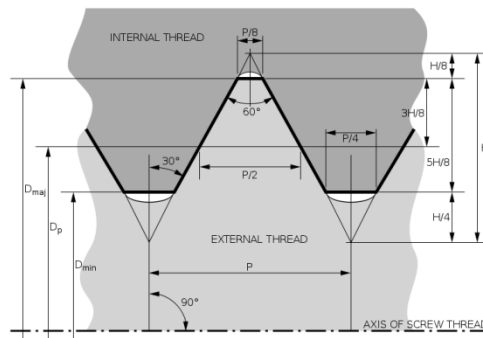


Figure 78. Profile of the Screw Thread

The external diameters have been chosen according to the standard sizes of bar and then verified as reported in the following table.

<i>External diameters</i>	<i>Gross Area (mm)</i>	<i>Threaded Area (mm): 0.7*Ag</i>	<i>Threaded Area (mm): 0.75*Ag</i>
16	201.1	140.7	150.8
20	314.2	219.9	235.6
24	452.4	316.7	339.3
32	804.2	563.0	603.2
32	804.2	563.0	603.2

<i>Threaded diameters min (mm)</i>	<i>Threaded diameters max (mm)</i>	<i>Fuse diameters (mm)</i>
13.4	13.9	12
16.7	17.3	16
20.1	20.8	20
26.8	27.7	24
26.8	27.7	26

Table 4. Threaded Diameters of the Dissipator Devices

Considering both cases of a thread root area of 70% or 75%, the threaded diameter is bigger than the fuse diameter.

The buckling is closely related to the slenderness of the element. Almost all the tests have been designed with a value of slenderness of 60 but for some of them a higher value has been considered ($\lambda = 75$ and $\lambda = 90$).

In this way another parameter of the experimental program is the influence of the slenderness.

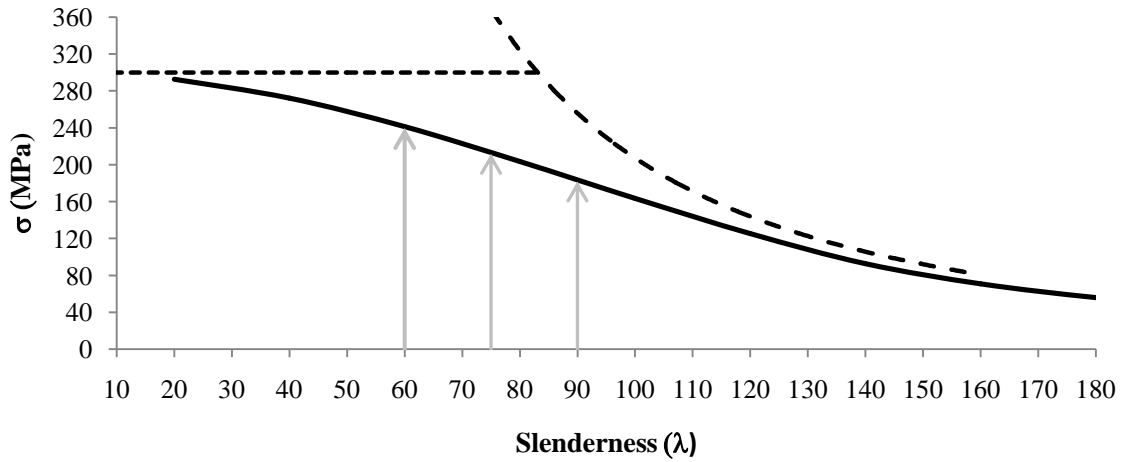


Figure 79. Stress - Slenderness Relationship

The specimens considered with their different parameters are described in the following graph.

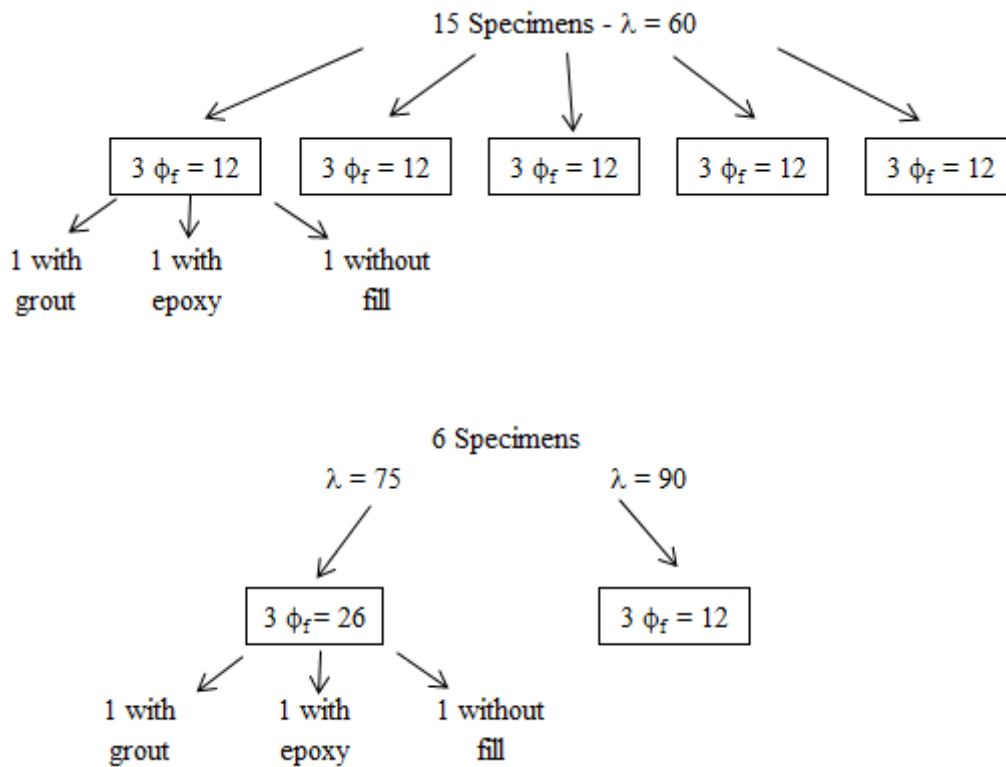


Figure 80. Dissipators to be Tested at University of Canterbury

According with the diameters considered and the slenderness chosen the lengths of the fused part of the specimens are calculated.

	<i>Diameters (mm)</i>	<i>r_{gyration}(mm)</i>	<i>Fuse Lengths (mm)</i>
$\lambda_1 = 60$	$\phi = 12$	3	180
	$\phi = 16$	4	240
	$\phi = 20$	5	300
	$\phi = 24$	6	360
	$\phi = 26$	6.5	390

	<i>Diameters (mm)</i>	<i>r_{gyration}(mm)</i>	<i>Fuse Lengths (mm)</i>
$\lambda_2 = 75$	$\phi = 26$	6.5	488
$\lambda_3 = 90$	$\phi = 26$	6.5	585

Table 5. Diameters and Lengths of the Dissipators

The steel tube has to be designed to resist to the lateral pressure due to the buckling of the bar that pushes on the confining material. The thickness of the tube has been chosen considering the worst case scenario which corresponds to the bar that, buckling, pushes the tube with a concentrated load at the mid length.

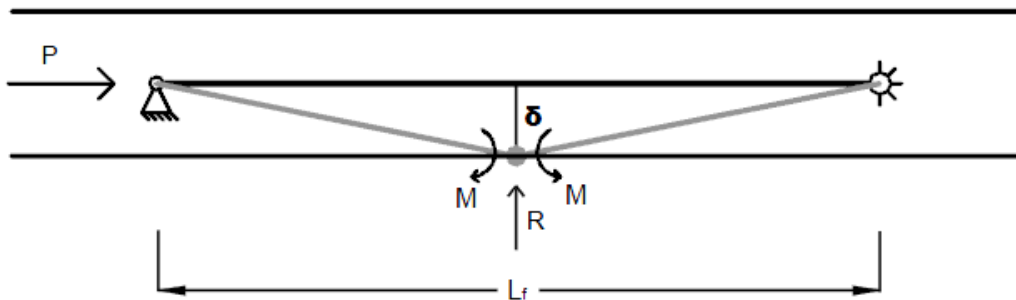


Figure 81. Simplified Scheme of Buckling

For the applied load P the maximum load of the Uni Axial Machine (250 kN) has been considered. The maximum displacement is the distance between the bar and the tube.

A value around 3 mm thickness of the tube can guarantee a value of stress within the elastic range (250 MPa for the first specimen, 300 MPa for all the others); the flexural yield in the middle of the external tube is so avoided.

The thicknesses of the tubes (t) have then been chosen according to the standard sizes.

ϕ (mm)	t (mm)	δ (m)	R (kN)	σ (MPa)
12	2.6	10.85	30.14	151.84
16	3.2	13.65	28.44	92.75
20	3.2	18.1	30.17	76.16
24	3	20.15	27.99	50.27
26	3	20.15	25.83	48.71
26	3	20.15	25.83	48.71
26	3	20.15	25.83	48.71

Table 6. Determination of the Thickness of the Tube

3.3 Materials

3.3.1 Grade 300 Mild Steel

The steel chosen for the dissipator is Grade 300 steel covered by NZS 3402:1973.

The typical stress strain relationship for the reinforcing steel when subjected to a monotonic tension is shown in the picture below.

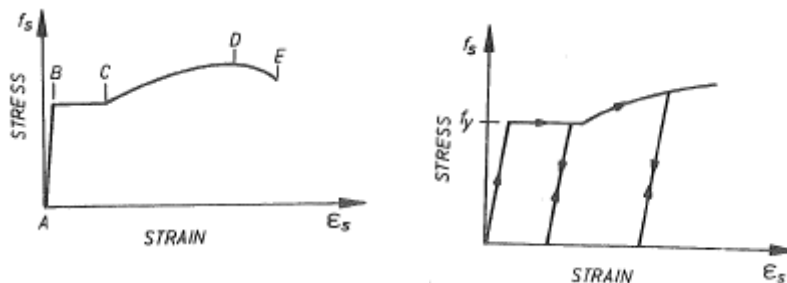


Figura 82. Typical Stress Strain Relationship for Steel Bars (left), Typical Stress Strain Relationship for Steel with repeated Loading of the Same Sign [5]

The slope is given for an elastic modulus of 200000 MPa and the curve is characterized by three major parts: the linear elastic portion A-B up to the yield point, a yield plateau B-C with little or no increase in stress and the strain hardening range C-D where the stress increase up to the maximum value and then decreases. Beyond the point D the remaining elongation takes place mainly over a small length of the bar where the necking occurs and the stress falls until fracture (point E).

The slope stress strain representing the behavior of the 275 steel when stress by a cyclic loading is shown in the picture below. The Grade 300 Steel generally considered being the same material as the earlier Grade 275 reinforcement.

After the first yield excursion the curve becomes non linear at a stress much lower than the initial yield strength.

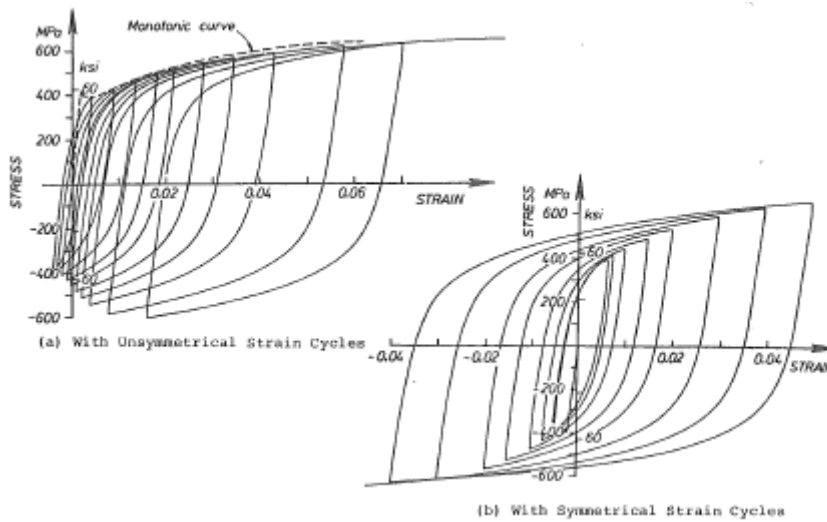


Figure 83. Typical Stress Strain Relationship for Steel with Cyclic Loading [5]

In the case of dissipator is important to know the value of yield strength in order to know at which strain the bar starts dissipate.

The yield strength of the bars depends on several factors. The main variation can be caused by the strength of the material, the area of the cross section of the bar, the bar diameter, the strain at which yield is defined and the rate loading.

The bar may have different strength because also if they are produced by the same manufacturer they have small variations in rolling. For this reason a range of values for the yield strength should be expected. The results of a statistical analysis based on a series of tests carried out by the Pacific Steel Ltd and the University of Christchurch shows the variation of the yield strength. It was assumed that the distribution of the samples follow the theoretical standard normal distribution.

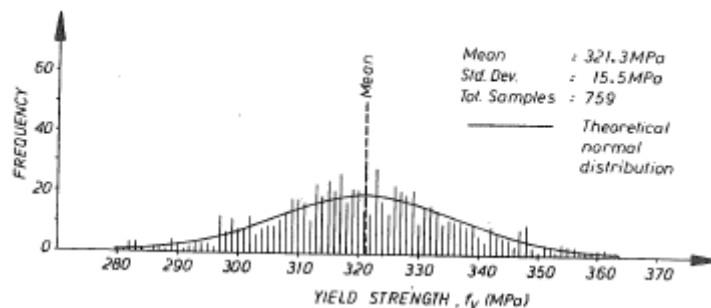


Figure 84. Histograms of Yield Strengths for Grade 275 Deformed Bars [5]

The cross sectional area shows some variations from the nominal area as a result of factors during the bar rolling process.

This detail has to be taken in account in particular in the case of dissipator where the internal thread diameter has to be bigger than the fuse diameter in order to guarantee that the yielding happens in the fuse area.

Another factor that can involve the variation in steel yield strength is the diameter of the bar. Five different diameters have been considered as case study and the table shows the minimum, average and maximum values of yield strength.

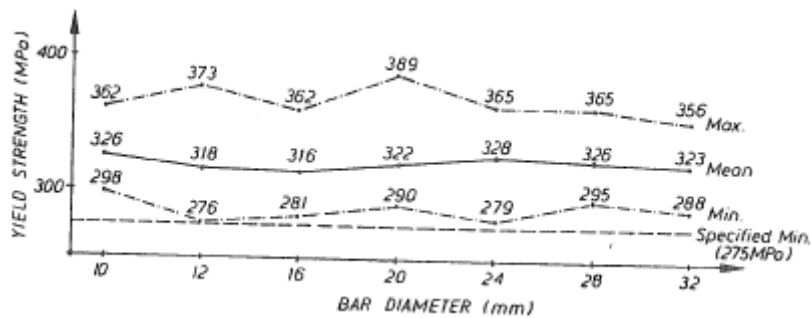


Figure 85. Yield Strength Values of Various Deformed Bars Diameter of Grade 275 [5]

The ultimate strength of a bar is a less important parameter for a dissipator. They are in fact designed to reach value of strain around the 0.02 at the design drift, design that prevents to reach the ultimate strength. Nevertheless it worth specify all the parameters in order to have a complete idea of the material.

NZS 3402P:1973 specifies that for grade 300 steel the minimum ultimate tensile strength shall be less than 380 MPa and the maximum shall not be greater than 520 MPa.

As for the yielding stress a histogram for the ultimate stress is shown in the picture below.

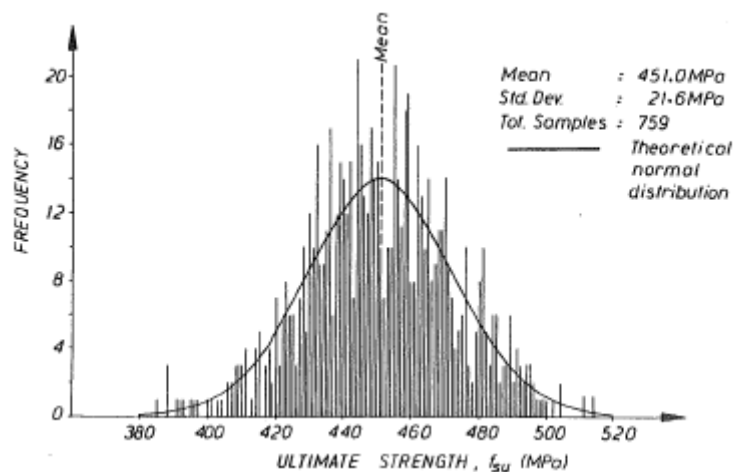


Figure 86. Histogram of the Ultimate Strength of Grade 275 Deformed Bars [5]

Some tests on the 275 steel that have been carried out at the University of Canterbury have shown that the average ultimate strain is around 0.202. The value of the Elasticity Modulus obtained by a statistical analysis based on 45 samples is 205.2 GPa.

All the average results obtained for the 275 steel are summarized in the table below.

Yield Strength	321.3 MPa
Ultimate Strength	451 MPa
Ultimate Strain	0.202
Elastic Modulus	205.2 GPa

Table 7. Properties of Grade 275 Steel

3.3.2 Epoxy

The epoxy resin has been used to confine the steel bar with the steel tube. The low viscosity of the resin is useful for the operation of fabrication of the dissipators because it will be injected between the bar and the steel tube. The epoxy chosen is design specifically to wet out and bond with wood, fiber glass and a variety of steel that is the case considered.

The main characteristics of the epoxy are summarized in the table below.

Compression yield	Tensile Strength	Elastic Modulus	Tensile Elongation
80 MPa	54 MPa	2850 MPa	4.50%

Table 8. Properties of Epoxy Resin

3.3.3 Grout

The grout has been prepared mixing cement sand with approximately 70% of water, as prescribed on the instructions in order to obtain a fluid grout.

The grout has to be in fact enough fluid to facilitate the injection in the space left between the bar and the tube.

The composite has then been mixed until obtaining the right consistence and then injected.

3.4 Fabrication of the Plug and Play Dissipators and Test Set Up

The Plug and Play dissipators have been fabricated by a private company and then prepared at the Civil Engineering Laboratory of the University of Canterbury. Around twenty bars with different lengths and diameters have been ordered already machined along bar with a reduced diameter over a specific length. The central length with a smaller diameter is the fuse length where the steel yield.

Seven types of bars have been ordered.

<i>External Diameters (mm)</i>	<i>Diameters (mm)</i>	<i>Fuse Lengths (mm)</i>	<i>Total Lengths (mm)</i>
$\phi = 16$	$\phi = 12$	180	524
$\phi = 20$	$\phi = 16$	240	624
$\phi = 24$	$\phi = 20$	300	686
$\phi = 32$	$\phi = 24$	360	760
$\phi = 32$	$\phi = 26$	390	824
$\phi = 32$	$\phi = 26$	488	929
$\phi = 32$	$\phi = 26$	585	1034

Table 9. Diameters and Lengths of the Dissipators

The fuse part is connected to the external part of bigger diameter with a transition length at an angle of 45 degree. The cross section of the fuse is smaller and more flexible than the adjacent segments, the reduce cross section can be represented by a hinge with springs. A transition length an angle of 45 degree might avoid a concentration of stress that might be present without a transition angle [6]

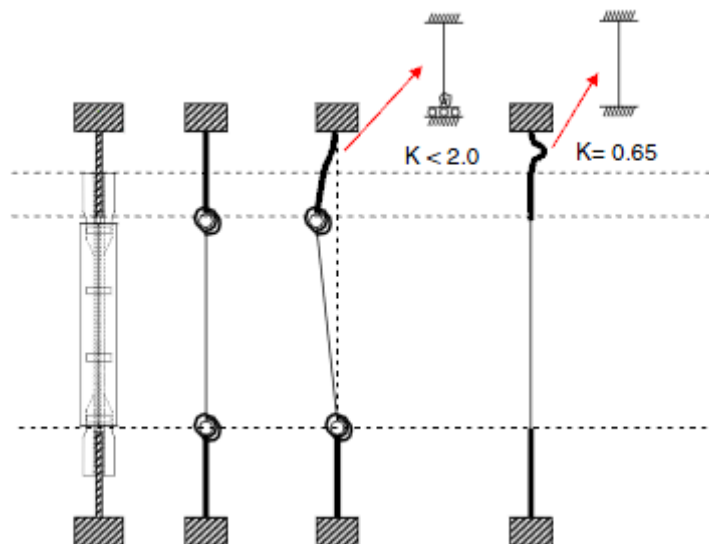


Figure 87. Possible Buckling Shapes [6]

An example of the dissipator is shown in Figure 88. Example of the Dissipator

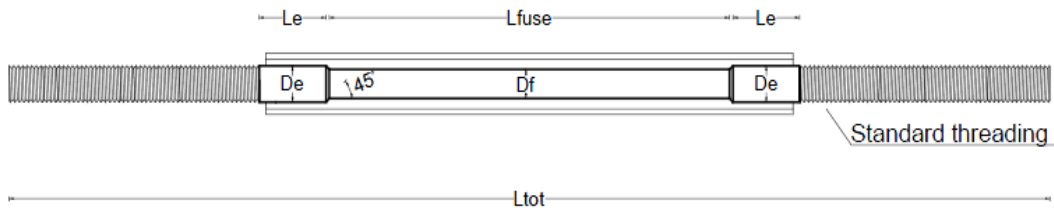


Figure 88. Example of the Dissipator

The steel bars have been strain gauged for instrumentation purposes only. The strain gauges are fixed to the bar with an adhesive and have been covered with two layers of water proof liquid. Strain gauges were used to provide data about the steel strain rates. A rigorous procedure needed to be followed in order to attach the strain gauges to the reinforcing steel. A small surface area on the steel bars had to be smoothed off. This was done without cutting into the core radius of the bar itself, so that it would not lose any strength. Next the strain gauge plate had to be connected to the prepared surface on the steel. A special glue must be used for this procedure. It is very important to place the longer side of the strain gauge plate lengthwise to the stress in the steel bar [7].

The highly sensitive plate at the end of the strain gauge can measure accurately. It is important to position the plate correctly to get an idea of the stress inside the bar.

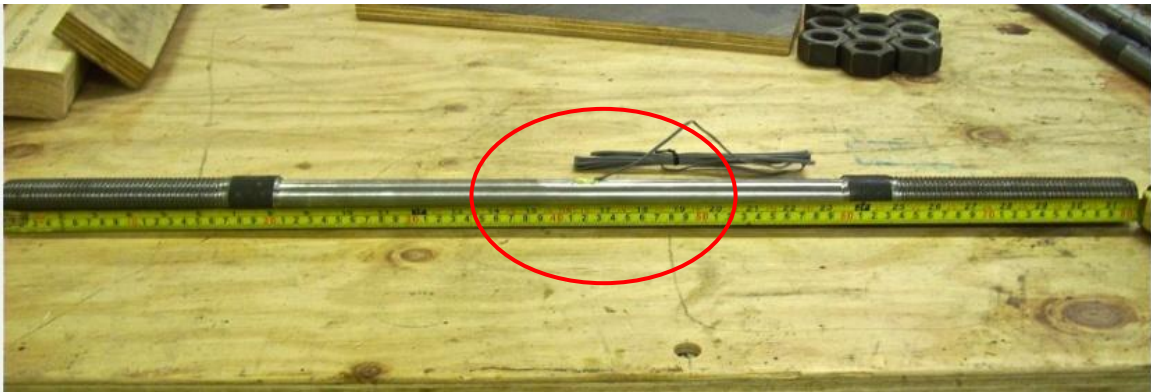


Figure 89. Strain Gauging of the Dissipator at the mid length (top), Detail of the Strain Gauging (bottom)

The steel tubes are located around the steel bars. The thickness of the steel tube has been chosen considering a concentrated force at the mid length as presented in the previous pages. Once that the minimum thickness have been calculated the different sizes of tubes have been chosen

according to the standard sizes. The length of the tube is such as to cover also the external parts. In this way the tube is never subjected to the axial load how can happen if the tube was long as the fuse. Without this condition under tension and compression cycles in fact the external part might hit the tube and start pushing it.

The tubes are kept very close to the bar that is immediately restrained when it starts buckling.

<i>Internal Diameters (mm)</i>	<i>External Diameters (mm)</i>	<i>Lengths (mm)</i>	<i>Thickness (mm)</i>	<i>σ (MPa)</i>
$\phi = 21.7$	$\phi = 26.9$	256	2.6	260
$\phi = 27.3$	$\phi = 33.7$	316	3.2	300
$\phi = 36$	$\phi = 42.4$	377	3.2	300
$\phi = 40.3$	$\phi = 48.3$	440	4	300
$\phi = 40.3$	$\phi = 48.3$	468	4	300
$\phi = 40.3$	$\phi = 48.3$	566	4	300
$\phi = 40.3$	$\phi = 48.3$	665	4	300

Table 10. Restrain Tubes Details

The grout has been prepared at the Laboratory of the University of Canterbury and it has to be enough fluid to facilitate the injection.



Figure 90. Manufacturing of External “Plug and Play” Dissipators

The test set up is shown in the picture below. The specimens are directly fixed to the load cell that has a hole of 50.8 mm (2 inches). Different adapters are screwed into the load cell and the specimens are screwed into the adapters.

In order to avoid the buckling in the upper part of the specimen before that the tube starts, the specimens is fixed as close as possible to the load cell.

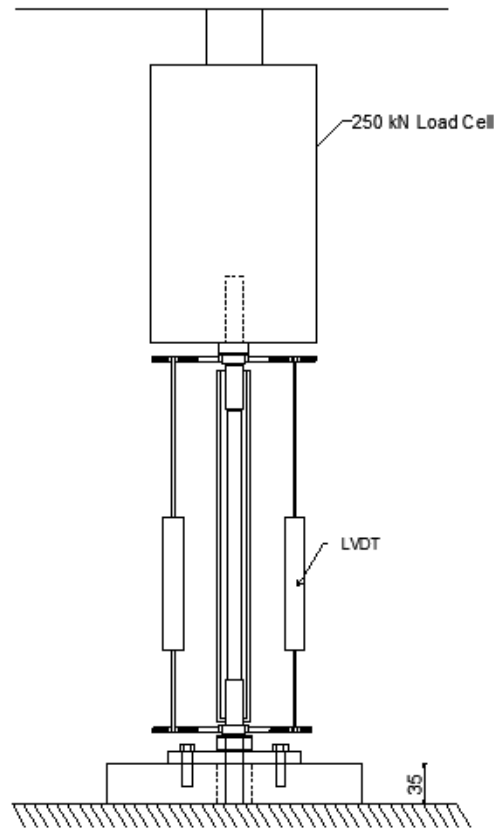


Figure 91. Dissipators Test Set Up

3.5 Displacement Time History

The displacement time history that has to be applied to the specimens is determined by considering a timber wall as a case study. The lateral load resisting system of the Carterton Events Center in Carterton (New Zealand) is realized with Press Lam walls with internal dissipators; the parallel with external dissipators is presented in the following pages. Comparing the post tensioned wall to an equivalent monolithic section it's possible to estimate the number of mild steel devices that is necessary to achieve the same amount of dissipation of the solution with internal dissipators. The values of displacements in tension and compression are consequently determined; the strain of the dissipators is limited to values of 0.02, 0.03.

The wall considered is 2400 mm long, 180 mm deep and 6700 mm height.

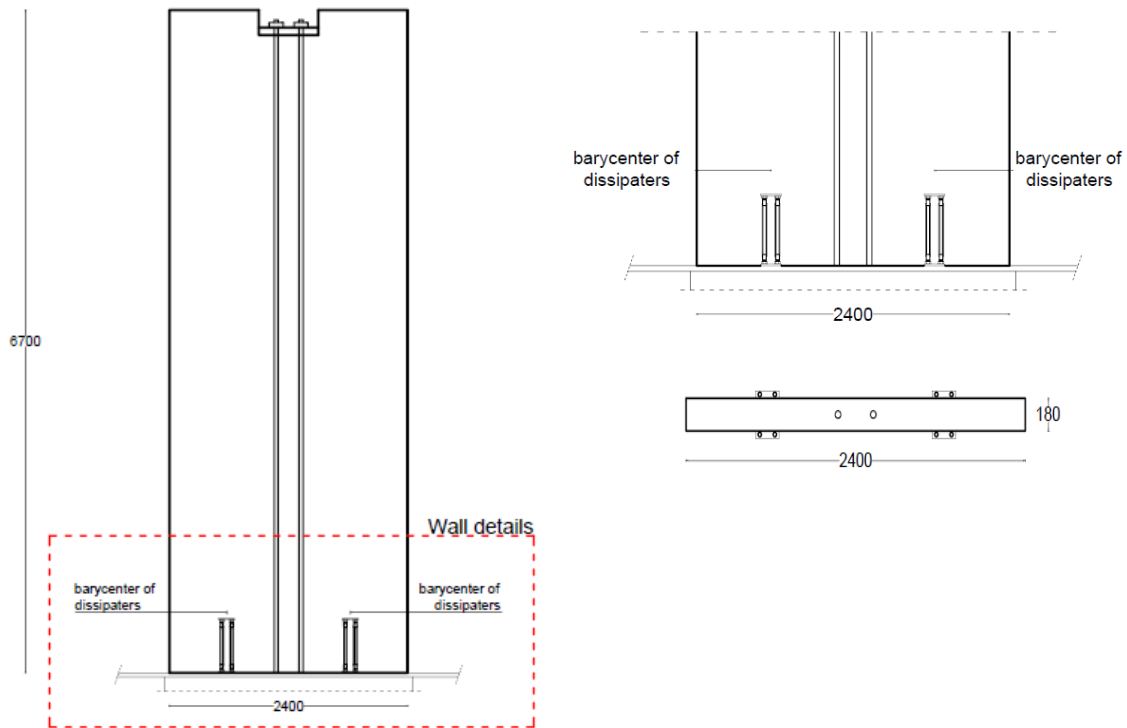


Figure 92. Details of the Wall. Vertical Section of the Wall (left), Detail of the base of the Wall (top right), Horizontal Section of the Wall (bottom right)

The axial loads on the wall are:

- Axial load due to dead loads: 32.5 kN
- Axial load due to self weight of the wall: 14.5 kN

The total axial load is so 47 kN.

The demand on the wall is:

$$V_w^* = 243 \text{ kN}$$

$$M_w^* = 243 \times 6.7 = 1630 \text{ kN m}$$

$$N_w^* = 47 \text{ kN}$$

The material properties are listed in the table below:

Mild steel

$E_s =$	200000 MPa
$\sigma_y =$	300 MPa

Table 11. Mild Steel Steel Properties

Post tensioned steel

$E_s =$	170000 MPa
$\sigma_y =$	835 MPa
$\phi =$	40 mm
$f_{ptu} =$	1030 MPa

Table 12. Post Tensioned Steel Properties

The procedure used to solve the problems of non strain compatibility of mild steel and timber due to the presence of the unbonded cables is the Monolithic Beam Analogy or MBA (Pampanin 2011).

According to the procedure, the compatibility is obtained imposing an equal member deflection between a system with hybrid connection and an equivalent monolithic solution.

The design of the equivalent monolithic solution is carried out considering the design moment

$$M^* = 1630 \text{ kNm.}$$

The required mild steel content can be determined from an estimate of the internal lever arm assuming a dimensionless neutral axis depth of $\gamma = c/L_w = 0.35$ and a reductive factor ϕ of 0.85.

Considering that the centroid of the resultant mild steel tension acts in the centre of the wall, the internal lever arm is:

$$jd = 843 \text{ mm}$$

Thus the amount of mild steel required to resist the entire design moment is:

$$A_s = \frac{M_w}{\phi \times jd \times f_y} \quad (0.12)$$

Where:

M_w is the design moment

jd is the internal lever arm

ϕ is a strength reduction factor.

The total amount of mild steel necessary is:

$$A_s \geq 7583 \text{ mm}^2.$$

As for the monolithic solution the design moment has to be less than the moment capacity of the post tensioned wall.

A ratio between the moment contribution provided by the mild steel and the moment contribution provided by the post tensioned cable is normally adopted in order to guarantee a controlled rocking mechanism.

The prestressed contribution provides the self centering capacity while the mild steel contribution provides the dissipation properties of the post tensioned wall.

Different shapes of hysteresis can be obtained varying the relation between the two contributions and a factor that keeps in account this relation is the value λ .

Thus the ratio between the self centering moment contribution provided by post tensioned steel tendons ($M_p + M_n$) to the dissipative contribution, M_s , is adopted as the main design parameter λ .

$$\lambda = \frac{M_p + M_n}{M_s} \geq \alpha \quad (0.13)$$

M_p is the moment contribution provided by the post tensioned tendons

M_n is the moment contribution provided by the axial load

M_s is the moment contribution provided by energy dissipation devices

α is post tensioned moment ratio.

In the design a value of λ equal to 1.5 has been chosen to guarantee enough recentering.

Having decided the value of λ is now possible to find out the values of α and β that are the post tensioned moment ratio and the mild steel moment ratio respectively.

$$\lambda = \frac{M_p + M_n}{M_s} \geq \alpha \quad (0.14)$$

$$\beta = \frac{M_s}{M_{total}} = \frac{1}{\lambda + 1} \quad (0.15)$$

The values are:

$$\alpha = 0.6$$

$$\beta = 0.4$$

These values obtained mean that this post tensioned hybrid connection would require the 60% of the capacity of a post tensioned solution and the 40% of the capacity of an equivalent monolithic solution.

$$\phi M_s \geq M_w^* \times 40\% \quad (0.16)$$

$$\phi [M_{pt} + M_n] \geq M_w^* \times 60\% \quad 0.17$$

$$\phi M_s > 652 \text{ kNm}$$

$$\phi (M_{pt} + M_N) > 978 \text{ kNm}$$

Considering so the value of β the amount of mild steel necessary is:

$$A_{ms} = 0.4 * A_s = 0.4 * 7583 = 3033 \text{ mm}^2$$

So the number of dissipators required is shown in the table below:

ϕ_f	$A_{\text{mild steel}} (\text{mm}^2)$	n	$n_{\text{cons tot}}$
12	113.10	26.82	28
16	201.06	15.09	16
20	314.16	9.65	12
24	452.39	6.70	8
26	530.93	5.71	8

Table 13. Number of Dissipators Required

The post-tensioned plus axial moment is given by:

$$\phi (M_{pt} + M_n) = \phi (T_{pt} + N_w) * jd$$

$$\phi (M_{pt} + M_n) \geq 978 \text{ kNm}$$

Where:

T_{pt} is the total force within the post tensioned tendons at the design drift

N_w is the axial load

jd is the lever arm of the section.

In order to estimate the number of post tensioned cables that are necessary to achieve at least the 60% of the design moment, the value of the total force in the post tensioned cables at the design drift has to be defined.

$$T_{pt} \geq \frac{M_w \times 0.6}{\phi \times jd} - \phi N_w$$

The internal lever arm considering tendons located at the centre of the wall is:

$$jd = 852 \text{ mm}$$

Rearranging the formula above the value of the total force is:

$$T_{pt} \geq \frac{M_w \times 0.6}{\phi \times jd} - \phi N_w = \frac{978}{0.85 \times 0.920} - 0.85 * 47 = 1210.69 \text{ kN}$$

$$T_{pt} = 1210.69 \text{ kN.}$$

The number of tendons that is needed to carry the value of force calculated is:

$$n \geq \frac{T_{pt}}{90\%A_{pt}f_{pty}} \quad (0.18)$$

For a diameter of the tendon of 32 mm, the number of tendons requested by the design is 2.

After having estimated the number of post tensioned tendons, the initial force in the tendons must be determined as the difference between the force at the design drift and the increment of force due to opening of the gap.

$$\varepsilon_{pt}(\theta) = \frac{n\Delta_{pt}}{l_{ub}} = \frac{n \times \theta \times l_w \times (0.5 - \gamma)}{l_{ub}} \quad (0.19)$$

With a value of l_{ub} of 7200mm and a Δ_{pt} of 3.6 mm, the strain in the tendon is equal to 0.005. The total increment in tendon load is given by:

$$\Delta T_{pt} = E_{pt}\varepsilon_{pt}(\theta)n_{pt}A_{pt} \quad (0.20)$$

$$\Delta T_{pt} = 136 \text{ kN}$$

The value of initial post tensioned force is defined by deduction of the value of force at the design drift and the positive contribution of the gap opening.

$$T_{pt, \text{initial}} = T_{pt} - \Delta T_{pt}$$

$$T_{pt, \text{initial}} = 1074 \text{ kN}$$

$$f_{pt, \text{initial}}/f_{py} = 51\%$$

The study provided an estimation of the number of mild steel dissipators and post tensioned cables necessary to achieve the moment demand considering a hypothetical neutral axis position. The following step is the verification of the design connection with an iterative procedure till obtaining the value of neutral axis depth that assures the section equilibrium.

The dissipation moment from the mild steel internal devices of the wall of the Carterton Events Center is equal to 965 kNm. The parallel with external dissipators is carried out trying to use a number of devices located at a certain distance that can provide the same amount of dissipation.

The first alternative solution considered is the one with $\phi 24$ mm diameter of dissipator; this size is realistic for the wall used as case study.

Eight bars of 24 mm diameters are considered for a total of 3620 mm² of mild steel; the fuse length is 300 mm and the un bonded length is 536 mm.

The final iteration is presented below. The neutral axis depth is equal to $c = 762$ mm, $\gamma = c/L_w = 0.31$.

The tendons elongation at the rockings interface is:

$$\Delta_{pt} = \theta(d_{pt,i} - c) \quad \begin{array}{l} = 3.1 \text{ mm for } d_{pt,1} = 1075 \text{ mm} \\ = 5.6 \text{ mm for } d_{pt,2} = 1325 \text{ mm} \end{array}$$

The tendons strain increments due to tendons elongations are:

$$\varepsilon_{pt}(\theta) = \frac{n\Delta_{pt}}{l_{ub}}$$

$$\varepsilon_{pt} = 0.0005$$

$$\varepsilon_{pt} = 0.0008$$

The increment in tendon force is:

$$\Delta T_{pt} = E_{pt} \varepsilon_{pt}(\theta) n_{pt} A_{pt}$$

The increments in tendons force are:

$$\Delta T_{pt1} = 99.7 \text{ kN}$$

$$\Delta T_{pt2} = 179.4 \text{ kN}$$

The total post tensioned forces are:

$$T_{pt} = T_{pt,initial} + \Delta T_{pt}$$

$$T_{pt1} = 598.2 \text{ kN}$$

$$T_{pt2} = 677.9 \text{ kN}$$

The stress in the tendons can't exceed the allowable limit of 90% of f_{pty} .

$$\varepsilon_{pt,initial} + \varepsilon_{pt} < 0.9 \varepsilon_y = 0.9 * 835/E = 0.004$$

$$\text{Tendon 1: } \varepsilon_{pt,initial} + \varepsilon_{pt} = 0.0028 < 0.004$$

$$\text{Tendon 2: } \varepsilon_{pt,initial} + \varepsilon_{pt} = 0.0032 < 0.004$$

The mild steel is lumped into 4 layers of 2 bars each, two on the left and two on the right side of the wall. The depth of each layer is:

$$\begin{aligned}d_1 &= 455 \text{ mm} \\d_2 &= 505 \text{ mm} \\d_3 &= 1895 \text{ mm} \\d_4 &= 1945 \text{ mm}\end{aligned}$$

TENSION STEEL LAYERS

The elongations and the strain of the tension steel layers are:

$$\Delta s_1 = 11.8 \text{ mm}$$

$$\Delta s_2 = 11.3 \text{ mm}$$

$$\begin{aligned}\varepsilon_s &= \varepsilon_{s1} = 0.032 \\&\varepsilon_{s2} = 0.031\end{aligned}$$

The stress is determined from a bilinear stress – strain relationship with $r = 0.8\%$.

$$f_s = f_y \left[1 + r \left(\frac{\varepsilon_s}{\varepsilon_y} - 1 \right) \right] \quad (0.21)$$

$$\begin{aligned}f_s &= f_{s1} = 350 \text{ MPa} \\&f_{s2} = 347 \text{ MPa}\end{aligned}$$

The force in the tension layer is given by:

$$\begin{aligned}T_s = f_s A_s &= T_{s1a} = 158 \text{ kN} \quad T_{s1b} = 158 \text{ kN} \\&T_{s2a} = 157 \text{ kN} \quad T_{s2b} = 157 \text{ kN}\end{aligned}$$

COMPRESSION STEEL LAYERS

The elongations and the strain of the tension steel layers are:

$$\Delta s_1 = -3.1 \text{ mm}$$

$$\Delta s_2 = -2.5 \text{ mm}$$

$$\begin{aligned}\varepsilon_s &= \varepsilon_{s1} = -0.0085 \\&\varepsilon_{s2} = -0.0071\end{aligned}$$

The stress is determined from a bilinear stress – strain relationship with $r = 0.8\%$.

$$f_s = f_y \left[1 + r \left(\frac{\varepsilon_s}{\varepsilon_y} - 1 \right) \right]$$

$$f_s = \begin{matrix} f_{s1a} = -311.2 \text{ MPa} \\ f_{s2a} = -309 \text{ MPa} \end{matrix}$$

The force in the tension layer is given by:

$$T_s = f_s A_s = \begin{matrix} C_{s1a} = -140.8 \text{ kN} & C_{s1b} = -140.8 \text{ kN} \\ C_{s2a} = -139.8 \text{ kN} & C_{s2b} = -139.8 \text{ kN} \end{matrix}$$

TIMBER

The timber compressive strain is defined as:

$$\varepsilon_t = \left(3 \frac{\vartheta_{imp}}{L_{cant}} + \phi_{dec} \right) c \quad (0.22)$$

Where:

$$E_t = 10 \text{ GPa}$$

$$E_{can} = 5.5 \text{ MPa}$$

The decompression curvature is:

$$\phi_{dec} = \frac{M}{E_{can} I_t} = \frac{T_{pt,t} + N}{E_{cant} I_t} \quad (0.23)$$

$$\phi_{dec} = 3.66\text{E-}07$$

Thus the timber strain is calculated:

$$\varepsilon_t = 3.69\text{E-}03$$

The compression force is so equal to:

$$C_t = -1394 \text{ kN.}$$

Checking the equilibrium:

$$-C_t - C_{s1a} - C_{s1b} = N + C_{t1a} + C_{t2b} + T_{pt1} + T_{pt2} = 0$$

Finally the moment capacity of the section is computed.

Centering moments from axial loads and Post – tensioned:

$$M_{pt} = 1261 \text{ kNm}$$

Dissipating moment from mild steel:

$$M_d = 925 \text{ kNm.}$$

The dissipating moment is approximately the 20% smaller than the one obtained with the internal dissipators. The reason is that the aim was to find the correct position of dissipators to ensure to achieve more or less the same moment but with a value of strain of 0.2, 0.3.

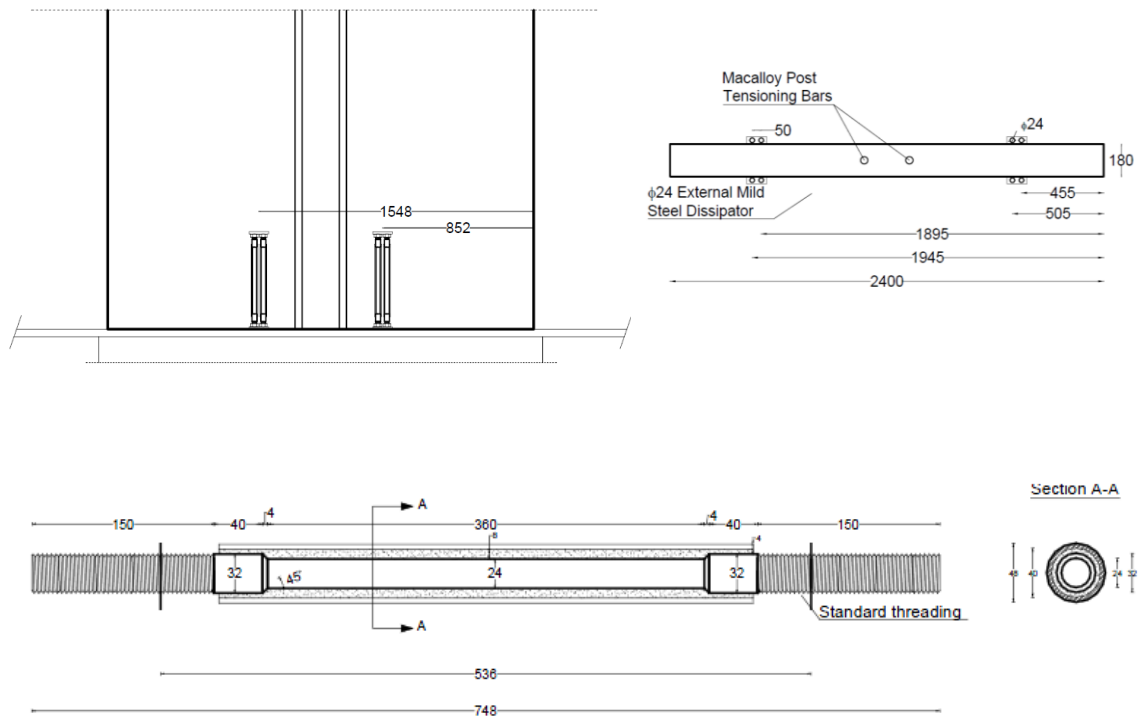


Figure 93. Post Tensioned Wall Sections with D24 External Mild Steel Dissipators

The same procedure for all the other diameters taken into account has been carried out (See APPENDIX A) and the drawings of the wall are herein reported.

External Mild Steel Dissipators $\phi 12$ mm

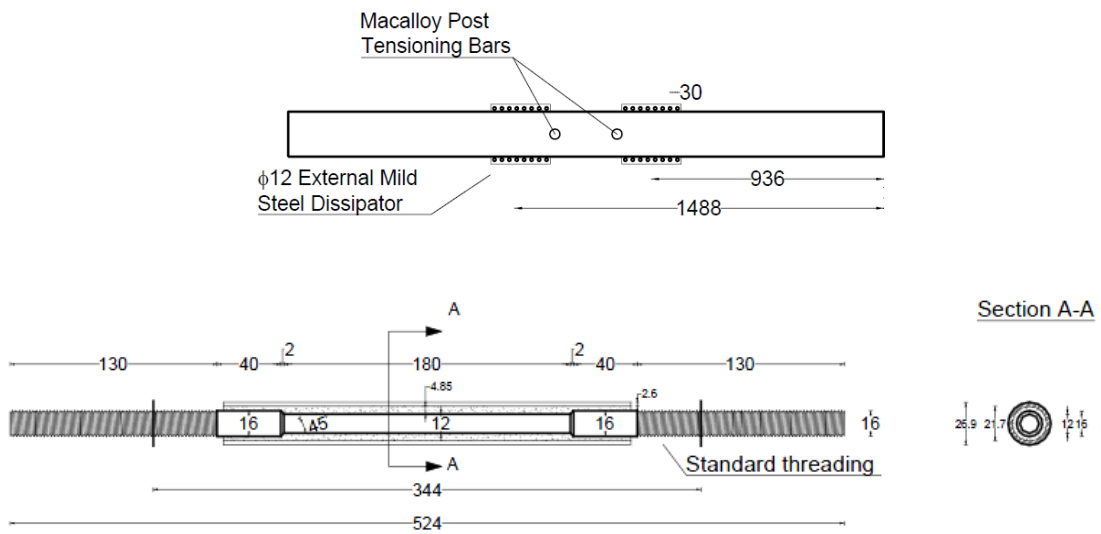


Figure 94. Post Tensioned Wall Section with $\phi 12$ External Mild Steel Dissipators

External Mild Steel Dissipators $\phi 16$ mm

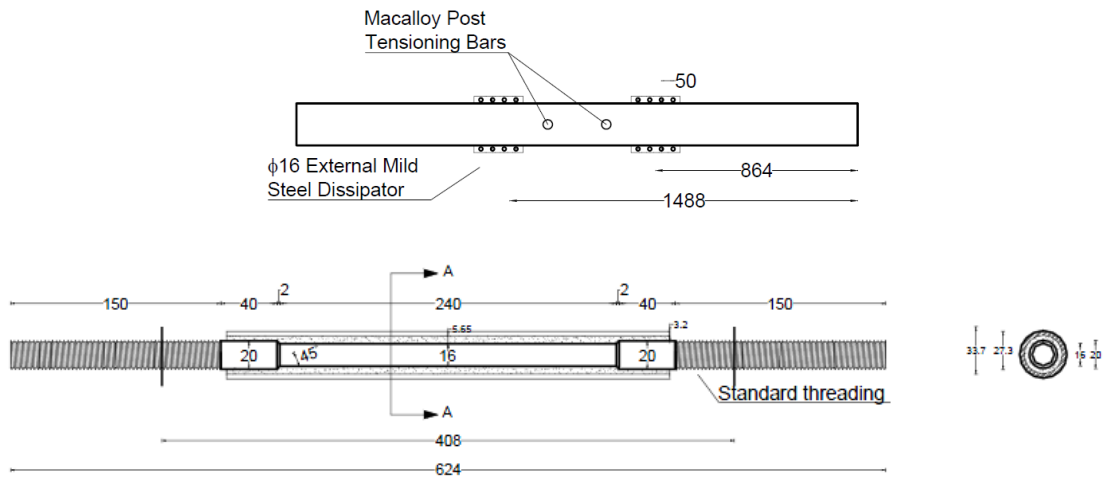


Figure 95. Post Tensioned Wall Section with $\phi 16$ External Mild Steel Dissipators

External Mild Steel Dissipators $\phi 20$ mm

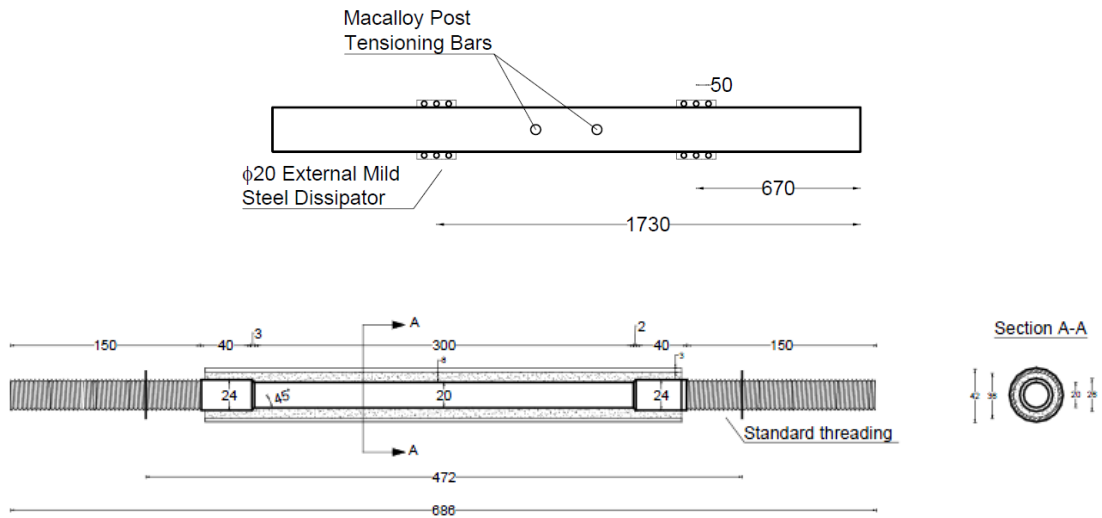


Figure 96. Post Tensioned Wall Section with $\phi 20$ External Mild Steel Dissipators

External Mild Steel Dissipators $\phi 26$ mm

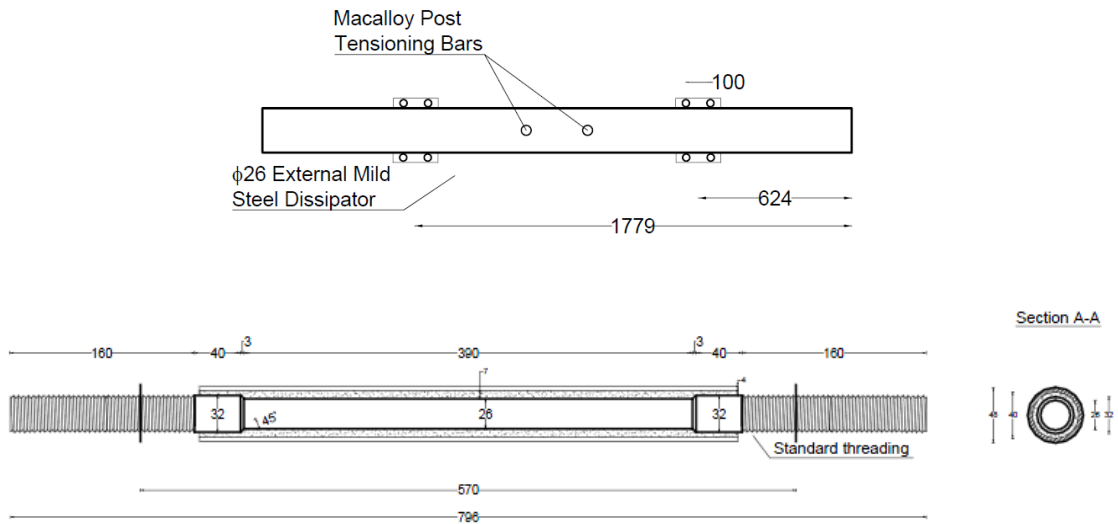


Figure 97. Post Tensioned Wall Section with $\phi 26$ External Mild Steel Dissipators

With a moment rotation analysis on the wall, the displacements for different values of drift are calculated.

3.5.1 Test Schedules

The load protocol used in the test assumes that the dissipator is stressed with three cycles at 0.1%, 0.2%, 0.5%, 0.75% and 1% of drift [8].

Displacement Time History External Mild Steel Dissipators $\phi 12$ mm

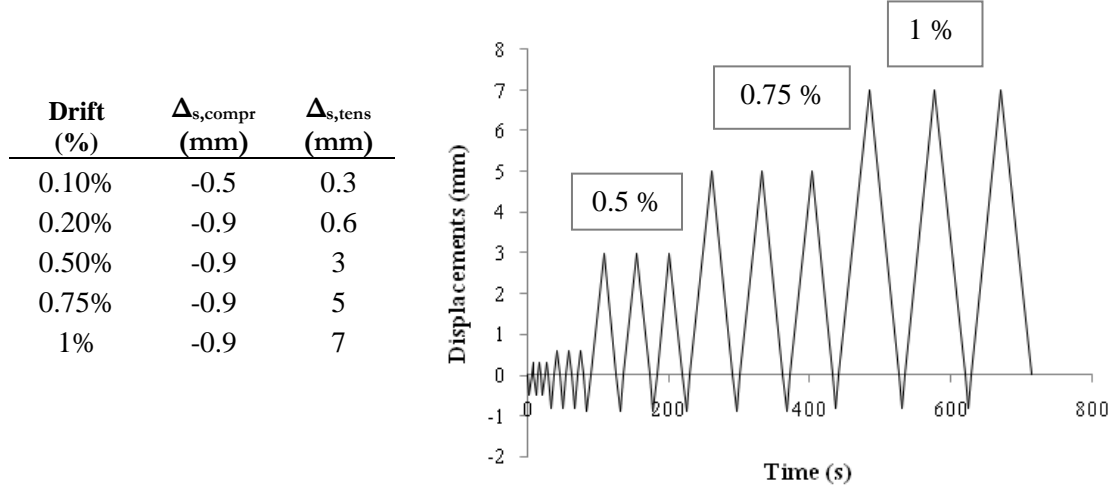


Figure 98. Test Schedule of $\phi 12$ External Mild Steel Dissipators

Displacement Time History External Mild Steel Dissipators $\phi 16$ mm

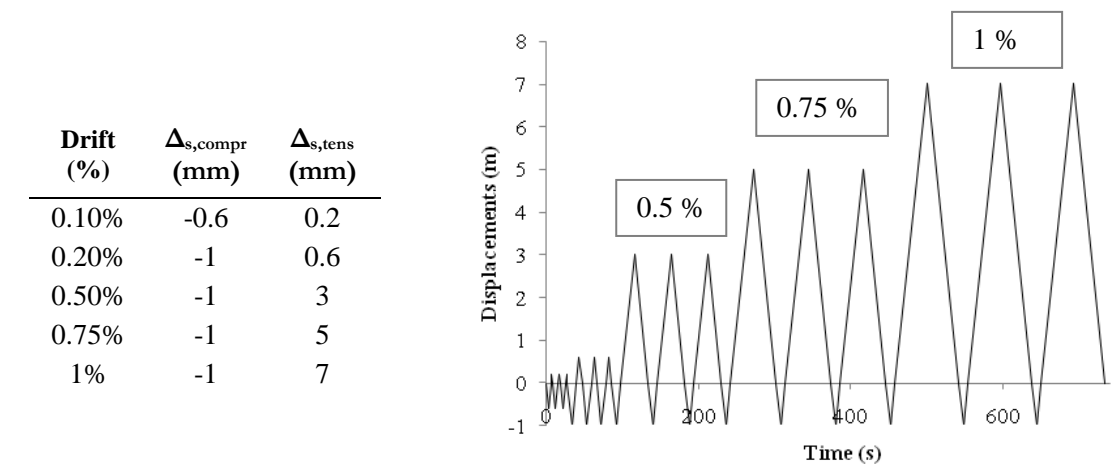


Figure 99. Test Schedule of $\phi 16$ External Mild Steel Dissipators

Displacement Time History External Mild Steel Dissipators $\phi 20$ mm

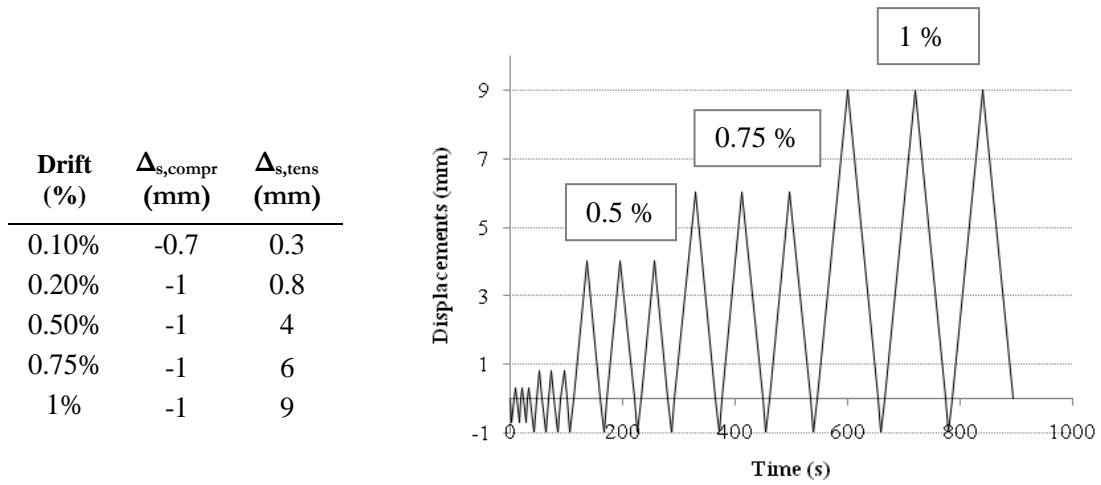


Figure 100. Test Schedule of $\phi 20$ External Mild Steel Dissipators

Displacement Time History External Mild Steel Dissipators $\phi 24$ mm

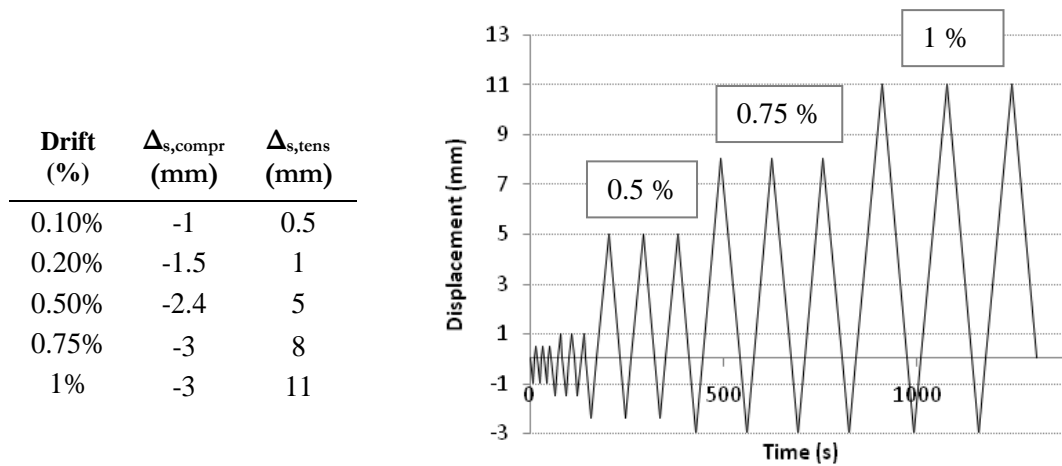


Figure 101. Test Schedule of $\phi 24$ External Mild Steel Dissipators

Displacement Time History External Mild Steel Dissipators $\phi 26$ mm

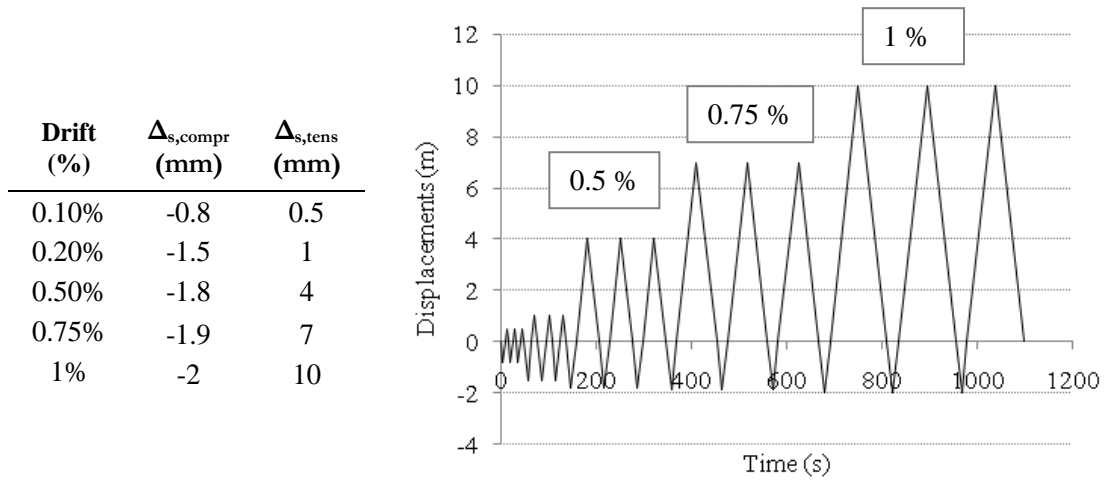


Figure 102. Test Schedule of $\phi 26$ External Mild Steel Dissipators

3.6 Conclusions and Future Applications

The Chapter investigates the key parameters regarding the design and test of Plug and Play dissipators. All the information needed to carry out the experimental tests on the devices are provided.

The diameters of the bar have been chosen according to the most used sizes in the previous research and applications. The length of the dissipators is in function of the slenderness and diameter of the bar; the value of slenderness is of 60 for the most of specimens but some of them have been designed with higher values (75 and 90).

The dissipators have been prepared for the tests: the strain gauges have been supplied, the restrain tube has been located around the bar and the filler material has been injected between the bar and the tube.

For every dissipator element the test schedule has been decided considering a case study of a timber wall with external devices.

The dissipators are ready to be tested at the University of Canterbury.

3.7 References

- [1] E. R. J. Ferdinand P. Beer "Mechanics of materials," p. 210, 2006.
- [2] C. M. Hewitt and C. J. Carter, "2005 AISC manual of steel construction and seismic manual," in *2005 Structures Congress and the 2005 Forensic Engineering Symposium - Metropolis and Beyond, Apr 20 - 24 2005*, New York, NY, United states, 2005, pp. 1643-1644.
- [3] W. A. Lopez and R. Sabelli, "Seismic Design of Buckling-Restrained Braced Frames," ed, 2004.
- [4] M. Le Haux, "Experimantal Proposal", unpublished|.
- [5] T. Andriono and R. Park, "Seismic Design Considerations of the Properties of New Zealand Manufactured Steel Reinforcing Bars," *Bulletin of the New Zealand Society for Earthquake Engineering*, vol. 19, p. 37, September 1986 1986.
- [6] K.-C. Tsai and P. C. Hsiao, "Pseudo-dynamic test of a full-scale CFT/BRB frame—Part II: Seismic performance of buckling-restrained braces and connections," *EARTHQUAKE ENGINEERING AND STRUCTURAL DYNAMICS*, vol. 37, pp. 1099–1115, 2008.
- [7] P. Loock, " LVL Wall with Varied External Dissipation Options - Lab Test Report", unpublished|.
- [8] T. Smith, *et al.*, "Post Tensioned Glulam Beam Column Joints with Advanced Damping Systems: Testing and Numerical Analysis," *Journal of Earthquake Engineering*, p. 56, 2012.
- [9] R. Vargas and M. Bruneau, "Experimental Response of Buildings Designed with Metallic Structural Fuses. II," *Journal of Structural Engineering*, 2009.
- [10] D. Marriott, "The Development of High-Performance Post-Tensioned Rocking Systems for the Seismic Design of Structures," Civil Engineering, University of Canterbury, Christchurch, New Zealand, 2009.
- [11] L. Muir and C. J. Duncan, "The AISC 2010 specification and the 14th edition steel construction manual," in *Structures Congress 2011, April 14, 2011 - April 16, 2011*, Las Vegas, NV, United states, 2011, pp. 661-675.
- [12] M. Dhanasekar, "Effect of grout confinement on the compressive strength of masonry," *Journal of the Institution of Engineers (India): Civil Engineering Division*, vol. 85, pp. 26-30, 2004.
- [13] Y. K. Ju, *et al.*, "Component tests of buckling-restrained braces with unconstrained length," *Engineering Structures*, vol. 31, pp. 507-516, 2009.
- [14] A. Amaris, *et al.*, "Uni and Bidirectional Quasi Static Tests on Alternative Hybrid Precast Beam Column Joint Subassembly," presented at the NZSEE Conference, 2006.

- [15] A. Amaris, "Advanced Seismic Performance of Jointed Ductile Precast Concrete Frame Systems," Department of Civil Engineer, University of Canterbury, Christchurch, 2010.
- [16] S. Pampanin, *et al.*, "EXPERIMENTAL INVESTIGATIONS ON HIGH-PERFORMANCE JOINTED DUCTILE CONNECTIONS FOR PRECAST FRAMES," presented at the First European Conference on Earthquake Engineering and Seismology, Geneva, 2006.
- [17] A. Iqbal, *et al.*, "Seismic Performance of Prestressed Timber Beam-Column Sub-Assemblies," presented at the 2010 NZSEE Conference, 2010.
- [18] J. E. Martinez-Ruedaa, "On the Evolution of Energy Dissipation Devices for Seismic Design," in *Earthquake Spectra* vol. Vol. 18, ed, 2002, pp. 309 - 346.

4 Buckling Restrained Braces Behaviour

In the last decades, buckling restrained braces (BRB) have become increasingly popular in Asia, especially in Japan, for their good earthquake performance. A conventional brace exhibits a non symmetric behavior in tension and compression due to the buckling; to preclude the buckling a restraining-unit is used around the bar. The following Chapter presents the characteristics and hysteretic behavior of the BRB. The load-deformation behavior of the BRBs can be compared to the one of the external dissipators object of this study.

4.1 Characteristics of Buckling Restrained Braces

Braced frames and moment frames are the most widely used framing systems for steel construction in seismic region. Conventional brace frames are expected to buckle and yield during a major seismic event. The disadvantage of conventional brace is the buckling in compression; to overcome this problem a restrained solution has been proposed. A conventional brace that incorporates a brace confined with a restraining unit is called a buckling restrained brace (BRB).

Buckling Restrained Braces (BRB) generally comprises a steel core element that carries the entire axial load and a restraining exterior element that prevents the core from buckling in compression. Due to the confining effect of the exterior element, a BRB yields in both compression and tension and dissipates a significant amount of hysteretic energy during earthquakes.

After the 1994 Northridge and 1995 Kobe earthquakes buckling restrained braces frames have emerged and have been used extensively for seismic application in Japan. The two earthquakes have demonstrated the susceptibility of steel moment resisting frames to various type of damage associated to various displacements. To alleviate such problems, engineers have improved the performance of concentrically braced frames through the development of buckling restrained braces with different structural configurations. Buckling restrained braces have then found widespread application in Japan and Taiwan and the use is developed later also in the US. The Berkeley Campus of the University of California has been one of the major early developers of

buckling restrained braced frames technology in the US. Most of the Barkley Campus, in fact, lies within approximately 2 km of the Hayward Fault. To mitigate the effect of a large near-by earthquake, buckling restrained braces have been used already in four building on the Barkley Campus.

Different types of BRBs developed to date have been patented but the concepts are similar. An example of a BRB is composed of five components:

- A restrained yielding segment where the deformation occurs;
- An extension of the restrained yielding segment with an enlarged area
- An un restrained non yielding segment commonly designed as a bolted connection
- Un bonding material that minimize the transfer of the shear force between the restrained steel and the mortar
- Buckling restraining mechanism that is typically composed of mortar and steel casing.

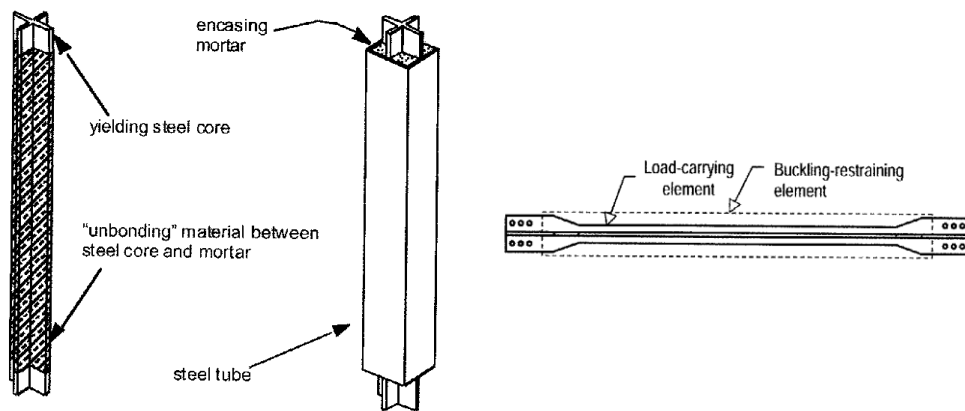


Figure 103. Component of BRB [1]

Research on BRBs was firstly carried out by Yoshino et al. (1971) that proposes a flat steel plate encased by reinforcing concrete panels with some de bonding material between them [2]. Different aspects of the BRB have then been investigated: different cross sections, several de bonding material and various reinforcing details have been studied.

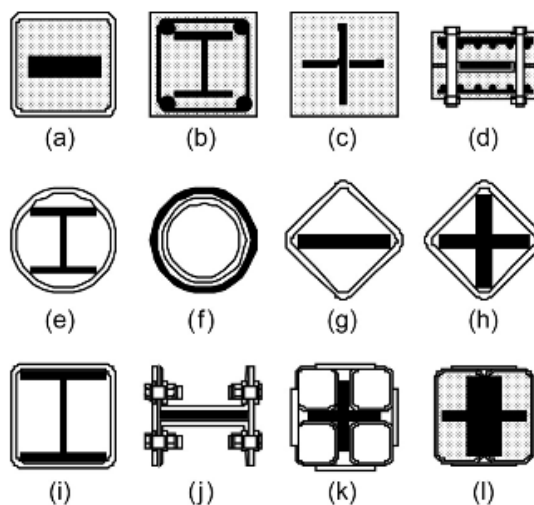


Figure 104. Cross Sections of BRBs [2]

Figure 104 shows a crisscross section plate stiffened by mortar-infilled steel tube. Figure 104b exhibits an H section steel brace enclosed by reinforcing concrete. Figure 104c exhibits crisscross section enclosed by a steel fiber reinforced concrete. Figure 104d show a type of steel plate brace stiffened by two bolt connected precast concrete panels. A wide flange section restrained against lateral buckling by an exterior steel tube is shown in Figure 104e. A cross section of the BRB with two circular steel tubes is presented in Figure 104f; the inner tube provides resistance against the lateral deformation whilst the outer tube is the one that carries axial load. A steel plate and a cruciform section encased by a square steel tube are shown in Figure 104g and 2h.

The H shaped brace restrained by a square tube is presented in Figure 104i. Figure 104j shows a steel plate enclosed by bolted channels and plate. Figure 104k shows double-Tee brace encased by four-connected square tubes. A double- Tee double tube is shown in Figure 104l.

4.2 Experimental Results on Buckling Restrained Braces

The buckling restrained braces have been introduced in the seismic engineer to overcome the deficiency of the conventional braces concerning the cyclic loading behavior. Buckling restrained braces are, in fact, able to dissipate a large amount of energy as in tension as in compression without incur in the buckling under compression.

The behavior of a buckling restrained brace compared to a conventional brace is shown in Figure 105.

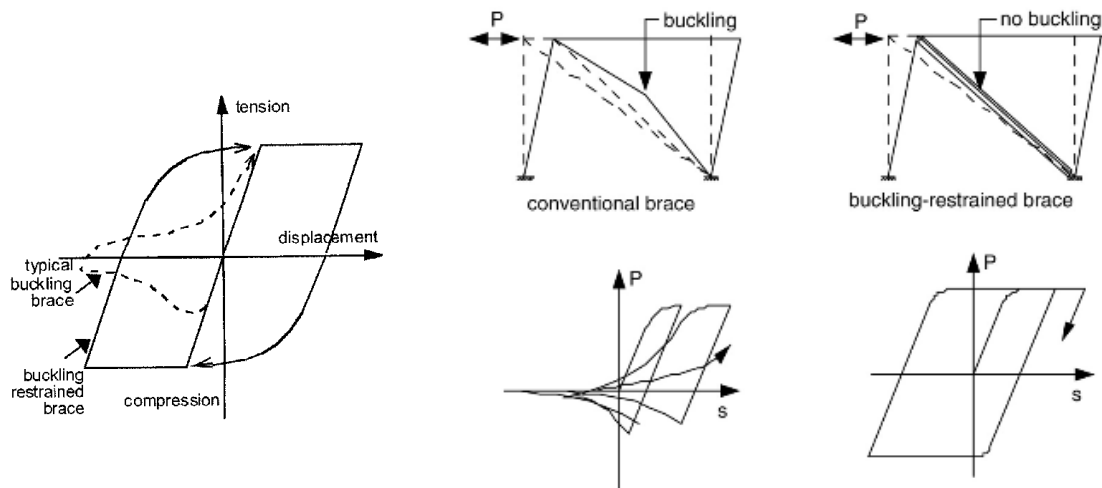


Figure 105. Behavior of Conventional Brace and BRB

Figure 105. Behavior of Conventional Brace and BRB depicts a comparison between the hysteretic behavior of BRB and ordinary braces. If the buckling resistant mechanism is designed properly, the core would yield in compression and exhibits similar tension and compression strengths. It would also perform a regular hysteretic behavior for considerable values of strain (around 2%).

Different experimental tests have been carried out on BRB. One of the first tests carried out on restrained braces regarded the behavior of several 1/5 scale specimens of X-shape braces encased by PC panels under cyclic loading.

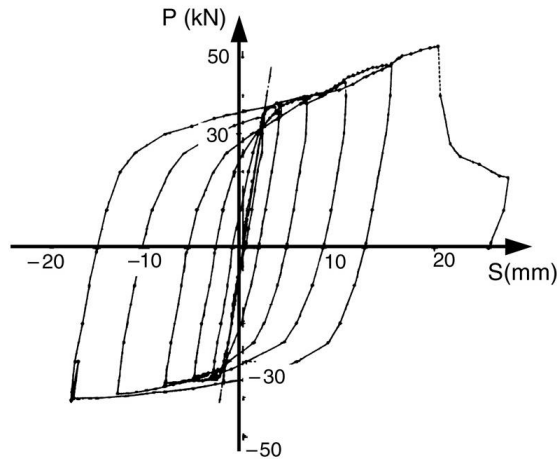


Figure 106. Buckling - Restrained Brace Hysteresis [2]

The hysteresis shows a stable behavior for different cycles before the rupture, after degradation, of the brace.

In order to check the behavior of real steel frames, two 1/2 scale tests were performed for final demonstration.

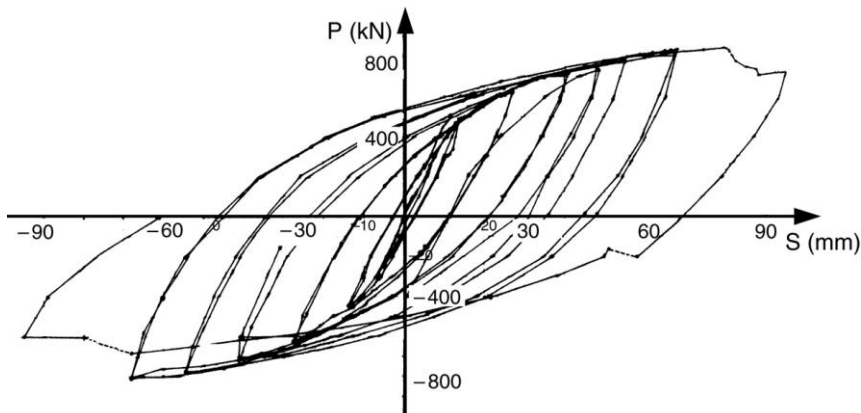


Figure 107. Frame test of X-Shape BRB [2]

Figure 107 shows that before the local buckling occurred in the steel plate, the behavior was stable showing the typical spindle-shape loop of the reinforcing steel.

At the University of California, Barkley, tests of large scale of buckling restrained braces subassembly have been performed; three frames subassembly have been subjected to the design level and beyond the design level cyclic lateral loading [3]. The first and second tests uses a yielding core plate and the third one a cruciform core. The tests are intended to subject the braces to a maximum deformation at least equal to the design one, and to a cumulative plastic ductility demand of at least 140. The loading protocol of test 1 is shown in Figure 108; the

general characteristics of the loading histories for Test 2 and 3 were similar varying only in terms of maximum lateral displacement.

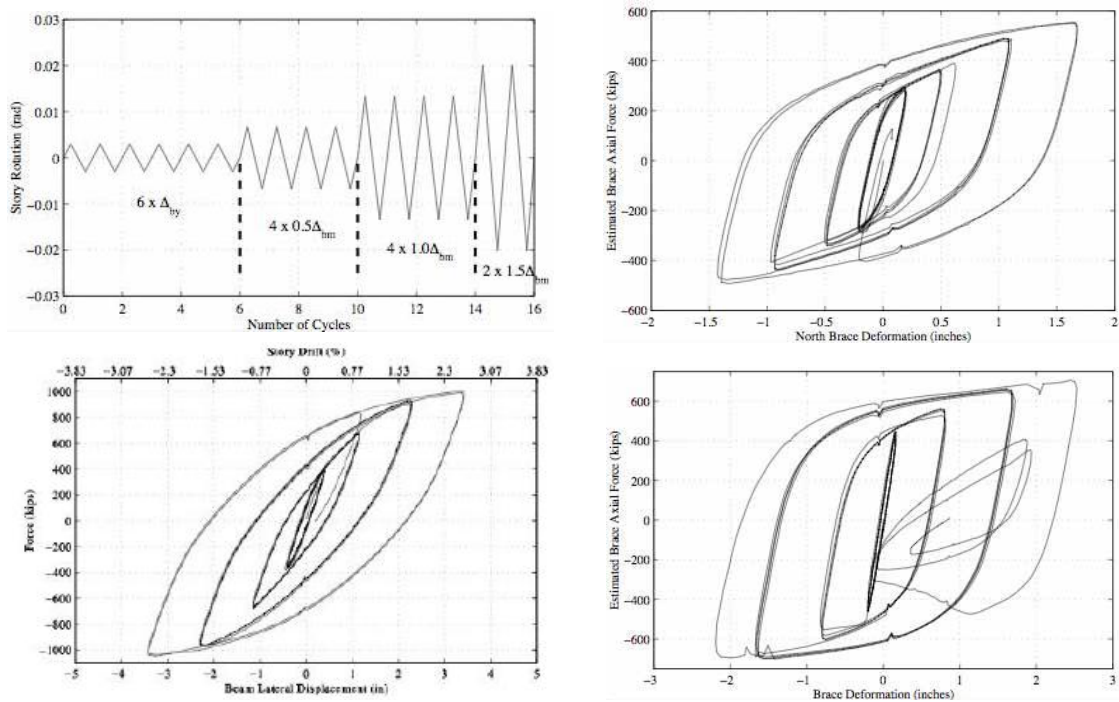


Figure 108. Brace Hysteretic Behavior : loading Protocol (top left), Test 1 (top right), Test 2 (bottom left), Test 3 (bottom right) [3]

The results of test 1 and test 2 shows a stable and repeatable hysteretic loop with a spindle-shape loop also for a drift more than 0.5% higher than the design one. A different behavior presents the Test 3; the beam to column connection developed a transverse crack that continued to extend during the remainder test. The un bonded brace shows a good behavior up to the point of the beam flange fracture but, because of the lateral displacements, the subsequent hysteretic loop of the brace is similar to the conventional one (See Figure 105). The plastic buckling of the brace occurs.

Several tests have been carried out on H shape braces by [4]. To reduce the cost of manufacturing the tube is not filled with any filler material; the external tubes have three different thicknesses of 3 mm, 4 mm, 5 mm. The un constrained length has been varied too, 200 mm and 300 mm long specimens have been considered. The results obtained are shown in Figure 109. Test 1 is the benchmark test of a bar subjected to tension and compression cycles without any restraint. Test 2 and Test 3 are both 200 mm long and are restrained by 3 and 4 mm thicknesses of the tube respectively. Test 4 and Test 5 are both 200 mm long but and are restrained by 4 and 5 mm thicknesses of the tube respectively and have a core end reinforcement. Test 6 and 7 are 300 mm long, the tube is 4 and 5 mm thick respectively and have core end reinforcement. The results are shown in Figure 109.

The results show that Test 1 fails by buckling at the first compressive loading cycle and presents the typical buckling of a conventional brace. Increasing the thickness of the tube, the axial load resisting capacity increase too; the higher thickness provides a higher bending stiffness and

strength of the external tube. All the tests present a buckling behavior after a certain number of cycles; a higher number of stable cycles are obtained increasing the restraining capacity. For economy the thickness of tube has to be optimized depending on the prevision of stress of the brace.

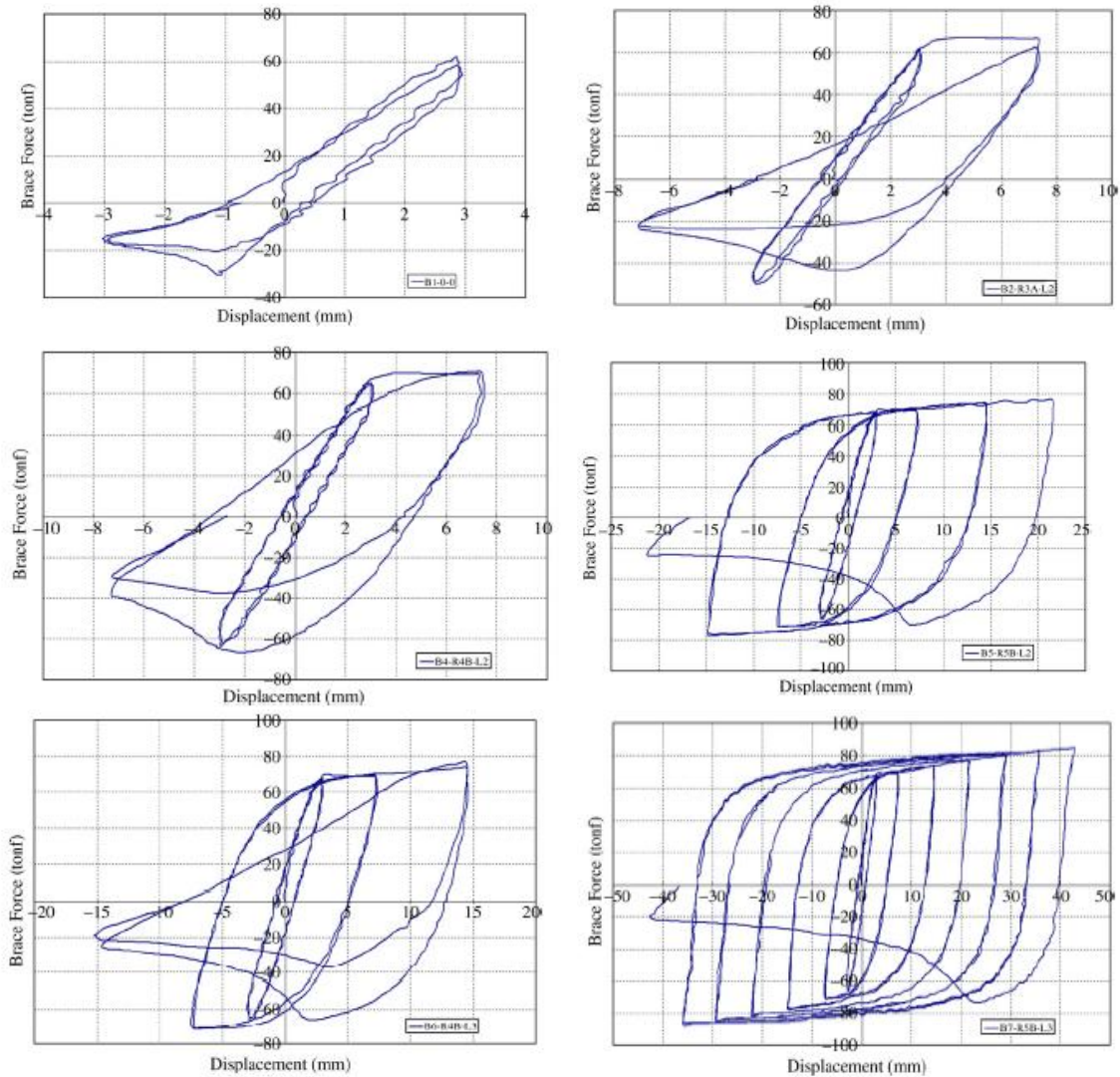


Figure 109 Load Displacement Relation of Test Specimens: Test 1 (top left), Test 2 (top right), Test 3 (middle left), Test 4 (middle right), Test 5 (bottom left), Test 6 (bottom right).

Different analyses have been carried out to study the behavior of BRB by considering different covering types include steel tube, PVC pipes, and FRP rolled sheets. Four specimens have been tested: the core of the first test was only covered by concrete without any covering; the other tests were covered by steel, FRP and PVC respectively.

The results are shown in Figure 110.

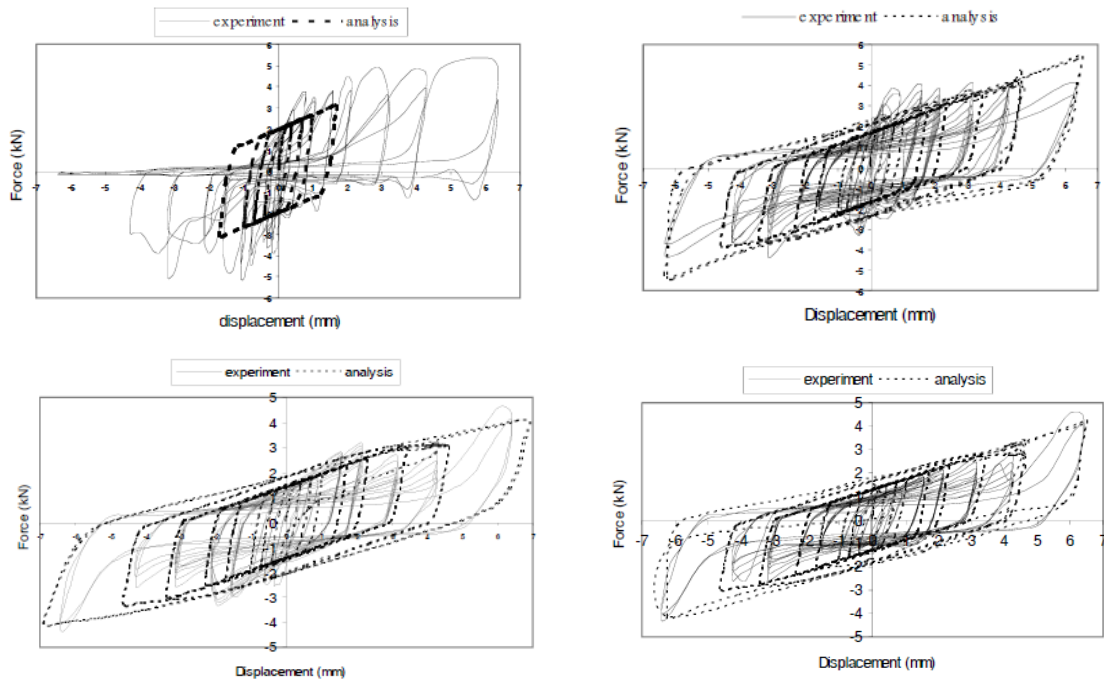


Figure 110. Experimental and Analytical Cyclic Response: Test 1 (top left), Test 2(top right), Test 3 (bottom left), Test 4 (bottom right) [5]

The hysteretic loop of the specimen whose core was only covered by concrete without any covering was irregular after few cycles presenting different behaviors in tension and compression. The reason is the low tensile strength of the concrete that cracked after few cycles. The other specimens present fairly identical behavior in tension and compression. The covering layer (steel or FRP or PVC) prevented the bracing from buckling guaranteeing a similar behavior in tension and compression [5].

The results of different tests have been presented and are useful to understand and delineate the general behavior of the buckling restrained braces. If properly designed, the BRB show a very stable behavior characterized by a hysteresis loop with spindle-shape. The BRB, after a reasonable number of cycles depending on the properties of the brace and the schedule drift, can fail. The failure is for rupture or, most often, for plastic buckling. A stocky brace will be subjected to a rupture due to the low cycle fatigue; a slender brace (that is the common case) will fail for plastic buckling for low cycle fatigue as well. Depending on the characteristics of the brace three different failure modes can happen:

- the brace is very slender or there is no confinement (or is not providing enough stiffness): the behavior is described by a Remennikov Steel Brace hysteresis loop.
- the brace is stocky: the behavior is described by a Ramberg- Osgood Hysteresis Loop that consider the low cycle fatigue of the brace
- the brace is quite slender and properly confined: the behavior is described by a Ramberg Osgood Hysteresis Loop for a certain number of cycles; the brace yield in both tension and compression. A plastic buckling occurs when the brace is not able to reach anymore

the yielding value. From this point a second loop describe better the behavior of the dissipator: the steel buckling hysteresis loop [6, 7]

Case 1: Buckling restrained brace not properly designed/ Conventional Brace
Remennikov Hysteresis Loop

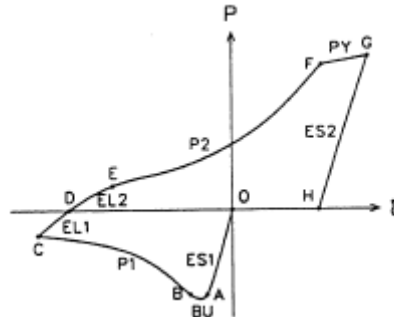


Figure 111. Steel Buckling Hysteresis Rule

Case 2: Buckling Restrained Brace properly confined:
Ramberg- Osgood Hysteresis Loop for a certain number of cycles then two types of failure might occur: plastic buckling failure or failure due to low cycle fatigue.

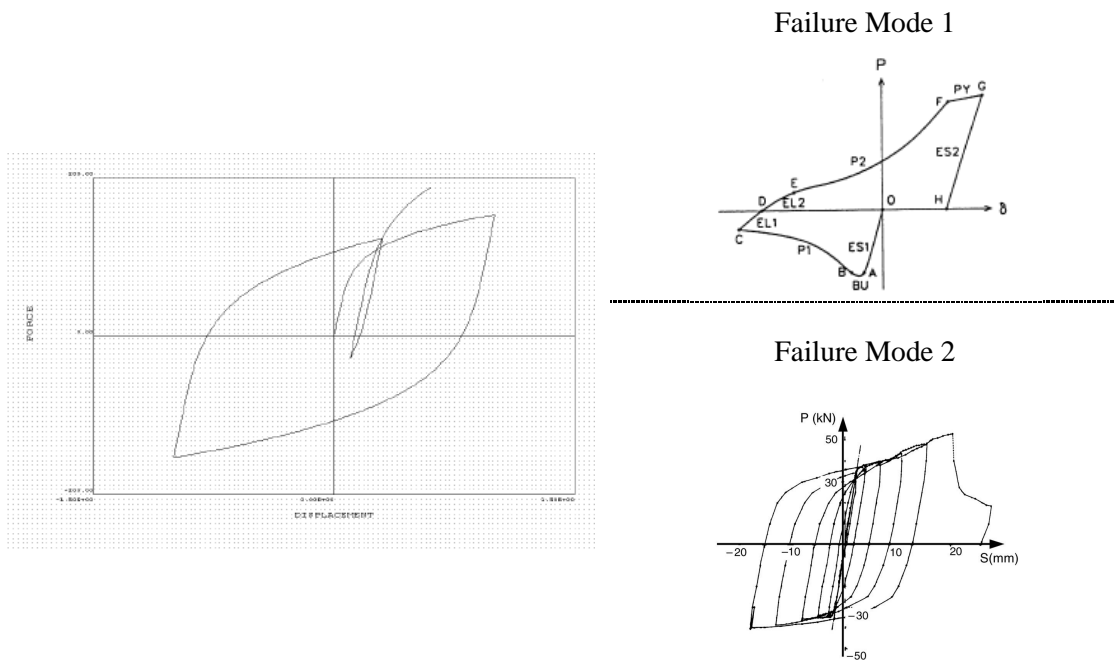


Figure 112. Different Failure modes of the brace: Plastic buckling (top right), Fatigue Failure mode (bottom right).

The global loop can be split in two different loops describing the behavior of the brace pre and post plastic buckling. A Ramberg-Osgood hysteresis [8] is able to describe the pre-buckling behavior while the Remennikov Steel Brace Hysteresis ([6], [7]) is appropriate to describe the buckling and post buckling behavior.

4.3 References

1. Ung, C.M., *Research and Application of Buckling Restrained Braces Frames*. Steel structures, 2004: p. 13.
2. Qiang, X., *State of the art of buckling-restrained braces in Asia*. Journal of Constructional Steel Research, 2005. **61**(6): p. 727-48.
3. MAHIN, S., et al., *SEISMIC PERFORMANCE OF BUCKLING RESTRAINED BRACED FRAME SYSTEMS*, in *13th World Conference on Earthquake Engineering*. 2004: Vancouver, Canada.
4. Ju, Y.K., et al., *Component tests of buckling-restrained braces with unconstrained length*. Engineering Structures, 2009. **31**(2): p. 507-516.
5. Rahai, A.R., M.M. Alinia, and S.M.F. Salehi, *Cyclic Performance of Buckling Restrained Composite Braces Composed of Selected Materials*. International Journal of Civil Engineering, 2009. **7**.
6. Remennikov, A.M.W., Warren R., *Analytical prediction of seismic behaviour for concentrically braced steel system*, in *EARTHQUAKE ENGINEERING AND STRUCTURAL DYNAMICS*. 1997. p. 859-874.
7. Remennikov, A.M., *Modelling the inelastic cyclic behaviour of a bracing member for work-hardening material*. International Journal of Solids and Structures, 1997. **34**(27): p. 3491-3515.
8. Carr, A.J., *Ruamoko Programme for Inelastic Dynamic Analysis - User Manual*. 2007, University of Canterbury, Christchurch.
9. Lopez, W.A. and R. Sabelli, *Seismic Design of Buckling-Restrained Braced Frames*. 2004.
10. Timothy R. Eckert, P.E., *Effect of modifying braces slenderness in concentrically braced frames*. 2009.
11. Kardomateas, G.A. and D.S. Dancila, *Buckling of moderately thick orthotropic columns: Comparison of an elasticity solution with the Euler and Engesser/Haringx/Timoshenko formulae*. International Journal of Solids and Structures, 1997. **34**(3): p. 341-357.

5 Plug and Play Hysteresis Loop

The study that follows is focused on the determination of all the parameters needed to modify the Remennikov Hysteresis Loop and to adapt it to the case of Plug and Play dissipators.

The Remennikov Hysteresis Loop is designed to represent the out of plane buckling of steel brace but there is no possibility to introduce the condition of an elastic restraint on the buckling.

The effect of the confinement is investigated with different methods in order to determine a general equation in function of the material and thickness of the filler material and of the outer diameter of the tube.

The presence of the confinement guarantee a higher value of critical load compared to the solution with the only bar, providing an increasing of stiffness or a decreasing of equivalent length.

5.1 Physical Model of the Dissipator

The Plug and Play dissipator is realized with a steel bar encased inside a steel tube filled with grout or epoxy.

The external device can be modeled in Ruaumoko as a beam element representing the bar and several spring elements modeling the restraint. The spring of the filler material and of the tube can be in series or the tube can be represented as a restraint as far as the grout/epoxy has still sufficient stiffness (See 5.4.1 The Effect of the Tube).

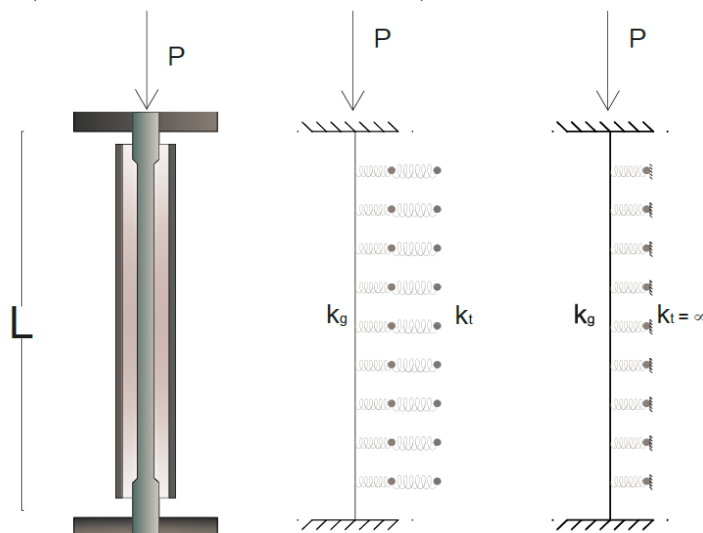


Figure 113. Dissipator and model of the dissipator

The spring elements have to be defined by at least two nodes; the node implies a division of the bar in several beam elements. Considering that the Remennikov Hysteresis Loop [1, 2] requires the value of the effective length parameter, if the bar is split in several parts the analysis is carried out considering not the effective length of the entire beam element but of all the single parts that compose the bar.

The new hysteresis loop tries to solve this modeling problem considering the bending moment at the cross section with the contribution of all the elements, bar, tube and filler material.

An additional information that will be available using the new hysteresis loop for external dissipator is the lateral displacement of the bar at the mid length. This function is introduced as an item of the spring without the need to insert a node that would involve the division of the beam as already explained.

5.2 Overall Buckling Criterion for Buckling Restrained Dissipators

The Plug and Play dissipator have to be analyzed as a composite system of a bar confined by a filler material encased in a steel tube.

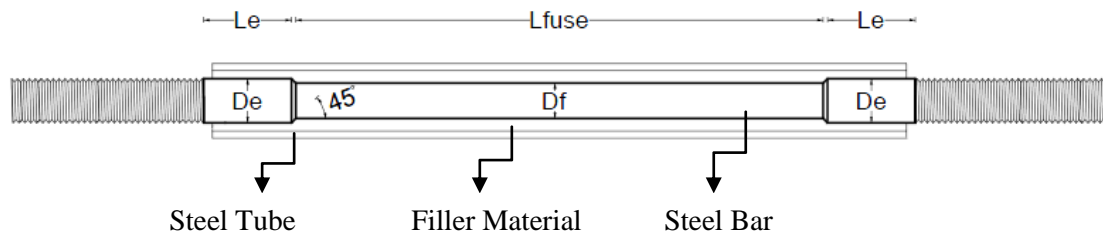


Figure 114. Detail of the Plug and Play Dissipators

The deformation of the grout/epoxy encased bar is sinusoidal [3] and can be expressed as:

$$\omega = \delta \sin \frac{\pi x}{l} \quad (5.1)$$

δ is the deflection in the midspan.

Assuming that the deflections of the bar and of the grout/epoxy are the same, the lateral distributed force in the grout/epoxy can be written as:

$$p = \frac{\pi^4}{L^4} \omega E_r I_r = \frac{\pi^4}{L^4} E_r I_r \delta \sin \frac{\pi x}{l} \quad (5.2)$$

Where:

$E_r I_r$ is the flexural stiffness of the restrain.

The bending moment at the cross section can be written as:

$$M(x) = -R(x) + \int_0^x p x dx + N\omega \quad (5.3)$$

$M(x)$ is the bending moment at the cross section;

R is the reaction in the hinge

x is the distance from the hinge to the calculation cross section

N is the axial force.

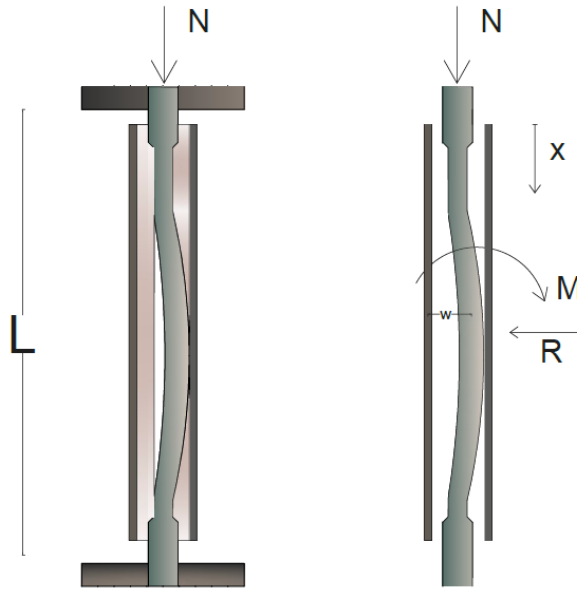


Figure 115. Analysis on a Dissipators, Force in the System

$$M(x) = -\sigma Ax + \int_0^x p x dx + N\omega = -\frac{M}{w} A x + \int_0^x p x dx + N\omega \quad (5.4)$$

$$\underbrace{\hspace{1.5cm}}_{\text{Tube contribution}} \underbrace{\hspace{1.5cm}}_{\text{Grout/epoxy encased bar contribution}} \underbrace{\hspace{1.5cm}}_{N = \frac{\pi^2}{L^2} (E_s I_s + E_r I_r)}$$

The critical value of force is function of the stiffness of the steel bar and the stiffness of the restrain. Assuming that the epoxy/grout has the same deflection of the steel bar, they can be considered as a single layer subjected to an axial force. The tube should not be considered in the determination of the critical load because is not subjected to an axial force but, confining the epoxy/grout, provide an additional stiffness that has to be considered. For these reasons the stiffness of the restrain is not the sum of the stiffnesses of the grout/epoxy and of the tube but it is a percentage of that value.

$$N = \frac{\pi^2}{L^2} (E_s I_s + \alpha E_r I_r) \quad (5.5)$$

The study that follows considered different ways to determine the effect of the confinement on the critical value of load.

5.3 The Effect of the Confinement

The confinement helps to avoid the buckling in compression and to allow the specimen to dissipate the same amount of energy as in tension as in compression. The tube is not subjected to the axial force but, confining the filler material, it contributes to the anti-buckling system.

The grout/ epoxy will deteriorate when the bar buckles. As long as the dissipator buckles in compression, the filler material is subjected to an increasing pressure. When the tension force is applied, the deflection of the bar reduces and the filler material can detach from the bar. If this happens there will be a gap between the bar and the filler material. Different cycles of tension and compression involve the decreasing of the stiffness of the material due to the reduction of its thickness. This phenomenon can happen if the material is stressed over its elastic limit and there is a residual deformation.

After some cycles of compression the specimen will have a deflection equal to the thickness of the filler material that is not working anymore and the tube is the only one that resists.

The system of the bar with confining material and the respective model with two different springs representing the grout/epoxy and the confining tube are shown in the figure below.

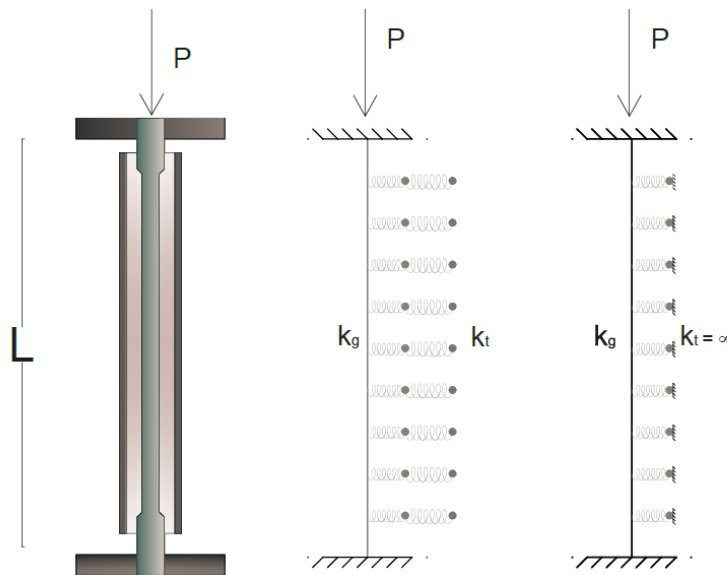


Figure 116. Dissipator and model of the dissipator

The tube can be assumed as a confinement of the grout and it starts working only when the steel bar starts pushing it. For this reason the spring that models the tube can also be replaced by a fully fixed restraint till when the deflection of the bar reaches the thickness of the filler material and so the length of the spring in the model.

Considering that the dissipator is subjected to tension and compression forces, a “step by step” analysis with the investigation of the buckling behavior for each value of load considered is carried out. The object is to define a simplified model for the most significant steps of a push pull test.

- *Step 1: $P < P_{cr}$*

The dissipator is compressed by a force smaller than the critical value, so the bar is supposed to remain straight considering the ideal situations. The straight form of elastic equilibrium is stable; the force produces a small deflection that disappears when the force is removed.

The grout confined by the tube gives an important contribution to the stability of the structure. The tube can be modeled as a fixed restraint because is not interested by any deformation for this value of force.

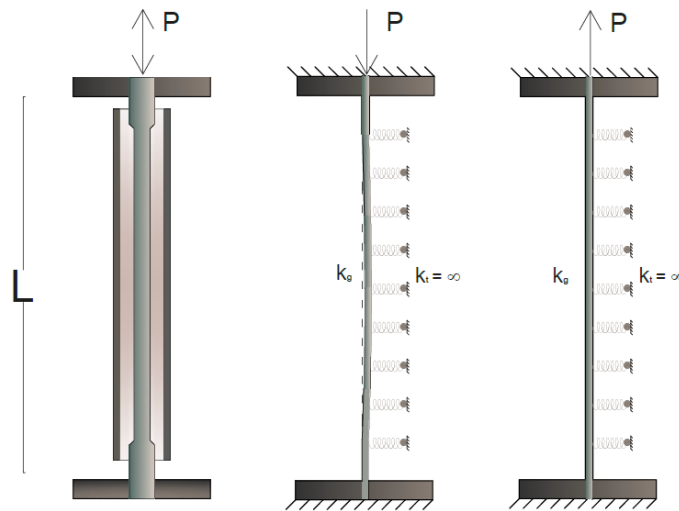


Figure 117. Dissipator and Model of the Dissipator for $P < P_{cr}$

- *Step 2: Compression with a value of $P \approx P_{cr}$*

If P gradually increases, a condition will be reached in which the straight form of equilibrium becomes unstable and a small lateral force will produce a deflection which does not disappear when the lateral force is removed.

The filler material is subjected to a pressure from the bar that buckles; this pressure is not uniform but more concentrated at the mid length. This pressure might cause a permanent deformation in the material that means a decreasing of thickness of the layer and of the stiffness consequently.

The model that best describes this situation is bar confined with a series of spring fixed at one end modeling the grout/epoxy. The stiffness of the spring is the one of the entire confinement (filler material restrained by the tube)z and can be estimated studying the displacement of two layers in their shape (pipe) when subjected to a unitary force applied at the mid length (Figure 125).

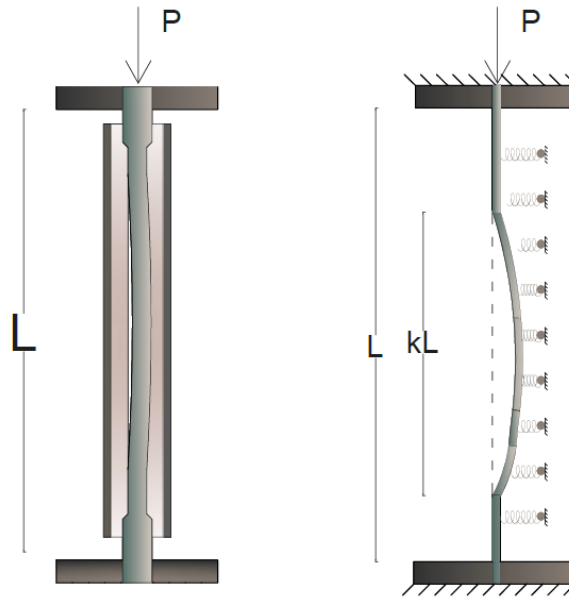


Figure 118. Dissipator and Model of the Dissipator for $P \approx P_{cr}$

- *Step 3: Tension with a value of $P \approx P_{cr}$*

Once that the compression force is removed the specimen still has a residual deformation as the critical value has been exceeded in compression. When a tension force is applied the dissipator tries to go back to the straight position, but, due to the permanent deflection, the shape of the deformation is slightly spiky at the mid length. Depending on the characteristics of the filler material it detaches from the bar and the two elements start having different deformations. For this reason a possible gap between the bar and the grout/epoxy might develop.

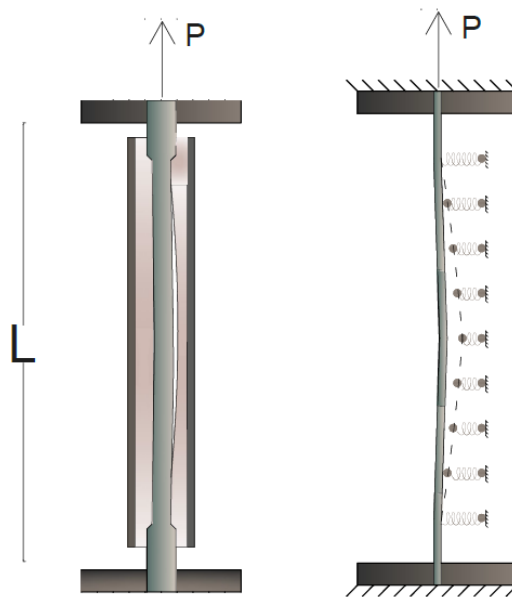


Figure 119. Dissipator and Model of the Dissipator for $P \approx P_c$

Step 4: Compression with a value of $P > P_{cr}$

At this stage the dissipator is compressed with a force higher of the critical value. The filler material might be no more attached to the specimen and there could be a gap between them. For this reason the bar will deflect without finding any resistance at the beginning until bar will start pressing again the epoxy/grout. The stiffness of the confinement is becomes smaller and smaller with the increasing of the gap. The value of the gap depends on the number of cycles and on the force applied.

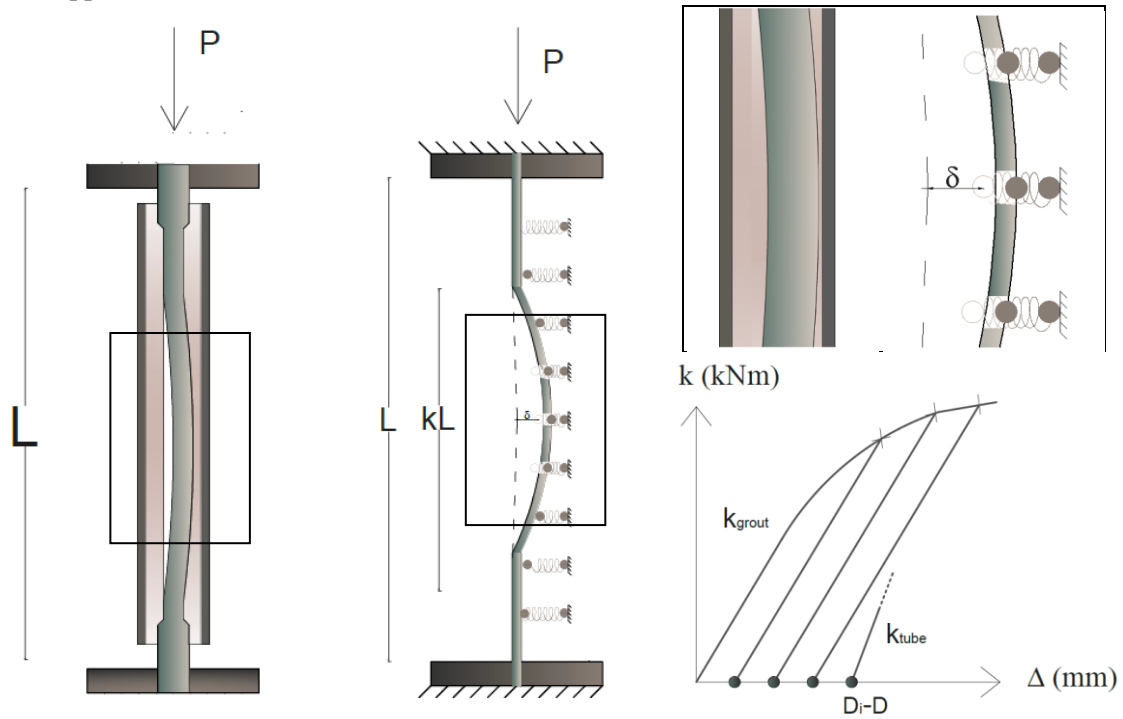


Figure 120. Dissipator and Model of the Dissipator for $P > P_{cr}$ (left), Detail of the Mid Length of the Dissipator (top right), Force – Displacement of the filler material

- *Step 5: Tension with a value of $P > P_{cr}$*

When a tension force is applied the dissipator shows the same deformed shape has already described in the step 3 but it will get spikier at the mid length increasing the lateral displacement.

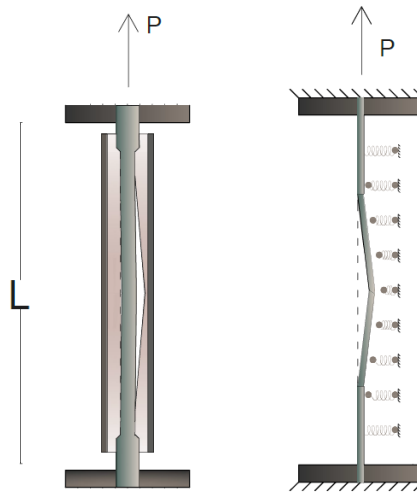


Figure 121. Dissipator and Detail of the Dissipator for $P > P_{cr}$

- *Step 6: Compression with a value of $P > P_{cr}$*

A higher value of compressive force is now applied. The springs modeling the filler material are now completely pressed in the central area and so their stiffness can be assumed as zero. At the end of the bar the springs are still working because the stresses are smaller. The dissipator can now deflect at the mid length without any resistance from the grout and so it pushes the tube. The tube provides additional stiffness and it is now modeled as a spring because its stiffness can not be assumed anymore as infinite.

The equivalent model is thus realized with the springs of the grout/epoxy that still provide resistance at the end parts of the rods, while in the center their stiffness is zero. A second spring in series is added in the most stressed part of the bar to describe the tube.

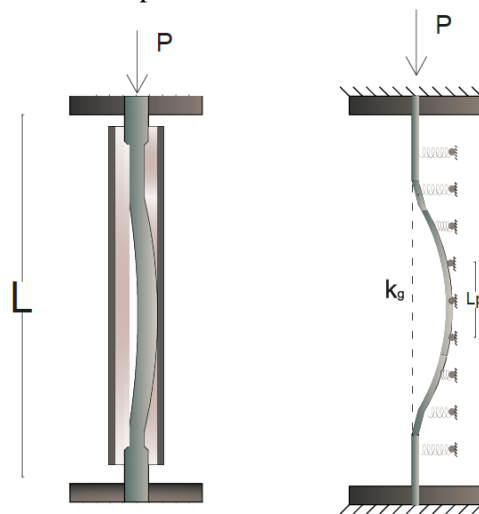


Figure 122. Dissipator and Detail of the Dissipator for $P > P_{cr}$

5.4 Buckling of a Bar on Elastic Supports

An approximate calculation of the critical load can be obtained with the Energy Method [4]. The solution presented by Timoshenko is for a bar on an elastic foundation; the same method can be adopted assuming the epoxy/grout as an elastic continuum.

If α is the stiffness of the individual support and a is the distance between them, the rigidity of the equivalent elastic medium is expressed by the quantity:

$$\beta = \alpha/a$$

The general expression for the deflection curve of a bar with hinged ends can be represented by a series:

$$y = a_1 \sin \frac{\pi x}{L} + a_2 \sin \frac{2\pi x}{L} + a_3 \sin \frac{3\pi x}{L} + \dots \quad (5.6)$$

The bending strain energy of the bar is:

$$\Delta U_1 = \frac{EI}{2} \int_0^l \left(\frac{d^2 y}{dx^2} \right)^2 dx = \frac{\pi^4 EI}{4l^3} \sum_{n=1}^{n=\infty} n^4 a_n^2 \quad (5.7)$$

The lateral reaction on an element dx of the bar is $\beta y dx$ and the corresponding energy is $(\beta y^2/2) dx$.

The total energy of deformation of the elastic medium is:

$$\Delta U_2 = \frac{\beta L}{4} \sum_{n=1}^{n=\infty} a_n^2 \quad (5.8)$$

The work done by the compressive forces P is:

$$\Delta T = \frac{P\pi^2}{4l} \sum_{n=1}^{n=\infty} n^2 a_n^2 \quad (5.9)$$

Considering that: $\Delta U_1 + \Delta U_2 = \Delta T$, P can be evaluated as a function of a_1, a_2, \dots

The deflection curve of the bar can be assumed as a sine curve:

$$y = a_m \sin \left(\frac{m\pi x}{l} \right) \quad (5.10)$$

The critical load is then defined:

$$P = \frac{\pi^2 EI}{l^2} \left(m^2 + \frac{\beta l^4}{m^2 \pi^4 EI} \right) \quad (5.11)$$

Where m is an integer number of half waves in which the bar subdivides when buckles. The lowest critical load may occur with different values of m depending on the values of the other constants.

The value of m is determined iteratively increasing at every step the value of β .

To find the number of β at which the number of half waves changes from m to $m+1$, the following equation is used:

$$\frac{\beta l^4}{\pi^4 EI} = m^2(m+1)^2 \quad (5.12)$$

For a given dimension of the bar and for a given value of b , this equation can be used for determining m , the number of half waves.

Once that m is known, it can be substituted in the formula of the critical load to find its value (See Eq. $\frac{\beta l^4}{\pi^4 EI} = m^2(m+1)^2$)

The formula of the critical load can also be written using a reduced length (L) that keeps into account the effect of the restrain:

$$P_{cr} = \frac{\pi^2 EI}{L^2} \quad (5.13)$$

Considering a confined bar the solution shows that increasing the load the number of half waves increases too (Figure 123).

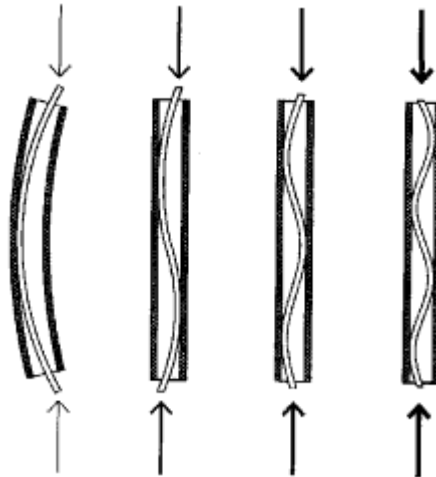


Figure 123. Deformation of a Column with Increasing Load [5]

5.4.1 The Effect of the Tube

The external tube has a stiffness that is higher than the one of the filler material in both cases of grout and epoxy. An analysis using Ruaumoko 2D [6] is carried out to define whether the steel tube can be approximated as a fully fixed joint that means that its deformation is irrelevant compared to the one of the filler material.

Two different springs in series are considered, one with the stiffness of the grout/epoxy and one with the stiffness of the tube.

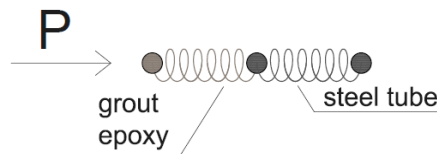


Figure 124. Two Springs in series modeling the grout/epoxy and the steel tube

The stiffness value that have to be assigned to the springs are calculated with a finite element model using Sap 2000 [7]. Different pipes modeling the grout, the epoxy and the tube are considered to evaluate the stiffness of the different layers. The pipe is fixed at one end and free to roll on the plane when subjected to a distributed force at one end.

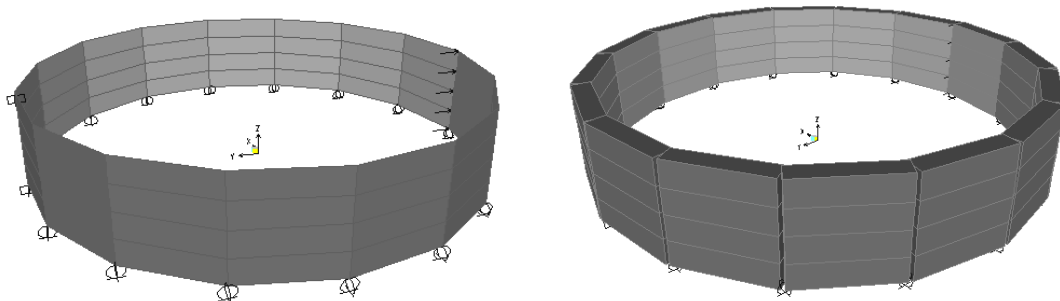


Figure 125. Sap Model of the Confinement subjected to a force in the Y axis

Firstly, the worst case is considered, so the smallest thickness and the highest external diameter of the tube. The most used thicknesses are 2, 3, 4, 5 mm and the outer diameter is usually between 20/25 mm to 50 mm depending on the bar diameter and thickness of the confinement. By increasing the external diameter the displacement is getting higher and higher; then worst situation is so the one with outer diameter of 50 mm and thickness of the tube of 2 mm. If for this case the tube can be considered as a restrain, all the more so will be for all the other cases.

The results of the static analysis show that the displacement of the second node is approximately 1/100 of the displacement of the first node if the filler material is epoxy. This means that to assume the tube as a restrain is a valid approximation. Considering then that the maximum

displacement of the bar is less than 1 cm the tube's displacement will be at the most 0.1 mm and then negligible.

The grout is stiffer than the epoxy and in this case the displacement of the tube when subjected to an axial force is 1/10 the one of the grout. For the same reason exposed above the tube will be considered as restrain.

5.4.2 Critical Load of Bars on Elastic Supports

Considering now a case study of a dissipator of 20 mm of diameter confined with a layer of epoxy and a steel tube, the reduce length can be evaluated; consequently the critical value for different lengths of the bar and different thicknesses of the confinement ensues.

Four different thicknesses and six different lengths are considered:

s_{epoxy} (mm)	2	4	6	8		
L (mm)	300	400	500	600	700	800

In order to evaluate the stiffness of the confinement a "slice" of the dissipator is considered but without the steel tube. This slice is fixed at one end at free to roll on the plane when subjected to a force F. In this way known the displacement of the node the value of stiffness of the confinement is obtained.

A sketch of the model is shown in the figure below.

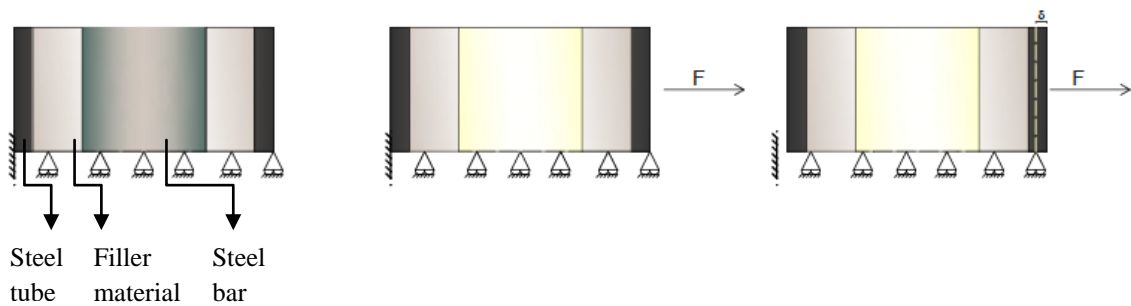


Figure 126. "Slice" of the Confinement subjected to a force F

The displacements due to a 1 kN force are shown in the table below.

s_{grout} (mm)	δ (m)	k_{system} (kN/m)	β (kN/m ²)
2	0.00052	1895.38	189537.5
4	0.00041	2408.48	240847.8
6	0.00029	3362.47	336247.5
8	0.00020	4943.15	494315.4

Table 14. Unitary Values of Stiffness of a "Slice" of Dissipator

For the different values of length of the bar, the number of half sine waves and the value of the critical load are calculated.

1) $L = 300$, P_{cr} without restrain: 172 kN

s_{grout} (mm)	β (kN/m ²)	$\beta l^4/\pi^4 EI$	m	P _{cr} (kN)	L/l
2	189537.53	10.03	2	356.86	0.39
4	240847.78	12.75	2	394.10	0.37
6	336247.48	17.80	2	463.33	0.34
8	494315.37	26.17	2	578.03	0.31

The reduce length L for the bar is:

$\beta l^4/\pi^4 EI$	10.03	12.75	17.80	26.17
L/l	0.3920	0.3730	0.34401	0.30799

Table 15. Critical Value of a L = 300 mm Dissipator

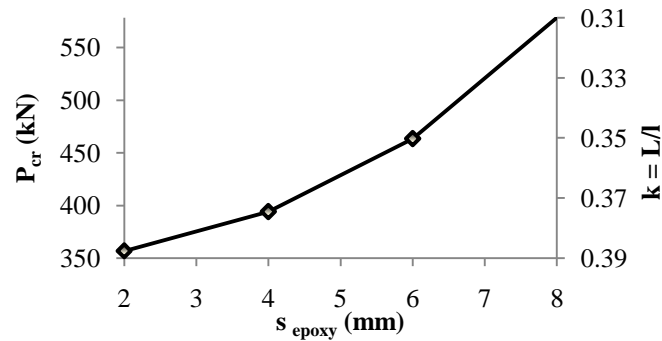


Figure 127. Critical Load and Effective Length Factor versus Thickness of the Confinement

2) $L = 400$, P_{cr} without restrain: 97 kN

s_{grout} (mm)	β (kN/m ²)	$\beta l^4/\pi^4 EI$	m	P _{cr} (kN)
2	189537.52	31.71	2	367.88
4	240847.78	40.30	2	434.07
6	336247.47	56.26	2	557.15
8	494315.37	82.70	2	761.06

The reduce length L for the bar is:

$\beta l^4/\pi^4 EI$	31.71	40.30	56.26	82.70
L/l	0.29	0.26	0.23	0.20

Table 16. Critical Value of a L = 400 mm Dissipator

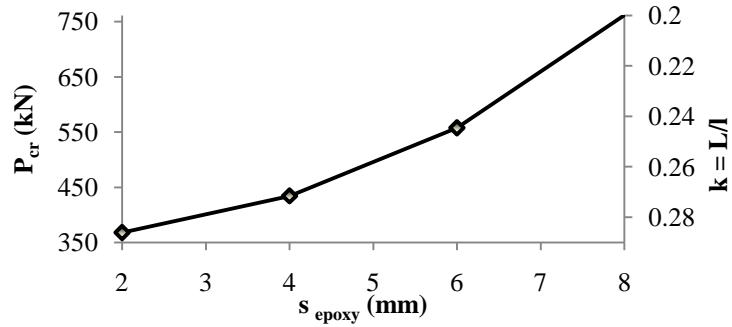


Figure 128. Critical Load and Effective Length Factor versus Thickness of the Confinement

3) $L = 500$, P_{cr} without restrain: 62 kN

s_{grout} (mm)	β (kN/m ²)	$\beta l^4/\pi^4 EI$	m	P _{cr} (kN)
2	189537.52	77.42	3	347.4
4	240847.78	98.38	3	393.42
6	336247.47	137.35	3	478.88
8	494315.37	201.91	3	620.49

The reduce length L for the bar is:

$\beta l^4/\pi^4 EI$	77.42	98.38	137.35	201.91
L/l	0.24	0.22	0.20	0.18

Table 17. Critical Value of a $L = 500$ mm Dissipator

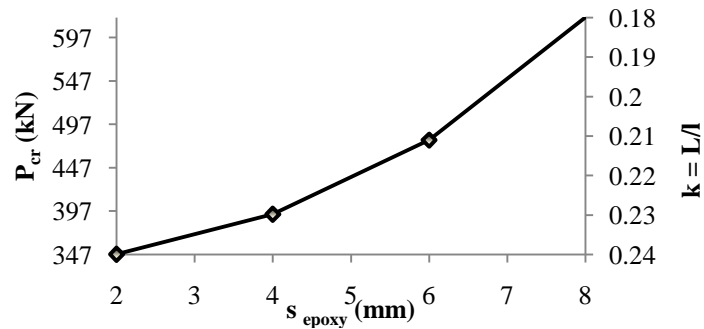


Figure 129. Critical Load and Effective Length Factor versus Thickness of the Confinement

4) $L = 600$, P_{cr} without restrain: 43 kN

s_{grout} (mm)	β (kN/m ²)	$\beta l^4/\pi^4 EI$	m	P _{cr} (kN)
2	189537.53	160.54	3	367.89
4	240847.78	204.00	4	394.10
6	336247.48	284.80	4	463.33
8	494315.37	418.69	4	578.03

The reduce length L for the bar is:

$\beta l^4/\pi^4 EI$	160.54	204.00	284.80	418.69
L/l	0.19	0.19	0.17	0.15

Table18. Critical Value of a L = 600 mm Dissipator

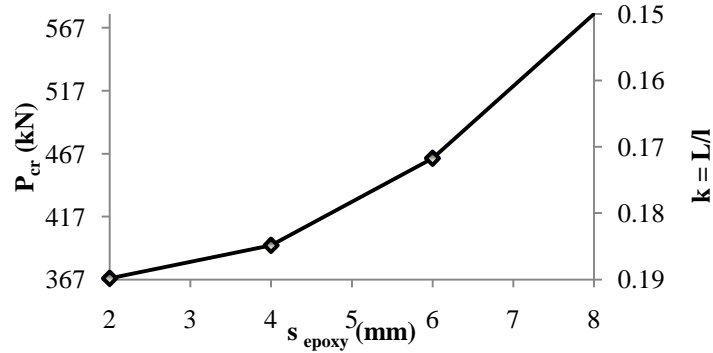


Figure 130. Critical Load and Effective Length Factor versus Thickness of the Confinement

5) $L = 700$, P_{cr} without restrain: 32 kN

s_{grout} (mm)	β (kN/m ²)	$\beta l^4/\pi^4 EI$	m	P _{cr} (kN)
2	189537.52	297.42	4	348.34
4	240847.78	377.93	4	399.02
6	336247.47	527.63	4	493.24
8	494315.37	775.67	5	564.24

The reduce length L for the bar is:

$\beta l^4/\pi^4 EI$	297.42	377.93	527.63	775.67
L/l	0.17	0.16	0.14	0.13

Table 19. Critical Value of a L = 600 mm Dissipator

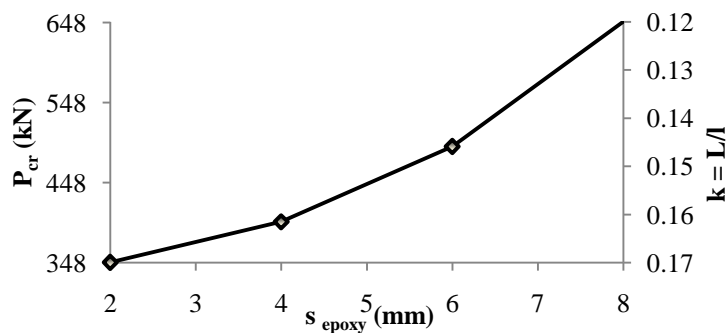


Figure 131. Critical Load and Effective Length Factor versus Thickness of the Confinement

6) $L = 800$, P_{cr} without restraint: 24 kN

s_{gROUT} (mm)	β (kN/m ²)	$\beta l^4/\pi^4 EI$	m	P_{cr} (kN)
2	189537.53	507.38	4	367.89
4	240847.78	644.74	5	391.62
6	336247.48	900.12	5	470.38
8	494315.37	1323.26	6	561.00

The reduce length L for the bar is:

$\beta l^4/\pi^4 EI$	507.38	644.74	900.12	1323.26
L/l	0.14	0.14	0.13	0.12

Table 20. Critical Value of a $L = 600$ mm Dissipator

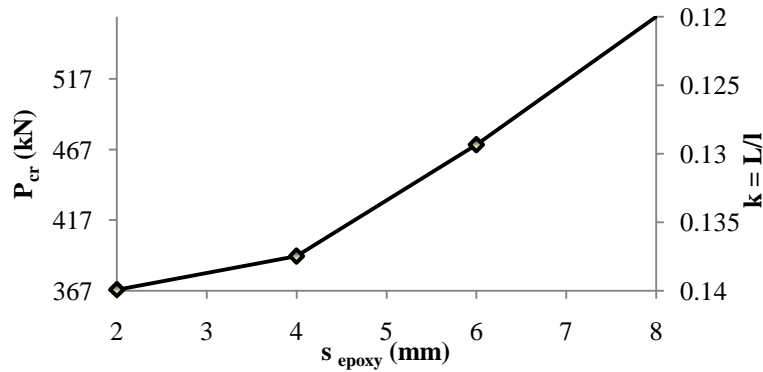


Figure 132. Critical Load and Effective Length Factor versus Thickness of the Confinement

The ratio of the reduce length and the total length in function of the length of the dissipator and of the thickness of the epoxy is shown in the graph below.

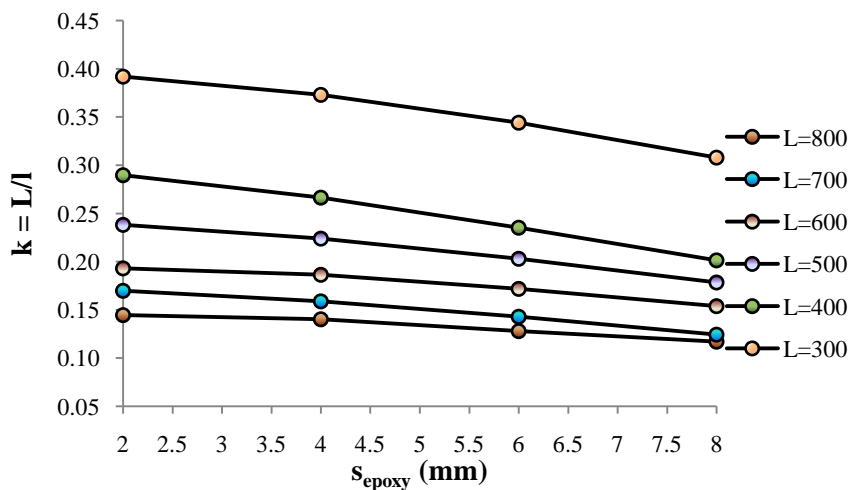


Figure 133. Graph of Effective Length Factor versus Thickness of the Epoxy

The critical value obtained for each length at the different thickness of the epoxy is shown in the figure below.

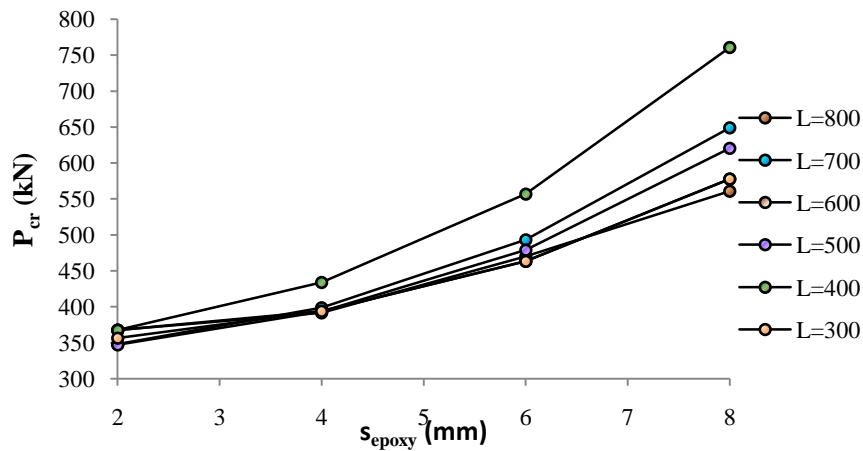


Figure 134. Graph of Critical Load versus Thickness of the Epoxy

The presence of the confinement is significant in order to obtain a higher value of critical load. Increasing the thickness of the epoxy, the reduce length become smaller and smaller while the critical value increases.

The effect of the thickness is more significant in the case of shorter specimen and become less important increasing the length of the specimen. The reason is that, increasing the value of β , the number of half sine waves raises, so the dissipator buckles different times along its length. Consequently the lateral displacement is smaller.

As β increases, the number of half sine waves also increases because the bar is so confined that it can only have a small deflection.

Without the confinement the dissipator will buckle in theory at the mid length; adding the confinement the static scheme of the bar changes and the bar behaves like a simply supported beam. To a higher stiffness corresponds a higher number of supports, a smaller effective length and, consequently, a higher number of half sine waves.

5.5 Finite Element Analysis

The same analysis is now carried out with the finite element program SAP 2000 [7]. The only way to have buckling is to give an eccentricity to at least one node. This means that the buckle mode is in a certain way “chosen”. The Timoshenko analysis has shown that the number of half waves increases with the length of the dissipator. Increasing the number of half waves the effective length and then the deflection become smaller and smaller. As a result a simplified analysis that assumes that the dissipator buckles in the middle is conservative because a higher effective length is used to calculate the critical load obtaining so a smaller value of it.

The length L of the dissipator is the distance between the supports. When subjected to an axial force the bar starts buckling and the two half parts of the beam are symmetric about their midpoints. These are points of inflection where the bending moment is zero. This means that the portion between these two points of the column behave as a pin ended column.

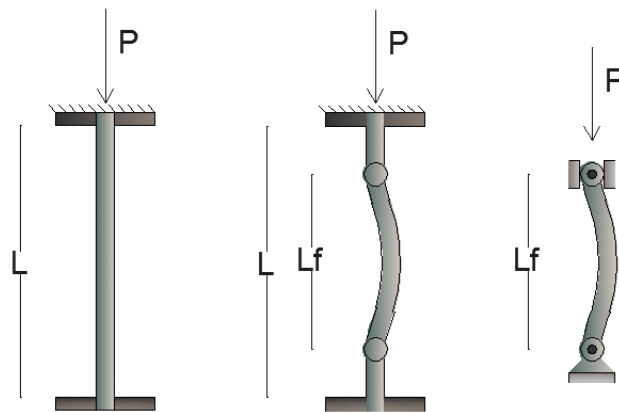


Figura 135. Fully Fixed Column Supporting a Load P

Considering that all the deformations occur in the fused part because the stiffness is lower than in the external ones, the effective length of the column can be assumed as the fuse length of the specimen. For this reason the dissipator has been modeled considering a pin ended column as long as the fuse.

The model used is shown in the picture below.

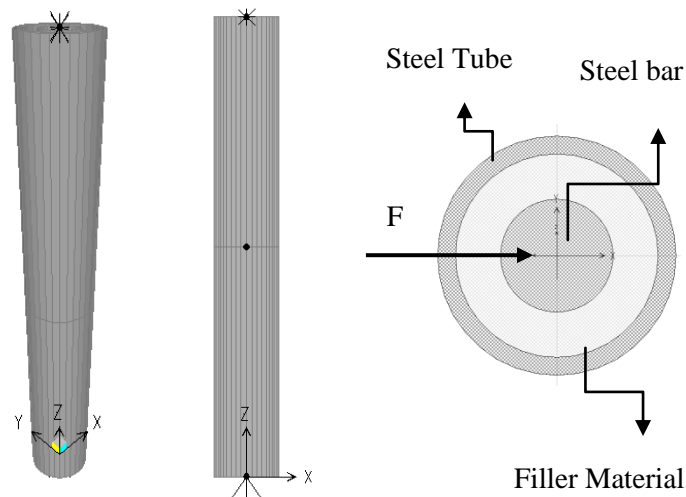


Figure 136. SAP 2000 Model (left) and Section of the model (right)

When the dissipator is subjected to an axial load, a lateral distributed pressure at the cross section will cause the deflection of the section. The maximum deflection occurs at the mid length and can be calculated as the deflection of a pin ended beam subjected to a point load concentrated at the mid length.

$$\delta = \frac{PL^3}{48EI}$$

The model can be simplified with a pin ended beam subjected to a shear force at the mid length. Once the deflection is known the stiffness of the composite system is calculated with the formula of the deflection of pin ended beams.

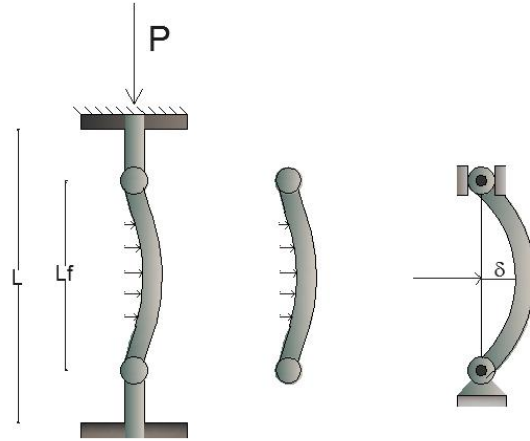


Figure 137. Fully Fixed Column Supporting a load P

The beam object of this study is 300 m long and has a diameter of 20 mm. The filler material and the tube are 8 mm and 3 mm thick respectively.

The elastic moduli are:

$$E_s = 200000 \text{ MPa}$$

$$E_g = 2400 \text{ MPa}$$

$$E_t = 200000 \text{ MPa}$$

The deflection increases directly proportional to the shear force applied, so the force value is not influencing the stiffness value of the composite.

In this example a 1 kN shear force is chosen.

The maximum deflection obtained with the bar without any confinement is:

$$\delta_x = 0.36 \text{ mm}$$

The stiffness of the steel bar is:

$$(EI)_s = FL^3 / (48 \delta) = 1.55 \text{ kNm}$$

This value of stiffness can be checked estimating the stiffness with the formula:

$$(EI)_s = E * \pi * (D^4 / 64) = 1.57 \text{ kNm}$$

The maximum deflection obtained at the mid length is:

$$\delta_x = 0.035 \text{ mm.}$$

The stiffness of the composite system is:

$$(EI)_{\text{comp}} = 16.07 \text{ kNm}$$

$$(EI)_{comp} = (EI)_s + \alpha (EI)_{conf} \quad (5.14)$$

$$(EI)_{comp} = (EI)_{steel} + \alpha (EI)_{conf} \quad (5.15)$$

$$\alpha = \frac{(EI)_{comp} - (EI)_{steel}}{(EI)_{conf}} \quad (5.16)$$

Considering that:

$$(EI)_{steel} = 1.55 \text{ kNm} ,$$

The value of $(EI)_{conf}$ is:

$$(EI)_{conf} = 16.07 - 1.55 = 14.52 \text{ kNm}.$$

The tube and grout stiffness are:

$$\begin{aligned} (EI)_{tube} &= && 15.24 && \text{kNm}^2 \\ (EI)_{grout} &= && 0.18 && \text{kNm}^2 \\ (EI)_{conf} = (EI)_{tube} + (EI)_{grout} &= && 15.42 && \text{kNm}^2. \end{aligned}$$

Once all the values are known, the value of the parameter α that takes in account the additional stiffness provided by the encasing can be obtained.

$$\alpha = 0.94.$$

The formula for estimating the critical value of load in the presence of an additional stiffness compared to the one of the only bar is [8]:

$$P_{cr} = \frac{\pi^2}{(kL)^2} [(EI)_s + \alpha (EI)_{conf}] \quad (5.17)$$

The critical value of load with the additional stiffness provided by the grout and the tube is herein calculated:

$$P_{cr} = 528 \text{ kN}$$

A different way to estimate the critical value is herein reported in order to check the accuracy of the previous method. The effect of the confinement can be seen as an increased value of the critical load or a decreased effective length. Assuming that the confinement has a stiffness that approaches infinite, the static scheme of the beam changes and the effect is that the beam is as supported on simply supported restrains. By increasing the number of restrains, the effective length becomes smaller. The second method is based on the assumption that the stiffness is the same (the one of the unconstrained bar) and the effect of the confinement comes out with a change of the value of the effective length parameter, k .

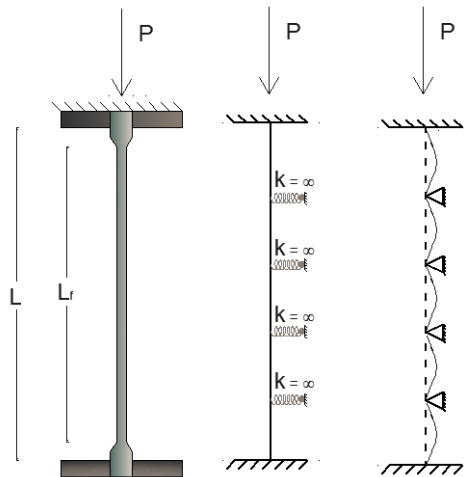


Figure 138. Fully Fixed Restrained Column Supporting a Load P

Also in this case a comparison between the two systems, the unconstrained bar and the confined bar, is carried out. The steel bar is subjected to the critical force and develops a deflection; increasing the force up to reach the same displacement of the confined bar, the effect of the confinement can be investigated..

Considering the bar without confinement the critical load can be calculated with the formula used for the design of steel columns under centric load ([9]) is:

$$\vartheta_{cr} = 0.658^{\vartheta_e} \times \vartheta_y \quad (5.18)$$

Where:

$$\vartheta_e = \frac{\pi^2 E}{\lambda^2} \quad (5.19)$$

λ is the slenderness of the bar and is defined as the ratio between the effective length of the column and the radius of gyration.

The fuse length can be considered as the effective length of the column as all the deformations occur there due to the lower stiffness.

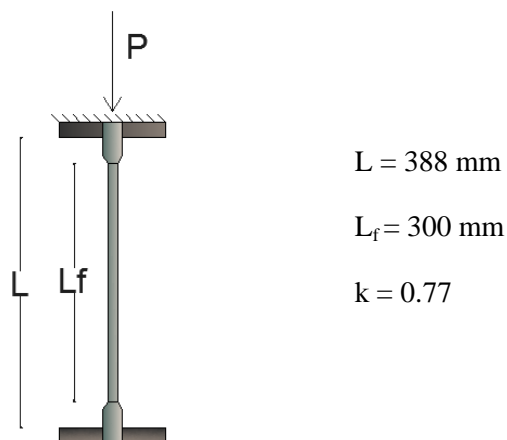


Figure 139. Fully Fixed Column Supporting a Load P

The critical value of force is:

$$F_{cr} = \sigma_{cr} * A$$

$\sigma_y =$	300	MPa
$\sigma_e =$	548.31	MPa
$\sigma_{cr} =$	238.60	MPa
$P_{cr} =$	74.96	kN

When the bar is subjected to the critical value of force, the lateral displacement is:

$$\delta_x = 0.24 \text{ mm.}$$

Considering now the dissipator, approximately the same value of deflection is obtained for 530 kN.

$$\delta_x = 0.25 \text{ mm.}$$

The new critical value is consistent with the one obtained with the previous method.

The critical load is defined as:

$$P_{cr} = \frac{\pi^2(EI)}{(kL)^2} \quad (5.20)$$

The new effective length factor is herein calculated:

$$k = \frac{1}{L} \sqrt{\frac{\pi^2 EI}{P}} \quad (5.21)$$

$$k_1 = 0.44.$$

This means that the new effective length is:

$$L_e = k_1 * L = 170 \text{ mm}$$

And so the confinement has provided a decreasing of the effective length of the 56%.

The results obtained with the two methods gives almost the same results in terms of critical value but compared to the ones calculated using the Energy Method they are slightly higher.

This is due to the fact that the finite element analysis is carried out imposing an initial eccentricity to the node at the mid length and so a way to buckle. On the other hand the method proposed by Timoshenko provides the number of half waves that, if higher than one, imply a reduction of the effective length.

The value of k obtained with the two methods with the same length of 300 mm and the same thickness of the tube are:

$k = 0.31$ $P_{cr} = 578$ kN Energy method, two half waves

$k = 0.44$ $P_{cr} = 528$ kN Finite Element Model, one half wave.

The difference between the two methods is quite significant and a different approach is proposed.

5.6 Parametric Analysis

A parametric analysis is carried out to define the stiffness of the confinement. Four values of the outer diameter of the tube and four values of thickness of the filler material are considered. Starting from the results obtained with these values of the two parameters a general equation will be determined, as a function of the outer diameter of the tube and the thickness of the confinement that can be grout or epoxy.

The outer diameters and the thicknesses considered are:

ϕ (mm)	$t_{\text{grout/epoxy}}$ (mm)
25	2
35	4
45	6
55	8

Table 21. Dimensions of the External Tube e Thicknesses of the Confinement

The values of stiffness are obtained with a Sap Model for each combination. Every diameter will be combined with each thickness proposed.

CASE 1: $s_{\text{epoxy}} = 2$ mm

$D_o = 25$ mm

δ (m)	k (kN/m)	β (kN/m ²)
0.00014	6891.78	689179.9

$D_o = 45$ mm

δ (m)	k (kN/m)	β (kN/m ²)
0.00089	1125.36	112536.6

$D_o = 35$ mm

δ (m)	k (kN/m)	β (kN/m ²)
0.00041	2442.56	244259.9

$D_o = 55$ mm

δ (m)	k (kN/m)	β (kN/m ²)
0.0016	606.98	60698.03

CASE 2: $s_{\text{epoxy}} = 4 \text{ mm}$

$$D_o = 25 \text{ mm}$$

δ (m)	k (kN/m)	β (kN/m ²)
0.0001	9990.01	999001

$$D_o = 45 \text{ mm}$$

δ (m)	k (kN/m)	β (kN/m ²)
0.00060	1666.11	166611.1

$$D_o = 35 \text{ mm}$$

δ (m)	k (kN/m)	β (kN/m ²)
0.00027	3593.245	359324.5

$$D_o = 55 \text{ mm}$$

δ (m)	k (kN/m)	β (kN/m ²)
0.0011	901.632	90163.2

CASE 3: $s_{\text{epoxy}} = 6 \text{ mm}$

$$D_o = 25 \text{ mm}$$

δ (m)	k (kN/m)	β (kN/m ²)
0.000062	16233.77	1623377

$$D_o = 45 \text{ mm}$$

δ (m)	k (kN/m)	β (kN/m ²)
0.00035	2824.86	282485.9

$$D_o = 35 \text{ mm}$$

δ (m)	k (kN/m)	β (kN/m ²)
0.00017	6016.847	601684.7

$$D_o = 55 \text{ mm}$$

δ (m)	k (kN/m)	β (kN/m ²)
0.00065	1538.70	153869.8

CASE 4: $s_{\text{epoxy}} = 8 \text{ mm}$

$$D_o = 25 \text{ mm}$$

δ (m)	k (kN/m)	β (kN/m ²)
0.000039	25641.03	2564103

$$D_o = 45 \text{ mm}$$

δ (m)	k (kN/m)	β (kN/m ²)
0.0002098	4766.444	476644.4

$$D_o = 35 \text{ mm}$$

δ (m)	k (kN/m)	β (kN/m ²)
0.0001006	9940.358	994035.8

$$D_o = 55 \text{ mm}$$

δ (m)	k (kN/m)	β (kN/m ²)
0.0003813	2622.607	262260.7

Table 22. Unitary Stiffness of the Dissipator Device for Different Values of Outer Diameter and Thickness of the Epoxy

The results for each thickness of the epoxy are summarized in the tables below.

$s_{\text{epoxy}} = 2$	D_o (mm)	k (kN/m)	β (kN/m ²)	$s_{\text{epoxy}} = 4$	D_o (mm)	k (kN/m)	β (kN/m ²)
	25	6891.80	689179.88		25	9990.01	999001.00
	35	2442.60	244259.89		35	3593.24	359324.47
	45	1125.37	112536.57		45	1666.11	166611.13
	55	606.98	60698.03		55	901.63	90163.20

$s_{\text{epoxy}} = 6$	D_o (mm)	k (kN/m)	β (kN/m ²)	$s_{\text{epoxy}} = 8$	D_o (mm)	k (kN/m)	β (kN/m ²)
	25	16233.77	1623376.62		25	25641.03	2564102.56
	35	6016.85	601684.72		35	9940.36	994035.79
	45	2824.86	282485.88		45	4766.44	476644.42
	55	1538.70	153869.83		55	2622.61	262260.69

Table 23. Unitary Stiffness of the Dissipator Device for Different Values of Outer Diameter and Thickness of the Epoxy

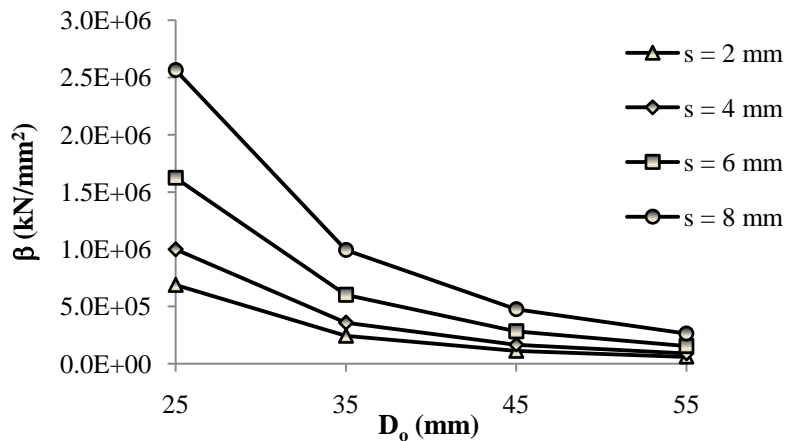


Figure 140. Graph of Stiffness versus Outer Diameter of the Tube

Depending on the outer diameter and the thickness of the tube the equation can be used to find out the value of β .

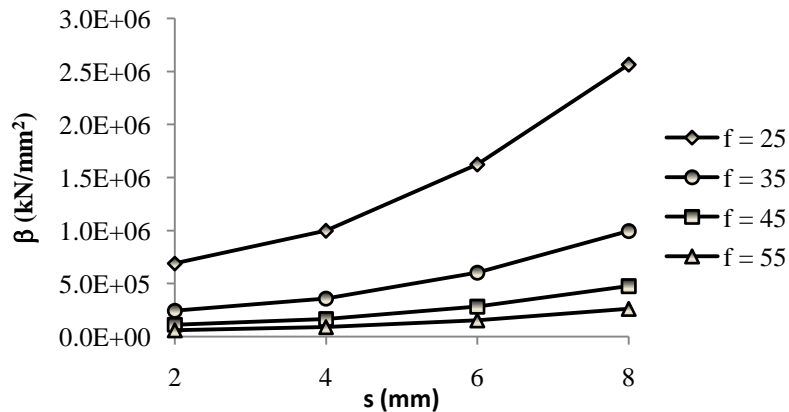


Figure 141 . Stiffness versus Thickness of the Confinement

The same analysis has been carried out for the grout.

$S_{grout} = 2$			$S_{grout} = 4$		
D_o (mm)	k (kN/m)	β (kN/m ²)	D_o (mm)	k (kN/m)	β (kN/m ²)
25	14577.26	1457725.95	25	38022.81	3802281.37
35	4149.38	414937.76	35	10729.61	1072961.37
45	2447.98	244798.04	45	7183.91	718390.80
55	606.98	60698.03	55	901.63	90163.20

$S_{grout} = 6$			$S_{grout} = 8$		
D_o (mm)	k (kN/m)	β (kN/m ²)	D_o (mm)	k (kN/m)	β (kN/m ²)
25	70422.54	7042253.52	25	103092.78	10309278.35
35	22371.36	2237136.47	35	37313.43	3731343.28
45	15797.79	1579778.83	45	27548.21	2754820.94
55	1538.70	153869.83	55	2622.61	262260.69

Table 24. Unitary Stiffness of the Dissipator Device for Different Values of Outer Diameter and Thickness of the Grout

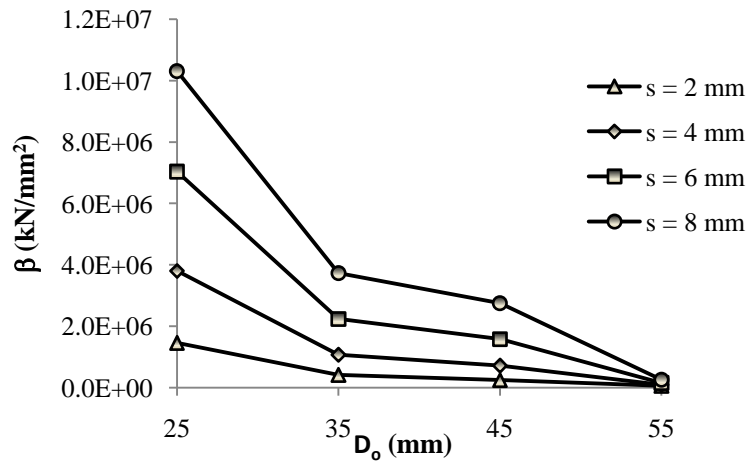


Figure 142. Graph of Stiffness versus Outer Diameter of the Tube

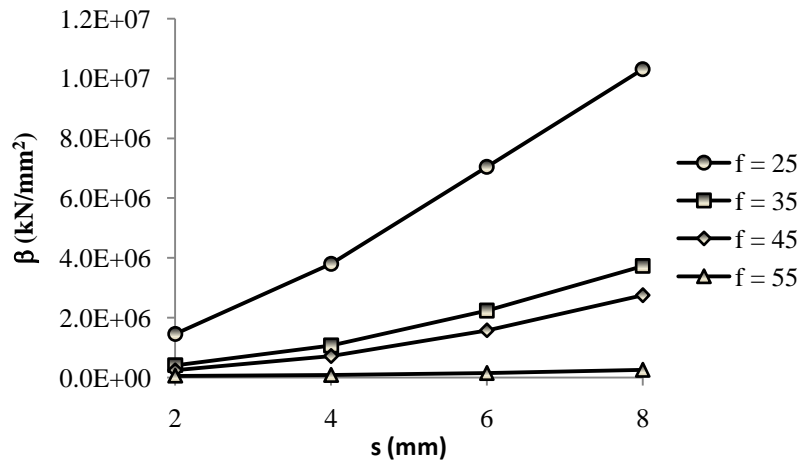


Figure 143. Stiffness versus Thickness of the Confinement

The loops obtained can be reduced to a bi linear relationship with two different equations that give the value of β .

With the parametric analysis the value of β is obtained for different diameters and thickness of the confinement in both cases, grout and epoxy.

The number of half waves is obtained by the equation:

$$\frac{\beta l^4}{\pi^4 EI} = m^2 (m + 1)^2 \quad (5.22)$$

Considering that the critical load is:

$$P = \frac{\pi^2 EI}{l^2} \left(m^2 + \frac{\beta l^4}{m^2 \pi^4 EI} \right) \quad (5.23)$$

and that it can be written in function of the effective length:

$$P_{cr} = \frac{\pi^2 EI}{L^2} \quad (5.24)$$

The value of the effective length factor, k , is:

$$k = \frac{L}{l} = \frac{1}{m^2 + \frac{\beta l^4}{m^2 \pi^4 (EI)_s}} \quad (5.25)$$

With tension and compression cycles, the filler material might deteriorate. When the bar is compressed there is an increasing pressure on the filler material that is pushed against the bar. When the tension force is applied the deflection of the bar reduces and the filler material can detach from the bar. If this happens, there will be a gap between the bar and the filler material. Different cycles of tension and compression will reduce the thickness of the filler material and increase the gap.

This phenomenon can happen if the material is stressed over its elastic limit and there is a residual deformation.

The epoxy is an elastic material and no residual deformation is expected. The grout on the contrary may have a residual deformation depending on the value of pressure and so its value of β changes in the course of time.

When the bar touches the tube the filler material is not going to contribute anymore to the anti-buckling and the tube is now the only one that restrains.

The behavior of the bar is changing also with relation to the displacement time history, and so if the dissipator is subjected before to compression or tension.

In the following pages all the different steps of the dissipator when stressed with tension and compression cycles are described in order to define its hysteresis loop.

5.7 Dissipator Hysteresis Loop Steps

A “step by step” analysis is presented in this paragraph and all the essential information to define the hysteresis loop are herein reported.

Two different cases are considered:

- Force time history starting with a compression on the dissipator
- Force time history starting with a tension on the dissipator

The first time history considered is shown in the picture below.

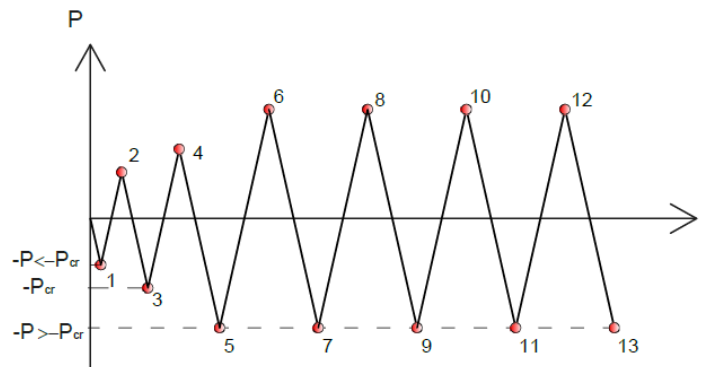
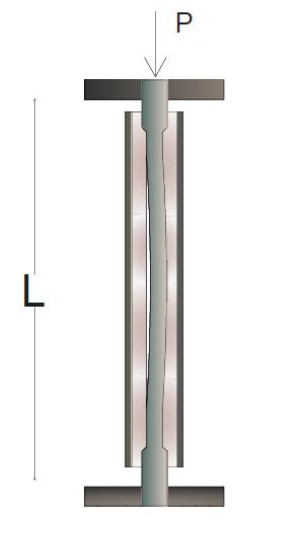
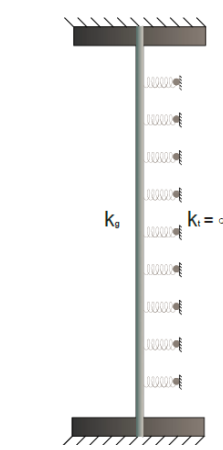
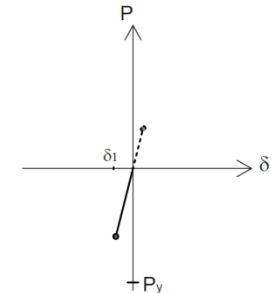


Figure 144. Displacement Time History, Compression - Tension

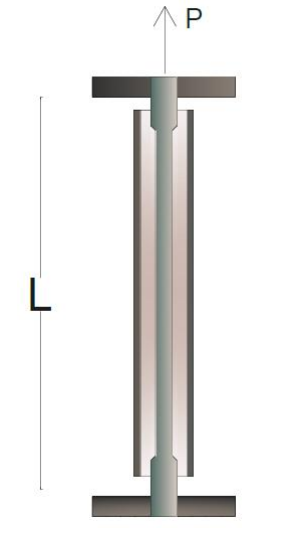
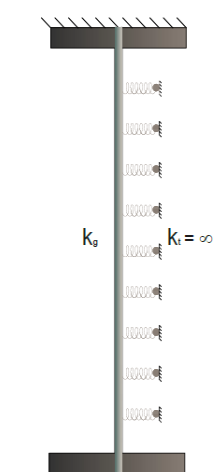
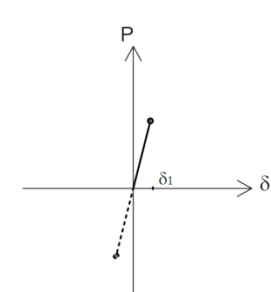
The different steps with the associated models are summarized in the table below.

	DISSIPATOR	MODEL	HYSTERESIS
1. $-P < -P_{cr,s}$: $P = \sigma A$ 2. $P < P_{cr,s}$: $P = \sigma A$			$P = k_{tot} \delta_1 = (k_s + k_r) \delta$ $\delta_1 = k_{tot} / P$
$k_r = f(\beta)$ $\beta = f(s, D_o)$ s: thickness of the grout/epoxy D_o: outer diameter of the tube			

At this stage the dissipator is stressed by a force with a smaller value than the critical one. The force-displacement hysteresis is elastic.

	DISSIPATOR	MODEL	HYSTERESIS
<p>3. $-P \approx -P_{cr,s}$:</p> $P_{cr} = \frac{\pi^2(EI)_s}{(kL)^2}$			$P = k_{tot} \delta_1 = (ks+kr) \delta_1$ $\delta_1 = k_{tot}/P$ 
<p>$k_r = f(\beta)$ $\beta = f(s, D_o)$</p> <p>s: thickness of the grout/epoxy</p> <p>D_o: outer diameter of the tube</p>			

At this stage the dissipator is stressed by a force with a value similar to the Euler one. The bar is restrained and so for this load the behavior is still elastic. The force-displacement hysteresis is elastic. The value of stiffness k_r of the restrain depends on the thickness of the grout/epoxy and the outer diameter of the tube. (See Eq. 5.7.2, 5.7.4)

<p>4. $P \approx P_{cr,s}$:</p> $P = \sigma A$			$P = k_{tot} \delta_1 = (ks+kr) \delta_1$ $\delta_1 = k_{tot}/P$ 
<p>$k_r = f(\beta)$ $\beta = f(s, D_o)$</p> <p>s: thickness of the grout/epoxy</p> <p>D_o: outer diameter of the tube</p>			

At this stage the dissipator is stressed by a force with a value similar to the Euler one. The bar is restrained and so for this load the behavior is still elastic. The force-displacement hysteresis is elastic. The value of stiffness k_r of the restrain depends on the thickness of the grout/epoxy and the outer diameter of the tube (See Eq. 5.7.2, 5.7.4)

Figura 145 "Step by Step" Analysis of the Dissipator

When the tension force is applied it may happen that the filler material detaches from the bar and it's possible the formation of a gap between the bar and the confinement. This means that when the dissipator is compressed the bar is no confined till when it reaches again the grout/epoxy. The epoxy is an elastic material and so it remains attached to the bar during all the tension and compression cycles. The grout on the contrary is an elasto plastic material; during

the loading phase it is compressed and during the unloading phase is not following the bar anymore if the yielding value has been exceeded.

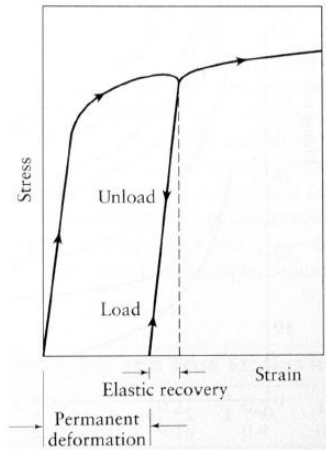
Considering that:

$$f_{yc} \approx 20 \text{ MPa}$$

$$E \approx 24000 \text{ MPa}$$

The value of strain is:

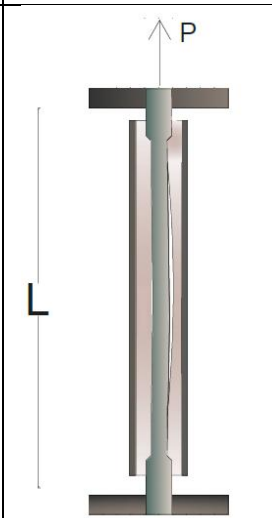
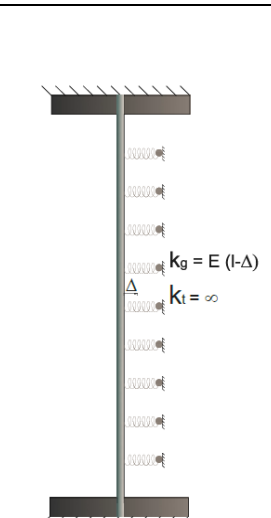
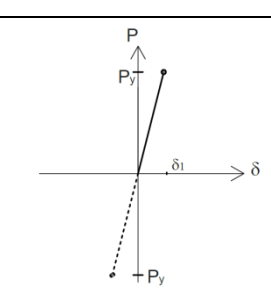
$$\varepsilon \approx 0.001$$



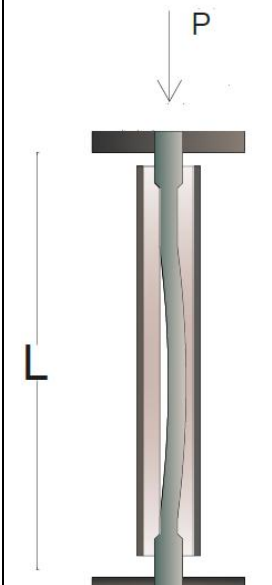
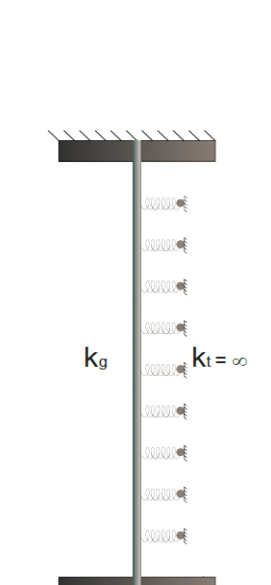
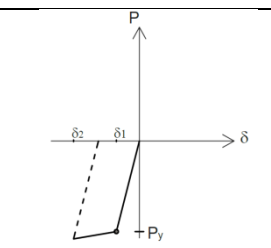
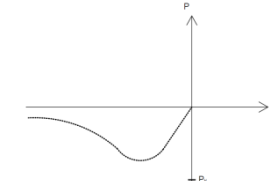
For this value of strain and considering the thicknesses of the filler material it's possible to assume that the yielding value will be exceeded already at the first loading.

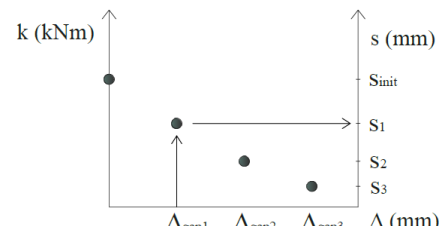
Figur3 146. Stress Strain Relationship

	DISSIPATOR	MODEL	HYSTERESIS
<p>5. $-P > -P_{cr,s}$</p> <p>5a) $P = \sigma_y A$</p> <p>5b) $P_{cr} = \frac{\pi^2(EI)_t}{(kL)^2}$</p>			<p>$P = k_{tot} \delta_1 = (ks+kr) \delta_1$ $\delta_1 = k_{tot}/P$</p>
<p>$k = f(\beta)$ $\beta = f(s, D_o)$</p> <p>s: thickness of the grout/epoxy D_o: outer diameter of the tube</p>			
<p>At this stage the dissipator is stressed with a value of load higher than the critical one of the only bar. There are two possibilities: the bar can reach the yielding point (case of a bar properly confined), the bar buckles. Depending on the situation two different hysteresis loops are possible. The dissipator, buckling, pushes the filler material.</p>			

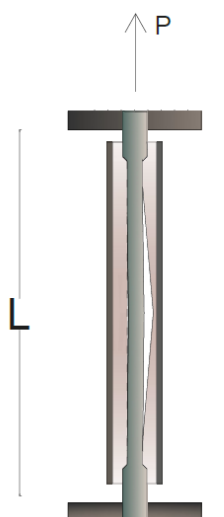
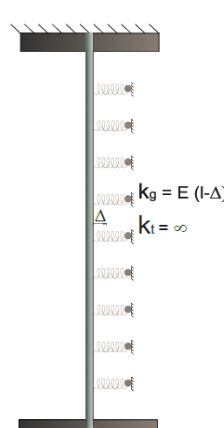
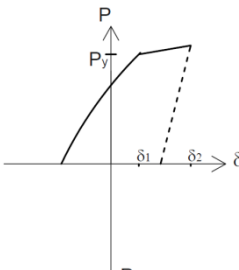
	DISSIPATOR	MODEL	HYSTERESIS
6. $P > P_{cr,s}$; $P = \sigma_y A$			$P = k_{tot} \delta_1 = (k_s + k_r) \delta_1$ $\delta_1 = k_{tot} / P$ 

The dissipator is stressed with a value higher than the critical one of the steel bar. Depending on the characteristics of the filler material, a gap between the tube and grout/epoxy might form.

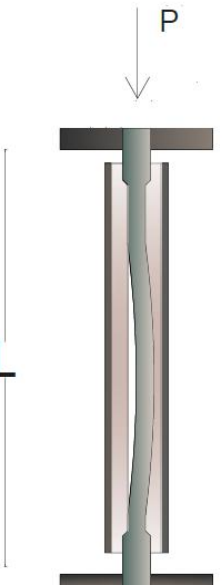
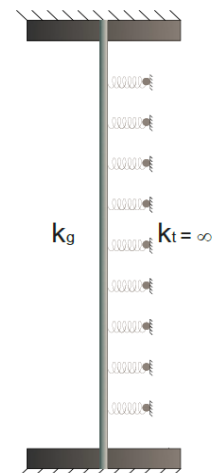
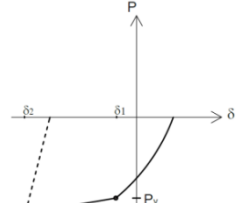
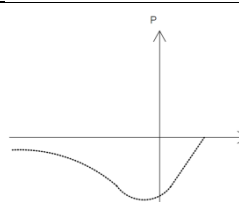
7. $-P > -P_{cr,s}$ 7a) $P = \sigma_y A$ 7b) $P_{cr} = \frac{\pi^2 (EI)_t}{(kL)^2}$ $k = f(\beta)$ $\beta = f(s, D_o)$ s : thickness of the grout / epoxy D_o : outer diameter of the tube If epoxy: s_{epoxy} is constant: $\sigma_e < \sigma_{ye}$ If grout: $\sigma_g < \sigma_{yg}$: no gap $s_{grout} = f(t)$ $\sigma_g > \sigma_{yg}$: gap			$P = (k_s + k_r) \delta_1 + BF(k_s + k_r) \delta_2$ $BF = \text{bilinear factor}$  
---	--	---	---

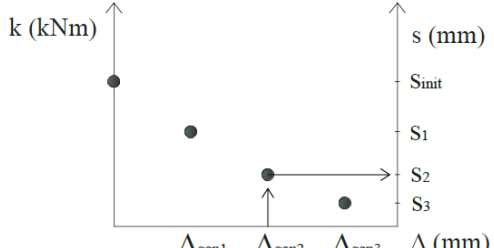
	IF GROUT: $\Delta < \Delta_{gap1}$: $P = (k_s + k_r) \delta_1 + BF(k_s + k_r) \delta_2$ $\Delta > \Delta_{gap1}$: $P = (k_s + k_{r1}) \delta_1 + BF(k_s + k_{r1}) \delta_2$ $k_r = f(\beta)$ $\beta = f(s_{init} - \Delta_{gap1}, D_o)$ switch of the equation for determine β .
---	--

The dissipator is stressed with a value higher than the critical one of the only bar. The dissipator is yielded. If the filler material detached from the bar, in the previous part the dissipator buckle without being confined. If the filler material has been pressed it is now characterized by a smaller thickness (switch of the equation for determine) (See Eq. 5.7.2, 5.7.4)

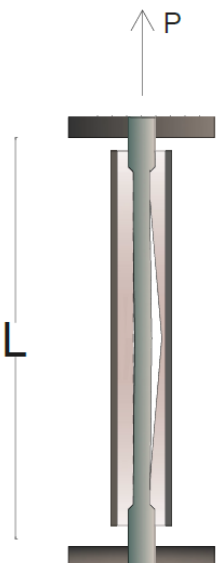
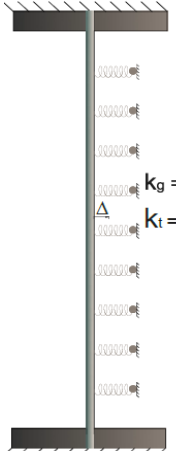
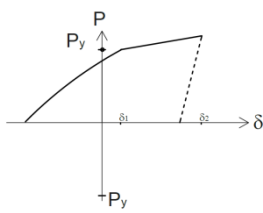
	DISSIPATOR	MODEL	HYSTERESIS
8. $P > P_{cr} : P = \sigma_y A$			$P = (ks+kr)\delta_1 + BF(ks+kr)\delta_2$ <p>BF = bilinear factor</p> 

The dissipator is stressed with a value higher than the critical one of the steel bar. Depending on the characteristics of the filler material, a gap between the tube and grout/epoxy might form. For k_r (See Eq. 5.7.2, 5.7.4)

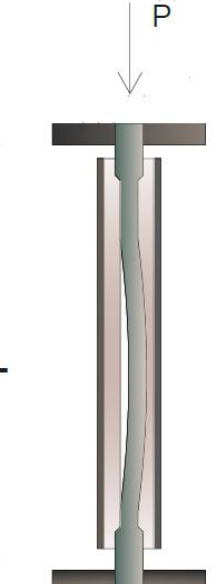
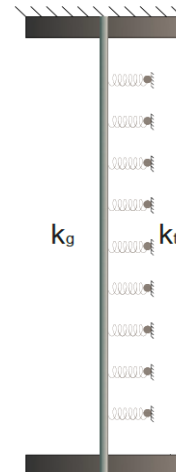
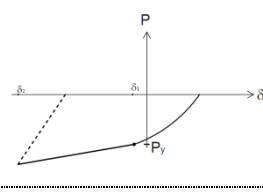
9. $-P > -P_{cr}$			$P = (ks+kr)\delta_1 + BF(ks+kr)\delta_2$ <p>BF = bilinear factor</p>
9a) $P = \sigma_y A$ 9b) $P_{cr} = \frac{\pi^2(EI)_t}{(kL)^2}$ $k = f(\beta)$ $\beta = f(s, D_o)$ s: thickness of the grout / epoxy D_o : outer diameter of the tube If epoxy: s_{epoxy} is constant: $\sigma_e < \sigma_{ye}$ If grout: $\sigma_g < \sigma_{yg}$: no gap $s_{grout} = f(t)$ $\sigma_g > \sigma_{yg}$: gap			
			

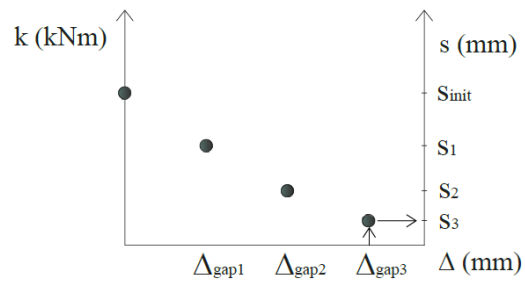
	<p>IF GROUT: $\Delta < \Delta_{gap2}$:</p> $P = (ks+k_{r1})\delta_1 + BF(ks+k_{r1})\delta_2$ <p>$\Delta > \Delta_{gap2}$:</p> $P = (ks+k_{r2})\delta_1 + BF(ks+k_{r2})\delta_2$ <p>$k = f(\beta)$ $\beta = f(s_{init} - \Delta_{gap2}, D_o)$ switch of the equation for determine β.</p>
---	---

The dissipator is stressed with a value higher than the critical one of the only bar. The dissipator is dissipating. If the filler material detached from the bar, in the previous part the dissipator buckle without being confined. If the filler material has been pressed it is now characterized by a smaller thickness (switch of the equation for determine β). (See Eq. 5.7.2, 5.7.4)

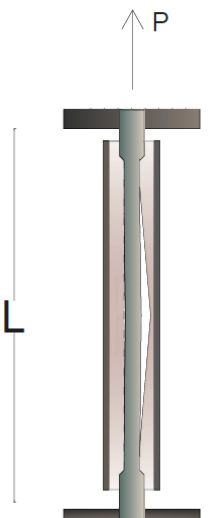
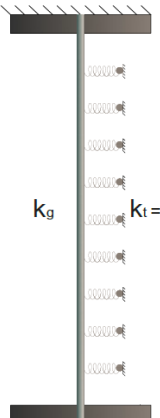
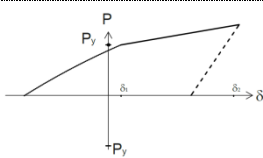
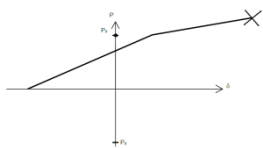
	DISSIPATOR	MODEL	HYSTERESIS
10. $P > P_{cr}$: $P = \sigma_y A$			$P = (ks+kr)\delta_1 + BF(ks+kr)\delta_2$ <p>BF = bilinear factor</p> 

The dissipator is stressed with a value higher than the critical one of the steel bar. Depending on the characteristics of the filler material, a gap between the tube and grout/epoxy might form. For kr see Eq. 5.7.2, 5.7.4

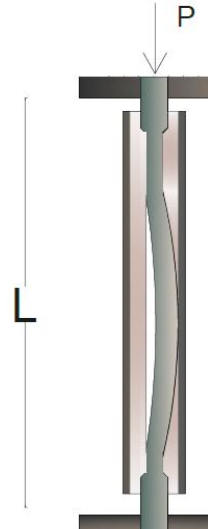
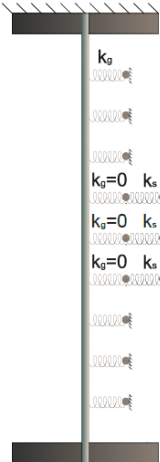
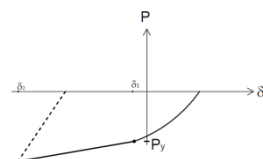
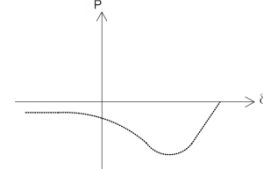
11. $-P > -P_{cr}$:			$P = (ks+kr)\delta_1 + BF(ks+kr)\delta_2$ <p>BF = bilinear factor</p>
11a) $P = \sigma_y A$ 11b) $P_{cr} = \frac{\pi^2(EI)_t}{(kL)^2}$ $k = f(\beta)$ $\beta = f(s, D_o)$ s : thickness of the grout / epoxy D_o : outer diameter of the tube If epoxy: S_{epoxy} is constant: $\sigma_e < \sigma_{ye}$ If grout: $\sigma_g < \sigma_{yg}$: no gap $S_{grout} = f(t)$ $\sigma_g > \sigma_{yg}$: gap			

	<p>IF GROUT: $\Delta < \Delta_{gap3}$:</p> $P = (ks+k_{r2})\delta_1 + BF(ks+k_{r2})\delta_2$ <p>$\Delta > \Delta_{gap2}$:</p> $P = (ks+k_{r3})\delta_1 + BF(ks+k_{r3})\delta_2$ <p>$k = f(\beta)$ $\beta = f(S_{init} - \Delta_{gap2}, D_o)$: switch of the equation for determine β.</p>
---	---

The dissipator is stressed with a value higher than the critical one of the only bar. The dissipator is dissipating. If the filler material detached from the bar, in the previous part the dissipator buckle without being confined. If the filler material has been pressed it is now characterized by a smaller thickness (switch of the equation for determine β) (See Eq. 5.7.2, 5.7.4)

	DISSIPATOR	MODEL	HYSTERESIS
12. $P > P_{cr}$: $P = \sigma_y A$			$P = (ks+kr)\delta_1 + BF(ks+kr)\delta_2$ <p>BF = bilinear factor</p>  

The dissipator is stressed with a value higher than the critical one of the steel bar. The dissipator can have still residual capacity or can fail reaching the rupture point. For kr (See Eq. 5.7.2, 5.7.4)

13. $-P > -P_{cr}$: $P_{cr} = \frac{\pi^2(E_r I)_t}{(kL)^2}$ <p>The grout is no more working in the center of the dissipator: $k = 0$</p> $k = f(\beta)$ $\beta = f(s_{tube}, D_o)$			$P = (ks+kr)\delta_1 + BF(ks+kr)\delta_2$ <p>BF = bilinear factor</p>  
--	--	---	---

The dissipator is stressed with a value higher than the critical one of the only bar. The filler material might have received the crack point. The tube can not be considered as a fully fixed restraint; the tube now is the only one that resists (See Eq. 5.7.5). The tube is the only one that restrains the bar. There are two possibilities: a residual capacity can be still present or there can be plastic buckling. (See Eq. 5.7.2, 5.7.4)

Figure 147. "Step by Step" Analysis of the Dissipator

The total loop is herein reported.

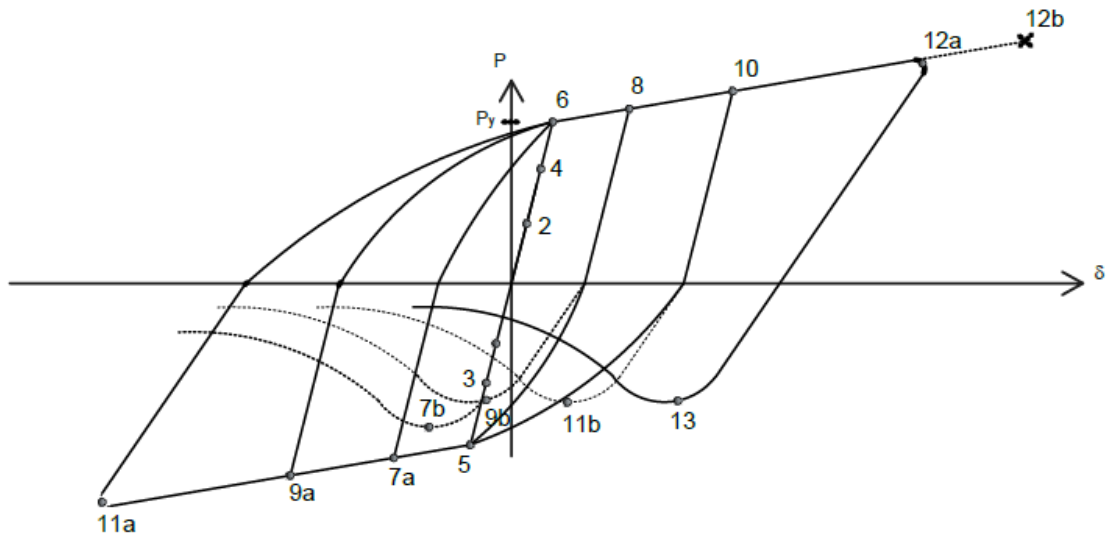


Figure 148. Force-Displacement Relationship of Dissipator

The second time history considered is shown in the picture below.

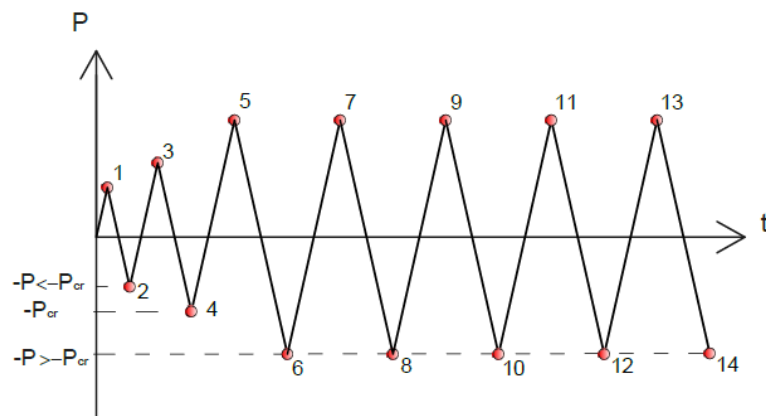
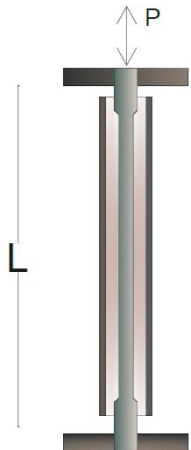
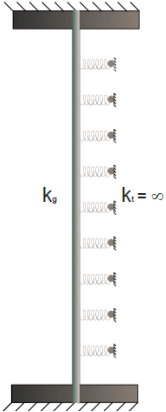
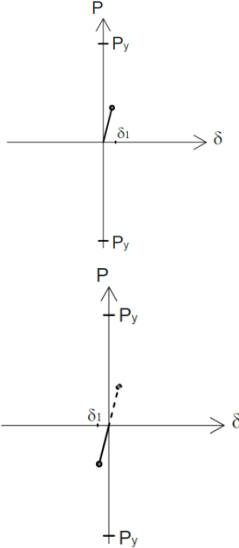
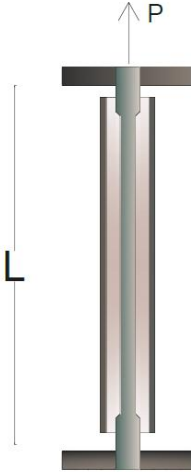
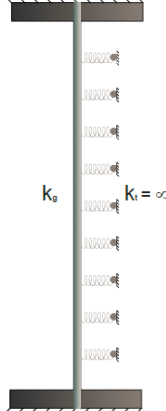
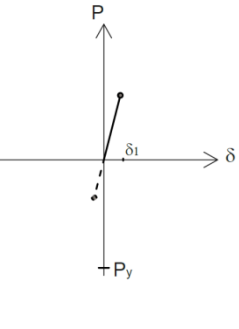


Figure 149. Displacement Time History, Compression - Tension

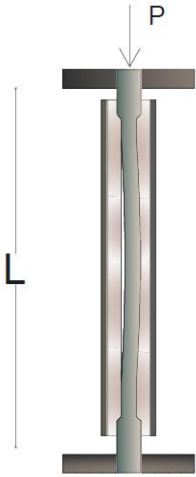
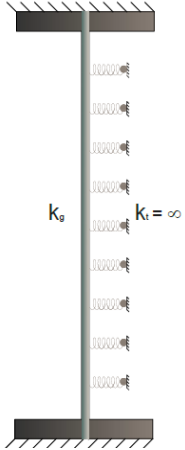
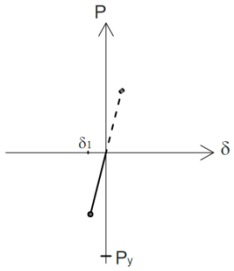
The different steps with the associated models are summarized in the table below.

	DISSIPATOR	MODEL	HYSTERESIS
<p>1. $P < P_{cr,s}$:</p> <p>$P = \sigma A$</p> <p>2. $-P < -P_{cr,s}$:</p> <p>$P = \sigma A$</p> <p>$k_r = f(\beta)$ $\beta = f(s, D_o)$</p> <p>s: thickness of the grout/epoxy D_o: outer diameter of the tube</p>			<p>$P = k_{tot} \delta = (k_s + k_r) \delta$ $\delta = k_{tot} / P$</p> 


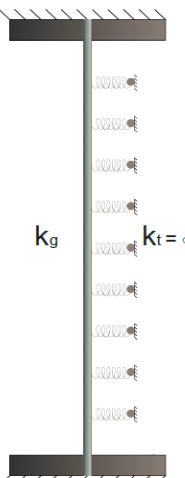
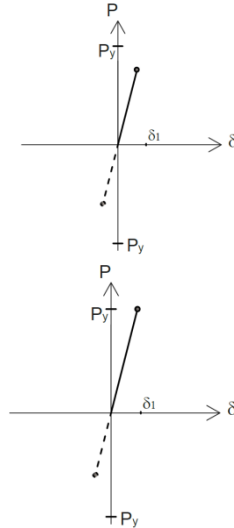
At this stage the dissipator is stressed by a force with a smaller value than the critical one. The force-displacement hysteresis is elastic.

<p>3. $P \approx P_{cr}$:</p> <p>$P = \sigma A$</p>			<p>$P = k_{tot} \delta = (k_s + k_r) \delta$ $\delta = k_{tot} / P$</p> 
--	---	--	--


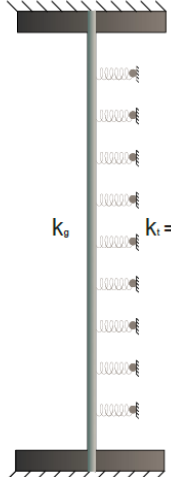
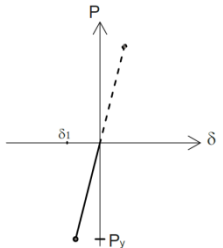
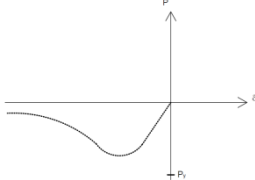
At this stage the dissipator is stressed by a force with a value similar to the Euler one. The bar is restrained and so for this load the behavior is still elastic. The force-displacement hysteresis is elastic. The value of stiffness k_r of the restraint depends on the thickness of the grout/epoxy and the outer diameter of the tube. (See Eq. 5.7.2, 5.7.4)

	DISSIPATOR	MODEL	HYSTERESIS
<p>4. $-P \approx -P_{cr}$:</p> $P_{cr} = \frac{\pi^2(EI)_s}{(kL)^2}$ <p>$k = f(\beta)$ $\beta = f(s, D_o)$</p> <p>s: thickness of the grout/epoxy D_o: outer diameter of the tube</p>			$P = k_{tot} \delta = (k_s + k_r) \delta$ $\delta = k_{tot} / P$ 

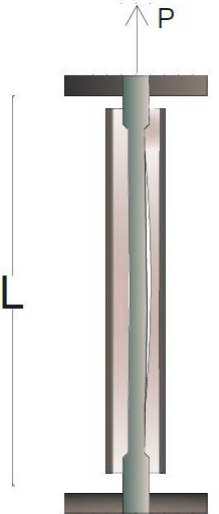
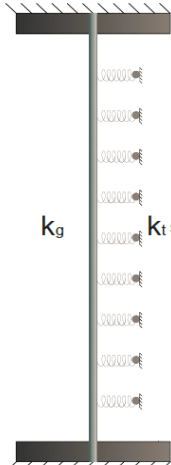
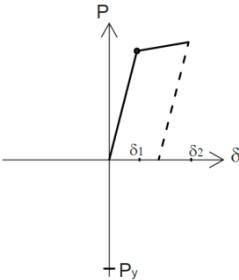
At this stage the dissipator is stressed by a force with a value similar to the Euler one. The bar is restrained and so for this load the behavior is still elastic. The force-displacement hysteresis is elastic. The value of stiffness k_r of the restrain depends on the thickness of the grout/epoxy and the outer diameter of the tube. (See Eq. 5.7.2, 5.7.4)

<p>5. $P > P_{cr,s}$:</p> <p>a) $P = \sigma A$ b) $P = \sigma_y A$</p>			$P = k_{tot} \delta = (k_s + k_r) \delta$ $\delta = k_{tot} / P$ 
---	---	--	--

The dissipator is stressed with a value higher than the critical one of the steel bar. Depending on the characteristics of the filler material, a gap between the tube and grout/epoxy might form.

	DISSIPATOR	MODEL	HYSTERESIS
<p>6. $-P > -P_{cr,s}$</p> <p>4a) $P = \sigma_y A$</p> <p>4b) $P_{cr} = \frac{\pi^2(EI)_t}{(kL)^2}$</p> <p>$k = f(\beta)$</p> <p>$\beta = f(s, D_o)$</p> <p>s: thickness of the grout / epoxy</p> <p>D_o: outer diameter of the tube</p> <p>If epoxy: s_{epoxy} is constant: $\sigma_e < \sigma_{ye}$</p> <p>If grout: $\sigma_g < \sigma_{yg}$: no gap $s_{grout} = f(t)$ $\sigma_g > \sigma_{yg}$: gap</p>			<p>$P = (ks+kr)\delta_1 + BF(ks+kr)\delta_2$</p> <p>BF = bilinear factor</p>  

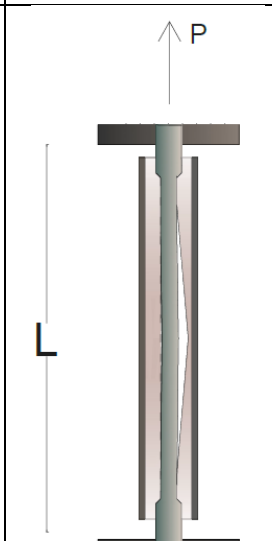
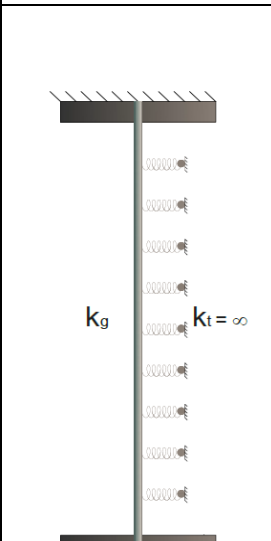
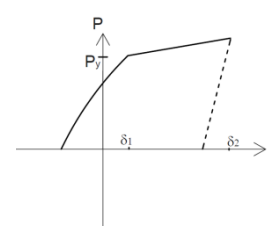
The dissipator is stressed with a value higher than the critical one of the only bar. The dissipator starts dissipating. If the filler material detached from the bar, in the previous part the dissipator buckle without being confined. If the filler material has been pressed it is now characterized by a smaller thickness (switch of the equation for determine β). (See Eq. 5.7.2, 5.7.4) . The dissipator can reach the yielding value or buckle for a smaller value than the yielding one.

<p>7. $P > P_{cr,s}$</p>			<p>$P = (ks+kr)\delta_1 + BF(ks+kr)\delta_2$</p> <p>BF = bilinear factor</p> 
--	---	--	---

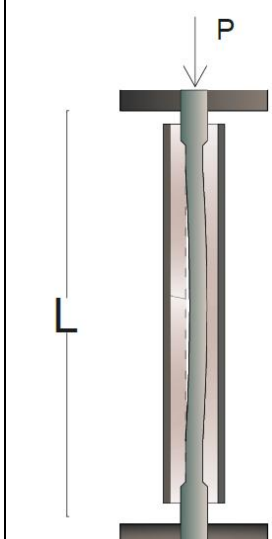
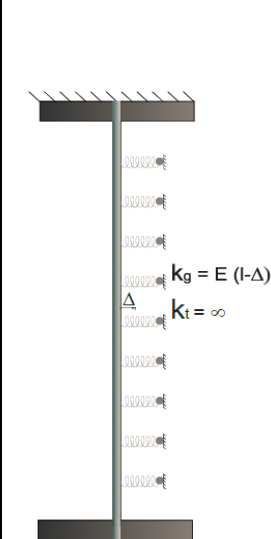
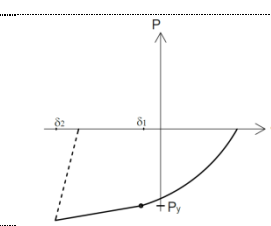
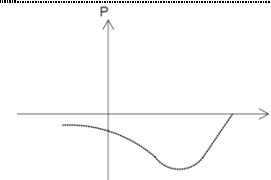
The dissipator is stressed with a value higher than the critical one of the steel bar. Depending on the characteristics of the filler material, a gap between the tube and grout/epoxy might form. For kr (See Eq. 5.7.2, 5.7.4)

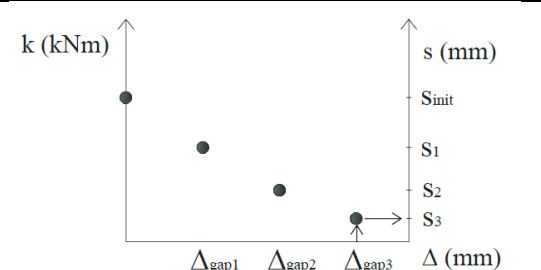
	DISSIPATOR	MODEL	HYSTERESIS
<p>8. $-P > -P_{cr}$:</p> <p>8a) $P = \sigma_y A$</p> <p>8b) $P_{cr} = \frac{\pi^2(EI)_t}{(kL)^2}$</p> <p>$k = f(\beta)$</p> <p>$\beta = f(s, D_o)$</p> <p>s: thickness of the grout / epoxy</p> <p>D_o: outer diameter of the tube</p> <p>If epoxy: S_{epoxy} is constant: $\sigma_e < \sigma_{ye}$</p> <p>If grout: $\sigma_g < \sigma_{yg}$: no gap $S_{grout} = f(t)$ $\sigma_g > \sigma_{yg}$: gap</p>			<p>$P = (ks+kr)\delta_1 + BF(ks+kr)\delta_2$</p> <p>BF = bilinear factor</p>
	<p>IF GROUT: $\Delta < \Delta_{gap1}$:</p> $P = (ks+kr)\delta_1 + BF(ks+kr)\delta_2$ <p>$\Delta > \Delta_{gap1}$: $P = (k_s+k_{r1})\delta_1 + BF(k_s+k_{r1})\delta_2$</p> <p>$k_r = f(\beta)$</p> <p>$\beta = f(S_{init} - \Delta_{gap1}, D_o)$:</p> <p>switch of the equation for determine β.</p>		

The dissipator is stressed with a value higher than the critical one of the only bar. The dissipator is dissipating. If the filler material detached from the bar, in the previous part the dissipator buckle without being confined. If the filler material has been pressed it is now characterized by a smaller thickness (switch of the equation for determine β). (See Eq. 5.7.2, 5.7.4). The dissipator can reach the yielding value or buckle for a smaller value than the yielding one.

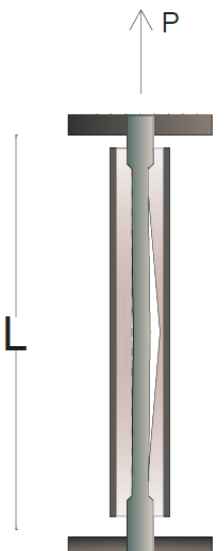
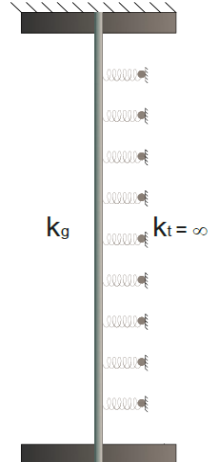
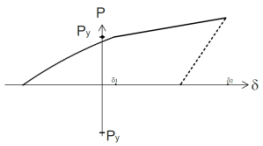
	DISSIPATOR	MODEL	HYSTERESIS
9. $P > P_{cr} : P = \sigma_y A$			$P = (ks+kr)\delta_1 + BF(ks+kr)\delta_2$ <p>BF = bilinear factor</p> 

The dissipator is stressed with a value higher than the critical one of the steel bar. Depending on the characteristics of the filler material, a gap between the tube and grout/epoxy might form. For k_r (See Eq. 5.7.2, 5.7.4)

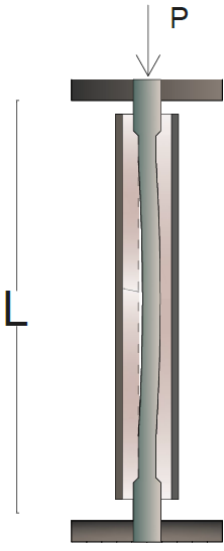
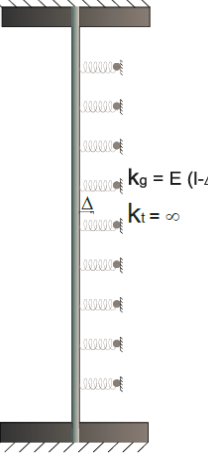
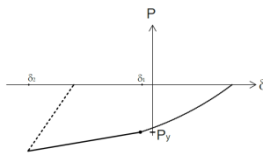
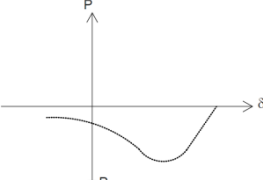
10. $-P > -P_{cr} :$ 10a) $P = \sigma_y A$ 10b) $P_{cr} = \frac{\pi^2(EI)_t}{(kL)^2}$ $k = f(\beta)$ $\beta = f(s, D_o)$ s: thickness of the grout / epoxy D_o : outer diameter of the tube If epoxy: s_{epoxy} is constant: $\sigma_e < \sigma_{ye}$ If grout: $\sigma_g < \sigma_{yg}$: no gap $s_{grout} = f(t)$ $\sigma_g > \sigma_{yg}$: gap			$P = (ks+kr)\delta_1 + BF(ks+kr)\delta_2$ <p>BF = bilinear factor</p>  
--	--	---	--

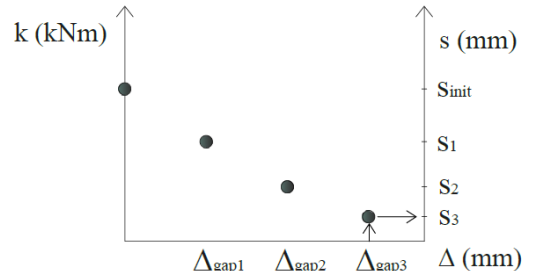
	<p>IF GROUT: $\Delta < \Delta_{gap3} :$</p> $P = (ks+k_{r2})\delta_1 + BF(ks+k_{r2})\delta_1$ <p>$\Delta > \Delta_{gap2} :$</p> $P = (ks+k_{r3})\delta_1 + BF(ks+k_{r3})\delta_1$ <p>$k = f(\beta)$</p> <p>$\beta = f(s_{init} - \Delta_{gap2}, D_o) :$</p> <p>switch of the equation for determine β.</p>
---	---

The dissipator is stressed with a value higher than the critical one of the only bar. The dissipator is dissipating. If the filler material detached from the bar, in the previous part the dissipator buckle without being confined. If the filler material has been pressed it is now characterized by a smaller thickness (switch of the equation for determine β). (See Eq. 5.7.2, 5.7.4).

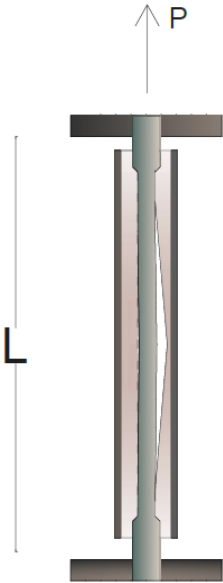
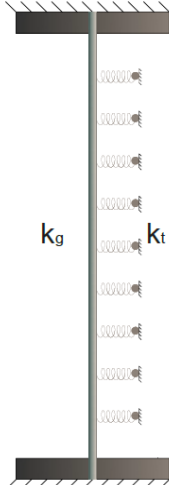
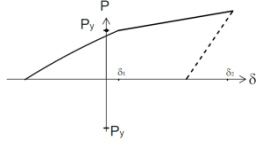
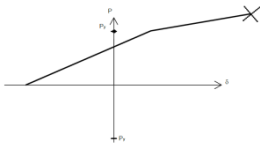
	DISSIPATOR	MODEL	HYSTERESIS
11. $P > P_{cr} : P = \sigma_y A$			$P = (ks+kr)\delta_1 + BF(ks+kr)\delta_2$ <p>BF = bilinear factor</p> 

The dissipator is stressed with a value higher than the critical one of the steel bar. Depending on the characteristics of the filler material, a gap between the tube and grout/epoxy might form. For kr (See Eq. 5.7.2, 5.7.4)

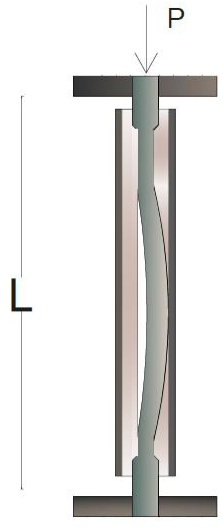
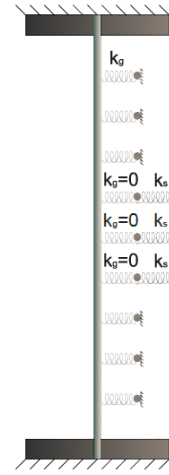
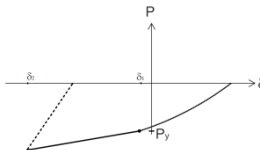
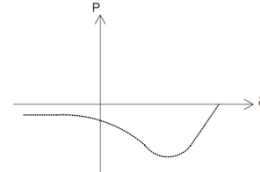
1. $-P > -P_{cr} :$ 12a) $P = \sigma_y A$ 12b) $P_{cr} = \frac{\pi^2(EI)_t}{(kL)^2}$ $k = f(\beta)$ $\beta = f(s, D_o)$ s: thickness of the grout / epoxy D_o : outer diameter of the tube If epoxy: s_{epoxy} is constant: $\sigma_e < \sigma_{ye}$ If grout: $\sigma_g < \sigma_{yg}$: no gap $s_{grout} = f(t)$ $\sigma_g > \sigma_{yg}$: gap			$P = (ks+kr)\delta_1 + BF(ks+kr)\delta_2$ <p>BF = bilinear factor</p>  
---	--	--	---

	<p>IF GROUT: $\Delta < \Delta_{gap3} :$</p> $P = (ks+k_{r2})\delta_1 + BF(ks+k_{r2})\delta_2$ <p>$\Delta > \Delta_{gap2} :$</p> $P = (ks+k_{r3})\delta_1 + BF(ks+k_{r3})\delta_2$ <p>$k = f(\beta)$</p> <p>$\beta = f(s_{init} - \Delta_{gap2}, D_o) :$</p> <p>switch of the equation for determine β.</p>
---	---

The dissipator is stressed with a value higher than the critical one of the only bar. The dissipator is dissipating. If the filler material detached from the bar, in the previous part the dissipator buckle without being confined. If the filler material has been pressed it is now characterized by a smaller thickness (switch of the equation for determine β). (See Eq. 5.7.2, 5.7.4)

	DISSIPATOR	MODEL	HYSTERESIS
2. $P > P_{cr} : P = \sigma_y A$			$P = (ks+kr)\delta_1 + BF(ks+kr)\delta_2$ <p>BF = bilinear factor</p>  

The dissipator is stressed with a value higher than the critical one of the steel bar. Depending on the characteristics of the filler material, a gap between the tube and grout/epoxy might form. For k_r (See Eq. 5.7.2, 5.7.4)

14. $-P > -P_{cr} :$ $P_{cr} = \frac{\pi^2(E_r I)_t}{(kL)^2}$ The grout is no more working in the center of the dissipator: $k = 0$ $k = f(\beta)$ $\beta = f(s_{tube}, D_o)$			$P = (ks+kr)\delta_1 + BF(ks+kr)\delta_2$ <p>BF = bilinear factor</p>  
---	--	--	---

The dissipator is stressed with a value higher than the critical one of the only bar. The filler material might have received the crack point. The tube can not be considered as a fully fixed restraint; the tube now is the only one that resists (See Eq. 5.7.5) The tube is the only one that restrains the bar. There are two possibilities: a residual capacity can be still present or there can be plastic buckling. (See Eq. 5.7.2, 5.7.4)

Figure 150. "Step by Step" Analysis of the Dissipator

The total loop is herein reported.

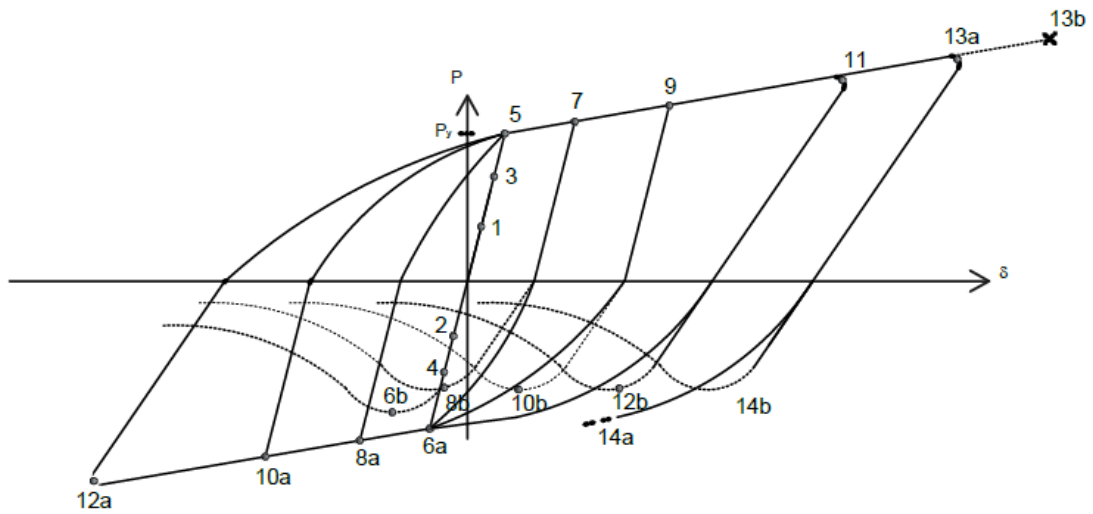


Figure 151. Force-Displacement Relationship of Dissipator

The results obtained with the parametric analysis can be used in Ruaumoko [6] to link every step to the right loop in terms of β .

Every loop is a function of the outer diameter of the tube and the thickness of the confinement material (grout or epoxy) and can be described by a parabolic equation or by two linear equations.

Epoxy Confinement

The results obtained for the epoxy confinement are shown in the picture below.

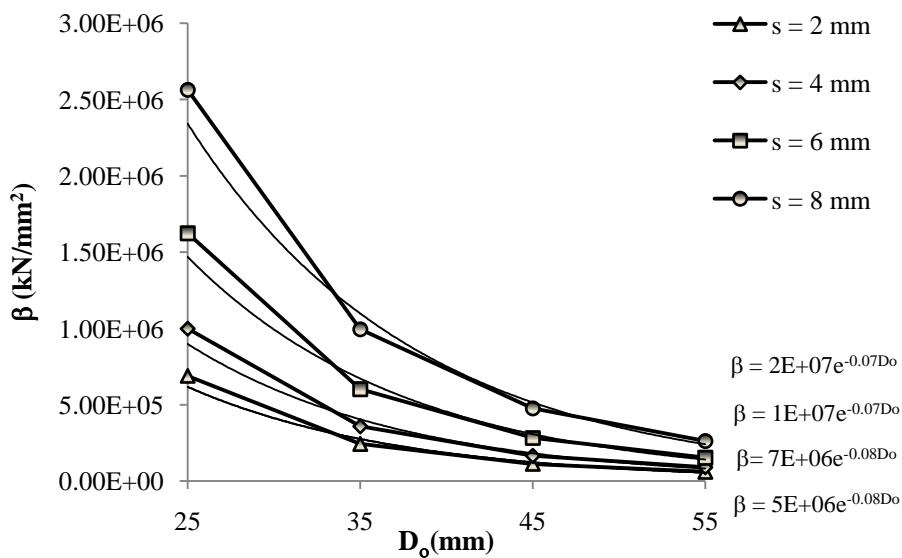


Figure 152. Stiffness versus Outer Diameter of the tube with an Epoxy Confinement

The loops obtained are useful only for the values of thickness of the epoxy considered. Starting from the graph that describe the case with 2 mm of epoxy, all the other cases have been derived considering the increment in stiffness as a function of the external diameter of the tube and the thickness of the epoxy. An extensive formula that gives β for any value of diameter and any thickness of the confinement is provided below.

$$\beta = 5^6 * e^{-0.08D_o} + 33716e^{-0.1D_o} * s_e^{(0.016D_o+2.9)} \quad (5.26)$$

Where:

β is the lateral stiffness of the confinement

D_o is the external diameter of the tube

s_e is the thickness of the epoxy.

The results obtained with the relation above are compared with the ones obtained using the formulas in [Figure 152](#).

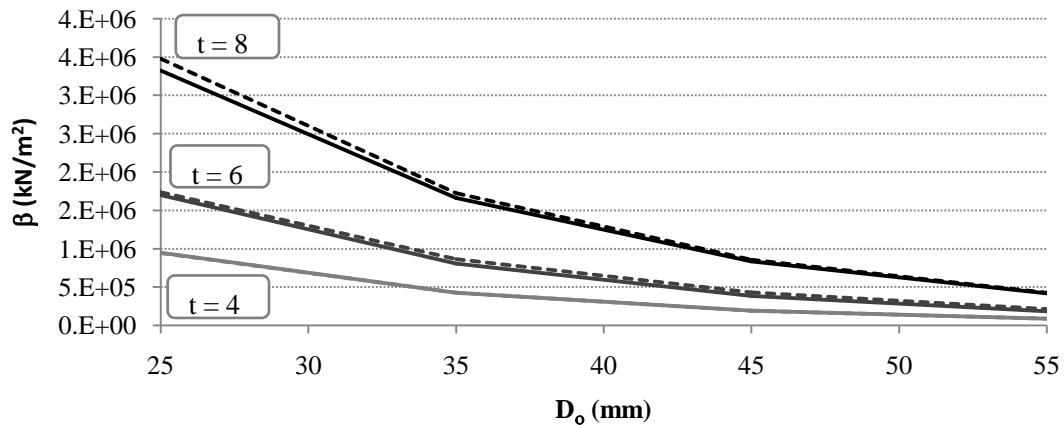


Figure 153. Fitting of Results

The difference between the two charts is irrelevant. The results obtained with the equation have then been compared with the results obtained with Sap 2000. A slightly modification of the equation to reduce the scatter between the results is proposed.

$$\beta = 5^6 * e^{-0.08D_o} + 33716e^{-0.1D_o} * s_e^{(0.01D_o+2.85)} \quad (5.27)$$

Where:

β is the lateral stiffness of the confinement

D_o is the external diameter of the tube

s_e is the thickness of the epoxy.

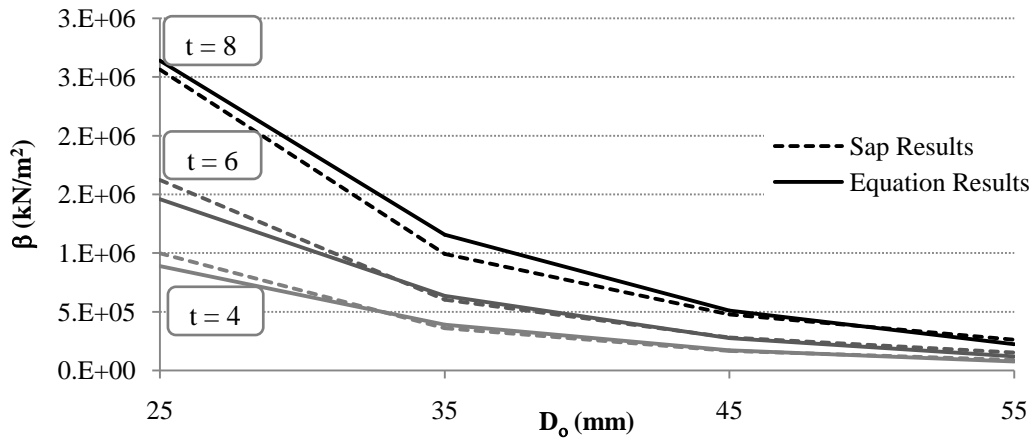


Figure 154. Fitting of Results obtained with the Equation and Sap 2000

The influence of the thickness of the confinement on the stiffness for each outer diameter is shown in the picture below.

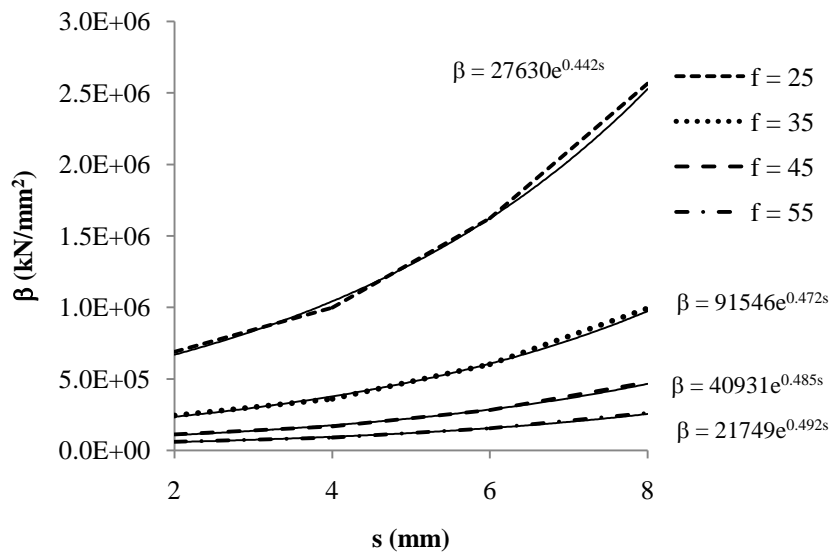


Figure 155. Stiffness versus Thickness of the Confinement

The results obtained with the parametric analysis are useful to extend the hysteresis also to other thicknesses of the confinement or to other outer diameters of the tube.

Grout Confinement

The results obtained for the grout confinement are shown in the picture below.

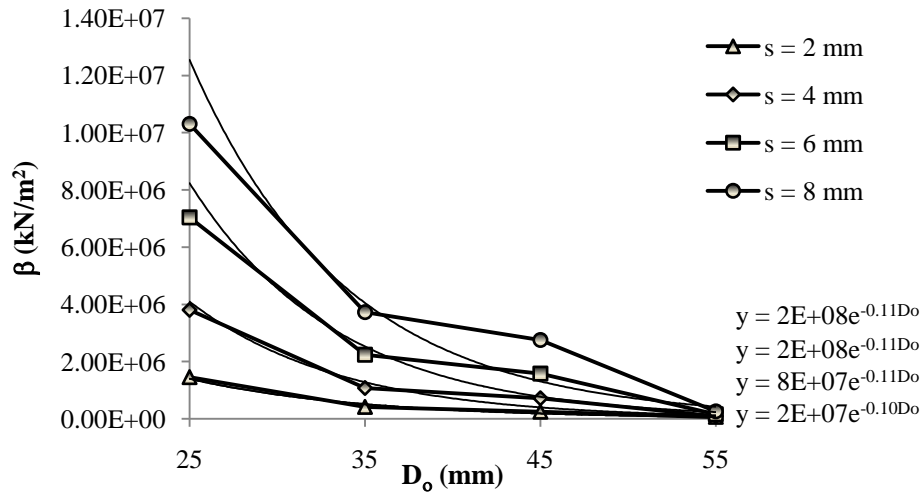


Figure 156. Stiffness versus Outer Diameter with a Grout Confinement

The loop can be described with two linear equations; one can be used if the outer diameter is smaller than 35 mm, the other one can be used if the outer diameter is bigger than 35 mm.

s = 2

$$\text{IF } D_o \leq 35 \text{ mm: } \beta = -10427 D_o + 4^6$$

$$\text{IF } D_o > 35 \text{ mm: } \beta = -17712 D_o + 1^6$$

s = 4

$$\text{IF } D_o \leq 35 \text{ mm: } \beta = -27293 D_o + 1^7$$

$$\text{IF } D_o > 35 \text{ mm: } \beta = -49140 D_o + 3^6$$

s = 6

$$\text{IF } D_o \leq 35 \text{ mm: } \beta = -48051 D_o + 2^7$$

$$\text{IF } D_o > 35 \text{ mm: } \beta = -10416 D_o + 6^6$$

s = 8

$$\text{IF } D_o \leq 35 \text{ mm: } \beta = -65779 D_o + 3^7$$

$$\text{IF } D_o > 35 \text{ mm: } \beta = -17345 D_o + 1^7$$

A general equation that allows the use of the hysteresis loop also for other thicknesses of the confinement is herein reported.

$$\beta = 1.7^7 * e^{-0.1D_o} + (-1101D_o + 63610) * s_g^{(0.018D_o+3.213)} \quad (5.28)$$

Where:

- β is the lateral stiffness of the confinement
- D_o is the external diameter of the tube
- s_g is the thickness of the grout.

The comparison between the results obtained with the equation above and the ones obtained with the formulas reported in Figure 156 is shown below.

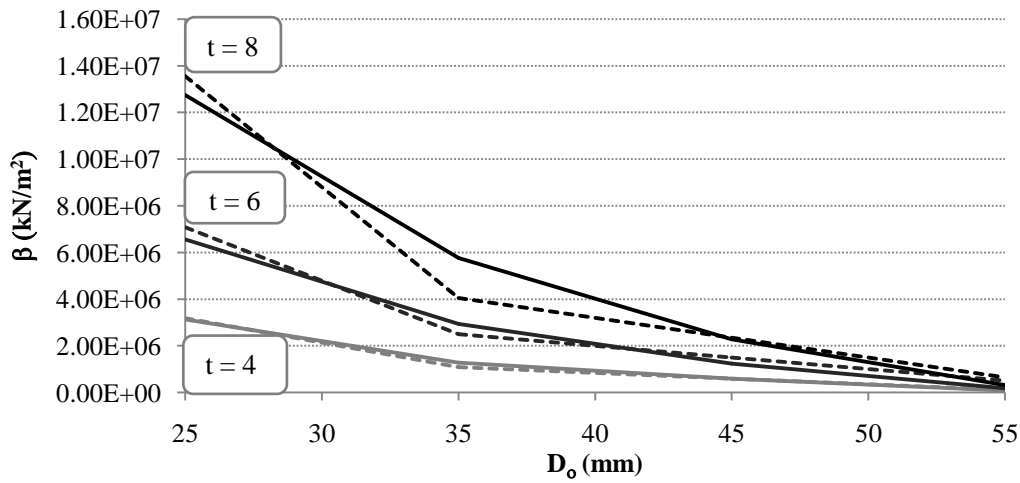


Figure 157. Fitting of the Results

The formula is slightly modified in order to be more similar to the one obtained plotting the Sap results.

$$\beta = 1.7^7 * e^{-0.1D_o} + (-1101D_o + 63610) * s_g^{(0.02D_o+3.213)} \quad (5.29)$$

Where:

- β is the lateral stiffness of the confinement
- D_o is the external diameter of the tube
- s_g is the thickness of the grout.

The comparison between the results obtained with the equation proposed above and the Sap results is shown in the picture below.

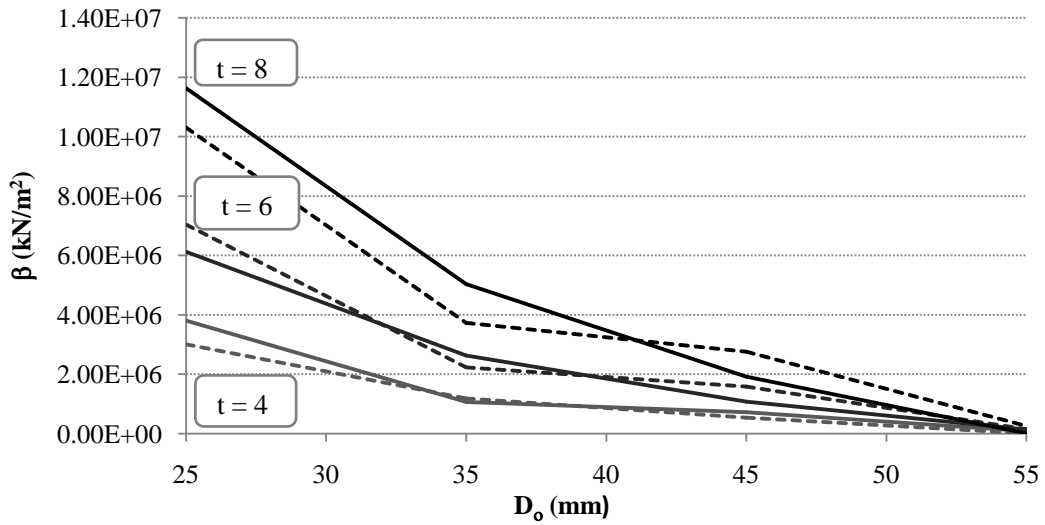


Figure 158. Fitting of the Results obtained with the Equation and Sap 2000

The influence of the thickness of the confinement on the stiffness for each outer diameter is shown in the picture below.

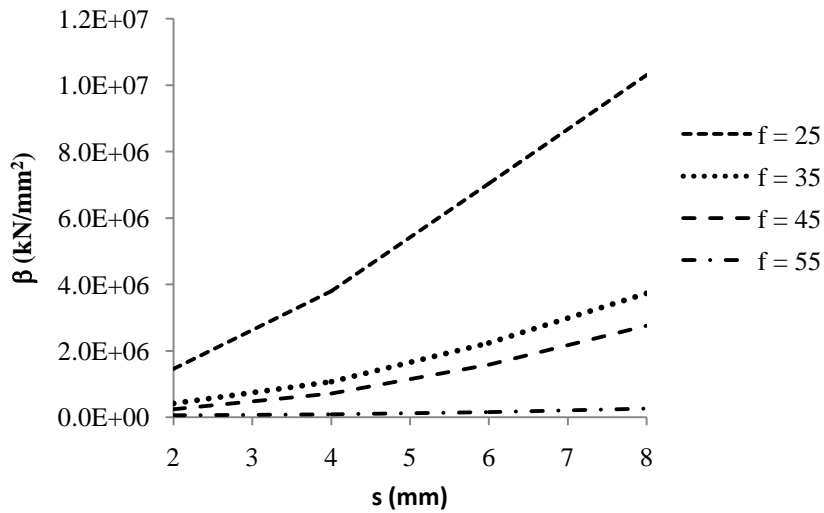


Figure 159. Stiffness versus Thickness of the Confinement

In the last step the grout is not working anymore in the area where the specimen is buckling. It's possible to consider that there is a length that can be approximated as the plastic hinge length where the stiffness of the filler material is zero and the tube is now the only one that restrains the bar. The tube can't be considered as a fully fixed restrain anymore and for this reason the thickness of the tube is now significant for the global behavior of the dissipator.

Tube

Different thicknesses of the tube are considered, according to the sizes of tube used for the dissipators. A 2, 3, 4, 5 mm thicknesses of the tube are considered. The results in terms of stiffness of the

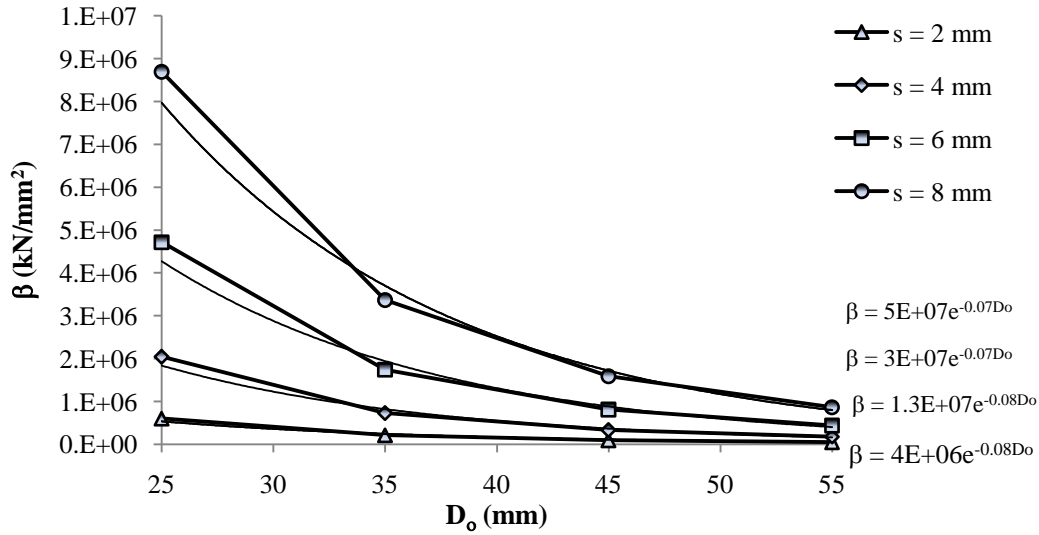


Figure 160. Stiffness versus Outer Diameter of the Tube

A general equation that allows the use of the hysteresis loop also for other thicknesses of the confinement is herein reported.

$$\beta = 4^6 * e^{-0.08D_o} + 2.27^5 * e^{-0.09D_o} * s_t^{(3.386e^{0.02D_o})} \quad (5.30)$$

Where:

β is the lateral stiffness of the confinement

D_o is the external diameter

s_t is the thickness of the tube

The comparison between the results obtained with the equation proposed above and the Sap results is shown in the picture below.

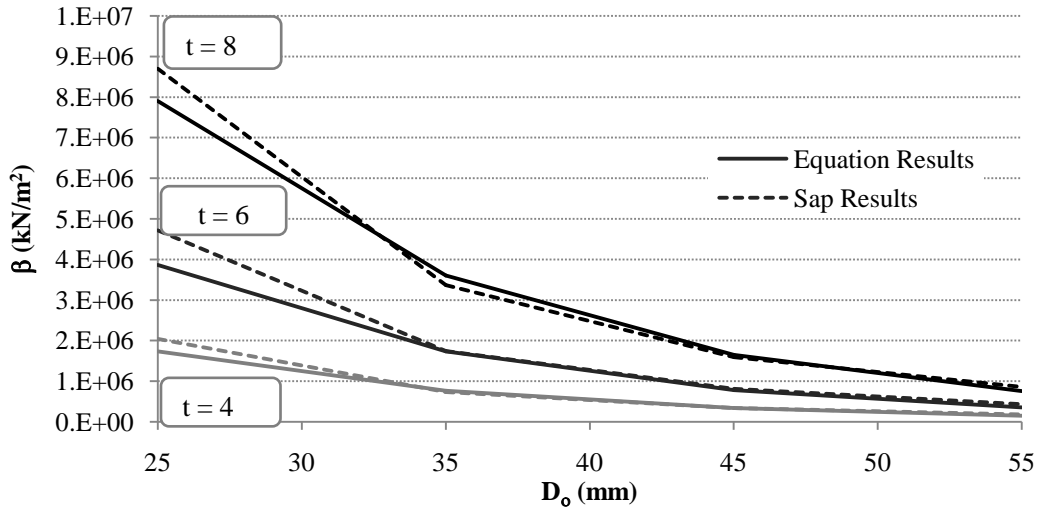


Figure 161. Fitting of Results obtained with the Equation and Sap 2000

With the parametric analysis the value of β is obtained for different diameters and thickness of the confinement in both cases, grout and epoxy.

The number of half waves is obtained by the equation:

$$\frac{\beta l^4}{\pi^4 EI} = m^2 (m + 1)^2 \quad (5.31)$$

Considering that the critical load is:

$$P = \frac{\pi^2 EI}{l^2} \left(m^2 + \frac{\beta l^4}{m^2 \pi^4 (EI)_s} \right) \quad (5.32)$$

and that it can be written in function of the effective length:

$$P_{cr} = \frac{\pi^2 EI}{L^2} \quad (5.33)$$

The value of the effective length factor, k , is:

$$k = \frac{L}{l_F} = \frac{1}{m^2 + \frac{\beta l^4}{m^2 \pi^4 (EI)_s}} \quad (5.34)$$

Where:

L is the effective length

l_F is the fuse length.

The k factor is function of the effective length of the dissipator calculated without considering the confinement and so it's equal to L_f . This is due to the fact that the Timoshenko theory of the bar on an elastic foundation is for a pin ended bar with effective length equal to the length of the bar.

5.8 Steel Dissipator Hysteresis Rule

The step by step analysis presented in 0 describes the behavior of the dissipator when subjected to an axial compression and tension loading history. To every step, a part of the hysteresis loop is associated. As already described in Chapter 4 for buckling restrained braces, different ways of failure are possible. At least three different possibilities can be considered:

- The dissipator is not confined/ not properly designed: an elastic buckling behavior has to be expected. The loop that describe this kind of dissipator is the buckling hysteresis loop ([1], [2]).

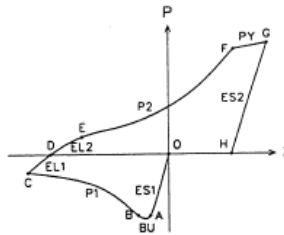
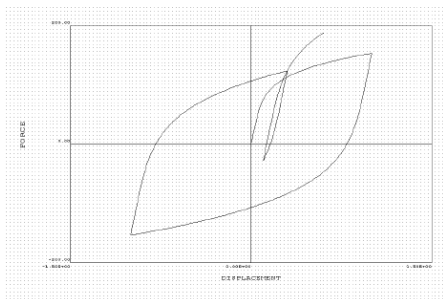
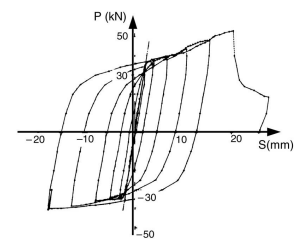


Figure 162. Steel Buckling Hysteresis Loop

- The dissipator is properly confined: the failure mode can be for low cycle fatigue after a certain number of cycles depending on the properties of the dissipator, the loading protocol, .. A Ramberg Osgood Hysteresis is suitable to describe a dissipator with the above mentioned characteristics (failure mode 1)
- The dissipator is properly confined and enough slender: the failure is for plastic buckling after a certain number of cycles; the plastic buckling occurs when the dissipator is not able to reach anymore the yielding value. To describe the behavior of a dissipator with the above mentioned properties Ramberg Osgood Hysteresis Loop is appropriate till when the dissipator is not able to reach anymore the yielding value: from this point a buckling steel hysteresis loop has to be used (failure mode 2)



Failure mode 1



Failure Mode 2

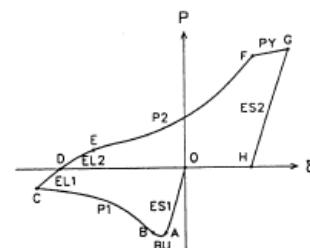


Figure 163. Different Failure modes of the Dissipator: Plastic buckling (top right), Fatigue Failure mode (bottom left).

The low cycle fatigue is one of the main causes of the crisis of the dissipator elements if properly designed. The general purpose of a fatigue model is to determine how much pre-ultimate strain cyclic loading a material can handle before the subject component fails. As Brown and Kunnath [10] have highlighted, the majority of fatigue models are created by experimentally, observing the relation between independent quantities, such as total strain amplitude or plastic strain amplitude, and relating them to dependent quantities, such as absorbed energy capacity or number of cycles to failure. These relations are then put into a fatigue life model that for constant amplitude experiments generally takes the form of:

$$y = a (x)^c \quad (5.35)$$

Where y is the independent quantity such as strain amplitude; x is the dependent quantity such as number of cycles to failure; and a and c are constants derived experimentally.

A model which adheres to this format that has been commonly used in experimental studies on fatigue life of concrete reinforcement, is the Coffin-Manson Model [11] model:

$$\varepsilon_{ap} = \frac{\Delta\varepsilon_p}{2} = \varepsilon'_f (2N_f)^c \quad (5.36)$$

Where ε_{ap} is the plastic strain amplitude; $\Delta\varepsilon_p$ is the plastic strain range; N_f is the number of whole cycles to failure, which implies that $2N_f$ is the number of half cycles to failure; ε'_f and c are again simply constants determined from experiments. The number of half cycles to failure ($f/2N$) is often used as a measure of fatigue resistance as it is generally simpler to deal with half-cycles when trying to quantify the cumulative damage from an earthquake loading. Number of half cycles can also be thought of as strain reversals.

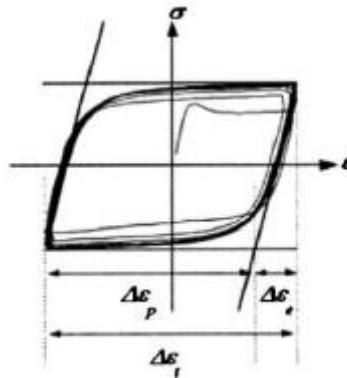


Figure 164. Hysteretic Loop

Manson [12] and Coffin [13] have indicated that the number of failure cycles N_f and each strain amplitude on steel material can be expressed as [14]:

$$\Delta\varepsilon_e = C_1 \times N_f^{m1} \quad (5.37)$$

$$\Delta\varepsilon_e = C_2 \times N_f^{m2} \quad (5.38)$$

$$\Delta\varepsilon_e = C_1 \times N_f^{m1} + C_2 \times N_f^{m2} \quad (5.39)$$

Where:

$\Delta\varepsilon_e$ is the elastic strain amplitude; $\Delta\varepsilon_p$ is the plastic strain amplitude, $\Delta\varepsilon_t$ is the total strain amplitude; C_i and m are constants that depend on the material. Maeda and Nagakomi have shown that this equation can be applied to the BRB. Plastic strain is generally distributed over the entire length of the core plates when sufficient restraint against buckling is provided and the core maintains positive stiffness after yield [14]. For this reason the same equation are used for determine an approximate value of number of failure cycles.

Considering a strain amplitude $\Delta\varepsilon_p$ equal to 0.05 the number of failure cycles is obtained.

$$\Delta\varepsilon_e = 300/200000 = 0.15\%$$

$$\Delta\varepsilon_p = 2\varepsilon_u - \Delta\varepsilon_e = 2 * 0.05 - 0.0015 = 9.85 \%$$

$$\Delta\varepsilon_t = 10\%$$

The third equation has to be used:

$$N_f = \left(\frac{\Delta\varepsilon_T}{54} \right)^{\frac{1}{0.71}} \quad (5.40)$$

$N_f = 10$ cycles to failure.

Considering a strain amplitude $\Delta\varepsilon_p$ equal to 0.03 the number of failure cycles is obtained.

$N_f = 22$ cycles to failure.

The hysteresis loop now available is a modified of the Remennikov Hysteresis Loop for Plug and Play dissipators.

The hysteresis is available for spring and multi-spring elements; if the multi-spring is used every single spring represent a dissipator with the stiffness of the single element. The multi-spring element is useful to model a series of external devices. The longitudinal stiffness, the axial yield force and the bi linear factor of the element (spring / multi-spring) must be supplied. The evaluation of the stiffness of the spring can be done considering the effect of the anchorage length of the dissipator as proposed in the next chapter. The deformations are manly concentrated in the fuse length but the higher stiffness of the external parts supply an additional stiffness that has to be considered. For this reason the member stiffness EA/L can be calculated using as L a length between the fuse length and the total length as proposed in the following chapter.

Two lines of data are required to represent the buckling of a steel dissipator element. The first line provides to the program all the information to characterize the steel bar of the dissipator, the second line gives details about the confinement. The yielding stress characterizes the filler material; the occurrence of the gap between the bar and the confinement due to tension and compression cycles depends on this value. If the material is enough elastic, there is no detachment between the bar and the grout/epoxy, otherwise a gap has to be expected. The

presence of the gap involves a not restrained deflection of the bar until the rod starts pushing again on the filler material left.

E	D	k	Dinit	ALFA	BETA	E1	E2	E3	E4
E			Elastic Modulus of Dissipator						
D			Diameter of the Bar						
k			Effective Length Parameter				$0.5 \leq k \leq 2$		
			$L_{eff} = kL$						
Dinit			Initial Lateral Displacement at mid length (if 0.0 uses L/1000)						
ALFA			Strain Hardening Alpha (if 0.0 uses a built-in rule)				$1 \leq k \leq 1.5$		
BETA			Beta factor recommended range 1.2 to 1.4				$\beta > 1$		
E1			Effective Modulus e1				> 0		
E2			Effective Modulus e2				> 0		
E3			Effective Modulus e3				> 0		
E4			Effective Modulus e4				> 0		

Restraint Data

Do	Di	Et	Eg	kR
Do		Outer Diameter of Restraint Tube		
Di		Inner Diameter of Restraint Tube		
Et		Ratio of Tube Elastic Modulus to Elastic Modulus of Dissipator		
Eg		Ratio of Grout Elastic Modulus to Elastic Modulus of Dissipator		
s		Grout/Epoxy Yield Strength		

Table 25. Data of Hysteresis Loop

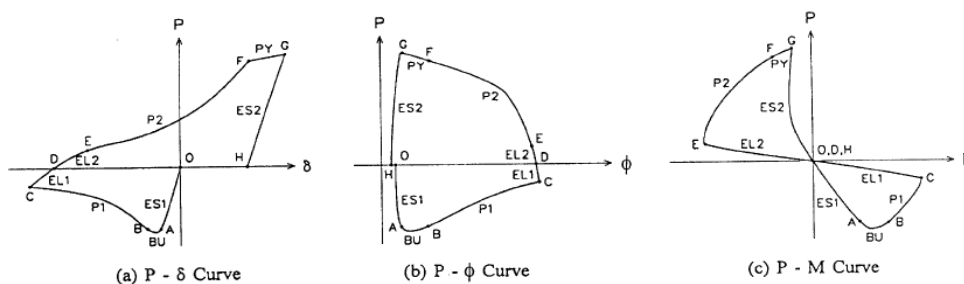


Figure 165. Required Datas of the Hysteresis Loop (top) and P- δ Curve, P- ϕ Curve, P - M Curve (bottom)

The dissipator is first subjected to an elastic compression (ESI). A buckling zone follows and it's characterized by the lateral displacement of the bar (BU). The value of compression force reached can be equal or less the yielding one; in the first situation there is no buckling and the dissipator is able to dissipate the right amount of energy. The compression force is then removed and an elongation zone follows (EL1). When a tension force is applied, there is an elastic elongation up to the yielding force (PY). The force is then removed and the first cycle compression- tension ended.

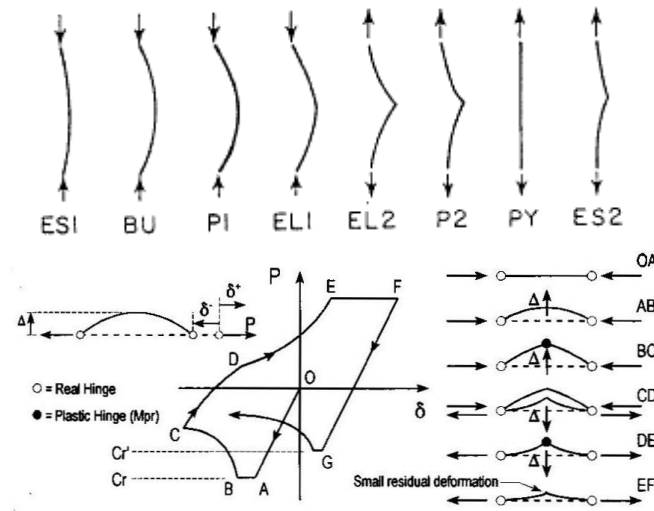


Figure 166. Deformation of the Dissipator when subjected to Compression-Tension Cycles

Considering Figure 165 loading begins at the origin (point O) and the dissipator is compressed elastically. The value reached in point A depends to the axial load and the bending moment; if the dissipator buckles this value will be smaller than the yielding one otherwise it will be similar to the yield load. At point B a plastic hinge forms where the plastic moment capacity is exceeded by the moment induced by the now eccentric load, $P\Delta$. With continued axial displacement the capacity of the dissipator falls. With unloading compression force, the still elastic portion of the device results in a reduction in the lateral deflections (C to D) with an exacerbation of the “kink”, which does not recover elastically.

When the force reverses into tension (D to E), the moments on the hinge reversed and the deflection is partially recovered. The resistance of the kinked region is significantly less compared to the axial stiffness of the dissipator, implying a region of very low stiffness between D to E. At point E the tensile capacity of the dissipator is achieved and maintained (E to F) although there is a residual displacement. When the force reverses again in compression, a plastic buckling derives; a lower value of compression is expected.

The loop is realized for a buckling behavior. For this reason also if the dissipator can reach the yielding point in compression, a decreasing of the capacity in the plastic zone follows. The loop has to be modified has proposed. At least three possibilities have to be taken into account:

- the buckling of the bar at the first cycle
- the rupture of the bar due to low cycle fatigue
- the plastic buckling of the bar after a certain number of cycles.

In the code a condition has to be applied based on the value of load reached.

Cycle n°1:

If $P < P_y$: Buckling Hysteresis Loop (Remennikov Hysteresis Loop)

If $P = P_y$: Steel Hysteresis Loop (Ramberg Osgood Hysteresis Loop)

After n cycles:

If $P < P_y$: Plastic buckling mode of failure: switch of loop from the Ramberg Osgood Hysteresis Loop to the Remennikov Hysteresis Loop

If $P = P_y$: Low cycle fatigue mode of failure: the dissipator after several cycles reach the rupture point.

5.1.1 Discussion

The hysteresis loop can provide the information useful to define which will be the failure mode of the dissipator. An example of dissipator device is represented in Figure 167.

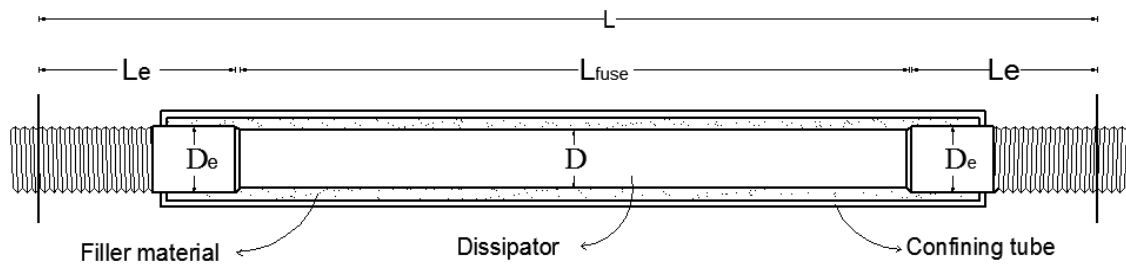


Figure 167. Example of Dissipator Device

The outer diameter of the tube and the thickness of the filler material are known, so the value of β can be determined with the equations 5.7.2 and 5.7.4. The stiffness of the bar can be calculated considering the section properties.

The dissipator is subjected to a tension and compression forces as shown in Figure 168.

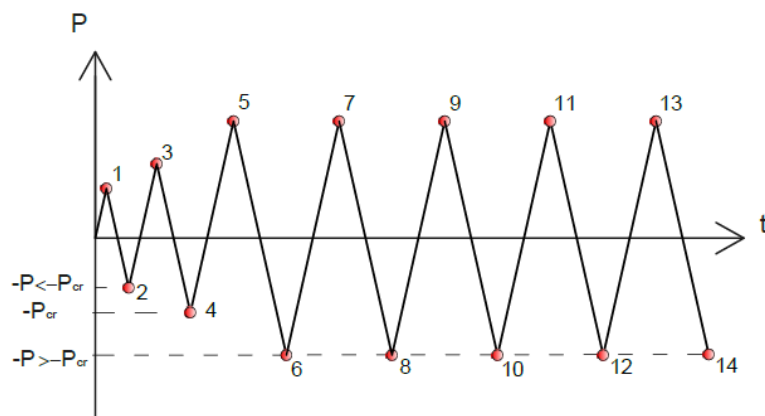


Figure 168. Test Schedule

The value of force reached by the dissipator is determined as:

$P = (k_s + k_r) * \delta_1$ In the elastic range.

$P = (k_s + k_r) * \delta_1 + BF (k_s + k_r) * \delta_2$ Elasto – plastic range.

With tension and compression cycles the stiffness of the restrain decrease depending on the increasing deflection of the bar. The stiffness of the steel bar can reduce as well due to the necking of the bar that involves a reduction of the section. The value of P is then function of the change of these parameters.

The first step is the determination of the number of cycles as function of the dissipator properties and of the strain amplitude and number of cycles that can determine the rupture of the dissipator.

The second step is to determine the value of P or δ depending if the schedule is on forces or displacement and verify if it's higher than the yielding one. If it's smaller the dissipator will buckle at the first cycle otherwise it will start dissipating.

The value of P or δ is then checked at every step. If a value of P smaller than the yielding one is reached, this means that a plastic buckling occurs. If the dissipator can reach the value of cycles that involve the fatigue rupture of the device with a yielding load, this means that the low cycle fatigue is the failure mode of the dissipator.

5.9 References

1. Remennikov, A.M.W., Warren R., *Analytical prediction of seismic behaviour for concentrically braced steel system*, in *EARTHQUAKE ENGINEERING AND STRUCTURAL DYNAMICS*. 1997. p. 859-874.
2. Remennikov, A.M., *Modelling the inelastic cyclic behaviour of a bracing member for work-hardening material*. *International Journal of Solids and Structures*, 1997. **34**(27): p. 3491-3515.
3. Qiang, X., *State of the art of buckling-restrained braces in Asia*. *Journal of Constructional Steel Research*, 2005. **61**(6): p. 727-48.
4. Timoshenko, S., *The theory of elasticity*. *Mechanical Engineering*, 1930. **52**(4): p. 494-496.
5. Uang, C.M., *Research and Application of Buckling Restrained Braces Frames*. *Steel structures*, 2004: p. 13.
6. Carr, A.J., *Ruaumoko Programme for Inelastic Dynamic Analysis - User Manual*. 2007, University of Canterbury, Christchurch.
7. SAP, A., *User Manual SAP*. 2002.
8. Lai, J.-W. and K.-C. Tsai, *Research and Application of Buckling Restrained Braces in Taiwan* 2004
9. Muir, L. and C.J. Duncan. *The AISC 2010 specification and the 14th edition steel construction manual*. in *Structures Congress 2011, April 14, 2011 - April 16, 2011*. 2011. Las Vegas, NV, United states: American Society of Civil Engineers (ASCE).
10. Brown, J. and S. Kunnath, *Low-Cycle Fatigue Failure of Reinforcing Steel Bars*. *ACI Materials Journal*, 2004: p. 457 - 466.
11. Coffin, L.F., *A Study of the Effect of Cyclic Thermal Stresses on a Ductile Metal*. American Society of Mechanical Engineers, 1954: p. 931-950.
12. Manson, S.S., *Thermal Stress and Low cycle Fatigue* ed. M.G. Hill. 1966, New York.
13. Coffin, L.F., *Experimental support for generalized equation predicting low cycle fatigue*. *Journal of Basic Engineer* 1962. **84**: p. 533-537.
14. Takeuchi, T., et al., *Estimation of Cumulative Deformation Capacity of Buckling Restrained Braces*. *Journal of Structural Engineering*, 2008.
15. Lopez, W.A. and R. Sabelli, *Seismic Design of Buckling-Restrained Braced Frames*. 2004.
16. Kardomateas, G.A. and D.S. Dancila, *Buckling of moderately thick orthotropic columns: Comparison of an elasticity solution with the Euler and Engesser/Haringx/Timoshenko formulae*. *International Journal of Solids and Structures*, 1997. **34**(3): p. 341-357.

17. Ju, Y.K., et al., *Component tests of buckling-restrained braces with unconstrained length*. Engineering Structures, 2009. **31**(2): p. 507-516.

6 The effect of anchorage length of Fused Type Dissipation

An important aspect of the dissipation devices that has to be known is the onset of dissipation and the value of displacement needed to reach the yielding load consequently.

The deformation is mainly concentrated in the fuse length but the external parts provide an additional stiffness that has to be considered in order to establish the right start of dissipation.

The following document studies the effect of the anchorage length of a dissipation element under axial loads.

The objective is to determine the “equivalent length” that has a value between the fused length and the total length and that keeps into account the effect of the terminal parts on the total displacement of the dissipater devices.

To define the “equivalent length” a factor k will be considered and it will be function of the relation between the diameters and the lengths of the fused and external parts respectively.

Two cases will be considered and two values of the factor k will be found, one before the yielding and the other one post yielding of the fused part. After the yielding point the deformation is concentrated on the fused part that is yielded (the external part are still in the elastic range) and the influence of the anchorage decreases.

6.1 Contribution of the Anchorage Length

The hysteretic dissipators have to go over the activation mark to start working and this imply that a certain displacement has to be reached in order to start dissipate (displacement activated dampers). It becomes so important to know the exact value of displacement needed to exceed the elastic limit.

The dissipator element is characterized by a total length defined as the length between the two anchorages, and a fuse length with smaller stiffness and where the deformation is mainly concentrated. The external parts provide an additional stiffness that involves a higher displacement (compared to the one of the bar without confinement) needed to start the dissipation.

A schematic example of the dissipator device is shown in the picture below.

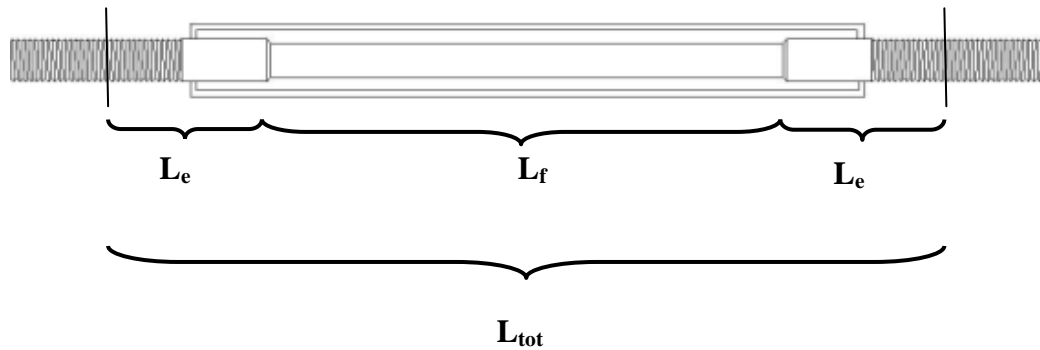


Figure 169. Specimen type - dissipator device

As shown in Figure 169, L_f is the fused length of the bar while L_e corresponds to the length of the two ends with higher stiffness. The external part is the length between the fuse and the point of application of the load and it is characterized by a higher diameter and a higher stiffness consequently.

The diameters for the fused and external lengths of the bar are ϕ_f and ϕ_e respectively.

The mechanical characteristics of the steel are summarized in the table below.

Mild steel G300

$$\sigma_y = 300 \text{ Mpa}$$

$$E = 200000 \text{ MPa}$$

$$\mathcal{G}_u = \mathcal{G}_y + rE(\varepsilon_u - \varepsilon_y)$$

$$r = 0.008 /$$

$$E_r = 1600 \text{ MPa}$$

$$\varepsilon_y = 0.00143 /$$

$$\varepsilon_u = 0.05 /$$

$$\sigma_u = 313.71 \text{ MPa}$$

As already presented in Chapter 3, different diameters and length of the dissipator have been considered.

Considering that:

ϕ_f : diameter of the fuse

ϕ_e : diameter of the external part

L_f : length of the fuse

L_e : length of the external part

The different diameters and lengths of the dissipators object of this study are summarized in the table below.

ϕ_f (mm)	ϕ_e (mm)	L_f (mm)	L_e (mm)	L_{tot} (mm)
12	16	180	82	344
16	20	240	84	408
20	24	300	86	472
24	32	360	88	536
26	32	390	90	570

Table 26. Diameters and Lengths of Dissipator Devices

A force- displacement analyses for all the dissipators object of this study are carried out in order to estimate the effect of the anchorage on the total displacement and determine for which value of displacement the device starts yielding.

Considering the displacements of the fused and external length up to a deformation of ϵ_u (0.05), the two hysteresis loops of the two sections are determined and the displacements are summed. The total displacement is consequently obtained.

The first specimen considered is the one with a fuse diameter of 12 mm and an external diameter of 16 mm.

$\phi_1 = 12$				$\phi_2 = 16$			
F (N)	σ (Mpa)	ϵ	Δ (mm)	F (N)	σ (Mpa)	ϵ	Δ (mm)
0	0.0	0.0000	0.00	0.00	0.00	0.00000	0.00000
20000	176.8	0.0009	0.16	20000.00	99.47	0.00050	0.04078
33929.2	300.0	0.0015	0.27	33929.20	168.75	0.00084	0.06919
34494.69	305.0	0.0046	0.83	34494.69	171.56	0.00086	0.07034
35060.17	310.0	0.0078	1.40	35060.17	174.38	0.00087	0.07149
42718.48	377.7	0.0501	9.01	42718.48	212.46	0.00106	0.08711
				60318.58	300.00	0.00150	0.12300
				75800.35	377.00	0.04963	4.06925

Table 27. Displacements of a 12 mm and 16 mm Diameter Bars

Under the hypothesis that all the deformations occurs in the fuse, the dissipator starts yielding when reached 0.27 mm of axial displacement.

If the anchorage effect is considered, the real displacement of the dissipator is obtained summing the values of displacements of the fuse and the two external parts. The hysteresis loops are represented in the graph below. A chart representing the force-displacement of the fuse part only, the external parts only and the global behavior of the dissipator is shown in Figure 170.

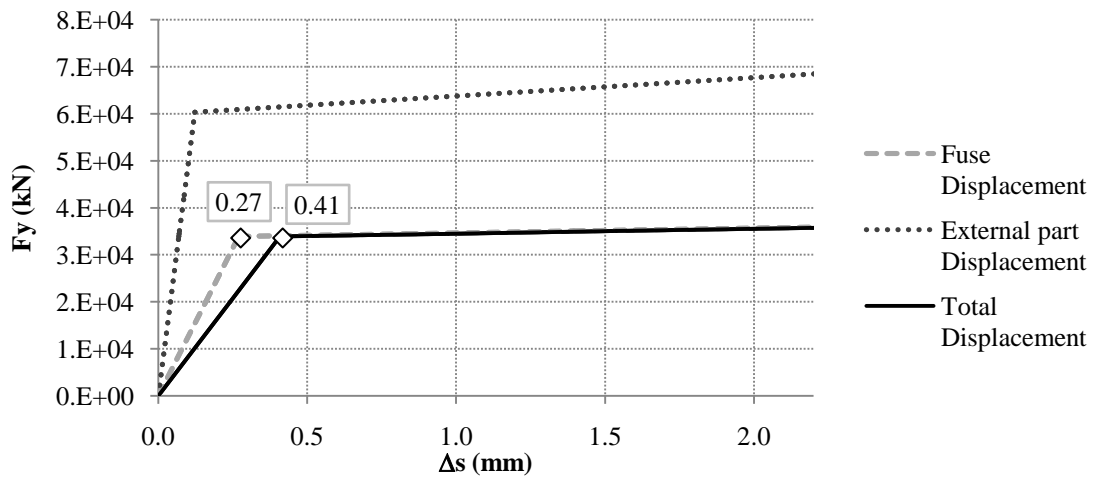


Figure 170. Displacement of the fuse, displacement of the external part and total displacement of specimen 1

As shown in Figure 170 when the fuse yield the external part is still in the elastic range; the fuse reaches the break point while the external part is still elastic.

Considering now all the other dissipator considered, the total displacements are shown in the figures below.

$$\phi_f = 16 \text{ mm and } \phi_e = 20 \text{ mm}$$

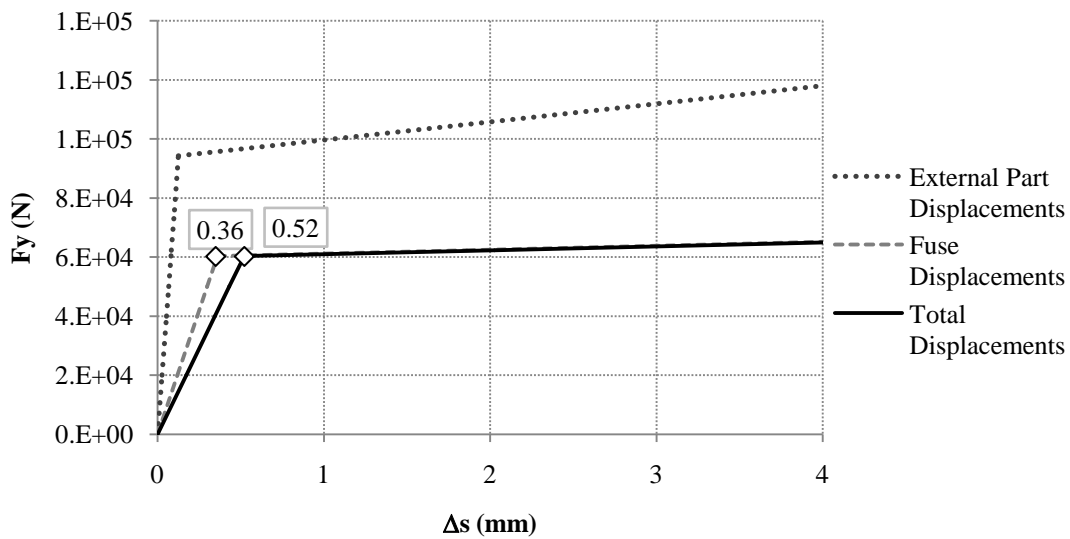


Figure 171. Displacement of the fuse, displacement of the external part and total displacement of specimen 2

$\phi_f = 20 \text{ mm}$ and $\phi_e = 24 \text{ mm}$

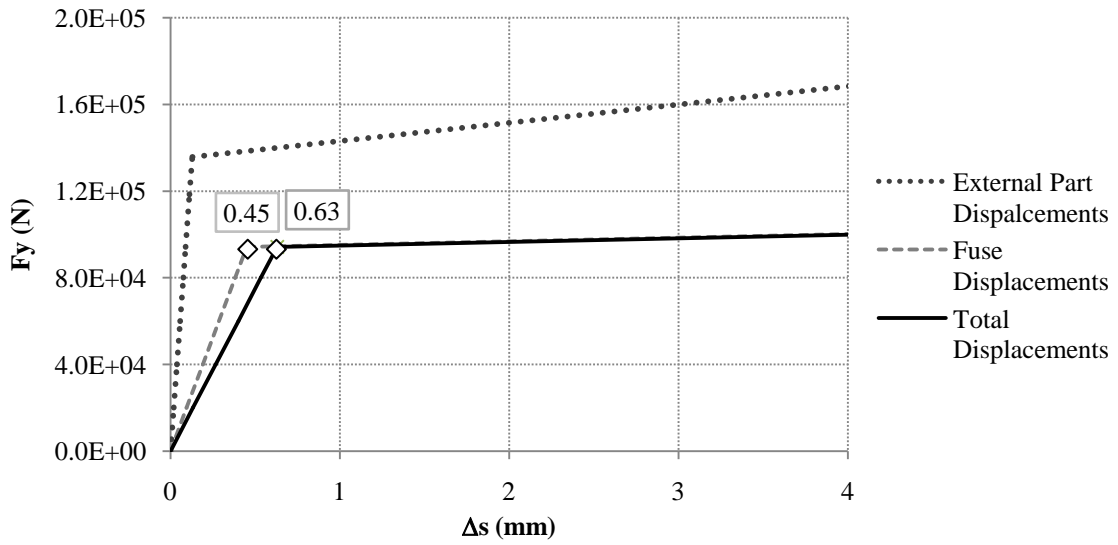


Figure 172. Displacement of the fuse, displacement of the external part and total displacement of specimen 3

$\phi_f = 24 \text{ mm}$ and $\phi_e = 32 \text{ mm}$

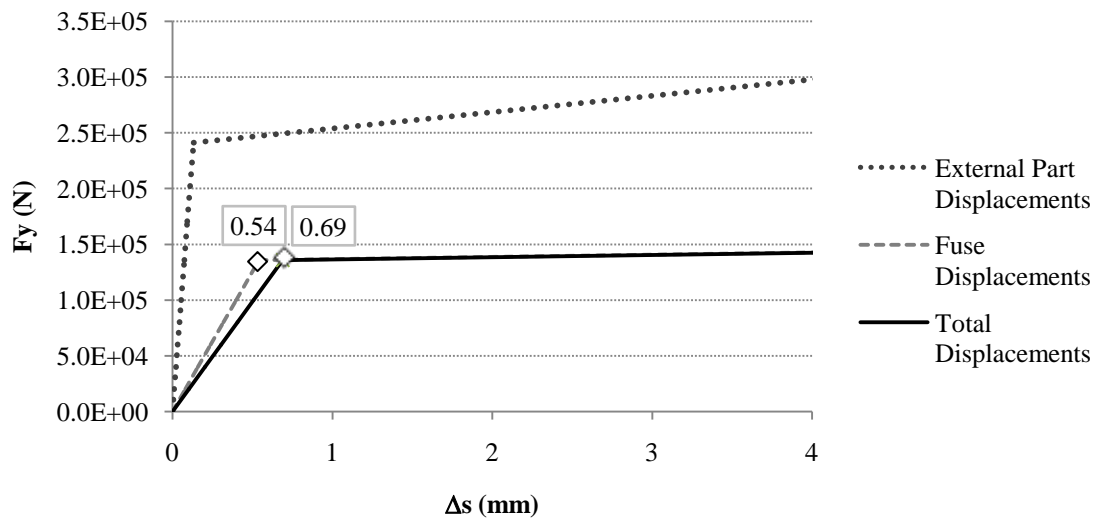


Figure 173. Displacement of the fuse, displacement of the external part and total displacement of specimen 4

$\phi_f = 26 \text{ mm}$ and $\phi_e = 32 \text{ mm}$

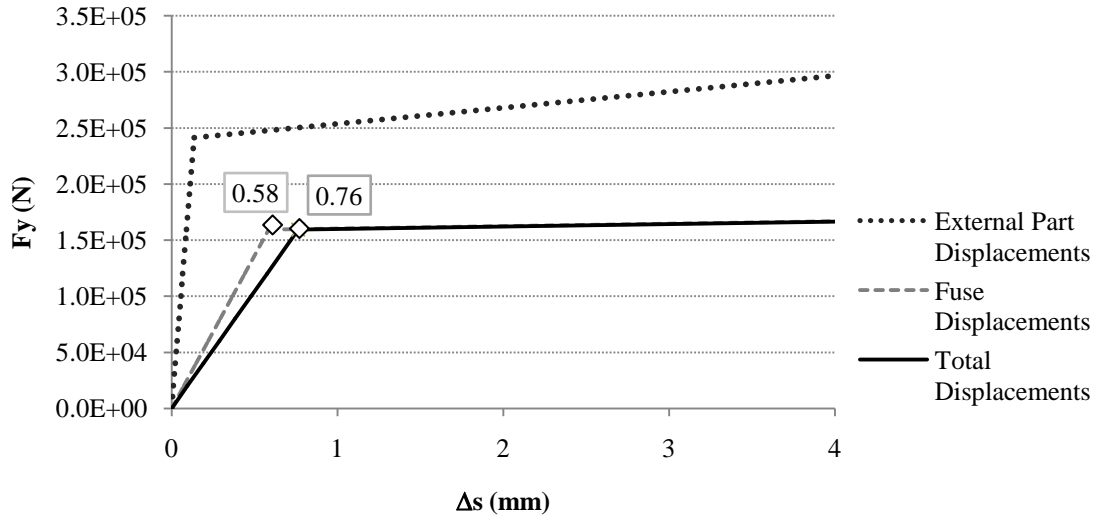


Figure 174. Displacement of the fuse, displacement of the external part and total displacement of specimen 5

6.2 The Effect of the Anchorage in the Elastic Range

Before reaching the yielding point the stress along the bar will be constant and so the displacement is defined as:

$$\Delta s = \epsilon_e L$$

$$\Delta s_{\text{tot}} = \Delta s_{e1} + \Delta s_f + \Delta s_{e2}$$

$\Delta s_{e1}, \Delta s_{e2}$: displacements of the external parts of the dissipator device

Δs_f : displacement of the fused part of the dissipator device

$$\Delta s = \frac{FL_{e1}}{EA_{e1}} + \frac{FL_f}{EA_{fuse}} + \frac{FL_{e2}}{EA_{e2}} \quad (6.1)$$

Considering that when yield occurs in the fused area :

$$F = f_y * A_{\text{fused}}$$

$$\Delta s = \frac{f_y A_{\text{fuse}} L_{e1}}{EA_{e1}} + \frac{f_y A_{\text{fuse}} L_f}{EA_{fuse}} + \frac{f_y A_{\text{fuse}} L_{e2}}{EA_{e2}} \quad (6.2)$$

In this particular case:

$$A_{e1} = A_{e2} \text{ and } L_{e1} = L_{e2}$$

$$\Delta S = \frac{f_y A_{fuse}(L_{e1} + L_{e2})}{EA_e} + \frac{f_y L_f}{E} \quad (6.3)$$

Where:

$$A = \pi \frac{\phi_f^2}{4} \quad A = \pi \frac{\phi_e^2}{4}$$

Rearranging the formula the value of Δs is:

$$\Delta S = \frac{f_y}{E} L_{tot} \left[\left(\frac{\phi_f}{\phi_e} \right)^2 \times \left(1 - \frac{L_f}{L_{tot}} \right) + \frac{L_f}{L_{tot}} \right] \quad (6.4)$$

The displacement is a function of the total length of the dissipator, the yielding stress, the elastic modulus and a factor that keep into account the ratio between the fuse and external diameters and the fuse and total lengths.

$$k_a = \left(\frac{\phi_f}{\phi_e} \right)^2 \times \left(1 - \frac{L_f}{L_{tot}} \right) + \frac{L_f}{L_{tot}} \quad (6.5)$$

The value of displacement can be written as:

$$\Delta S = \frac{f_y}{E} L_{tot} k_a \quad (6.6)$$

The values of Δs have already been calculated and the values of the equivalent lengths of the dissipators are herein reported. The equivalent length keeps into account the effect of the terminal parts on the total displacement of the dissipater devices and it's defined as:

$$L_{eq} = k L_{tot} \quad (6.7)$$

ϕ_f (mm)	ϕ_e (mm)	L_f (mm)	L_e (mm)	L_{tot} (mm)	k_a	Δy (mm)	L_{eq} (mm)
12	16	180	164	344	0.79	0.41	272.3
16	20	240	168	408	0.85	0.52	347.5
20	25	300	172	472	0.87	0.63	410.1
24	32	360	176	536	0.86	0.69	459.0
24	32	390	180	570	0.86	0.76	491.3

Table 28. Equivalent Lengths for the Different Dissipators

Considering now the following ranges of ratios:

$$0.5 \leq \phi_f / \phi_e \leq 1$$

$$0.1 \leq L_f / L_e \leq 1$$

The values of k_a is calculated for the ranges of diameters and length ratios considered; known k_a and the total length, the equivalent lengths can be obtained (See

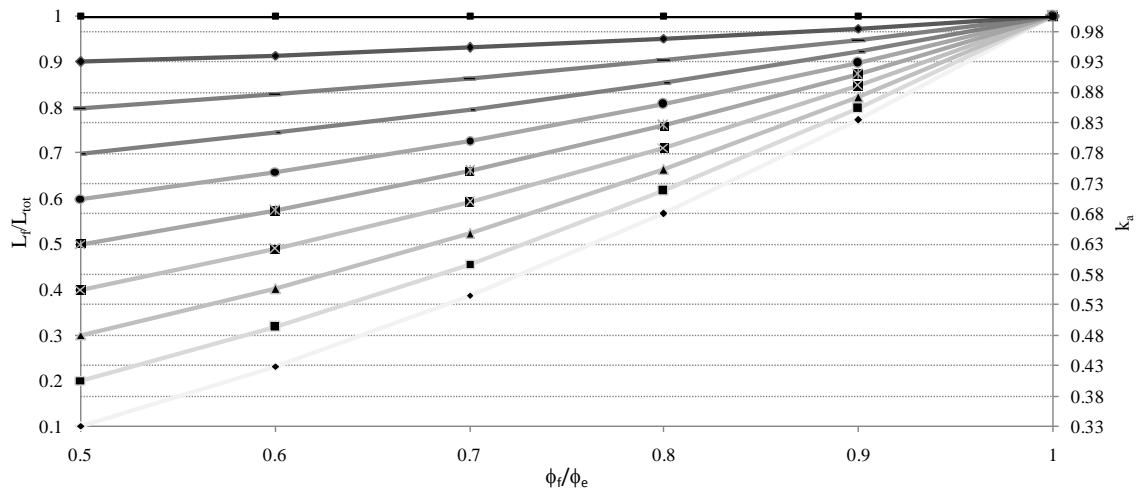


Figure 175. Values of k with relation to ϕ_f/ϕ_e and L_f/L_{tot}

As the fuse diameter gets close to the external diameter and the fuse length gets close to the total length, the equivalent length approaches the total length. The effect of the anchorage is relevant if there is a considerable change in stiffness, otherwise is non essential. In the design of the dissipators studied, the diameter of the external part has been chosen considering that the internal diameter has to be bigger than the fuse diameter. For this reason the ratio of diameters is comprised between 0.75 and 0.85, and the ratio of length is comprised between 0.5 and 0.7 and so the value of k is around 0.8 to 0.9.

6.2.1 Example of application of the k factor

The above calculation method has been applied to the specimen in the figure below of upcoming testing to be performed in order to characterize the performance of the fused type dissipation device.

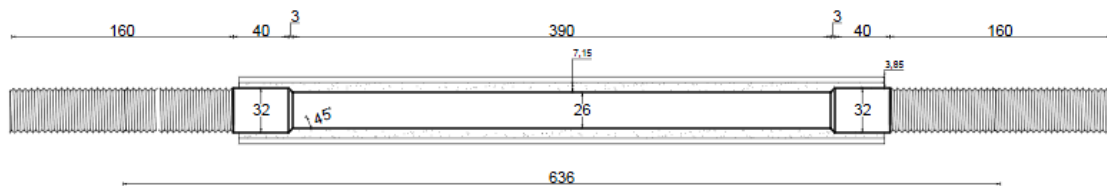


Figure 176. Specimen of upcoming UoC testing

The total length is the one between the point of application of the uni axial testing machine and the value is 636 mm. The fused length is 390 mm. The diameters are of 26 mm and 32 mm respectively of the fuse and of the external part.

The use of mild steel is also assumed ($f_y = 300$ MPa, $E = 200$ GPa).

$$k_a = \left(\frac{\phi_f}{\phi_e}\right)^2 \times \left(1 - \frac{L_f}{L_e}\right) + \frac{L_f}{L_{tot}} = \left(\frac{26}{32}\right)^2 \times \left(1 - \frac{390}{636}\right) + \frac{390}{636} = 0.86$$

$$\Delta s = \frac{f_y}{E} L_{tot} k = \frac{300}{200000} \times 636 \times 0.86 = 0.82 \text{ mm}$$

It is worth noting that without the introduction of the k factor and so considering that all the deformations happens in the fuse, the yield displacement, Δs , would be estimated at 0.58 mm which would have effect on the final ductility demand of the device.

6.3 The Effect of the Anchorage in the Plastic Range

After the yielding point the total displacement is defined as the sum of the displacements of the different parts of the specimen.

The fused part is now in the plastic range while the external parts are still elastic.

The total displacement is so defined as the sum of the two elastic components of the external parts ($\Delta\varepsilon_{e1}$, $\Delta\varepsilon_{e2}$) and of the displacement of the fused part that is given by an elastic contribution and a plastic one ($\Delta\varepsilon_{ef}$, $\Delta\varepsilon_{pf}$).

Considering that the specimen has reached a stress f_1 in the plastic range, the formula of the total displacement is:

$$\Delta S = \underbrace{\frac{f_y A_{fuse} L_{e1}}{E A_{e1}}}_{\Delta\varepsilon_{e1}} + \underbrace{\frac{f_y A_{fuse} L_f}{E A_{fuse}}}_{\Delta\varepsilon_{ef}} + \underbrace{\frac{(f_1 - f_y) \times (L_f - \Delta L_f)}{E_1}}_{\Delta\varepsilon_{pf}} + \underbrace{\frac{f_y A_{fuse} L_{e2}}{E A_{e2}}}_{\Delta\varepsilon_{e2}} \quad (6.8)$$

Where f_1 is the stress considered.

Considering that:

$$L_{e1} + L_{e2} = L_e; \quad L_{e1} = L_{e2}$$

And that on the plastic range the Young modulus is reduced ($E_1 = 0.008 E$):

$$E_1 = 0.008 E = 1600 \text{ MPa}$$

the total displacement can be written as:

$$\Delta S = \frac{f_y L_f}{E} + \frac{(f_u - f_y) \times (L_f - \Delta L_f)}{E_1} + \frac{f_y A_f L_e}{E A_e} \quad (6.9)$$

Simplifying $L_f - \Delta L_f$ with L_f and multiplying the terms for the displacement of the fuse part (elastic and plastic displacements) the formula becomes:

$$\Delta S = \left[\frac{f_y L_f}{E} + \frac{(f_u - f_y) \times L_f}{E_1} \right] \times \left[1 + \left(\frac{\phi_f}{\phi_e} \right)^2 \times \frac{f_1}{E} \times \frac{L_e}{L_f} \times \frac{1}{\left(\frac{f_y}{E} + \frac{f_1 - f_y}{0.008 E} \right)} \right] \quad (6.10)$$

The equation can be written in function of L_f/L_{tot} in order to find out a value of the factor k that depends only from the diameters and lengths ratios.

$$\Delta S = \left[\frac{f_y L_f}{E} + \frac{(f_1 - f_y) \times L_f}{E_1} \right] \times \underbrace{\left[1 + \left(\frac{\phi_f}{\phi_e} \right)^2 \times \frac{f_1}{E} \times \frac{1}{\left(\frac{L_f}{L_{tot}} - 1 \right)} \times \frac{1}{\left(\frac{f_y + f_1 - f_y}{E + 0.008E} \right)} \right]}_{k_1} \quad (6.11)$$

$$k_1 = 1 + \left(\frac{\phi_f}{\phi_e} \right)^2 \times \frac{f_1}{E} \times \frac{L_e}{L_f} \times \frac{1}{\left(\frac{f_y + f_1 - f_y}{E + 0.008E} \right)} \quad (6.12)$$

The factor k_1 is function of the relation between the lengths of the fuse and total length and of the relation between the diameters (fused diameter and external diameter) and keeps into account the level of stress reached (f_1).

$$L_{eq} = k_1 \times L_f \quad (6.13)$$

As case study the equivalent length of the specimens considered for the value of elongation equal to $\varepsilon_1 = 0.01$.

Considering $\varepsilon_1 = 0.01$ as elongation the equivalent lengths are summarized in the table below.

ϕ_f (mm)	ϕ_e (mm)	L_f (mm)	L_e (mm)	L_{tot} (mm)	k_1	L_{eq} (mm)
12	16	180	122	424	1.12	473.52
16	20	240	84	408	1.07	436.00
20	24	300	86	472	1.06	500.78
24	32	360	88	536	1.04	558.58
26	32	390	90	570	1.05	596.60

Table 29. Values of k_1 and equivalent lengths for $\varepsilon = 0.01$

For the second value of elongation, $\varepsilon_u = 0.05$, the equivalent lengths are:

ϕ_f (mm)	ϕ_e (mm)	L_f (mm)	L_e (mm)	L_{tot} (mm)	k_1	L_{eq} (mm)
12	16	180	122	424	1.03	436.28
16	20	240	84	408	1.02	414.94
20	24	300	86	472	1.02	479.14
24	32	360	88	536	1.01	541.60
26	32	390	90	570	1.01	576.60

Table 30. Values of k_1 and equivalent lengths for $\varepsilon = 0.01$

It is worth to notice that increasing the total displacement the equivalent length approaches to the fused length.

6.1.1 Influence of the Anchorage after Yielding

Estimating the influence of the anchorage after the yielding, the formula described above is used for different values of displacements imposed (0.8, 1, 2, 5, 10, 15, 20 mm) and for a specimen of $L_f = 420$ mm and $L_{tot} = 525$ mm chosen by way of example.

The total displacement is defined as:

$$\Delta s = \left[\frac{f_y L_f}{E} + \frac{(f_n - f_y) \times L_f}{E_1} \right] \times \left[1 + \left(\frac{\phi_f}{\phi_e} \right)^2 \times \frac{f_n}{E} \times \frac{1}{\left(\frac{L_f}{L_{tot}} - 1 \right)} \times \frac{1}{\left(\frac{f_y + f_n - f_y}{E + 0.008E} \right)} \right] \quad (6.14)$$

Δs (mm)	f_n (Mpa)	k	$\Delta \varepsilon_1 = \Delta s / L_{eq}$	$\Delta \varepsilon_2 = \Delta s / L_f$	$\Delta \varepsilon_3 = \Delta s / L_{tot}$	$\Delta \varepsilon_1 / \Delta \varepsilon_2$
1	304.08	1.13	0.001	0.001	0.001	0.89
1	306.13	1.10	0.002	0.002	0.002	0.91
2	310.23	1.07	0.004	0.005	0.003	0.94
5	322.52	1.03	0.012	0.012	0.008	0.97
10	343.01	1.02	0.023	0.024	0.017	0.98
15	363.50	1.01	0.035	0.036	0.025	0.99
20	383.98	1.01	0.047	0.048	0.033	0.99

Table 31. Comparison between the values of strain

f_n is the value of stress corresponding to the different values of elongation considered.

The three loops $\Delta \varepsilon_1$, $\Delta \varepsilon_2$, $\Delta \varepsilon_3$ are represented in the figure below.

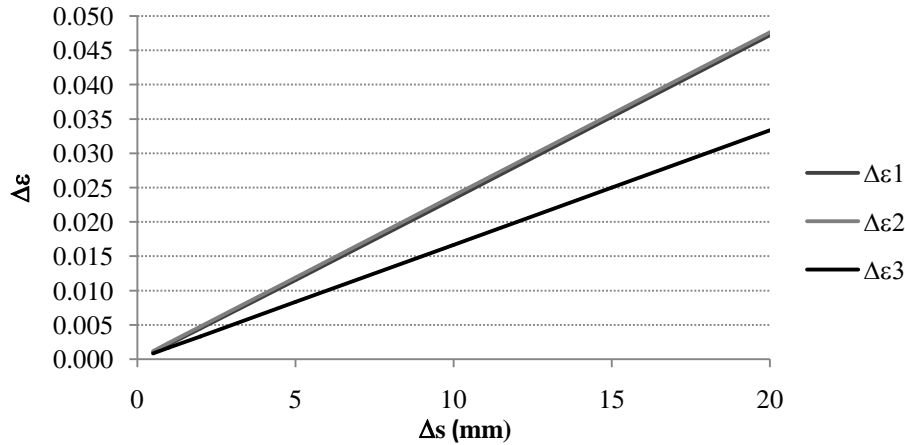


Figure 177. Comparison between the values of strain

When the fuse yields, all the stress falls in the fuse area. The effect of the anchorage becomes less relevant as the displacement increase (the fuse and total length ratio approaches 1).

Increasing the value of displacement the equivalent length tends to the fuse length.

Δs	f_n	k	$L_{eq}(\text{mm})$	$L_f(\text{mm})$	$L_{tot}(\text{mm})$
0.8	300.25	1.40	588		
1	301.01	1.31	550		
2	304.81	1.15	483		
5	316.23	1.06	445	420	664
10	335.25	1.03	432		
15	354.27	1.02	428		
20	373.30	1.02	428		

Table 32. Values of equivalent length obtained with different displacements

As shown in the graph after the yielding the elongation considering the L_{eq} and the elongation considering the L_f are almost the same and they are getting close increasing the displacement. The values of $\Delta\varepsilon_1/\Delta\varepsilon_2$ approach 1 increasing the displacement. At the same time the value of k_l approaches 1 increasing the displacement and that means that the equivalent length becomes almost equal to the fused length.

6.4 Application of the Equivalent Length

The study that follows considers some applications of the equivalent length. The first one refers to the possibility to use the equivalent length when calculating the axial stiffness of the spring in a Ruumoko model of the dissipator [1].

In the second application the use of the equivalent length when calculating the strain of the external dissipator during a moment rotation analysis of a hybrid connection is proposed.

6.1.2 Determination of the Axial Stiffness of the Spring or Multi-Spring

The equivalent length provides a value of length of the dissipator that considers the effect of the anchorage on the global displacement. The anchorage supplies an additional stiffness that could be considered in the modeling of the dissipator as already proposed in Chapter 4.

Modeling the dissipator the properties of the spring or multi-spring depending on the model have to be supplied. The first line of data with the basic section properties requires the value of stiffness of the spring.

A not exact value of stiffness implies a not exact determination of the displacement and so of the onset of dissipation.

Considering for example a dissipator with the following characteristics:

$$\begin{aligned}
D &= 20 \text{ mm} & A &= 314 \text{ mm}^2 \\
D_o &= 24 \text{ mm} & A_e &= 452 \text{ mm}^2 \\
L_f &= 300 \text{ mm} \\
L_{tot} &= 470 \text{ mm}
\end{aligned}$$

The value of displacement at the yielding point has been calculated as:

$$\Delta_s = \frac{f_y}{E} L_{tot} k_a = \frac{f_y}{E} L_{eq}$$

The stiffness is so defined:

$$k = \frac{F}{\Delta_s} = \frac{f_y A_F}{\frac{f_y}{E} L_{eq}} = \frac{E A_f}{L_{eq}}$$

Considering that:

$$L_f / L_{tot} = 0.64$$

$$\phi_f / \phi_e = 0.83$$

the value of L_{eq} is equal to 420 mm.

The value of stiffness of the dissipator element is equal to:

$$k = E A_f / L_{eq} = (200000 * 314) / 420 = 149.523 \text{ kN/mm.}$$

The other two possibilities to define the value of stiffness provide values that are overestimating or underestimating this section property.

$$k_1 = E A_f / L_{tot} = (200000 * 314) / 470 = 133.617 \text{ kN/mm}$$

$$k_2 = E A_f / L_f = (200000 * 314) / 300 = 209.333 \text{ kN/mm}$$

The use of the equivalent parameters provides a valid value of stiffness that considers the right contribution of the external parts in the global behavior.

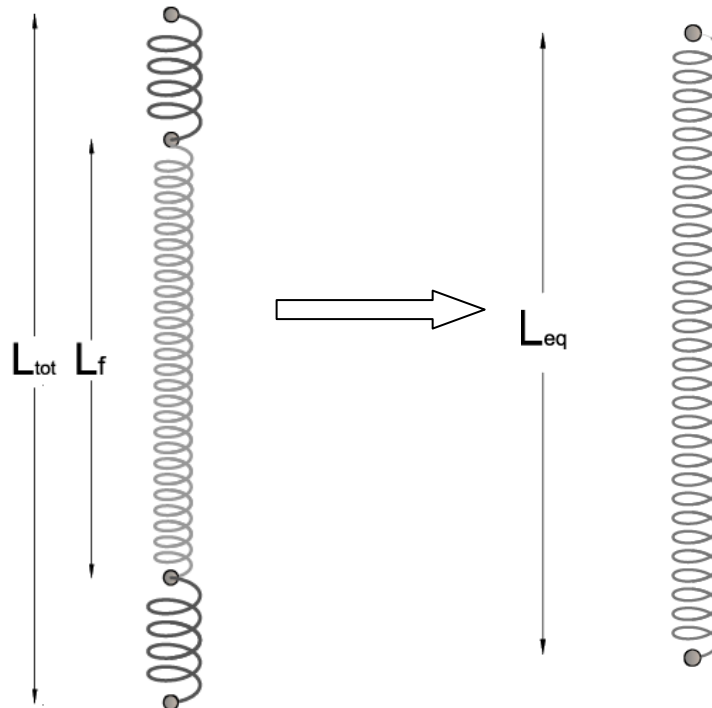


Figure 178. Alternative Solution using the Equivalent Length

6.4.1 Evaluation of the Strain of the External Dissipator

The moment – rotation analysis procedure for hybrid connection is based on the Monolithic Beam Analogy presented by [2] and then implemented by [3]. The analogy has already been presented in Chapter 2 with all the different steps needed to have the section equilibrium.

The first step of the procedure is to fix the rotation and guess the position of the neutral axis. In this way the strain in the unbonded post tension tendons and mild steel dissipators can be evaluated.

If the hybrid section is realized with Plug and Play dissipators the strain of the devices is calculated as:

$$\varepsilon_{se} = \frac{\Delta_{si}}{L_{ubi}}$$

Where:

Δ_{si} is the displacement on the bar of mild steel due to the gap opening

$$\Delta_{si} = \vartheta * (d - c)$$

L_{ubi} is the unbonded length of the dissipator.

It has to be considered that calculating the stress using the unbonded length we are supposing that the stress is normally distributed along the length of the bar. Otherwise there is a different distribution of the stress in the fused part with a diameter smaller than the one of the external part that can be partially unbonded.

The use of the equivalent length is proposed evaluating the strain.

$$\epsilon_{se} = \frac{\Delta_{si}}{L_{eq}}$$

6.5 Conclusions

The study investigates the influence of the anchored length on the total displacement of the dissipator device.

In order to keep into account the effect of the anchorage, a factor k has been considered and it's needed to find an equivalent length.

According to the results it's possible to notice that the effect of the external parts are significant till when the fuse yields; this means that an equivalent length has to be considered to find the total displacement of the dissipator to reach the yield point. To consider the fuse length or the total length instead of the equivalent length will lead to a wrong value of total displacement and so to a wrong value of the onset of dissipation.

After having reached the yielding point the fuse is in the plastic range and all the dissipation is there.

The effect of the anchorage decreases while increasing the elongation and the equivalent length approaches the fused length.

The difference between equivalent length and fuse length become less and less important raising the displacement imposed as shown in the table 19.

6.6 References

1. Carr, A.J., *Ruaumoko Programme for Inelastic Dynamic Analysis - User Manual*. 2007, University of Canterbury, Christchurch.
2. Pampanin, S., M.J.N. Priestley, and S. Sritharan, *Analytical Modelling of the Seismic Behaviour of Precast Concrete Frames Designed with Ductile Connections*. *Journal of Earthquake Engineering*, 2001. **Vol. 5**: p. 40.
3. Palermo, A., *The use of controlled rocking in the seismic design of bridges*, 2004, Politecnico di Milano.
4. NZCS, *Press Design Handbook*. 2010, Wellington, New Zealand.

7 Case Study – Carterton Events Center

The Carterton Events Center is a multi purposes community events center in the center of the town. The building was selected as a suitable case study due to use of the Press Lam System for the lateral resisting frame. Post tensioned walls realized with post tensioned wall and internal mild steel dissipators provide the re-centering and dissipating capacity of the building. The results of a finite element analysis of the building are presented in the following pages. For the purpose of this study the structure will be re designed using external dissipators.

7.1 Introduction to the Carterton Events Center

The Carterton Events Center is a multi purposes community events center in the center of the town. The building includes an auditorium and town hall, exhibition spaces and information center and then an existing refurbished Youth Centre is encapsulated along with new Community Meeting rooms, Archive storage and many other facilities.

A plan of the building is shown in the picture below Figure 179.

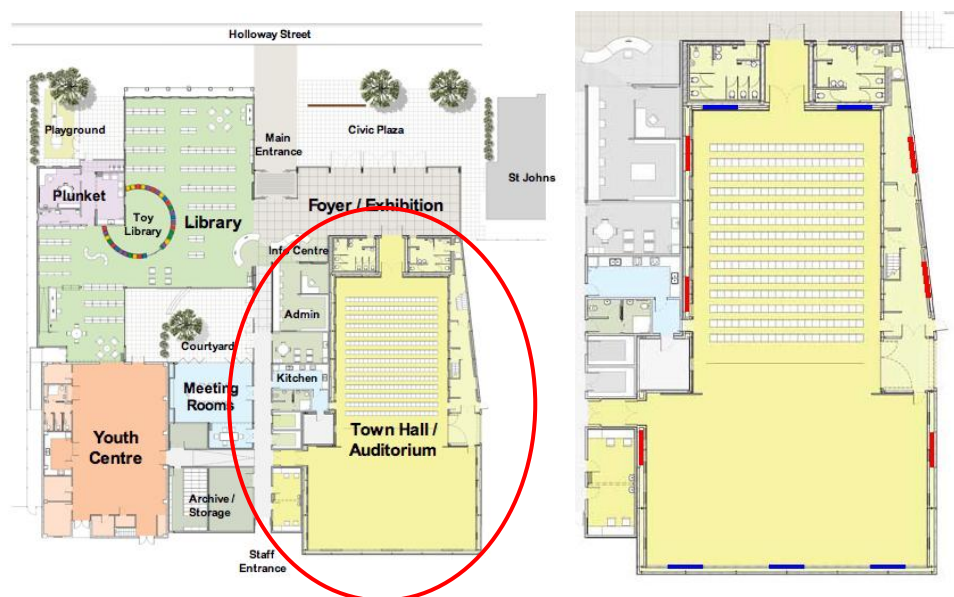


Figure 179. Plan of the Carterton Events Centre (left); Auditorium Plan showing walls locations (right) [1]

As shown in Figure 1 the Auditorium forms part of the Carterton Events Centre complex. The space is multi use and has the ability to hold up to 300 people. The auditorium can also be used as an emergency welfare and so it's important to guarantee the use after a natural disaster. The Press-Lam system has been chosen for the lateral resisting frame; post tensioned tendons are installed through the center of timber wall and provide the re-centering capacity while mild steel bars provide the energy dissipation. The Pres Lam system relies upon a controlled rocking mechanism and the connection allows the walls to remain virtually free of damage during an earthquake event.

The building is the second one in the world that uses the Pres-Lam system after the Nelson-Marlborough Institute of Technology's Arts and Media building Figure 180.



Figure 180. Photos taken during construction and installation of LVL post-tensioned and coupled shear panels, NMIT Arts & Media Building

The width of the auditorium of the Carterton Events Center is 14 meters over the auditorium and 20 meters over the stage area. To create a large open space timber trusses are used for the roof system supported on steel columns.

Eleven shear walls are installed, six in the longitudinal direction (N S) and five in the transversal direction (E-W). They are made of four layers of 45 mm LVL sheets, glue-laminated together to form a 180 mm thick wall. As a result each wall of 6.7 m high and 2.4 m length and 0.18 m depth contains approximately 22 sheets of LVL (3m x 1.2m x45mm) which equates to a total 231 sheets. Also made in LVL are the Carterton Auditorium roof trusses.

7.1.1 Material and Section Properties

Laminated Veneer Lumber (LVL)

A fairly recent addition to the world of engineered woods, Laminated Veneer Lumber is made from plantation-grown softwood veneers that are bonded together with a waterproof adhesive.

Developed in 1970s for the general market, LVL popularity as a structural material has grown recently.

Structural LVL is an engineered wood composite made from rotary peeled veneers, glued with a durable adhesive and laid up with parallel grain orientation to form long continuous sections.

It is suited to structural applications such as beams, rafters and columns in wide range of building including houses, commercial, industrial and rural structures. It is suited to structural applications such as beams, rafters and columns in wide range of building including houses, commercial, industrial and rural structures [2]

LVL is manufactured in Australasia in mills operated by Carter Holt Harvey Futurebuild (at Marsden Point in Northland and Nangwarry, South Australia), Nelson Pine Industries (Nelson), WESbeam (Perth, Western Australia) and Juke Nissho Ltd (Gisborne); Juke focus mainly on production for Japan.

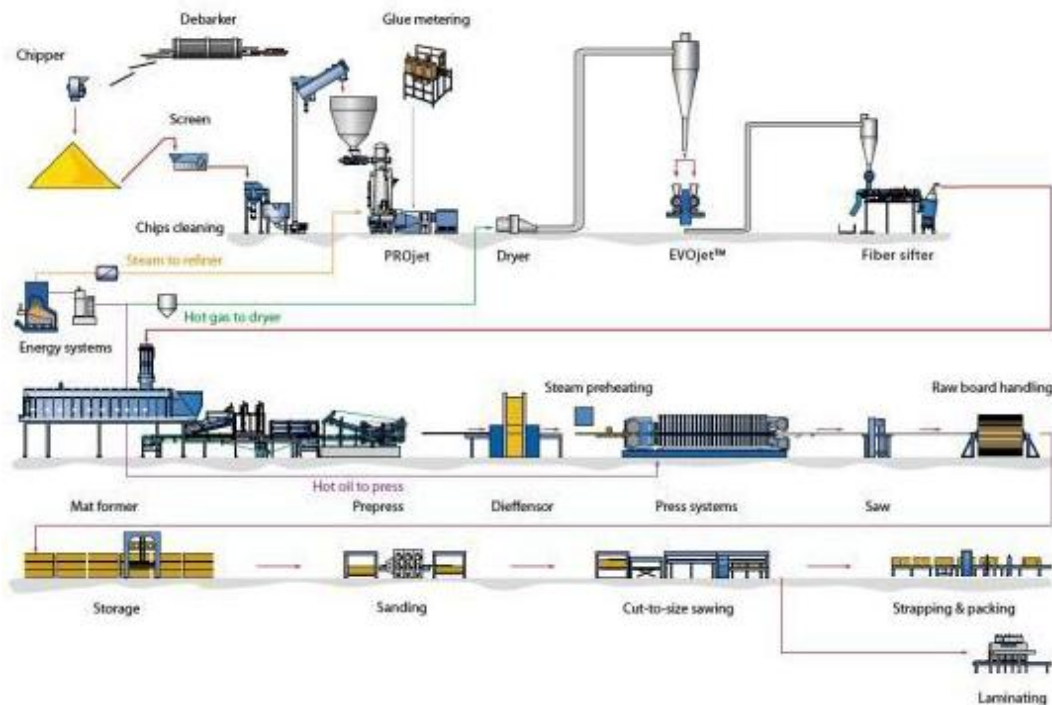


Figure 181. Manufacturing Process of LVL

LVL is manufactured by laminating veneer, using phenolic adhesive in a continuous process. The grain direction of all veneers is usually in the longitudinal direction. The logs are selected for appropriate quality, cut to length and heated by soaking or spraying with hot water to enhance “peel ability” before the process in the rotary lathe. In the drier jets of hot air perpendicular to the veneer surface dry the veneer in about 10 minutes to a target moisture content of about 6%. Veneers are then measured for stiffness and graded width, moisture content and visual appearance. A combination of grades allow manufacturer to produce LVL of specific properties for specific purposes.

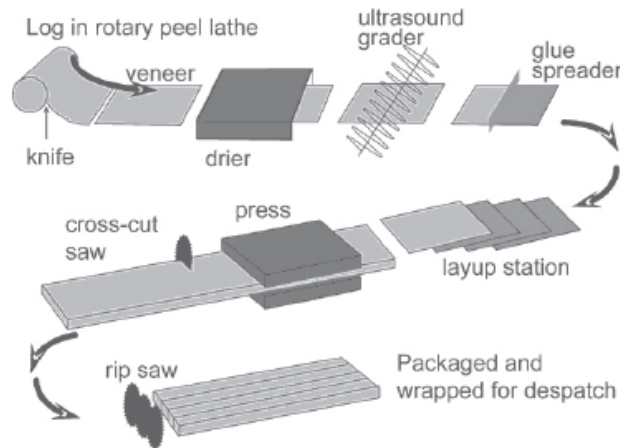


Figure 182. Schematic View of LVL Manufacturing Process

Veneers are delivered to press in a pre-determinate sequence, passed through a glue applicator and are then positioned to form a continuous slab that is subjected to heat and pressure to cure the structural phenol formaldehyde resin. The cured billets of LVL are then ripped and cross cut for further processing or customer requirements.

The adhesive used in LVL manufacturer is the phenol formaldehyde (PF); the bond is fully water proof.

Structural LVL is manufactured to conform with AS/NZS 4357: Structural Laminated Veneer Lumber. Structural properties are determined in accordance with AN/NSZ 4063: Characterization of structural timber.

The nominal 1200 mm wide billets are usually made in thickness from 35 to 105 mm. The billets are sawn into smaller sizes which are integer factors of the 1200 dimension, such as 150, 200, 240, 300, 360, 400 and 600 mm.

The structural properties of the LVL are shown in the table below.

	Bending Strength f_b (MPa)	Compr. Strength f_c (MPa)	Tension Strength f_t (MPa)	Shear in beams f_s (MPa)	Compr. Perpendic. f_p (MPa)	Modulus of Elasticity E (GPa)	Modulus of Rigidity G (GPa)
Nelson Pine LVL	48	45	30	6	12	10.7	535

Table 33. Structural Properties of LVL Wall

The dimensions of the transverse walls and of the truss above them are defined in the table below.

LVL Wall

$$b = 2400 \text{ mm}$$

$$t = 180 \text{ mm}$$

$$h = 6700 \text{ mm}$$

LVL Truss

$$b = 24582 \text{ mm}$$

$$t = 180 \text{ mm}$$

$$h = 4821 \text{ mm}$$

Table 34. Dimensions of LVL Wall and LVL Truss

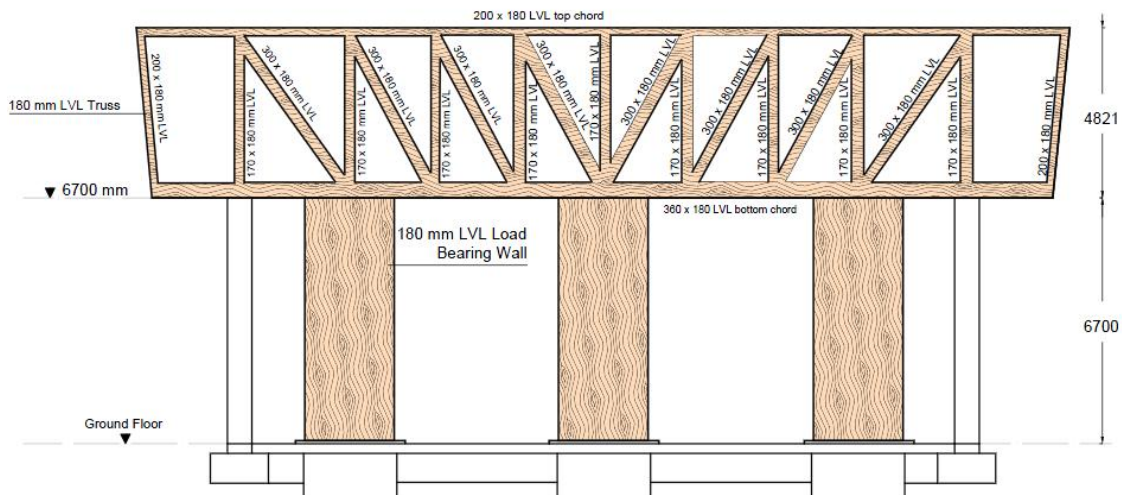


Figure 183. Walls - Truss System

Steel

The grade 300 mild steel is used for the dissipators and Macalloy bars for the post tensioning cables.

Grade 300 Mild Steel

$$f_y = 300 \text{ MPa}$$

$$A_s = 452 \text{ mm}^2$$

$$E = 200 \text{ GPa}$$

Macalloy Bars

$$f_y = 835 \text{ MPa}$$

$$A_{pt} = 1963.5 \text{ mm}^2$$

$$E_{pt} = 170 \text{ GPa}$$

Table 35. Materials Properties

The mild steel bars are fitted at the end of the wall. The unbonded length of the dissipators is different; this was done so that the two bars would yield at the same time. The unbonded lengths have also been limited due to the possibility of buckling of the bar under compressive loads. The bars had to be spaced so that the development cone of the timber could be developed without coinciding with the pull out cone of adjacent bars. This was essential, as to activate the unbonded section (energy dissipation) of the mild steel bar there had to be sufficient fixity at both ends of the bar. The unbonded length of the internal bars differed to the external bars. This was done so that the two bars would yield at the same time.

The Macalloy bars are inserted in a central slot that is width of two plies (90 mm) and there is sufficient room to fix them into place easily. This also takes advantage by the dimension of the tendons that have a small diameter (24 mm). Two smaller Macalloy bars were used instead a large bar also to have a better distribution of the loads.

The axial load providing self centering comes from the self weight of the wall and the Macalloy bar used for the post tension. In the design of the walls a ratio 60:40 of the contribution of the self centering capacity and the energy dissipation has been chosen.

Some pictures of the construction of the building are shown below.



Figure 184. Wall Panel Erection



Figure 185. Macalloy Bar Connection (left); Construction Progress (right)

Using a displacement based design philosophy, slightly modified for timber, the drift level of the walls was set to 1% of the height of the wall. This is a total displacement of 67 millimeters at the top of the walls. This drift level was found to provide the optimum solution, minimizing deflection yet also limiting the amount of stress induced on the Macalloy post tensioned bar and mild steel dissipator elements. With higher drift levels the structure will have a higher fundamental period, which in turn will reduce the base shear. However with higher drift levels there will be greater elongation in the steel elements.

A representation of the wall and a comparison between the monolithic solution and an hybrid solution is shown in the picture below.

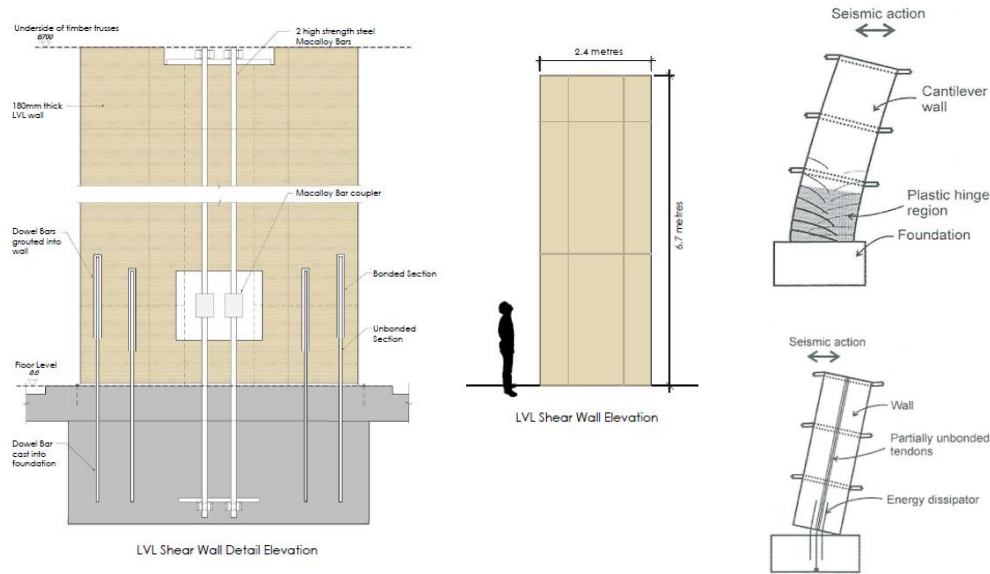


Figure 186. Pres-Lam Wall General Arrangement (left); comparative response of a monolithic system and a dissipative rocking post-tensioned solution (right) [3]

The objective of the study is to provide an assessment about the seismic performance of the system laminated veneer lumber walls and laminated veneer lumber truss above them used in the Carterton Events Centre town hall/auditorium.

Figure 5 shows the layout of the wall and the lumped plasticity model that have been adopted in the Ruaumoko 2D analysis [4].

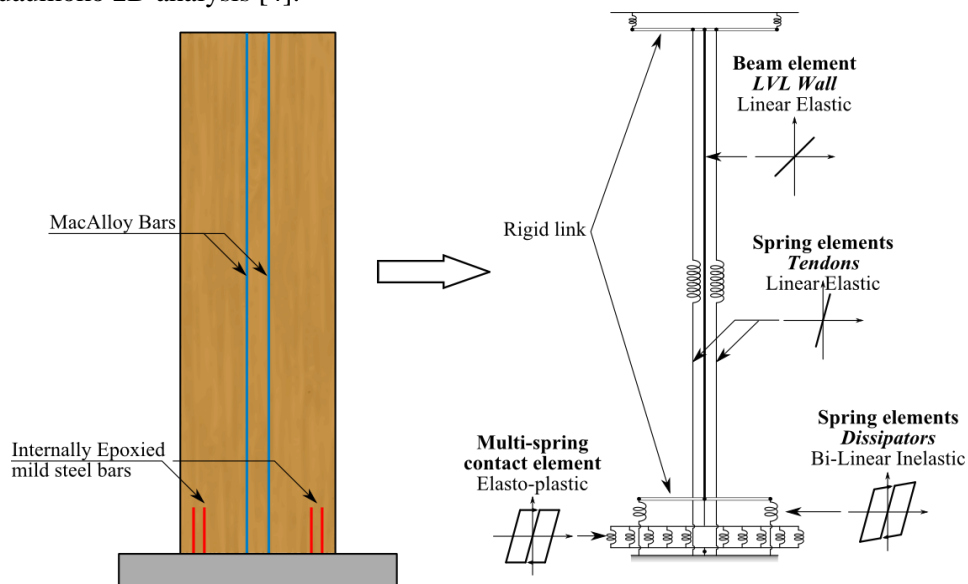


Figure 187 Post Tensioned Wall and Lumped Plasticity Model

The truss to wall system and the connection details are shown in the picture below.

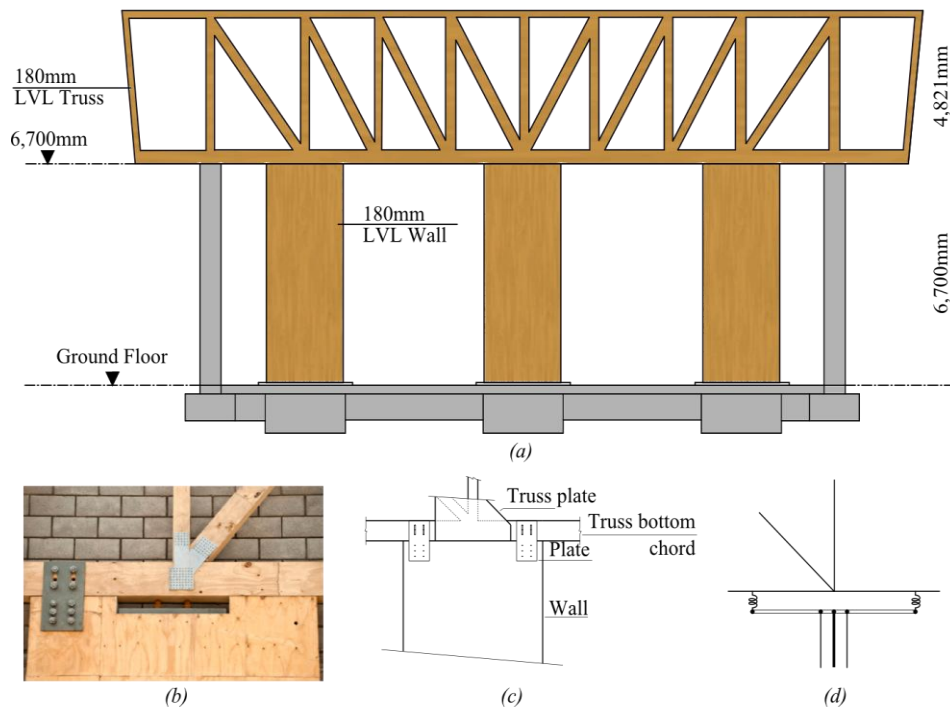


Figure 188 . (a) Side view of truss-wall system; (b) Transverse wall connection during construction; (c) Sketch and (d) Model of the truss-to-wall connection

The connection between wall and truss is realized with a couple of plates on the left and the right sides of the wall. The steel plates with slotted holes are intended to transfer the horizontal load from the truss bottom chord only, while allowing the wall to rotate.

A summary of design values is given in Table 5.

Target drift:	1.0%
Period:	0.57 s
Re-centring ratio:	1.5
Design equivalent viscous damping:	12.38%
Seismic weight:	1500 kN
Effective stiffness:	18100 kN/m
Design base shear (no torsion or P-Δ):	$V_{base} = 1215$ kN
Number of walls in longitudinal direction:	6
Number of walls in transverse direction:	5
Design base shear per longitudinal wall:	$V_{base} = 202.5$ kN
Design base shear per transverse wall:	$V_{base} = 243.0$ kN

Table 36. Design values of the Wall

A 2D Multi-Spring model [5] is used to represent the walls; the complete model is shown in Figure 189.

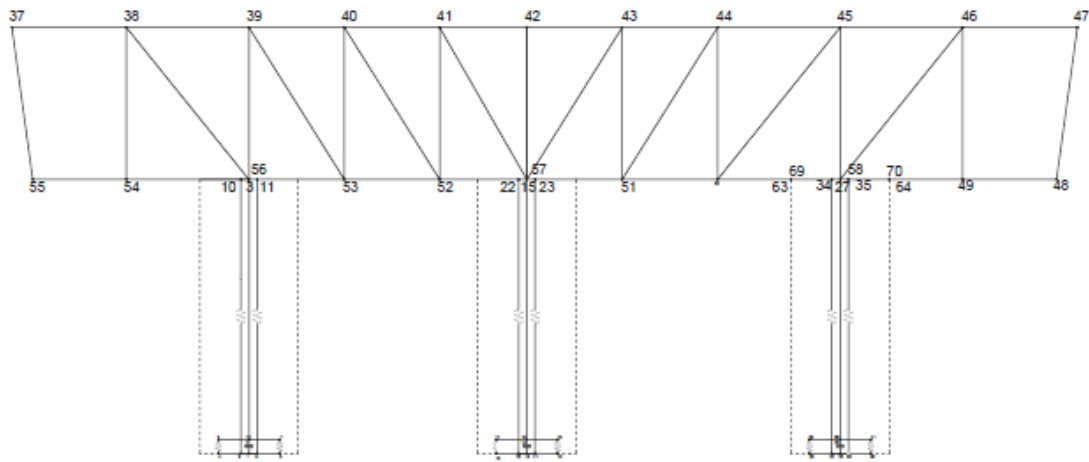


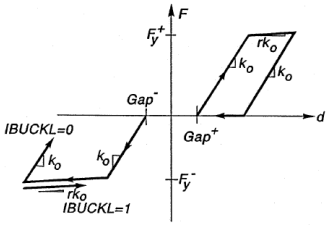
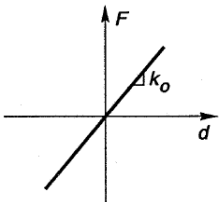
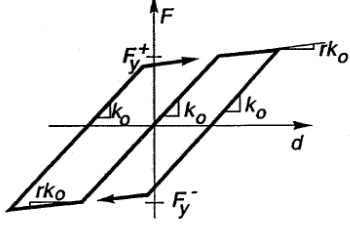
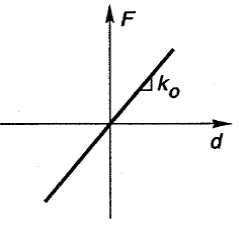
Figure 189. Ruaumoko Model of the Walls-Truss System

7.2 Multi Spring Model

The multi-spring model used for the wall consists in 7 elements. A frame member correspond to the LVL wall, each post tension bar is represented by a spring element and the mild steel dissipaters are represented by a spring element too. The joint interface between the bottom of the wall and the foundation is modeled with a multi-spring element. Because the rocking walls gap at the base is allowed, every spring representing the timber interface is a contact spring, able to adequately represent the behavior of timber both in tension and compression. This is achieved with a “gap hysteresis” rule for the multi spring element which does not exhibit any strength in tension and does not allow compression resistance until the closure of the gap previously formed has taken place. A value of stiffness has to be defined; such stiffness can be regarded as the effective stiffness of that part of wall foundation that resists in compression once the rocking starts. A value of a third of length has been adopted for this study [6].

Above the wall there is the truss modeled with a frame members and the joint between the wall and the truss is represented with two spring elements. The design connection is realized with two steel plates with slotted holes and three bolts in each hole and it transfers the horizontal load from the truss bottom chord only, while allowing the wall to rotate.

Table 37 summarizes the members of the model and their hysteresis rules.

<i>Member type</i>	<i>Physical representation</i>	<i>Hysteresis rule</i>
		Bi-linear with Gap
Multi-Spring	Rocking joint	 <p>The diagram shows a force-displacement (F-d) plot for a bi-linear with gap hysteresis rule. The vertical axis is Force (F) and the horizontal axis is Displacement (d). The plot shows a hysteresis loop with a gap. The initial loading path starts at the origin with a slope of k_o until it reaches a yield force F_y^+. At this point, the force drops to zero, creating a gap. The loading then resumes with a steeper slope $r k_o$ until it reaches a peak force F_y^+. The unloading path follows a parallel line with slope $r k_o$ back to zero force. The reverse loading path starts at zero force with a slope of k_o until it reaches a yield force F_y^-. At this point, the force drops to zero, creating a gap. The loading then resumes with a steeper slope $r k_o$ until it reaches a peak force F_y^-. The unloading path follows a parallel line with slope $r k_o$ back to zero force. The diagram is labeled with $IBUCKL=0$ and $IBUCKL=1$ at the origin, and Gap^+ and Gap^- at the points where the force drops to zero.</p>
Frame	Laminated Veneer Lumber (LVL) wall	Linear elastic
		 <p>The diagram shows a linear elastic hysteresis rule. The vertical axis is Force (F) and the horizontal axis is Displacement (d). The plot shows a single straight line passing through the origin with a slope of k_o. The loading and unloading paths are identical, indicating no energy dissipation.</p>
		Bi-linear inelastic
Linear Spring	Mild steel dissipators	 <p>The diagram shows a bi-linear inelastic hysteresis rule. The vertical axis is Force (F) and the horizontal axis is Displacement (d). The plot shows a hysteresis loop with a yield plateau. The initial loading path starts at the origin with a slope of k_o until it reaches a yield force F_y^+. The force then remains constant at F_y^+ until it reaches a peak force $r k_o$. The unloading path follows a parallel line with slope k_o back to zero force. The reverse loading path starts at zero force with a slope of k_o until it reaches a yield force F_y^-. The force then remains constant at F_y^- until it reaches a peak force $r k_o$. The unloading path follows a parallel line with slope k_o back to zero force.</p>
		Linear elastic
Linear Spring	Macalloy bar post - tensioning	 <p>The diagram shows a linear elastic hysteresis rule. The vertical axis is Force (F) and the horizontal axis is Displacement (d). The plot shows a single straight line passing through the origin with a slope of k_o. The loading and unloading paths are identical, indicating no energy dissipation.</p>

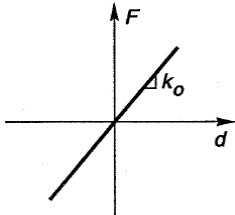
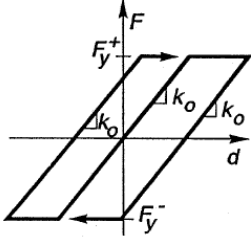
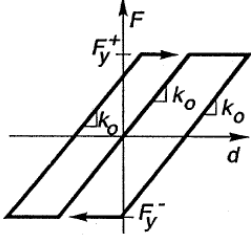
Frame	Wall – truss joint	<p style="text-align: center;">Bi – Linear</p>  <p>A graph showing a single bi-linear relationship between force F (vertical axis) and drift d (horizontal axis). The line passes through the origin with a constant slope labeled Δk_o.</p>
Frame	Truss beam 1	<p style="text-align: center;">Bi – Linear</p>  <p>A graph showing a bi-linear relationship between force F (vertical axis) and drift d (horizontal axis). The curve is symmetric about the origin. The peak force is labeled F_y^+ and the trough force is labeled F_y^-. The slope of the initial linear portion is labeled Δk_o.</p>
Frame	Truss beam 2	<p style="text-align: center;">Bi – Linear</p>  <p>A graph showing a bi-linear relationship between force F (vertical axis) and drift d (horizontal axis). The curve is symmetric about the origin. The peak force is labeled F_y^+ and the trough force is labeled F_y^-. The slope of the initial linear portion is labeled Δk_o.</p>

Table 37. Multi Spring Model Members

7.2.1 Quasi Static Analysis

Quasi static analysis refers to loading where the inertial effects are negligible. Essentially the test happens infinitely slowly so that time and inertial mass are insignificant. Two types of quasi static analyses are conducted: push-over and push-pull. The former provides information about the capacity of the wall, pushing the system to a top drift of 1.5% (0.5% more than the design drift). The latter has been carried out imposing a cyclic schedule at $\pm 1\%$ drift.

The analysis is carried out for the longitudinal walls that support the truss. The truss analyzed is the external one at grid N, see picture 5.

Presented on the following pages there are the results of push-over and push-pull analysis of the system of three walls and the truss above them using the multi-spring model in order to represent the rocking joint wall –foundation.

7.2.1.1 Push-over and push-pull analysis

Push Over Analysis

The push over analysis pushes the system at the top of the truss and so the three walls are subjected to different stresses. The neutral axis of the first wall will be more external compared to the ones of the other two walls.

Show in Figure 190 is the force displacement behavior of the three longitudinal walls during the push-over.

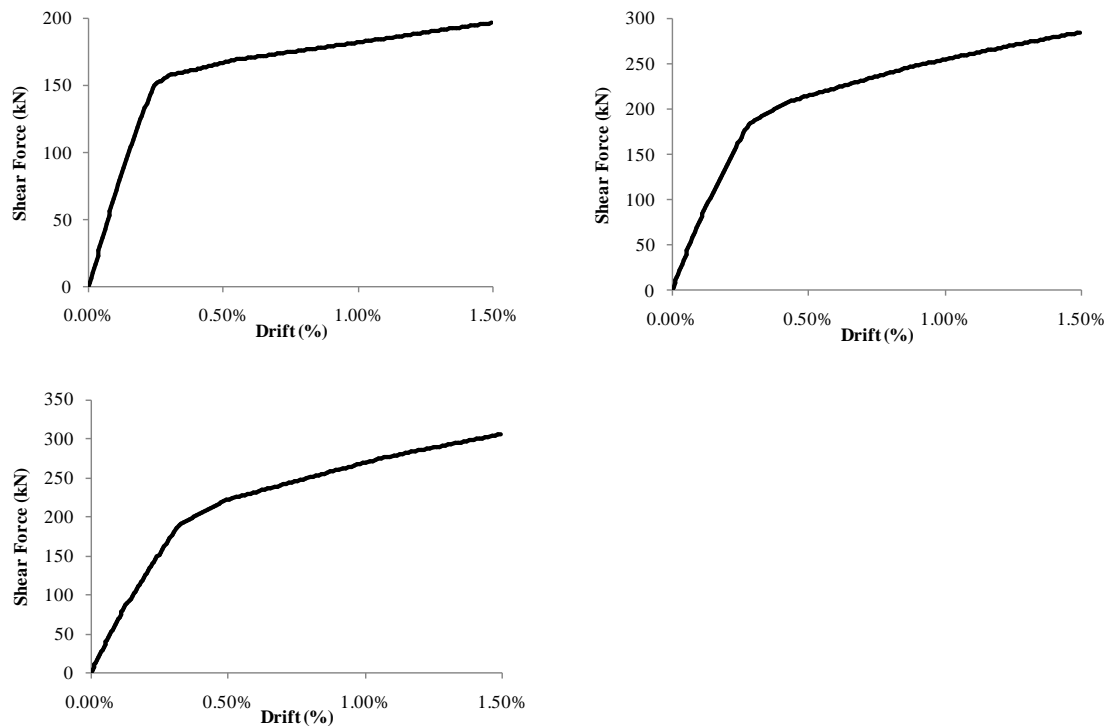


Figure 190. Push Over Capacity of the Walls. Capacity of Wall 1 (top left), Capacity of Wall 2 (top right), Capacity of wall 3 (bottom left)

Capacity Spectrum Method

The Capacity Spectrum Method (CSM) has been used to make an explicit comparison between the structural capacity and the earthquake demand. This method estimates the deformation of inelastic Single Degree of Freedom system consistent with the selected inelastic design spectrum [7].

The intersection between the capacity curve and the demand spectra is the required “performance point”, which should match the design drift value. The intersection represents the behavior of the structure in an earthquake represented by the demand. If for example a structure

is required to remain elastic in an earthquake, then the capacity spectrum should cross the elastic response spectrum for that earthquake in its elastic range (i.e. before the yielding point).

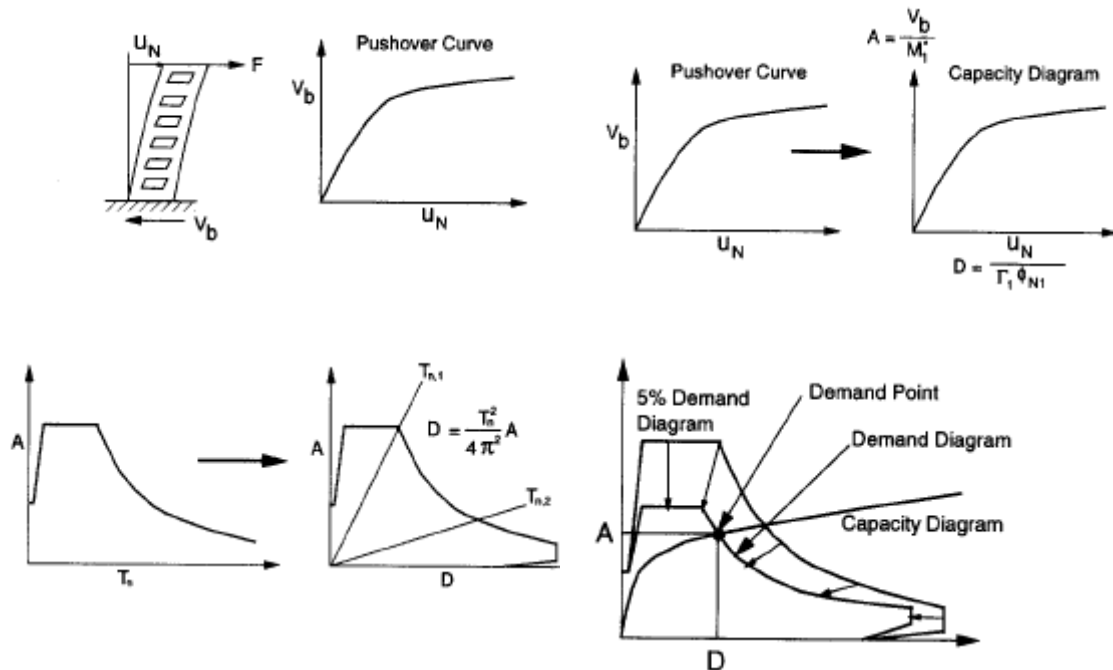


Figure 191. Capacity Spectrum Method. Development of Push Over Curve (top left), Conversion of Push Over Curve to Capacity Diagram (top right), Conversion from Acceleration Spectrum to Displacement Spectrum (bottom right) [7]

In order to account for the uncertainty in estimating the capacity of a structure, a reductive factor (less than one) is commonly used to multiply the capacity calculated with a push over analysis.

Two principal limits states are used: the serviceability limit state (SLS) and the ultimate limit state (ULS). SLS is intended to ensure that the structure remains functional and this means that deflection, vibration crack widths are within permissible limits specified in the codes. ULS is to ensure that a design structure does not collapse when subjected to the peak design action.

In order to obtain to do the comparison we have to find the elastic spectra in the site for the two states: ULS and SLS.

According to the NZS 1170.5 [8], [9]:

$$C(T) = C_h(T) Z R N(T,D)$$

Where:

$C_h(T)$ is the spectral shape factor

Z is the hazard factor

R is the return period factor different for R_s and R_u

$N(T, D)$ is the near fault factor.

For the site considered Z is equal to 0.42 and the distance to the nearest major fault is from 6 to 10 km.

Considering that the probability of exceedance is 1/1000 for the ultimate limit and 1/25 for the serviceability limit the factor are 1.3 and 0.25 respectively.

The near fault factor is equal to 1.

On the table below the values of $C_h(T)$ and so the values of $C(t)$ are calculated.

<i>Period T (s)</i>	<i>Spectral shape factor $C_h(T)$</i>	<i>$C(T)$ ULS demand (g)</i>	<i>$C(T)$ SLS demand (g)</i>
0	1.33	0.72618	0.13965
0.1	2.93	1.59978	0.30765
0.2	2.93	1.59978	0.30765
0.3	2.93	1.59978	0.30765
0.4	2.36	1.28856	0.2478
0.5	2	1.092	0.21
0.6	1.74	0.95004	0.1827
0.7	1.55	0.8463	0.16275
0.8	1.41	0.76986	0.14805
0.9	1.29	0.70434	0.13545
1	1.19	0.64974	0.12495
1.5	0.88	0.48048	0.0924
2	0.66	0.36036	0.0693
2.5	0.53	0.28938	0.05565
3	0.44	0.24024	0.0462
3.5	0.32	0.17472	0.0336
4	0.25	0.1365	0.02625
4.5	0.2	0.1092	0.021

Table 38. Spectrum Values

The acceleration spectrum is shown in the picture below. The displacement spectrum can be derived by the acceleration spectrum.

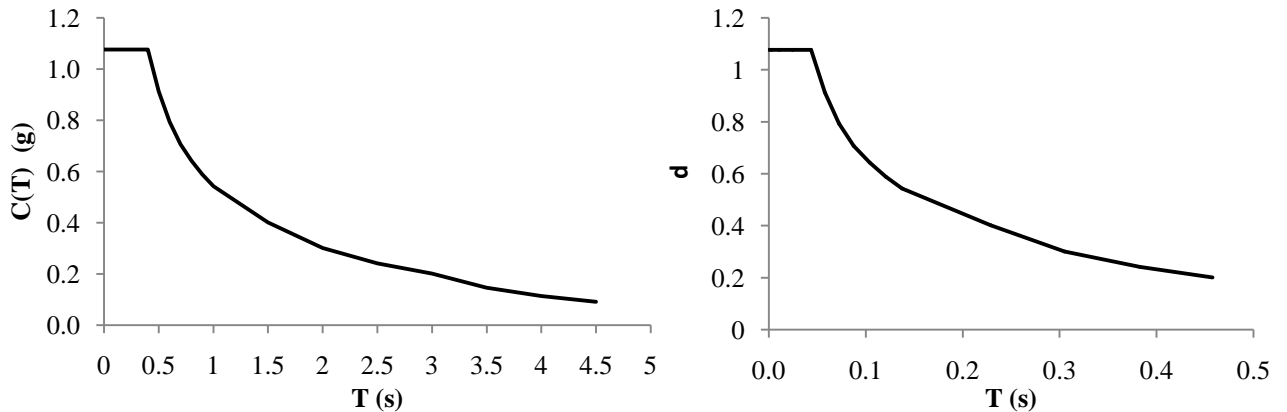


Figure 192. ULS Response Spectrum and ULS Displacement Spectrum

The comparison between the structural capacity and the earthquake demand is obtained overlapping the pushover of the three walls and the ULS design spectrum.

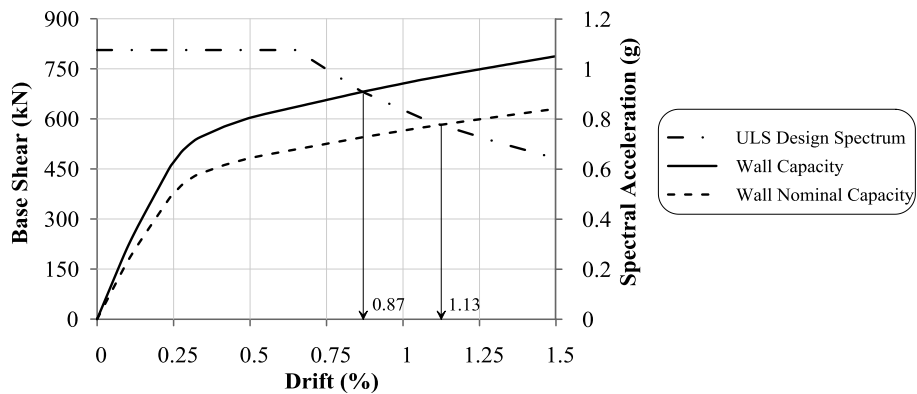


Figure 193. Seismic Performance Assessment

Capacity Spectrum Method results in Figure 193 shows 0.87% drift level corresponding to the wall capacity and 1.13% to the nominal capacity. Considering the wall capacity and the nominal wall capacity the results show that for an earthquake represented by the ULS Spectrum the wall will respond with a value of drift of 0.87% and 1.13% respectively.

Those values are successively compared to the results of the dynamic analysis presented in the next pages.

Push Pull Analysis

The push pull analysis cycles the “wall-truss” system at the top of the truss and so the walls are stressed in a different ways.

The results obtained are shown in the picture below.

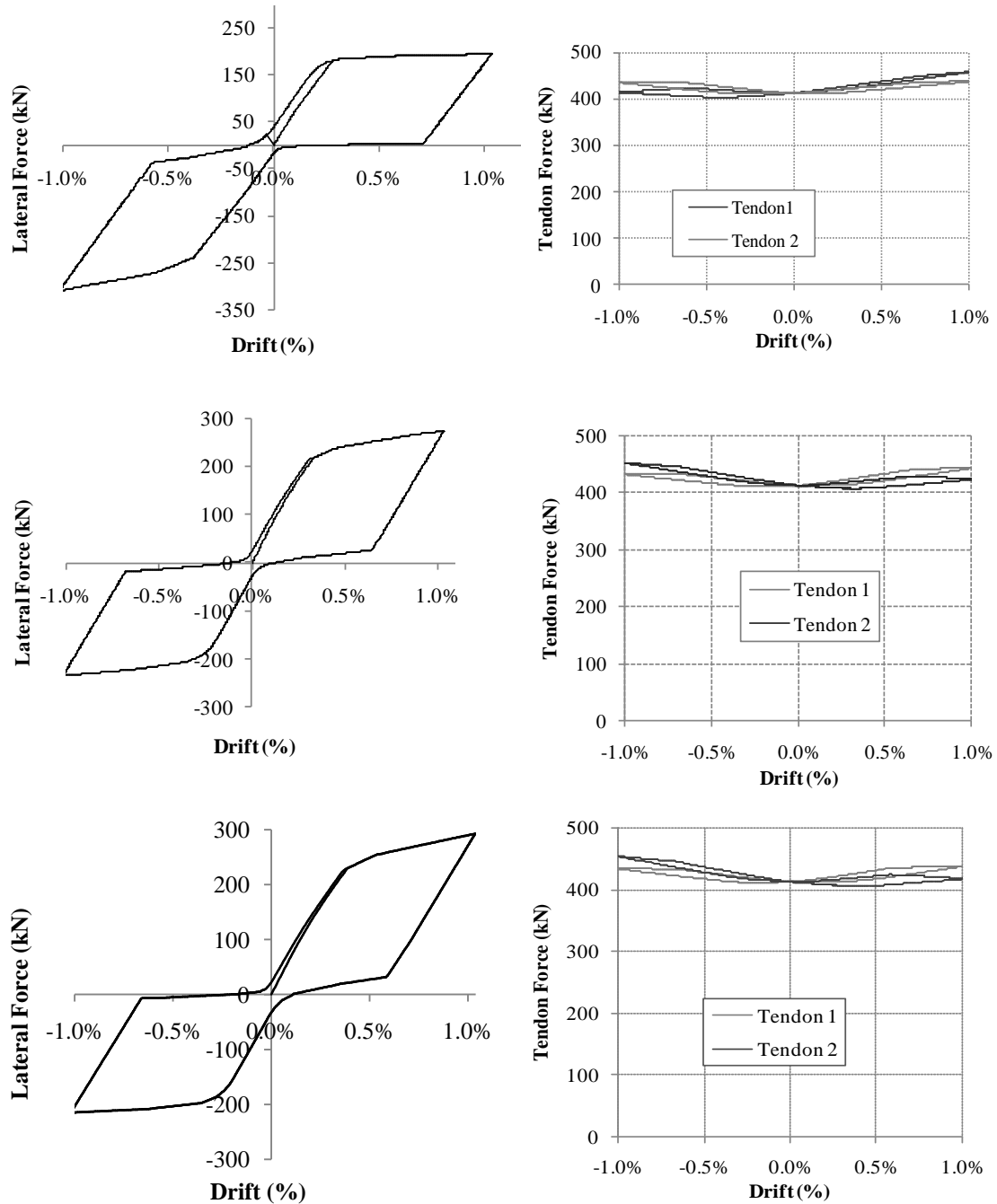


Figure 194. Quasi Static Analysis. Lateral Force and Tendons Force Wall 1 (top left and right), Lateral Force and Tendons Force Wall 2 (center left and right), Lateral Force and Tendon Force Wall 3 (bottom left and right)

The results show a non symmetric behavior of the external walls due to the distribution of the forces in the walls-truss system. The tendons of the first wall keep more force at the positive drift while the tendons of the third wall work more at the negative drift.

Considering the wall subjected to more load cycles, the hysteresis loop of the total moment and total shear of the three walls is shown in the picture below.

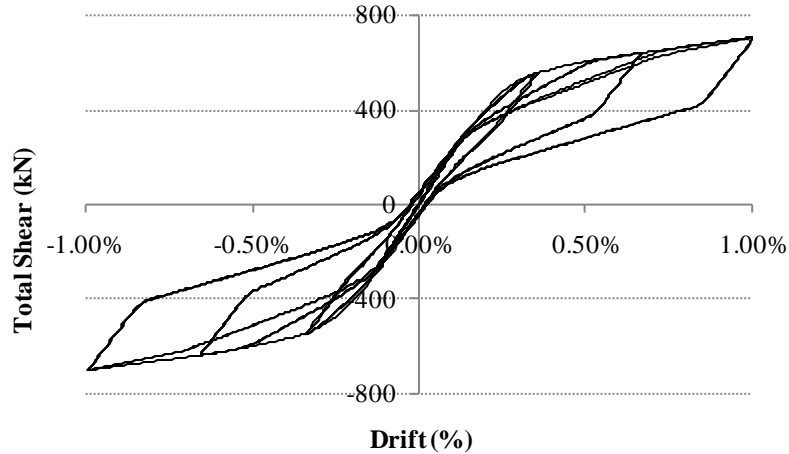


Figure 195. Quasi Static Analysis Total Shear Force – Drift

Observing the shear force- drift analysis, the connection exhibits stiffness degradation; a significant part it's probable that was associated to the bond slip within the epoxy as highlighted by [10].

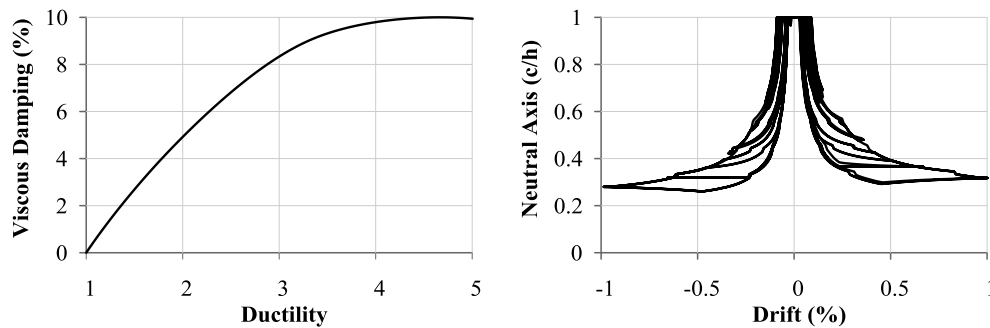


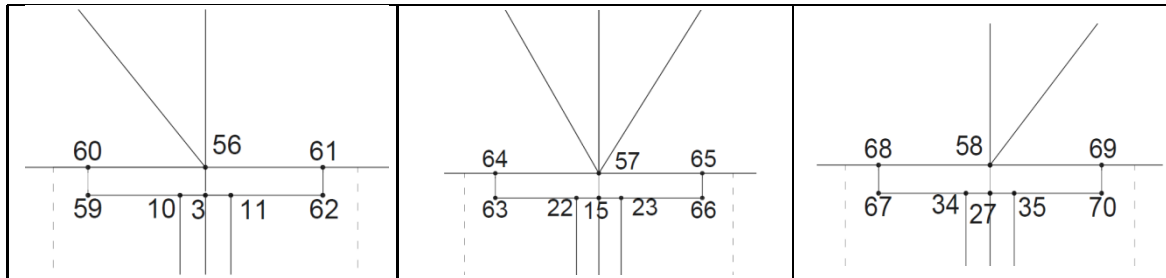
Figure 196. Quasi Static Analysis: Viscous Damping (left) and neutral axis vs. Drift (right)

The equivalent viscous damping has values quite consistent with the design phase. The neutral axis stabilizes at 0.3h for 1% drift level (Figure 196).

Truss to Wall Connection Analysis

The connection between walls and truss is realized with a couple of plates on the left and on the right side of the wall. The steel plates with slotted holes are intended to transfer the horizontal load from the truss bottom chord only, while allowing the wall to rotate.

The connection has been modeled with a beam element representing each plate as shown in the pictures below.



The vertical displacements of the nodes for the different values of drift are shown in the picture below.

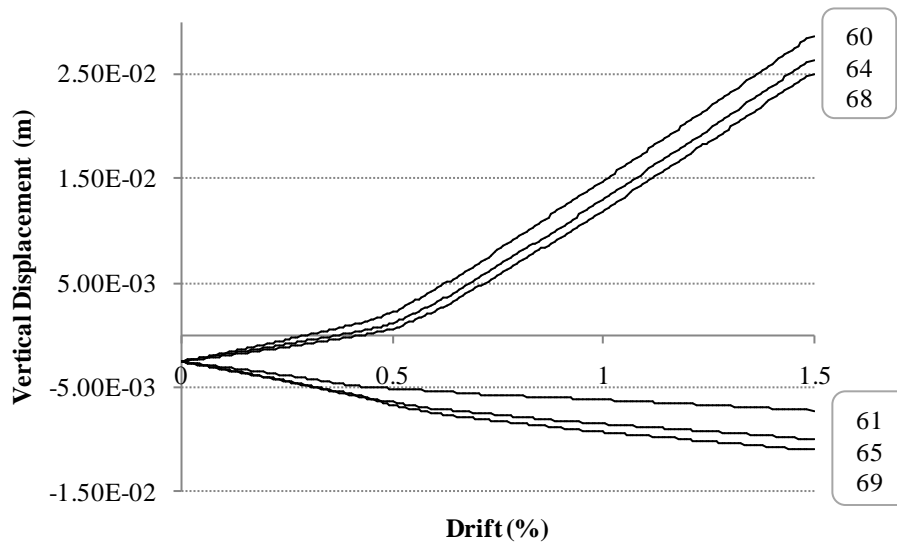


Figure 197. Vertical Displacement of the Walls

The maximum displacement of 30 mm is the one of the wall 1 that is closer to the point of application of the force.

An analysis of the connection is carried out in order to define the values of stress at the 1% and 1.5% drifts.

The bending moment, shear force and axial force of the beams in proximity of the connections are shown below.

The convention used is the one shown in the drawing below.

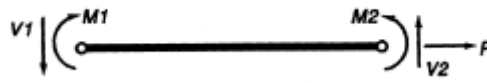


Figure 198. Beam sign convention

Connection between wall 1 and truss:

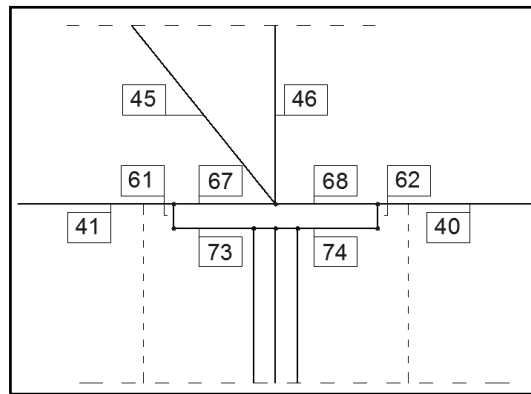


Figure 199. Wall 1 - Truss connection

Moments (kNm)

Drift 1%

Drift 1.5%

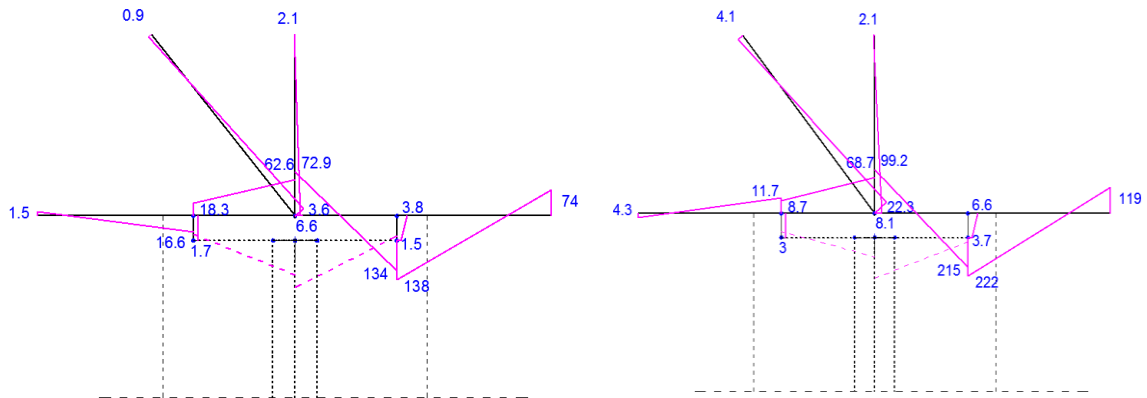


Figure 200. Bending Moment, drift 1% (left), Drift 1.5% (right)

Axial forces (kN) -red compression, blue tension-

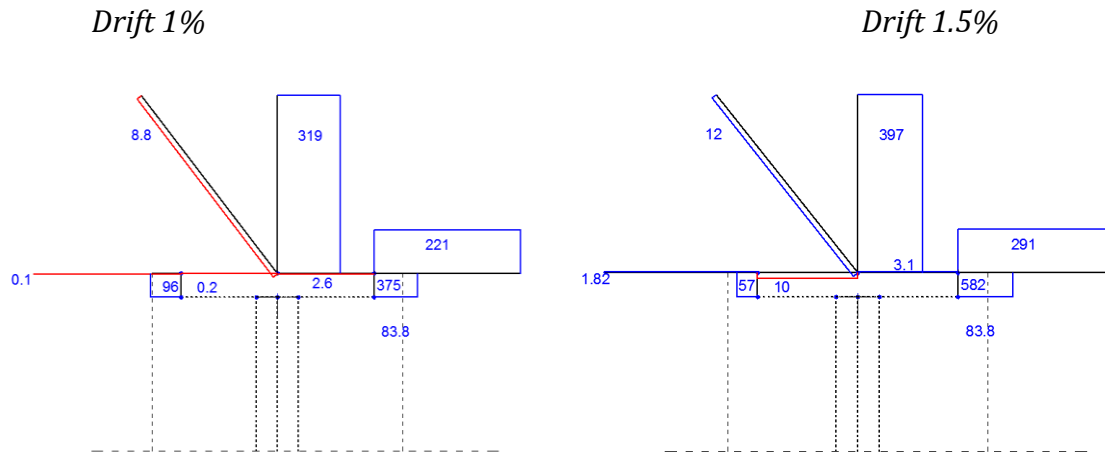


Figure 201. Axial Forces, Drift 1% (left), Drift 1.5% (right)

Shear forces (kN) -red negatives, blue positives-

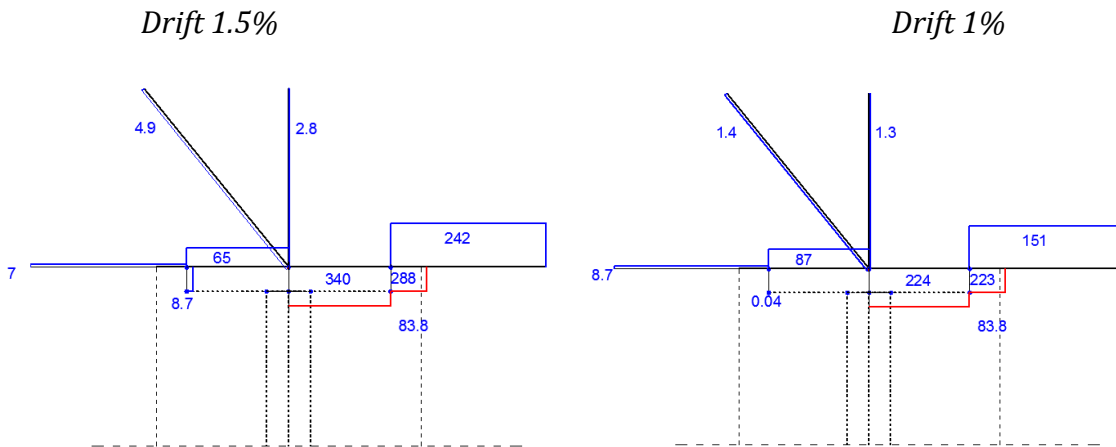


Figure 202. Shear Forces, Drift 1% (left), Drift 1.5% (right)

Connection between wall 2 and truss:

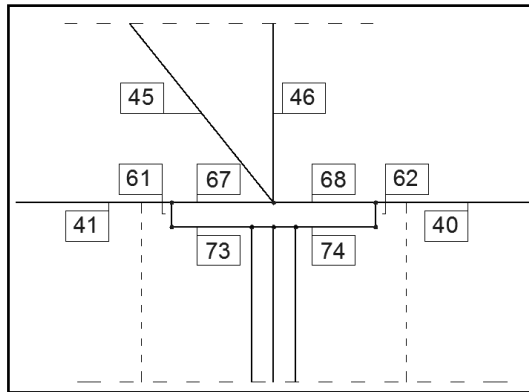


Figure 203. Wall 2 - Truss connection

Moments (kNm)

Drift 1%

Drift 1.5%

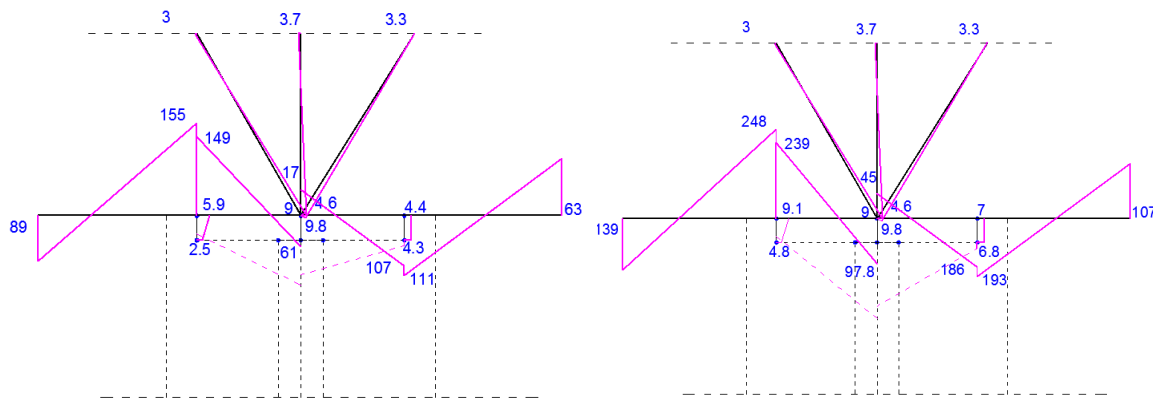


Figure 204. Bending Moment, drift 1% (left), Drift 1.5% (right)

Axial forces (kN) -red compression, blue tension-

Drift 1%

Drift 1.5%

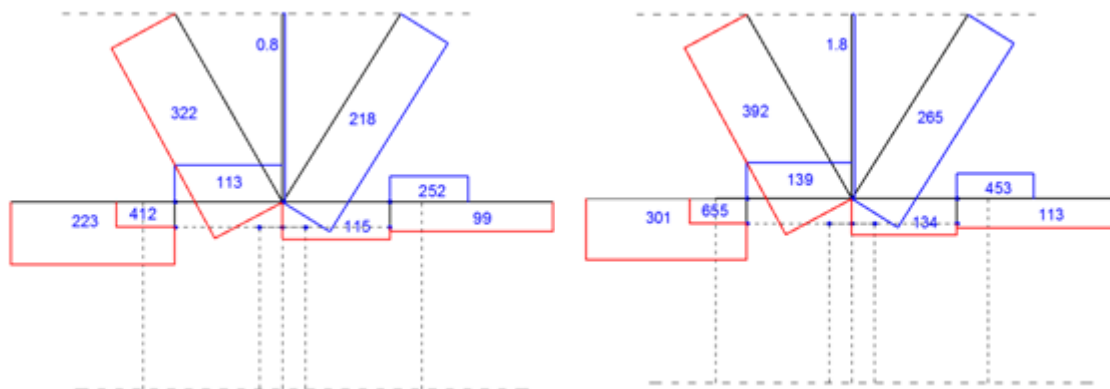


Figure 205. Axial Forces, Drift 1% (left), Drift 1.5% (right)

Shear forces (kN) -red negatives, blue positives-

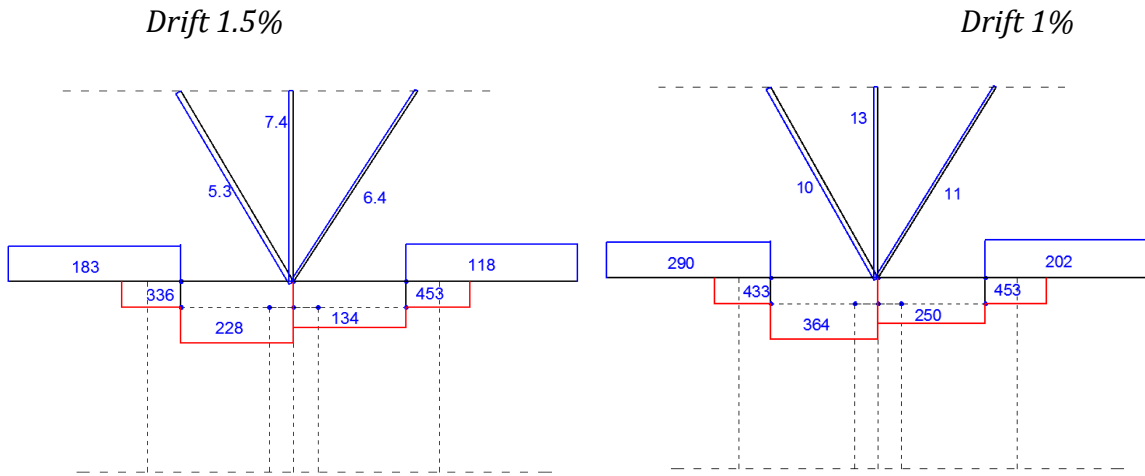


Figure 206. Shear Forces, Drift 1% (left), Drift 1.5% (right)

Connection between wall 3 and truss:

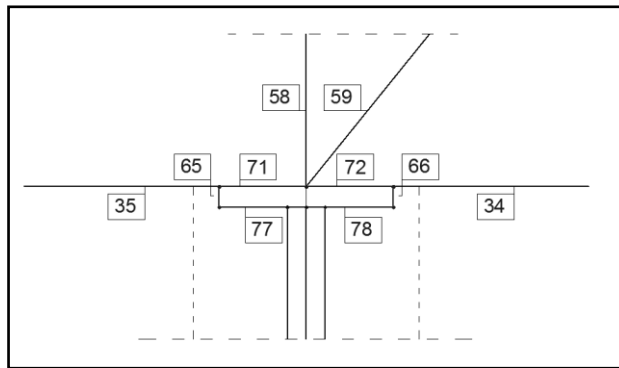


Figure 207. Wall 3- truss connection

Moments (kNm)

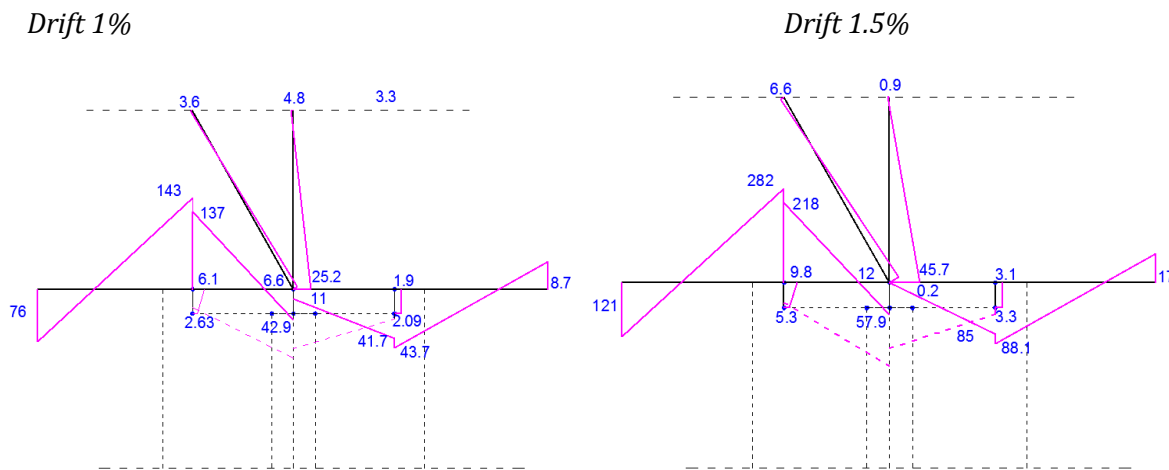


Figure 208. Bending Moment, drift 1% (left), Drift 1.5% (right)

Axial forces (kN) -red compression, blue tension-

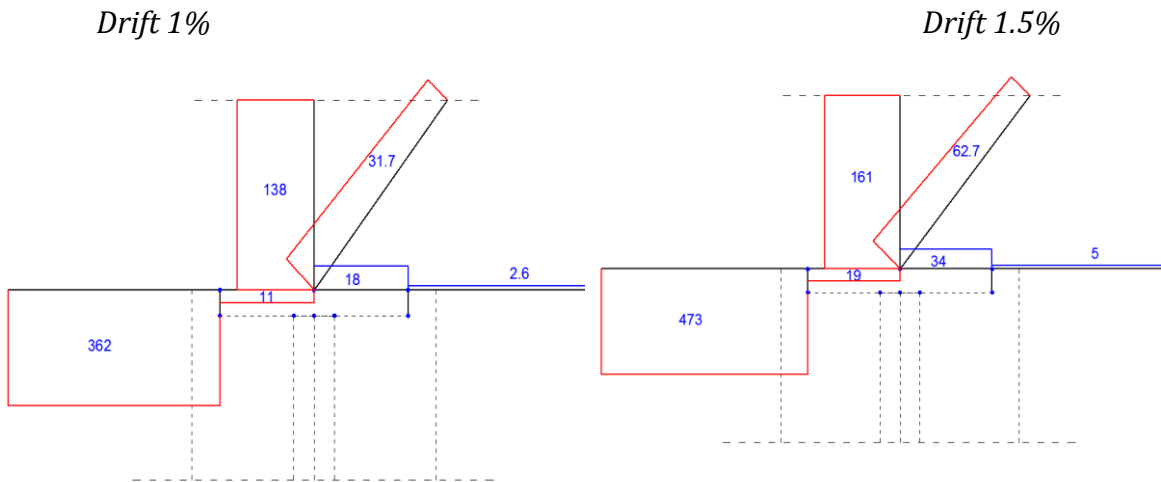


Figure 209. Axial Forces, Drift 1% (left), Drift 1.5% (right)

Shear forces (kN) -red negatives, blue positives-

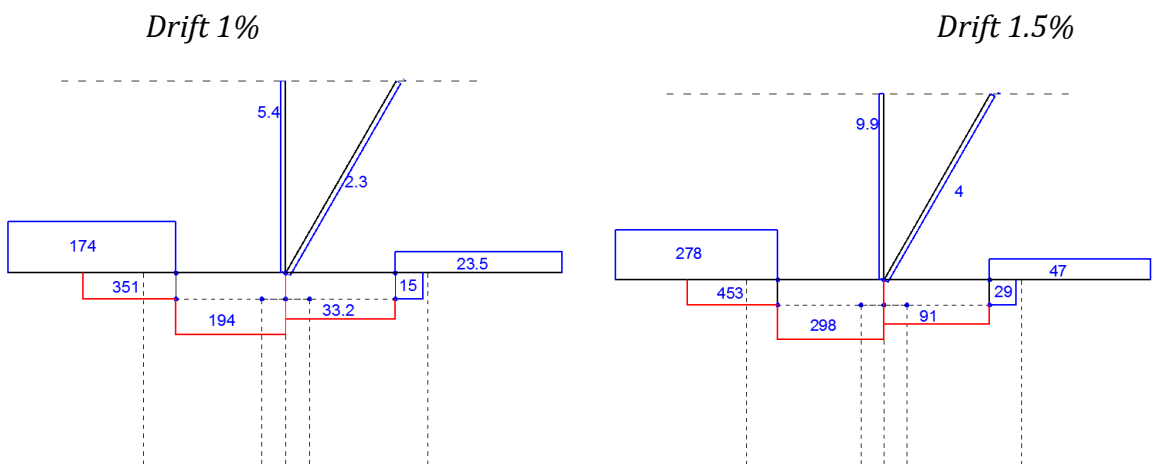


Figure 210. Shear Forces, Drift 1% (left), Drift 1.5% (right)

7.2.2 Dynamic Time History Analyses

The performance of the system when subjected to dynamic non-linear time history is herein presented. The walls have been subjected to a suite of ground motions scaled individually according to the NZS 1170.5 (Standard New Zealand 2004 [8] elastic spectra. Importance level 3, annual probability of exceedance 1/1000, soil class C, hazard factor of 1.3, return period factor of 1.3 and near fault factor of 1.0 are assumed.

The twenty earthquake records are shown in the table below.

Name	Earthquake Event	Year	Mw	Station	Soil Type	T (s)	Unscaled PGA	Scaling Factor	Scaled PGA (g)
EQ1	Superstition Hills	1987	6.7	Brawley	D	22	0.1335	6.1	0.626
EQ2	Superstition Hills	1987	6.7	El Centro Imp. Co. Cent	D	40	0.2899	2.8	0.711
EQ3	Superstition Hills	1987	6.7	Plaster City	D	22.2	0.155	3.4	0.634
EQ4	Northridge	1994	6.7	Beverly Hills 14145 Mulhol	C	30	0.469	1.6	0.673
EQ5	Northridge	1994	6.7	Canoga Park – Topanga Clan	D	25	0.356	1.6	0.568
EQ6	Northridge	1994	6.7	Glendale – Las Palmas	D	30	0.357	1.9	0.696
EQ7	Northridge	1994	6.7	LA – Hollywood Stor	D	40	0.231	2.7	0.615
EQ8	Northridge	1994	6.7	LA – N Faring Rd	D	30	0.273	2.3	0.631
EQ9	Northridge	1994	6.7	N Hollywood – Coldwater Can	C	21.9	0.271	2.4	0.641
EQ10	Northridge	1994	6.7	Sunland – Mt Gleason Ave	C	30	0.1406	4.4	0.690
EQ11	Loma Prieta	1989	6.9	Capitola	D	40	0.4798	1.2	0.608
EQ12	Loma Prieta	1989	6.9	Gilroy Array #3	D	39.9	0.4717	1.1	0.622
EQ13	Loma Prieta	1989	6.9	Gilroy Array #4	D	40	0.3038	1.4	0.604
EQ14	Loma Prieta	1989	6.9	Gilroy Array #7	D	40	0.226	2.7	0.618
EQ15	Loma Prieta	1989	6.9	Hollister Diff. Army	D	39.6	0.2762	1.9	0.528
EQ16	Loma Prieta	1989	6.9	USGS Anderson Dam	D	40	0.2399	2.7	0.651
EQ17	Cape Mendocino	1992	7.1	Fortuna Fortuna Blvd	C	44	0.116	4.9	0.569
EQ18	Cape Mendocino	1992	7.1	Rio Dell Overpass – FF	C	36	0.4443	1.4	0.550
EQ19	Landers	1992	7.3	Desert Hot Springs	C	50	0.153	2.4	0.582
EQ20	Landers	1992	7.3	Yemo Fire Station	D	44	0.2095	2.2	0.451

Table 4. Characteristics of ground motion records used for time history analysis

As shown in Figure 211 the maximum drift value of 0.95 is obtained under ground motion EQ 13. The maximum drift value reached is consistent with the one obtained with the Capacity Spectrum Method shown in Figure 193 and it is below the design value of 1%. Thus the results confirm the consistency of the design methodology with the numerical analysis.

Key parameters such as the maximum and minimum moment, the base shear, the drift and the residual drift, the displacement and the residual displacement, the top acceleration are shown in the table below.

	Average	Max	SD	Design
Max Drift (%)	0.68	0.95	0.19	1
Max Moment (kNm)	1809	2053	158	1644
Max Displacement (mm)	45	63	13	67
Max Base Shear Force (kN)	304	381	33	243
Max Top Acceleration (g)	1.85	2.88	0.63	/
Residual Displacement (mm)	7.66	23.070	7.27	
Residual Drift (%)	0.114	0.344	0.109	

Figure 211. Multi Spring Model Results

Considering for example the ground motion called EQ12 the flag shape hysteresis is shown in the picture below.

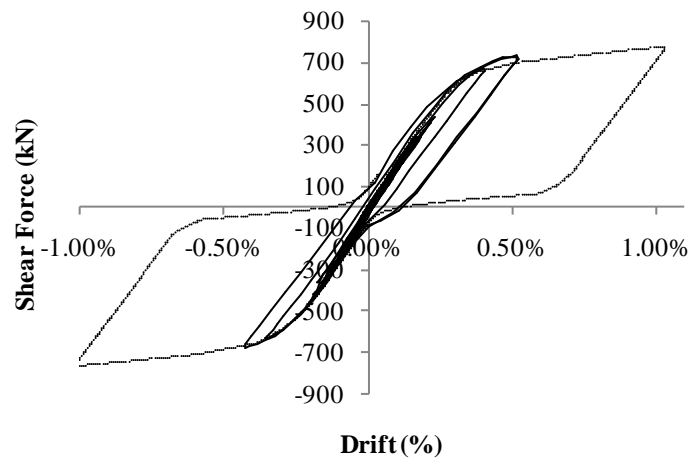


Figure 212. Flag Shape Hysteresis, Push Pull Analysis and Ground Motion Analysis (EQ2)

7.3 Carterton Events Center – Parallel with “Plug And Play” Dissipator

The walls of the Carterton Events Center have been realized coupling post tensioned cables to internal mild steel dissipators. A new solution replacing the internal dissipators with the external one is proposed in the following pages. The advantages of the Plug and Play dissipators have already been highlighted as first of all the replaceability after an earthquake event. It worth noting that very stable flag shape hysteresis loops with no stiffness degradation due to bond losses can be obtained with the external dissipator, when compared to internally grouted mild steel bars. The same analyses with external mild steel dissipators are carried out in order to do a comparison between the two cases.

The comparison is carried out using 26 mm diameter of the dissipators; the number of devices is the one calculated in Chapter 3. Eight external dissipators of 26 mm diameter provide a dissipating moment equal to 858 kNm, similar to the value obtained with internal devices (926 kNm). The location of the external devices is shown in the picture below.

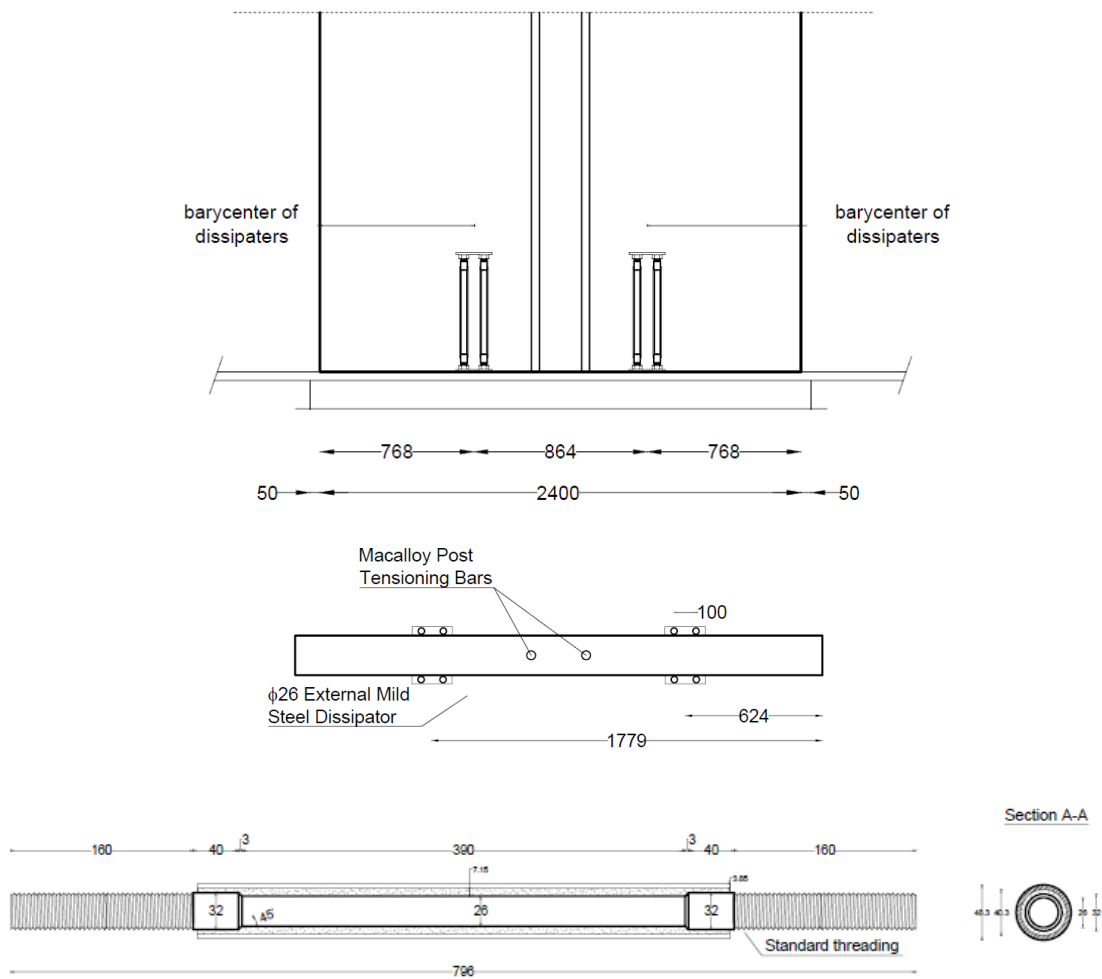


Figure 213. Case Study with External Dissipator Devices; Sections of the Wall (top and center), Detail of the Dissipator (bottom)

Figure 214 shows the layout of the wall and the lumped plasticity model that have been adopted in the Ruaumoko 2D [4] analysis.

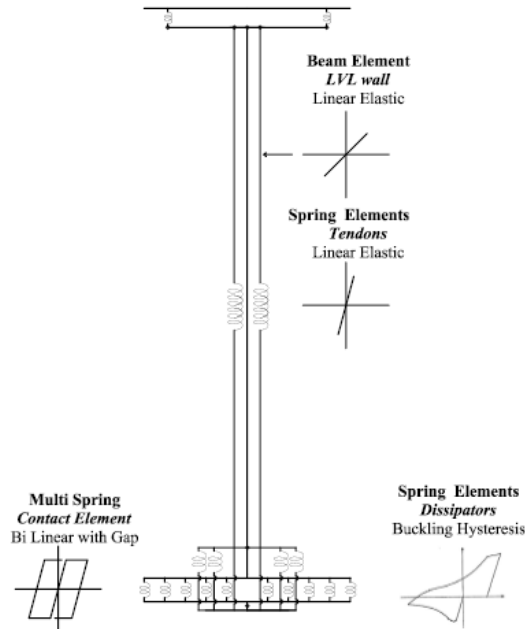


Figure 214. Lumped Plasticity Model of the Wall with External Dissipators

7.3.1 Multi Spring Model

As for the case with internal devices the multi-spring model used for the wall consists in seven elements. A frame member correspond to the LVL wall, each post tension bar is represented by a spring element and the mild steel dissipaters are described by a spring element too. Every spring describes the behavior of two dissipaters, one on the front and one on the back size of the wall. The join interface between the bottom of the wall and the foundation is modeled with a multi-spring element. This element is able to describe the rocking interface between wall and foundation because it is realized with a series of springs located to a different distances between the middle and the end of the wall and so it's possible to find out the compression and tension forces which the springs are subjected to and so the global moment of the element and their displacements.

Above the wall there is the truss modeled with a frame members and the joint between the wall and the truss is represented with two spring elements. The design connection is realized with two steel plates with slotted holes and three bolts in each hole and it transfers the horizontal load from the truss bottom chord only, while allowing the wall to rotate.

The main difference between the two models (internal and external dissipators) is the hysteresis used for the external dissipators that consider the possibility of the buckling of the devices when subjected to a compression force.

Table xx summarize the members of the model and their hysteresis rules.

<i>Member type</i>	<i>Physical representation</i>	<i>Hysteresis rule</i>
		Bi Linear with Gap
Multi-Spring	Rocking joint	
Frame	Laminated Veneer Lumber (LVL) wall	Linear elastic
Linear Spring	Mild steel dissipators	Buckling Hysteresis
Linear Spring	Macalloy bar post - tensioning	Linear elastic

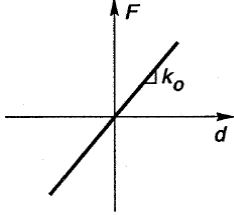
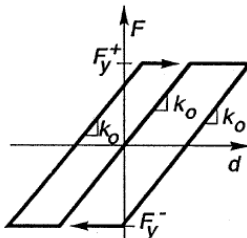
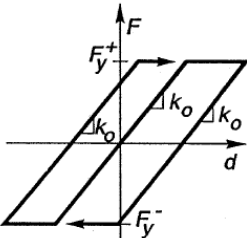
Frame	Wall – truss joint	<p style="text-align: center;">Bi – Linear</p>  <p>A graph showing a single straight line passing through the origin on a coordinate system where the vertical axis is Force (F) and the horizontal axis is Drift (d). The slope of the line is labeled as Δk_o.</p>
Frame	Truss beam 1	<p style="text-align: center;">Bi – Linear</p>  <p>A graph showing a hysteresis loop on a coordinate system where the vertical axis is Force (F) and the horizontal axis is Drift (d). The loading path (top half) is a straight line with slope Δk_o up to a yield force F_y^+, then becomes horizontal. The unloading path (bottom half) is a straight line with slope Δk_o down to a residual force F_y^-, then becomes horizontal. The slope of the unloading path is labeled as Δk_o.</p>
Frame	Truss beam 2	<p style="text-align: center;">Bi – Linear</p>  <p>A graph showing a hysteresis loop on a coordinate system where the vertical axis is Force (F) and the horizontal axis is Drift (d). The loading path (top half) is a straight line with slope Δk_o up to a yield force F_y^+, then becomes horizontal. The unloading path (bottom half) is a straight line with slope Δk_o down to a residual force F_y^-, then becomes horizontal. The slope of the unloading path is labeled as Δk_o.</p>

Table 39. Multi Spring Model Members

7.3.2 Quasi Static Analysis

Quasi static analysis refers to loading where the inertial effects are negligible. Essentially the test happens infinitely slowly so that time and inertial mass are insignificant. Two types of quasi static analyses are conducted: push-over and push-pull. The former provides information about the capacity of the wall, pushing the system to a top drift of 1.5% (0.5% more than the design drift). The latter has been carried out imposing a cyclic schedule at $\pm 1\%$ drift.

The analysis is carried out for the longitudinal walls that support the truss. The truss analyzed is the external one at grid N, see picture 5.

Presented on the following pages there are the results of push-over and push-pull analysis of the system of three walls and the truss above them using the multi-spring model in order to represent the rocking joint wall –foundation.

7.3.2.1 Push-over and push-pull analysis

Push Over Analysis

The push over analysis pushes the system at the top of the truss and so the three walls are subjected to different stresses. The neutral axis of the first wall will be more external compared to the ones of the other two walls.

Figure 10 shows the force displacement behavior of the three longitudinal walls during the push-over.

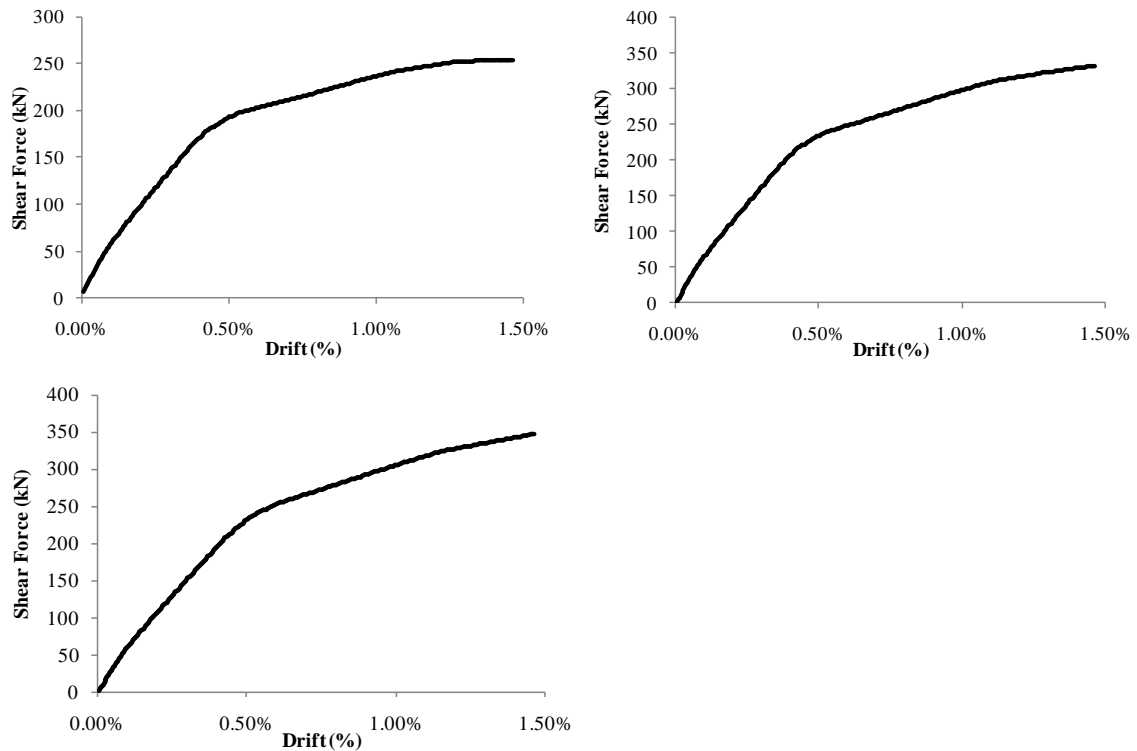


Figure 215. Push Over Capacity of the Wall; Capacity of Wall 1 (top left), Capacity of Wall 2 (top right), Capacity of Wall 3 (bottom left)

A push over analysis that pushes the system up to the failure point is shown in Figure 216. The rupture point is reached for a value of drift of 2.25% in the first wall; the other two walls still have a residual capacity. The dissipator reaches the ultimate curvature and the degradation starts.

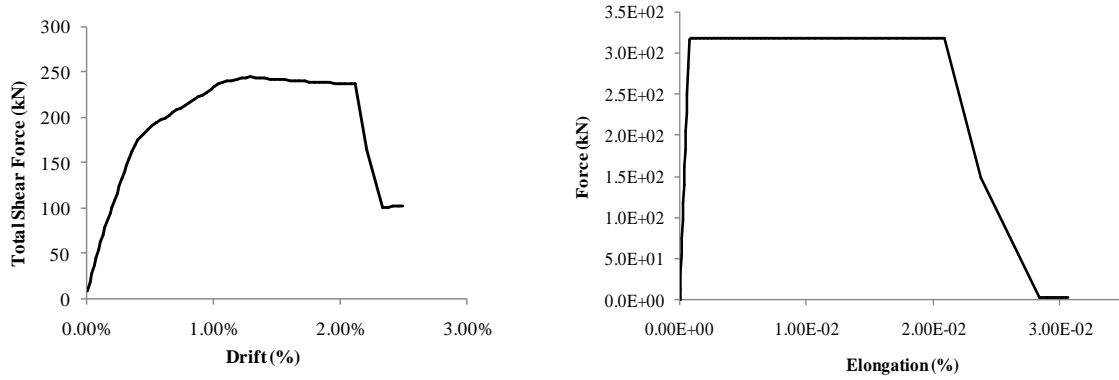
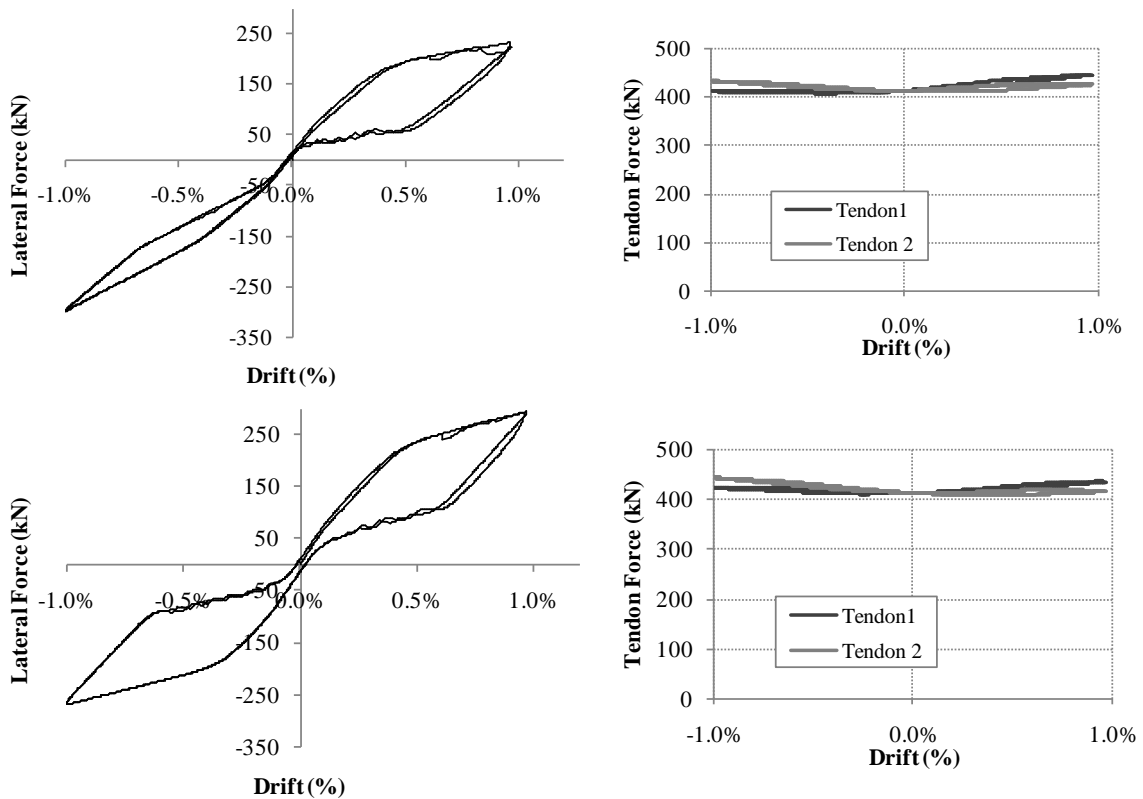


Figure 216. Push Over Analysis up to Failure Point (left), Hysteresis of External Dissipator (right)

Push Pull Analysis

The push pull analysis cycles the “wall-truss” system at the top of the truss and so the walls are stressed in a different ways.

The results obtained are shown in the picture below.



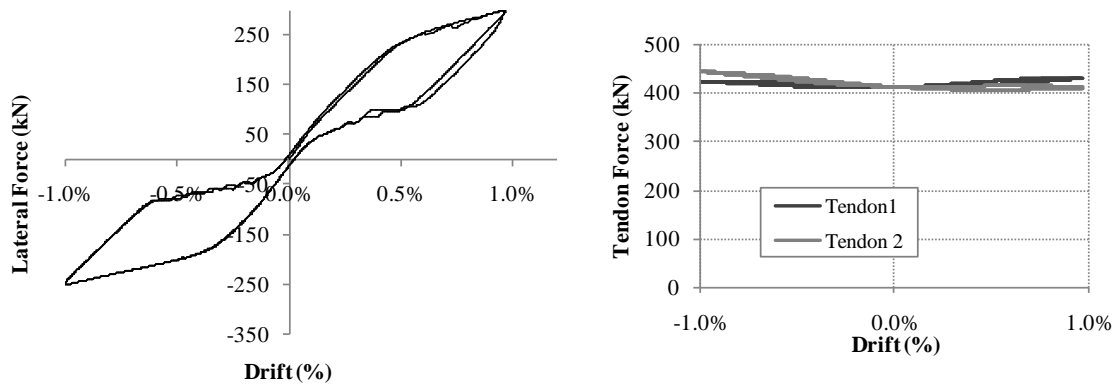


Figura 217 _Quasi Static Analysis. Lateral Force and Tendons Force Wall 1 (top left and right), Lateral Force and Tendons Force Wall 2 (center left and right), Lateral Force and Tendon Force Wall 3 (bottom left and right)

Increasing the number of cycles the loop is stable and there is no stiffness degradation (Figure 218); this is one of the main differences in behavior of the external devices compared to the internal ones (Figure 195).

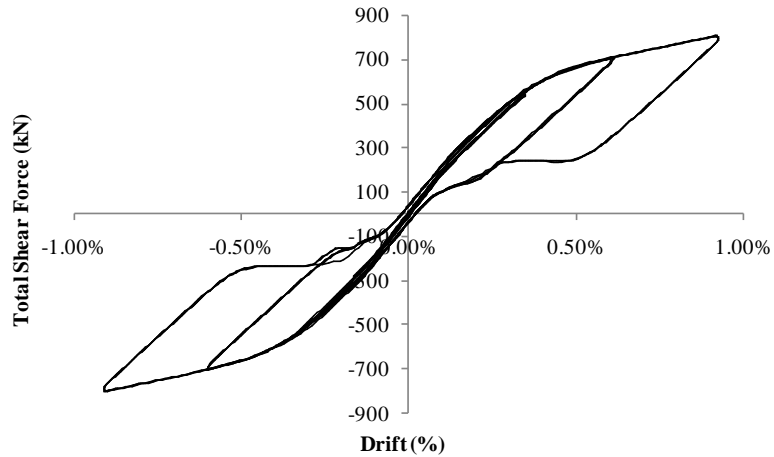


Figure 218. Quasi Static Analysis Total Shear Force - Drift

The hysteresis of the dissipator is shown in Figure 218. The first stretch of the graphic shows an elastic behavior up to the yield point (313 kN). A yield plateau with no increase in stress follows till when the decompression starts. The tension force on the dissipator decrease up to zero and then the device is compressed. In compression a smaller value of force (-160 kN) is reached because the dissipator has already yielded in tension (*plastic buckling*).

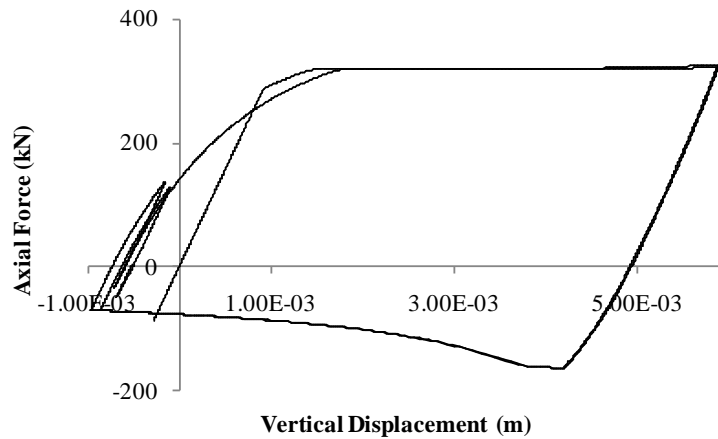


Figure 219. Hysteresis Loop of External Dissipator Devices

Figure 220 shows the results of the push pull analysis carried out with increasing tension-compression cycles up to failure (three cycles at 0.5% drift, three cycles at 0.1% drift, 3 cycles at 1.15% drift and three cycles at 2.2% drift).

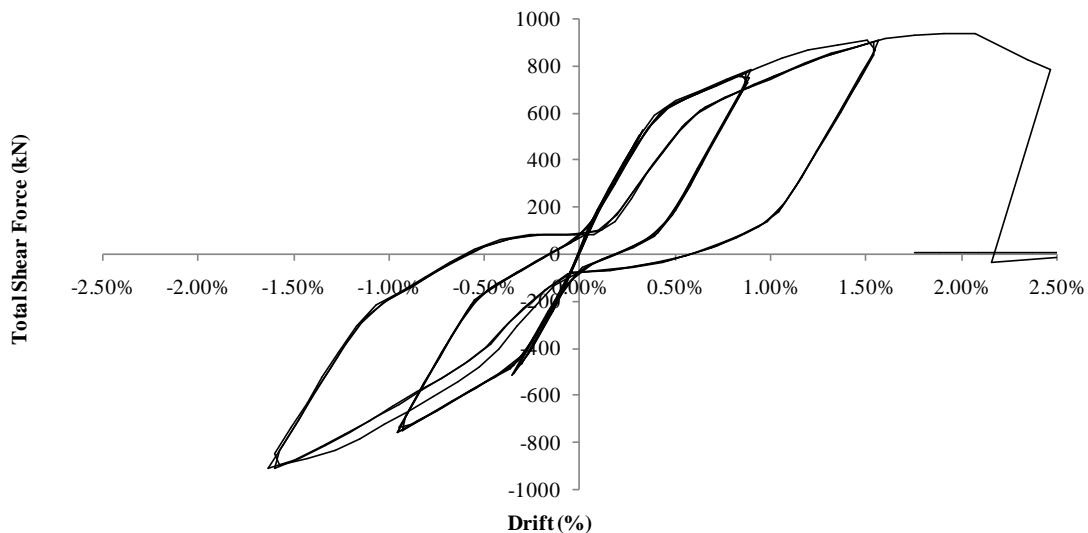


Figure 220. Push Pull Analysis up to Failure Point

The Push Pull analysis reflects the results obtained with the Push Over analysis; the external dissipator of the wall 1 reaches the failure point and the degradation starts.

7.3.2.2 Dynamic Time History Analyses

The performance of the system when subjected to dynamic non-linear time history is herein presented.

As for the model with internal devices as energy dissipators, the flag shape obtained when the system is subjected to the ground motion called EQ 12 is shown in the figure below.

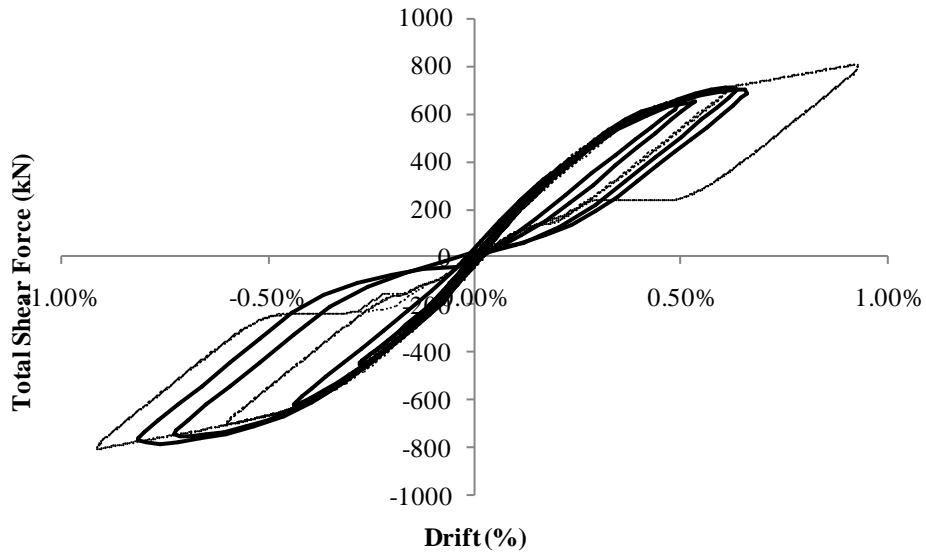


Figure 221. Flag Shape Hysteresis, Push Pull Analysis and Ground Motion Analysis

7.4 References

1. Dekker, D., S. Chung, and A. Palermo, *Carterton Events Centre Auditorium Pres-Lam Wall Design and Construction*, in NZSEE 2012.
2. Buchanan, A., *Timber Design Guide*, ed. Z.T.I.F. Inc. 2007.
3. NZCS, *Press Design Handbook*. 2010, Wellington, New Zealand.
4. Carr, A.J., *Ruaumoko Programme for Inelastic Dynamic Analysis - User Manual*. 2007, University of Canterbury, Christchurch.
5. Palermo, A., S. Pampanin, and A.J. Carr, *Efficiency Of Simplified Alternative Modelling Approaches To Predict The Seismic Response Of Precast Concrete Hybrid Systems*, in *fib Symposium 2005*: Budapest.
6. Pennucci, D., G.M. Calvi, and T.J. Sullivan. *Displacement-based design of precast walls with additional dampers*. 2009. 4 Park Square, Milton Park, Abingdon, Oxfordshire, OX14 4RN, United Kingdom: Taylor and Francis Ltd.
7. Chopra, A.K. and R.K. Goel, *Capacity-demand-diagram methods based on inelastic design spectrum*. *Earthquake Spectra*, 1999. **15**(4): p. 637-655.
8. Committee, T., *Structural Design Actions*, in *Part 5: Earthquake actions - New Zealand - Commentary*. 2004. p. 86.
9. Committee, T., *Structural Design Actions*, in *Part 5: Earthquake actions - New Zealand*. 2004. p. 82.
10. Newcombe, M., *Beam to Column and Wall to Foundation Tests with Internal Dissipaters*. 2005.
11. Palermo, A., *The use of controlled rocking in the seismic design of bridges* 2004, Politecnico di Milano.
12. Newcombe, M., et al., *Section Analysis and Cyclic Behavior of Post-Tensioned Jointed Ductile Connections for Multi-Story Timber Buildings*. *Journal of Earthquake Engineering* 2008. **Vol. 12**: p. 83-110.
13. Palermo, A., et al., *Seismic Design of Multi-Storey Buildings using Laminated Veneer Lumber (LVL)*, in *NZSEE Conference*. 2005. p. 8.

8 Conclusions

The work done has crossed several issues and aspects concerning the external dissipator devices used in hybrid joints. Following the declared target to achieve a no (or at least low) damage solution, the external replaceable mild steel dissipators have been developed and investigated at the University of Canterbury (New Zealand).

This study tries to provide further information more focused on the modeling and design of dissipators. If not properly designed, in fact, the devices can be subjected to instability; if buckling occurs, the dissipators are not able to dissipate the same amount of energy as in compression as in tension.

A preliminary study on the previous applications of dissipators (both internal and external) has been necessary to define the properties and characteristics of the devices. Following and trying to improve the design of the devices, several information useful for the manufacture of the “Plug and Play” are provided. Grade 300 mild steel is chosen for the bar due to its capacity to cumulate a large amount of plastic deformation. The external diameters of the bars have been verified considering that the thread root area has to be higher than the fuse area in order to guarantee that the buckling, if occurs, happens in the fuse. The fuse part is connected to the external part with a transitional length at an angle of 45° degree in order to avoid a concentration of stress. Following these last devices in the design of dissipators, the possibilities that buckling occurs out of the fuse length are reduced. In any case the restraining tube has been designed to be as long as to cover even the external length partly, so the restraining effect is not limited to the fuse length only. Another good effect of designing the tube longer than the fuse is to avoid that it is subjected to an axial compression with the risk of buckling as well. The tube is kept very close to the bar involving an almost immediate effect of the restrain.

The dissipators have been strain gauging and filled with the grout and epoxy and are ready for the forthcoming testing at the University of Canterbury.

An important aspect of the dissipation devices that has to be known is the onset of dissipation, so the value of displacement needed to reach the yielding load. The deformation is mainly concentrated in the fuse length but the external parts provide an additional stiffness that has to be considered in order to establish the right start of dissipation. An equivalent length whose value is between the fuse length and the total length is defined and depends on the fuse and external diameters ratio and fuse and total lengths ratio. As the fuse diameter gets close to the external diameter and the fuse length gets close to the total length, the equivalent length approaches the total length. The effect of the anchorage is relevant if there is a considerable change in stiffness, otherwise is non essential.

When the fuse yields, all the stress falls in this area. The effect of the anchorage becomes less relevant as the displacement increase (the fuse and total length ratio approaches 1).

The second part of the work has been more focused on the model of the dissipators. If not properly designed or if not restrained, the dissipator can buckle since the first cycle when subjected to compression. On the contrary if the dissipator has been properly designed the crisis of the device can occur for low cycle fatigue that involves the rupture of the dissipator or plastic buckling (due to low cycle fatigue) after a certain number of cycles. For this reason the behavior of the dissipator has to be described with different loops depending on its characteristics. The Remennikov Hysteresis loop is appropriate to describe the buckling of the device while the Ramberg Osgood Hysteresis represents the steel behavior with the typical spindle-shape. The two loops can be combined to describe the global behavior of the dissipator. If at the first cycle the device can't reach the yielding value, the shape of the hysteresis will be similar to the buckling one (Remennikov Hysteresis Loop). If the dissipator can reach the yielding value, different tension and compression cycles may follow with a force displacement loop typical of the steel (Ramberg Osgood Hysteresis). After a certain number of cycles, depending on the properties of the dissipator and the values of drift, the crisis of the device occurs due to the rupture or a plastic buckling behavior. The loop can reach the failure point or keeps on with the buckling hysteresis loop.

The presence of the restrain implies an increasing of the critical load (or a decreasing of the effective length). Starting from parametrical analyses considering different thicknesses of the epoxy and grout, the stiffness of the restrain (filler material restrained by a steel tube) is obtained. The results achieved with the parametrical analyses fit with good approximation an exponential loop; the solution has so been generalized for all values of thickness of the filler material and for all values of outer diameter of the tube.

The lateral resisting system of the Carterton Events Center has been chosen as case study. A push over analysis on the timber walls re-designed with external dissipators up to the failure point has shown that the crisis of the wall is due to the fracture of the dissipator. When the ultimate curvature is reached the degradation of the dissipator starts. The results show that the failure occurs for a value of drift of 2.25 % (1% design drift). Compared to the connection with internal dissipators that exhibits stiffness degradation associated to the bond slip, the external dissipator guarantee a more stable loop.

Further Objective of the Research

The dissipators will be tested at the University of Canterbury following the indications provided in this work. The hysteresis loop has to be updated considering the switch of loop depending on the values of stress reached by the dissipator when subjected to tension and compression cycles. Design charts on dissipators are the next step of the research.

The analytical prediction has to be compared with the experimental data in order to verify the correspondence of results. The experimental results will be also useful to calibrate the loop if necessary, in particular concerning the stiffness of the confinement.

APPENDIX A

Introduction

In the following appendix all the calculation performed to determine the dissipating moment supplied by the mild steel dissipators of 12, 16, 20, 26 mm of diameter are reported.

$\phi 12$ Diameter of the Bars

Twenty-eight bars of 12 mm diameters are considered for a total of 3166 mm² of mild steel; the fuse length is 180 mm and the un bonded length is 344 mm.

The final iteration is presented below. The neutral axis depth is equal to $c = 909$ mm, $\gamma = c/L_w = 0.378$.

The tendons elongation at the rocking interface is:

$$\Delta_{pt} = \theta(d_{pt,i} - c) \quad \begin{array}{l} = 1.6 \text{ mm for } d_{pt,1} = 1075 \text{ mm} \\ = 4.2 \text{ mm for } d_{pt,2} = 1325 \text{ mm} \end{array}$$

The tendons strain increments due to tendons elongations are:

$$\varepsilon_{pt}(\theta) = \frac{n\Delta_{pt}}{l_{ub}}$$

$$\varepsilon_{pt} = 0.0002$$

$$\varepsilon_{pt} = 0.0006$$

The increment in tendon force is:

$$\Delta T_{pt} = E_{pt}\varepsilon_{pt}(\theta)n_{pt}A_{pt}$$

The increments in tendons force are:

$$\Delta T_{pt1} = 52.92 \text{ kN}$$

$$\Delta T_{pt2} = 132.63 \text{ kN}$$

The total post tensioned forces are:

$$T_{pt} = T_{pt,initial} + \Delta T_{pt}$$

$$T_{pt1} = 551.45 \text{ kN}$$

$$T_{pt2} = 631.16 \text{ kN}$$

The stress in the tendons can't exceed the allowable limit of 90% of f_{pty} .

$$\varepsilon_{pt,initial} + \varepsilon_{pt} < 0.9 \varepsilon_y = 0.9 * 835/E = 0.004$$

$$\text{Tendon 1: } \varepsilon_{pt,initial} + \varepsilon_{pt} = 0.0026 < 0.004$$

$$\text{Tendon 2: } \varepsilon_{pt,initial} + \varepsilon_{pt} = 0.0030 < 0.004$$

The mild steel is lumped into 12 layers of 2 bars each, two on the left and two on the right side of the wall. The depth of each layer is:

$$d1 = 831 \text{ mm}$$

$$d2 = 861 \text{ mm}$$

$$d3 = 891 \text{ mm}$$

$$d4 = 921 \text{ mm}$$

$$d5 = 951 \text{ mm}$$

$$d6 = 981 \text{ mm}$$

$$d7 = 1011 \text{ mm}$$

$$d8 = 1041 \text{ mm}$$

$$d9 = 1359 \text{ mm}$$

$$d10 = 1389 \text{ mm}$$

$$d11 = 1419 \text{ mm}$$

$$d12 = 1449 \text{ mm}$$

$$d13 = 1479 \text{ mm}$$

$$d14 = 1509 \text{ mm}$$

$$d15 = 1539 \text{ mm}$$

$$d16 = 1569 \text{ mm}$$

TENSION STEEL LAYERS

The elongations and the strain of the tension steel layers are:

$$\Delta s_1 = 4.5 \text{ mm}$$

$$\Delta s_1 = 4.8 \text{ mm}$$

$$\Delta s_3 = 5.1 \text{ mm}$$

$$\Delta s_4 = 5.4 \text{ mm}$$

$$\Delta s_5 = 5.7 \text{ mm}$$

$$\Delta s_6 = 6 \text{ mm}$$

$$\Delta s_7 = 6.3 \text{ mm}$$

$$\Delta s_8 = 6.6 \text{ mm}$$

The values of strain are:

$$\varepsilon_{s1} = 0.025$$

$$\varepsilon_{s2} = 0.026$$

$$\varepsilon_{s3} = 0.028$$

$$\varepsilon_{s4} = 0.030$$

$$\varepsilon_{s5} = 0.032$$

$$\varepsilon_{s6} = 0.033$$

$$\varepsilon_{s7} = 0.035$$

$$\varepsilon_{s8} = 0.037$$

The stress is determined from a bilinear stress – strain relationship with $r = 0.8\%$.

$$f_s = f_y \left[1 + r \left(\frac{\varepsilon_s}{\varepsilon_y} - 1 \right) \right]$$

$$f_{s1} = 337.598 \text{ MPa}$$

$$f_{s2} = 340.264 \text{ MPa}$$

$$f_{s3} = 342.931 \text{ MPa}$$

$$f_{s4} = 345.598 \text{ MPa}$$

$$f_{s5} = 348.264 \text{ MPa}$$

$$f_{s6} = 350.931 \text{ MPa}$$

$$f_{s7} = 353.598 \text{ MPa}$$

$$f_{s8} = 356.264 \text{ MPa}$$

The force in the tension layer is given by:

$$T_s = f_s A_s$$

$$T_{1a} = 38.18 \text{ kN}$$

$$T_{1b} = 38.18 \text{ kN}$$

$$T_{2a} = 38.48 \text{ kN}$$

$$T_{2b} = 38.48 \text{ kN}$$

$$T_{3a} = 38.78 \text{ kN}$$

$$T_{3b} = 38.78 \text{ kN}$$

$$T_{4a} = 39.09 \text{ kN}$$

$$T_{4b} = 39.09 \text{ kN}$$

$$T_{5a} = 39.39 \text{ kN}$$

$$T_{5b} = 39.39 \text{ kN}$$

$$T_{6a} = 39.69 \text{ kN}$$

$$T_{6b} = 39.69 \text{ kN}$$

$$T_{7a} = 39.99 \text{ kN}$$

$$T_{7b} = 39.99 \text{ kN}$$

$$T_{8a} = 40.29 \text{ kN}$$

$$T_{8b} = 40.29 \text{ kN}$$

COMPRESSION STEEL LAYERS

The elongations and the strain of the tension steel layers are:

$$\Delta s_1 = -0.78 \text{ mm}$$

$$\Delta s_1 = -0.48 \text{ mm}$$

$$\Delta s_3 = -0.18 \text{ mm}$$

$$\Delta s_4 = +0.12 \text{ mm}$$

$$\Delta s_5 = +0.42 \text{ mm}$$

$$\Delta s_6 = +0.72 \text{ mm}$$

$$\Delta s_7 = +1.02 \text{ mm}$$

$$\Delta s_8 = +1.3 \text{ mm}$$

The values of strain are:

$$\varepsilon_{s1} = -0.004$$

$$\varepsilon_{s2} = -0.003$$

$$\varepsilon_{s3} = -0.001$$

$$\varepsilon_{s4} = 0.0007$$

$$\varepsilon_{s5} = 0.002$$

$$\varepsilon_{s6} = 0.004$$

$$\varepsilon_{s7} = 0.005$$

$$\varepsilon_{s8} = 0.007$$

The stress is determined from a bilinear stress – strain relationship (if the elastic limit is not exceeded) with $r = 0.8\%$.

$$f_s = f_y \left[1 + r \left(\frac{\varepsilon_s}{\varepsilon_y} - 1 \right) \right]$$

$$f_{s1} = -304.536 \text{ MPa}$$

$$f_{s2} = -301.869 \text{ MPa}$$

$$f_{s3} = -200.308 \text{ MPa}$$

$$f_{s4} = 133.026 \text{ MPa}$$

$$f_{s5} = 301.331 \text{ MPa}$$

$$\begin{aligned}
f_{s6} &= 303.998 \text{ MPa} \\
f_{s7} &= 306.664 \text{ MPa} \\
f_{s8} &= 309.331 \text{ MPa}
\end{aligned}$$

The force in the compression layer is given by:

$$C_s = f_s A_s$$

$$\begin{array}{llll}
C_{1a} = & -34.44 & \text{kN} & C_{1b} = & 34.44 & \text{kN} \\
C_{2a} = & -34.14 & \text{kN} & C_{2b} = & 34.14 & \text{kN} \\
C_{3a} = & -22.65 & \text{kN} & C_{3b} = & 22.65 & \text{kN} \\
C_{4a} = & 15.04 & \text{kN} & C_{4b} = & -15.04 & \text{kN} \\
C_{5a} = & 34.08 & \text{kN} & C_{5b} = & -34.08 & \text{kN} \\
C_{6a} = & 34.38 & \text{kN} & C_{6b} = & -34.38 & \text{kN} \\
C_{7a} = & 34.68 & \text{kN} & C_{7b} = & -34.68 & \text{kN} \\
C_{8a} = & 34.98 & \text{kN} & C_{8b} = & -34.98 & \text{kN}
\end{array}$$

TIMBER

The timber compressive strain is defined as:

$$\varepsilon_t = \left(3 \frac{\vartheta_{imp}}{L_{cant}} + \phi_{dec} \right) c$$

Where:

$$E_t = 10 \text{ GPa}$$

$$E_{can} = 5.5 \text{ MPa}$$

The decompression curvature is:

$$\phi_{dec} = \frac{M}{E_{can} I_t} = \frac{T_{pt,i} + N}{E_{cant} I_t}$$

$$\phi_{dec} = 3.66\text{E-}07$$

Thus the timber strain is calculated:

$$\varepsilon_t = 4.4 \text{ E-}03$$

The compression force is so equal to:

$$C_t = -1981 \text{ kN.}$$

Checking the equilibrium:

$$C = T = 0$$

$$2163.75 = 2163.75$$

Finally the moment capacity of the section is computed.

Centering moments from axial loads and Post – tensioned:

$$M_{pt} = 1070 \text{ kNm}$$

Dissipating moment from mild steel:

$$M_d = 838 \text{ kNm.}$$

$\phi 16$ Diameter of the Bars

Sixteen bars of 16 mm diameters are considered for a total of 3217 mm^2 of mild steel; the fuse length is 240 mm and the un bonded length is 408 mm.

The final iteration is presented below. The neutral axis depth is equal to $c = 865 \text{ mm}$, $\gamma = c/L_w = 0.361$.

The tendons elongation at the rocking interface is:

$$\begin{aligned} \Delta_{pt} = \theta(d_{pt,i} - c) &= 2.1 \text{ mm for } d_{pt,1} = 1075 \text{ mm} \\ &= 4.6 \text{ mm for } d_{pt,2} = 1325 \text{ mm} \end{aligned}$$

The tendons strain increments due to tendons elongations are:

$$\varepsilon_{pt}(\theta) = \frac{n\Delta_{pt}}{l_{ub}}$$

$$\varepsilon_{pt} = 0.0003$$

$$\varepsilon_{pt} = 0.0007$$

The increment in tendon force is:

$$\Delta T_{pt} = E_{pt} \varepsilon_{pt}(\theta) n_{pt} A_{pt}$$

The increments in tendons force are:

$$\Delta T_{pt1} = 66.75 \text{ kN}$$

$$\Delta T_{pt2} = 146.5 \text{ kN}$$

The total post tensioned forces are:

$$T_{pt} = T_{pt,initial} + \Delta T_{pt}$$

$$T_{pt1} = 565.3 \text{ kN}$$

$$T_{pt2} = 644.9 \text{ kN}$$

The stress in the tendons can't exceed the allowable limit of 90% of f_{pty} .

$$\varepsilon_{pt,initial} + \varepsilon_{pt} < 0.9 \varepsilon_y = 0.9 * 835/E = 0.004$$

$$\text{Tendon 1: } \varepsilon_{pt,initial} + \varepsilon_{pt} = 0.0026 < 0.004$$

$$\text{Tendon 2: } \varepsilon_{pt,initial} + \varepsilon_{pt} = 0.0030 < 0.004$$

The mild steel is lumped into 12 layers of 2 bars each, two on the left and two on the right side of the wall. The depth of each layer is:

$$d1 = 789 \text{ mm}$$

$$d2 = 839 \text{ mm}$$

$$d3 = 889 \text{ mm}$$

$$d4 = 939 \text{ mm}$$

$$d5 = 1461 \text{ mm}$$

$$d6 = 1511 \text{ mm}$$

$$d7 = 1561 \text{ mm}$$

$$d8 = 1611 \text{ mm}$$

TENSION STEEL LAYERS

The elongations and the strain of the tension steel layers are:

$$\Delta s_1 = 7.4 \text{ mm}$$

$$\Delta s_2 = 6.9 \text{ mm}$$

$$\Delta s_3 = 6.4 \text{ mm}$$

$$\Delta s_4 = 5.9 \text{ mm}$$

The values of strain are:

$$\varepsilon_{s1} = 0.031$$

$$\varepsilon_{s2} = 0.029$$

$$\varepsilon_{s3} = 0.027$$

$$\varepsilon_{s4} = 0.025$$

The stress is determined from a bilinear stress – strain relationship with $r = 0.8\%$.

$$f_s = f_y \left[1 + r \left(\frac{\varepsilon_s}{\varepsilon_y} - 1 \right) \right]$$

$$f_{s1} = 347.3 \text{ MPa}$$

$$f_{s2} = 343.9 \text{ MPa}$$

$$f_{s3} = 340.6 \text{ MPa}$$

$$f_{s4} = 337.3 \text{ MPa}$$

The force in the tension layer is given by:

$$T_s = f_s A_s$$

$$T_{1a} = 69.8 \text{ kN}$$

$$T_{1b} = 38.18 \text{ kN}$$

$$T_{2a} = 69.2 \text{ kN}$$

$$T_{2b} = 38.48 \text{ kN}$$

$$T_{3a} = 68.5 \text{ kN}$$

$$T_{3b} = 38.78 \text{ kN}$$

$$T_{4a} = 67.8 \text{ kN}$$

$$T_{4b} = 39.09 \text{ kN}$$

COMPRESSION STEEL LAYERS

The elongations and the strain of the tension steel layers are:

$$\Delta s_1 = -0.77 \text{ mm}$$

$$\Delta s_2 = -0.26 \text{ mm}$$

$$\Delta s_3 = -0.23 \text{ mm}$$

$$\Delta s_4 = -0.73 \text{ mm}$$

The values of strain are:

$$\varepsilon_{s1} = 0.003$$

$$\varepsilon_{s2} = 0.001$$

$$\varepsilon_{s3} = -0.001$$

$$\varepsilon_{s4} = -0.003$$

The stress is determined from a bilinear stress – strain relationship (if the elastic limit is not exceeded) with $r = 0.8\%$.

$$f_s = f_y \left[1 + r \left(\frac{\varepsilon_s}{\varepsilon_y} - 1 \right) \right]$$

$$\begin{aligned}
f_{s1} &= 302.7 \text{ MPa} \\
f_{s2} &= 222.1 \text{ MPa} \\
f_{s3} &= -194.6 \text{ MPa} \\
f_{s4} &= -302.5 \text{ MPa}
\end{aligned}$$

The force in the compression layer is given by:

$$C_s = f_s A_s$$

$$\begin{array}{llll}
C_{1a} = & 60.8 & \text{kN} & C_{1b} = & 60.8 & \text{kN} \\
C_{2a} = & 44.6 & \text{kN} & C_{2b} = & 44.6 & \text{kN} \\
C_{3a} = & -39.1 & \text{kN} & C_{3b} = & -39.1 & \text{kN} \\
C_{4a} = & -60.8 & \text{kN} & C_{4b} = & -60.8 & \text{kN}
\end{array}$$

TIMBER

The timber compressive strain is defined as:

$$\varepsilon_t = \left(3 \frac{\vartheta_{imp}}{L_{cant}} + \phi_{dec} \right) c$$

Where:

$$E_t = 10 \text{ GPa}$$

$$E_{can} = 5.5 \text{ MPa}$$

The decompression curvature is:

$$\phi_{dec} = \frac{M}{E_{can} I_t} = \frac{T_{pt,i} + N}{E_{cant} I_t}$$

$$\phi_{dec} = 3.66E-07$$

Thus the timber strain is calculated:

$$\varepsilon_t = 4.2 \text{ E-03}$$

The compression force is so equal to:

$$C_t = -1797 \text{ kN.}$$

Checking the equilibrium:

$$C = T = 0$$

$$2007.73 = 2007.73$$

Finally the moment capacity of the section is computed.

Centering moments from axial loads and Post – tensioned:

$$M_{pt} = 1113.1 \text{ kNm}$$

Dissipating moment from mild steel:

$$M_d = 703.2 \text{ kNm.}$$

$\phi 16$ Diameter of the Bars

Sixteen bars of 16 mm diameters are considered for a total of 3217 mm^2 of mild steel; the fuse length is 240 mm and the un bonded length is 408 mm.

The final iteration is presented below. The neutral axis depth is equal to $c = 865 \text{ mm}$, $\gamma = c/L_w = 0.31$.

The tendons elongation at the rocking interface is:

$$\begin{aligned} \Delta_{pt} = \theta(d_{pt,i} - c) &= 2.1 \text{ mm for } d_{pt,1} = 1075 \text{ mm} \\ &= 4.6 \text{ mm for } d_{pt,2} = 1325 \text{ mm} \end{aligned}$$

The tendons strain increments due to tendons elongations are:

$$\varepsilon_{pt}(\theta) = \frac{n\Delta_{pt}}{l_{ub}}$$

$$\varepsilon_{pt} = 0.0003$$

$$\varepsilon_{pt} = 0.0007$$

The increment in tendon force is:

$$\Delta T_{pt} = E_{pt} \varepsilon_{pt}(\theta) n_{pt} A_{pt}$$

The increments in tendons force are:

$$\Delta T_{pt1} = 66.75 \text{ kN}$$

$$\Delta T_{pt2} = 146.5 \text{ kN}$$

The total post tensioned forces are:

$$T_{pt} = T_{pt,initial} + \Delta T_{pt}$$

$$T_{pt1} = 565.3 \text{ kN}$$

$$T_{pt2} = 644.9 \text{ kN}$$

The stress in the tendons can't exceed the allowable limit of 90% of f_{pty} .

$$\varepsilon_{pt,initial} + \varepsilon_{pt} < 0.9 \varepsilon_y = 0.9 * 835/E = 0.004$$

$$\text{Tendon 1: } \varepsilon_{pt,initial} + \varepsilon_{pt} = 0.0026 < 0.004$$

$$\text{Tendon 2: } \varepsilon_{pt,initial} + \varepsilon_{pt} = 0.0030 < 0.004$$

The mild steel is lumped into 12 layers of 2 bars each, two on the left and two on the right side of the wall. The depth of each layer is:

$$d1 = 789 \text{ mm}$$

$$d2 = 839 \text{ mm}$$

$$d3 = 889 \text{ mm}$$

$$d4 = 939 \text{ mm}$$

$$d5 = 1461 \text{ mm}$$

$$d6 = 1511 \text{ mm}$$

$$d7 = 1561 \text{ mm}$$

$$d8 = 1611 \text{ mm}$$

TENSION STEEL LAYERS

The elongations and the strain of the tension steel layers are:

$$\Delta s_1 = 7.4 \text{ mm}$$

$$\Delta s_2 = 6.9 \text{ mm}$$

$$\Delta s_3 = 6.4 \text{ mm}$$

$$\Delta s_4 = 5.9 \text{ mm}$$

The values of strain are:

$$\varepsilon_{s1} = 0.031$$

$$\varepsilon_{s2} = 0.029$$

$$\varepsilon_{s3} = 0.027$$

$$\varepsilon_{s4} = 0.025$$

The stress is determined from a bilinear stress – strain relationship with $r = 0.8\%$.

$$f_s = f_y \left[1 + r \left(\frac{\varepsilon_s}{\varepsilon_y} - 1 \right) \right]$$

$$f_{s1} = 347.3 \text{ MPa}$$

$$f_{s2} = 343.9 \text{ MPa}$$

$$f_{s3} = 340.6 \text{ MPa}$$

$$f_{s4} = 337.3 \text{ MPa}$$

The force in the tension layer is given by:

$$T_s = f_s A_s$$

$$T_{1a} = 69.8 \text{ kN}$$

$$T_{1b} = 38.18 \text{ kN}$$

$$T_{2a} = 69.2 \text{ kN}$$

$$T_{2b} = 38.48 \text{ kN}$$

$$T_{3a} = 68.5 \text{ kN}$$

$$T_{3b} = 38.78 \text{ kN}$$

$$T_{4a} = 67.8 \text{ kN}$$

$$T_{4b} = 39.09 \text{ kN}$$

COMPRESSION STEEL LAYERS

The elongations and the strain of the tension steel layers are:

$$\Delta s_1 = -0.77 \text{ mm}$$

$$\Delta s_1 = -0.26 \text{ mm}$$

$$\Delta s_3 = 0.23 \text{ mm}$$

$$\Delta s_4 = 0.73 \text{ mm}$$

The values of strain are:

$$\varepsilon_{s1} = -0.003$$

$$\varepsilon_{s2} = -0.001$$

$$\varepsilon_{s3} = 0.001$$

$$\varepsilon_{s4} = 0.003$$

The stress is determined from a bilinear stress – strain relationship (if the elastic limit is not exceeded) with $r = 0.8\%$.

$$f_s = f_y \left[1 + r \left(\frac{\varepsilon_s}{\varepsilon_y} - 1 \right) \right]$$

$$\begin{aligned}
f_{s1} &= -302.7 \text{ MPa} \\
f_{s2} &= -222.1 \text{ MPa} \\
f_{s3} &= 194.6 \text{ MPa} \\
f_{s4} &= 302.5 \text{ MPa}
\end{aligned}$$

The force in the compression layer is given by:

$$C_s = f_s A_s$$

$$\begin{array}{llll}
C_{1a} = & 60.8 & \text{kN} & C_{1b} = & 60.8 & \text{kN} \\
C_{2a} = & 44.6 & \text{kN} & C_{2b} = & 44.6 & \text{kN} \\
C_{3a} = & -39.1 & \text{kN} & C_{3b} = & -39.1 & \text{kN} \\
C_{4a} = & -60.8 & \text{kN} & C_{4b} = & -60.8 & \text{kN}
\end{array}$$

TIMBER

The timber compressive strain is defined as:

$$\varepsilon_t = \left(3 \frac{\vartheta_{imp}}{L_{cant}} + \phi_{dec} \right) c$$

Where:

$$E_t = 10 \text{ GPa}$$

$$E_{can} = 5.5 \text{ MPa}$$

The decompression curvature is:

$$\phi_{dec} = \frac{M}{E_{can} I_t} = \frac{T_{pt,i} + N}{E_{cant} I_t}$$

$$\phi_{dec} = 3.66E-07$$

Thus the timber strain is calculated:

$$\varepsilon_t = 4.2 \text{ E-03}$$

The compression force is so equal to:

$$C_t = -1797 \text{ kN.}$$

Checking the equilibrium:

$$C = T = 0$$

$$2007.73 = 2007.73$$

Finally the moment capacity of the section is computed.

Centering moments from axial loads and Post – tensioned:
 $M_{pt} = 1113.1 \text{ kNm}$

Dissipating moment from mild steel:
 $M_d = 703.2 \text{ kNm}$.

$\phi 20$ Diameter of the Bars

Twelve bars of 20 mm diameters are considered for a total of 3769 mm^2 of mild steel; the fuse length is 300 mm and the un bonded length is 472 mm.

The final iteration is presented below. The neutral axis depth is equal to $c = 789 \text{ mm}$, $\gamma = c/L_w = 0.329$.

The tendons elongation at the rocking interface is:

$$\Delta_{pt} = \theta(d_{pt,i} - c) \quad \begin{array}{l} = 2.8 \text{ mm for } d_{pt,1} = 1075 \text{ mm} \\ = 5.3 \text{ mm for } d_{pt,2} = 1325 \text{ mm} \end{array}$$

The tendons strain increments due to tendons elongations are:

$$\varepsilon_{pt}(\theta) = \frac{n\Delta_{pt}}{l_{ub}}$$

$$\varepsilon_{pt} = 0.0004$$

$$\varepsilon_{pt} = 0.0008$$

The increment in tendon force is:

$$\Delta T_{pt} = E_{pt} \varepsilon_{pt}(\theta) n_{pt} A_{pt}$$

The increments in tendons force are:

$$\Delta T_{pt1} = 91.94 \text{ kN}$$

$$\Delta T_{pt2} = 170.75 \text{ kN}$$

The total post tensioned forces are:

$$T_{pt} = T_{pt,initial} + \Delta T_{pt}$$

$$T_{pt1} = 589.5 \text{ kN}$$

$$T_{pt2} = 669.3 \text{ kN}$$

The stress in the tendons can't exceed the allowable limit of 90% of f_{pty} .

$$\varepsilon_{pt,initial} + \varepsilon_{pt} < 0.9 \varepsilon_y = 0.9 * 835/E = 0.004$$

$$\text{Tendon 1: } \varepsilon_{pt,initial} + \varepsilon_{pt} = 0.0026 < 0.004$$

$$\text{Tendon 2: } \varepsilon_{pt,initial} + \varepsilon_{pt} = 0.0030 < 0.004$$

The mild steel is lumped into 6 layers of 2 bars each, two on the left and two on the right side of the wall. The depth of each layer is:

$$d1 = 670 \text{ mm}$$

$$d2 = 720 \text{ mm}$$

$$d3 = 770 \text{ mm}$$

$$d4 = 1630 \text{ mm}$$

$$d3 = 1680 \text{ mm}$$

$$d4 = 1730 \text{ mm}$$

TENSION STEEL LAYERS

The elongations and the strain of the tension steel layers are:

$$\Delta s_1 = 9.4 \text{ mm}$$

$$\Delta s_1 = 8.9 \text{ mm}$$

$$\Delta s_3 = 8.4 \text{ mm}$$

The values of strain are:

$$\varepsilon_{s1} = 0.031$$

$$\varepsilon_{s2} = 0.030$$

$$\varepsilon_{s3} = 0.028$$

The stress is determined from a bilinear stress – strain relationship with $r = 0.8\%$.

$$f_s = f_y \left[1 + r \left(\frac{\varepsilon_s}{\varepsilon_y} - 1 \right) \right]$$

$$f_{s1} = 347.7 \text{ MPa}$$

$$f_{s2} = 345.1 \text{ MPa}$$

$$f_{s3} = 342.4 \text{ MPa}$$

The force in the tension layer is given by:

$$T_s = f_s A_s$$

$T_{1a} =$	109.2	kN	$T_{1b} =$	109.2	kN
$T_{2a} =$	108.4	kN	$T_{2b} =$	108.4	kN
$T_{3a} =$	107.6	kN	$T_{3b} =$	107.6	kN

COMPRESSION STEEL LAYERS

The elongations and the strain of the tension steel layers are:

$$\Delta s_1 = -1.19 \text{ mm}$$

$$\Delta s_2 = -0.69 \text{ mm}$$

$$\Delta s_3 = -0.19 \text{ mm}$$

The values of strain are:

$$\varepsilon_{s1} = -0.004$$

$$\varepsilon_{s2} = -0.002$$

$$\varepsilon_{s3} = -0.006$$

The stress is determined from a bilinear stress – strain relationship (if the elastic limit is not exceeded) with $r = 0.8\%$.

$$f_s = f_y \left[1 + r \left(\frac{\varepsilon_s}{\varepsilon_y} - 1 \right) \right]$$

$$f_{s1} = -303.9 \text{ MPa}$$

$$f_{s2} = -301.3 \text{ MPa}$$

$$f_{s3} = -129.8 \text{ MPa}$$

The force in the compression layer is given by:

$$C_s = f_s A_s$$

$C_{1a} =$	-95.5	kN	$C_{1b} =$	-95.5	kN
$C_{2a} =$	-94.6	kN	$C_{2b} =$	-94.6	kN
$C_{3a} =$	-40.8	kN	$C_{3b} =$	-40.8	kN

TIMBER

The timber compressive strain is defined as:

$$\varepsilon_t = \left(3 \frac{\vartheta_{imp}}{L_{cant}} + \phi_{dec} \right) c$$

Where:

$$E_t = 10 \text{ GPa}$$

$$E_{can} = 5.5 \text{ MPa}$$

The decompression curvature is:

$$\phi_{dec} = \frac{M}{E_{can} I_t} = \frac{T_{pt,i} + N}{E_{cant} I_t}$$

$$\phi_{dec} = 3.66\text{E-}07$$

Thus the timber strain is calculated:

$$\varepsilon_t = 3.82 \text{ E-}03$$

The compression force is so equal to:

$$C_t = -1494 \text{ kN.}$$

Checking the equilibrium:

$$C = T = 0$$

$$1956.3 = 1956.3$$

Finally the moment capacity of the section is computed.

Centering moments from axial loads and Post – tensioned:

$$M_{pt} = 1189.3 \text{ kNm}$$

Dissipating moment from mild steel:

$$M_d = 716.2 \text{ kNm.}$$

φ 26 Diameter of the Bars

Eight bars of 26 mm diameters are considered for a total of 4247 mm² of mild steel; the fuse length is 390 mm and the un bonded length is 570 mm.

The final iteration is presented below. The neutral axis depth is equal to $c = 763$ mm, $\gamma = c/L_w = 0.32$.

The tendons elongation at the rocking interface is:

$$\Delta_{pt} = \theta(d_{pt,i} - c) \quad \begin{array}{l} = 3.1 \text{ mm for } d_{pt,1} = 1075 \text{ mm} \\ = 5.3 \text{ mm for } d_{pt,2} = 1325 \text{ mm} \end{array}$$

The tendons strain increments due to tendons elongations are:

$$\varepsilon_{pt}(\theta) = \frac{n\Delta_{pt}}{l_{ub}}$$

$$\varepsilon_{pt} = 0.0005$$

$$\varepsilon_{pt} = 0.0008$$

The increment in tendon force is:

$$\Delta T_{pt} = E_{pt} \varepsilon_{pt}(\theta) n_{pt} A_{pt}$$

The increments in tendons force are:

$$\Delta T_{pt1} = 99.26 \text{ kN}$$

$$\Delta T_{pt2} = 178.9 \text{ kN}$$

The total post tensioned forces are:

$$T_{pt} = T_{pt,initial} + \Delta T_{pt}$$

$$T_{pt1} = 597.8 \text{ kN}$$

$$T_{pt2} = 677.5 \text{ kN}$$

The stress in the tendons can't exceed the allowable limit of 90% of f_{pty} .

$$\varepsilon_{pt,initial} + \varepsilon_{pt} < 0.9 \varepsilon_y = 0.9 * 835/E = 0.004$$

$$\text{Tendon 1: } \varepsilon_{pt,initial} + \varepsilon_{pt} = 0.0028 < 0.004$$

$$\text{Tendon 2: } \varepsilon_{pt,initial} + \varepsilon_{pt} = 0.0032 < 0.004$$

The mild steel is lumped into 6 layers of 2 bars each, two on the left and two on the right side of the wall. The depth of each layer is:

$$\begin{aligned}d_1 &= 574 \text{ mm} \\d_2 &= 674 \text{ mm} \\d_3 &= 1726 \text{ mm} \\d_4 &= 1826 \text{ mm}\end{aligned}$$

TENSION STEEL LAYERS

The elongations and the strain of the tension steel layers are:

$$\begin{aligned}\Delta s_1 &= 9.4 \text{ mm} \\ \Delta s_2 &= 8.9 \text{ mm} \\ \Delta s_3 &= 8.4 \text{ mm}\end{aligned}$$

The values of strain are:

$$\begin{aligned}\varepsilon_{s1} &= 0.027 \\ \varepsilon_{s2} &= 0.025\end{aligned}$$

The stress is determined from a bilinear stress – strain relationship with $r = 0.8\%$.

$$f_s = f_y \left[1 + r \left(\frac{\varepsilon_s}{\varepsilon_y} - 1 \right) \right]$$

$$\begin{aligned}f_{s1} &= 341.2 \text{ MPa} \\ f_{s2} &= 337.1 \text{ MPa}\end{aligned}$$

The force in the tension layer is given by:

$$T_s = f_s A_s$$

$$\begin{aligned}T_{1a} &= 181.1 \text{ kN} & T_{1b} &= 181.1 \text{ kN} \\ T_{2a} &= 178.9 \text{ kN} & T_{2b} &= 178.9 \text{ kN}\end{aligned}$$

COMPRESSION STEEL LAYERS

The elongations and the strain of the tension steel layers are:

$$\begin{aligned}\Delta s_1 &= -1.89 \text{ mm} \\ \Delta s_2 &= -0.89 \text{ mm}\end{aligned}$$

The values of strain are:

$$\varepsilon_{s1} = -0.005$$

$$\varepsilon_{s2} = -0.002$$

The stress is determined from a bilinear stress – strain relationship (if the elastic limit is not exceeded) with $r = 0.8\%$.

$$f_s = f_y \left[1 + r \left(\frac{\varepsilon_s}{\varepsilon_y} - 1 \right) \right]$$

$$f_{s1} = -305.4 \text{ MPa}$$

$$f_{s2} = -301.3 \text{ MPa}$$

The force in the compression layer is given by:

$$C_s = f_s A_s$$

$$C_{1a} = -162.1 \text{ kN}$$

$$C_{2a} = -159.9 \text{ kN}$$

$$C_{1b} = -162.1 \text{ kN}$$

$$C_{2b} = -159.9 \text{ kN}$$

TIMBER

The timber compressive strain is defined as:

$$\varepsilon_t = \left(3 \frac{\vartheta_{imp}}{L_{cant}} + \phi_{dec} \right) c$$

Where:

$$E_t = 10 \text{ GPa}$$

$$E_{can} = 5.5 \text{ MPa}$$

The decompression curvature is:

$$\phi_{dec} = \frac{M}{E_{can} I_t} = \frac{T_{pt,i} + N}{E_{cant} I_t}$$

$$\phi_{dec} = 3.66E-07$$

Thus the timber strain is calculated:

$$\varepsilon_t = 3.7 \text{ E-}03$$

The compression force is so equal to:

$$C_t = -1398 \text{ kN.}$$

Checking the equilibrium:

$$C = T = 0$$

$$2042.5 = 2042.5$$

Finally the moment capacity of the section is computed.

Centering moments from axial loads and Post – tensioned:

$$M_{pt} = 1215.68 \text{ kNm}$$

Dissipating moment from mild steel:

$$M_d = 858.21 \text{ kNm.}$$